Introducing Bis(silylene) and Bis(germylene) Pincer Type Ligands in Catalysis

vorgelegt von

M. Sc. Chemie

Daniel Gallego Mahecha

aus Bogotá D. C., Kolumbien

Von der Fakultät II – Mathematik und Naturwissenschaften
der Technischen Universität Berlin
Institut für Chemie
zur Erlangung des akademischen Grades

Doktor der Naturwissenschaften
- Dr. rer. nat. -
genehmigte Dissertation

Promotionsausschuss:
Vorsitzender: Prof. Dr. Martin Kaupp (TU Berlin)
1. Gutachter: Prof. Dr. Matthias Driess (TU Berlin)
2. Gutachter: Prof. Dr. Thomas Braun (HU Berlin)
Tag der wissenschaftlichen Aussprache: 21-04-2015

Berlin 2015

D83

DISSERTATION

Introducing Bis(silylene) and Bis(germylene) Pincer Type Ligands in Catalysis

by

M. Sc. Chemistry

Daniel Gallego Mahecha

from Bogotá D. C., Colombia

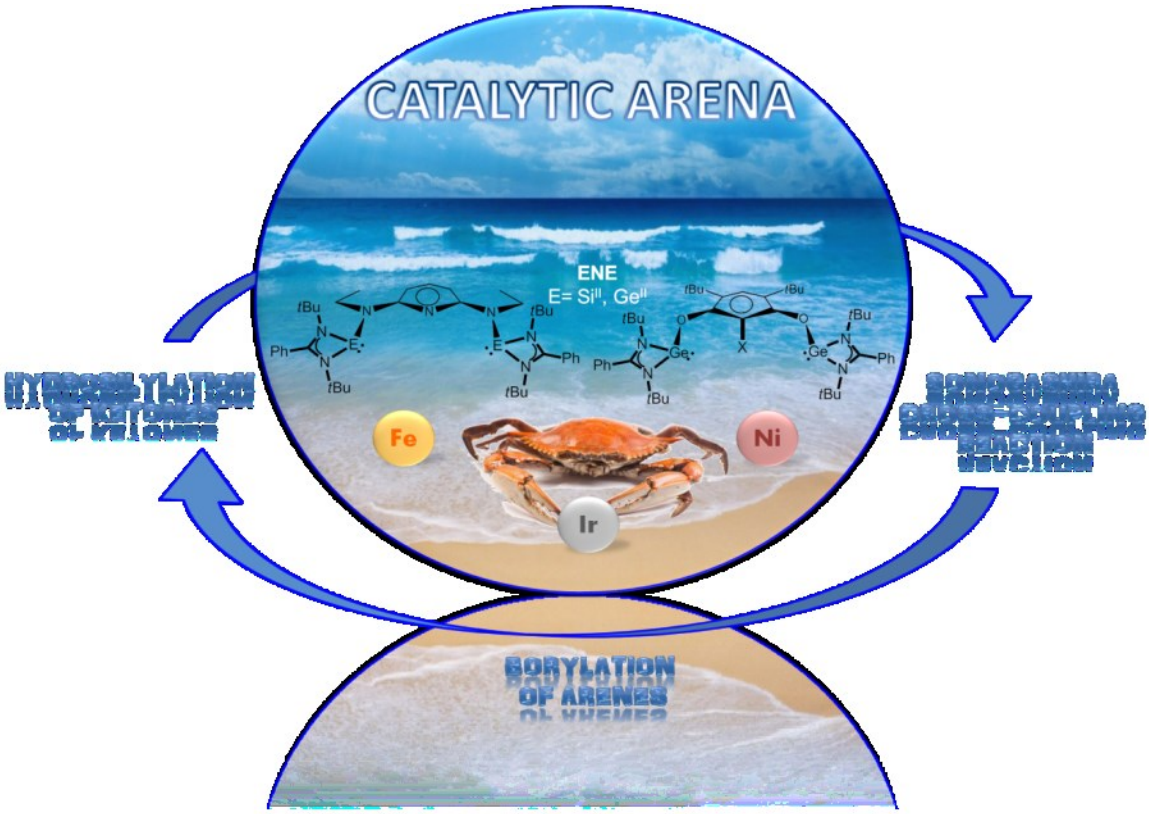

Erklärung

Die vorliegende Arbeit entstand in der Zeit von Sep. 2011 bis Mar. 2015 unter der Betreuung von Prof. Dr. Matthias Driess am Institut für Chemie der Technischen Universität Berlin.

Von Herzen kommend gilt mein Dank meinem verehrten Lehrer

Herrn Professor Dr. Matthias Drieß

für die Aufnahme in seinen Arbeitskreis, für seine engagierte Unterstützung,

und für die Forschungsfreiheit.

To my family,

Maria del Mar, Diego, Ariel y Nima, Che, Má y Pá,

for being always there despite the distance.

"Erfahren, was ist es, ernst genommen zu werden und über das andere zu lachen"
"Learn what is to be taken seriously and laugh at the rest"
Hermann Hesse

"Grau, teurer Freund, ist alle Theorie
Und grün des Lebens goldner Baum"
"Grey, dear friend, is all theory
And green the golden tree of life"
Faust I – Mephistopheles
Goethe

"The beauty of a living thing is not the atoms that go into it,
but the way those atoms are put together"
Cosmos
Carl Sagan

Acknowledgements

At the beginning of this PhD, the way looked very long and with plenty of unknown and some scary difficulties. However, thanks to the help of many people this journey has been amenable and enjoyable.

First, I would like to thank my supervisor Prof. Dr. Matthias Driess who gave me the possibility to work in this very interesting and challenging project independently. It has been very satisfying to learn about main group and organometallic chemistry under his supervision, I am in debt for his commitment in this field. Secondly, I would like to thank Prof. Dr. Thomas Braun for accepting reviewing this dissertation and be part of the jury committee. I would also want to thank the collaboration partners who have been very important for the successful achievements of my scientific research. I thank Prof. Dr. John F. Hartwig at University of California, Berkeley, who through the Einstein Foundation Fellowship worked during the projects of Iridium and Nickel pincer complexes; for his insightful discussions about catalysis and mechanistic studies, and his commitment in chemistry in general. Also I thank Dr. Andreas Brück who took part as the *"catalytic partner"* in these two projects from Hartwig's group, *Dankeschön*. I feel very thankful with the people who helped for the theoretical calculations for a better and complete understanding of the experiments. I thank Prof. Dr. Martin Kaupp and his co-worker Mr. Florian Meier for their passionate, careful and detailed work about the reaction intermediate of the Sonogashira cross-coupling reaction, *Dankeschön*. Also I thank Prof. Dr. Shigeyoshi Inoue for his contribution on the calculation of the electronic structure of the iron(0) complexes and for his friendship along this PhD, *Arigatou gozaimasu Shige Sensei!* And Dr. Tibor Szilvási at the University of Budapest, who appeared just at the right time for calculating the key intermediate of the hydrosilylation of ketones; I am happy that at the end the match *theory vs. experiment* finalized in a draw, *köszönöm szépen Tibi!* Finally, I feel gratified with the collaboration with Prof. Dr. Martin Oestreich and his co-worker Toni T. Metsänen during the understanding of the catalytic mechanism of the hydrosilylation of ketones. It was great to see the successful organic-inorganic fusion for a deep understanding in the unexpected mechanism for this system, *Dankeschön* and *Kiitos!*

I am strongly in debt with the people who in one or other way always stayed open for a scientific discussion, suggestion or just to give constant support during the tough days. First, I would like to thank my partner and *bro'* Gengwen Tan, it has been really incredible to work with such a passionate and bright chemist. Man, thanks to you this journey was more than simple research but a travel to wonderful and deep understanding of our crazy reactions day by day. I learnt a lot from you not only from chemistry but life as well, *Xièxiè wǒ de péngyǒu!* I also thank Dr. Burgert Blom, mostly known as Dr. UNO, who became a constant support and a really important guide during my scientific research. Man, I am thoroughly in debt with you for your careful revision of this dissertation. It has been a pleasure to work to your side with our little paws and to laugh as well, despite the stressful moments, *Thanks a lot UNO!* I am in debt with my mentor at the beginning of my PhD Dr. Wenyuan Wang, who with his patience I got to know the difficulties during this type of chemistry. Also, he taught me that science is an universal language and even when we could not understand each other quite well either in English, German, Chinese, or Spanish, at the end the chemistry knowledge could be transferred without any inconvenient, *Xièxiè!* My office partners deserve also big thanks because of their constant support, discussions and relaxing chats during the working days. Arindam and Prashant, you both are great, still I have to learn more about Indian *cousine* and its special and spiiiiiiicy taste! I would also like to thank Nils, who has been a very important friend and support during the last year of the PhD, *vielen Dank für deine Unterstützenden Worte mein Freund!* Also I am thoroughly in debt with Dr. Stephan Enthaler for his scientific discussions, suggestions and revision of this dissertation, *Dankeschön!*

I also thank all the group members of Metalorganics and Inorganic Materials group under the supervision of Prof. Dr. Matthias Driess, and the groups of Dr. Stephan Enthaler and Prof. Dr. Shigeyoshi Inoue, for their daily support. I especially thank the secretary Andrea Rahmel for all the help in the bureaucratic work during my PhD, *Vielen Dank!* I also thank all technicians from the Institute für Chemie at the Technische Universität Berlin for their constant help and work. Especially, I would like to thank Paula Nidorf and Dr. Elisabeth Irran for the measuring of single crystals and solving the disordering of the XRD crystallographic structures. Mrs. Christine Klose and Dr. Maria Schlangen for their help

during the mass spectra acquisition of the sensitive metal complexes. And, Samantha Voges and Dr. Jan Dirk Epping for their help during the NMR spectra acquisition.

I am thoroughly thankful with the *Cluster in Catalysis UniCat* in Berlin for giving me the scholarship during my PhD studies. It has been a pleasure to work in such interdisciplinary environment learning from the different fields of catalysis. Also, I thank the graduate school BIG-NSE, in which I took part as fellow, especially to Dr. Jean-Philippe Lonjaret for coordinating the different activities and act as a *catalyst* for the social meetings with the BIG-NSE students.

I thank all my BIG-NSE batch mates who became part of my family in Berlin. *Meine liebe* crazy Fanni, thanks for all your happiness and football matches either as spectator or player, I am your fan # 1! Mopsi I will always remember your monstrous speed of drinking beer and your flirting skills after the 6^{th} one hahaha. Paddy my rock star and party man, I enjoyed a lot each of your gigs and hic(s)…cops hehehe. *Meine liebe katze* Laura, happiness and craziness is a perfect mix to being just you, you became like my dear German sister *Miaaauuu!* Seti, your passion and courage are an inspiration to demand the rights for people for a better world, thanks for keeping this flame alive. Linyu, you and your Chinese wine will always produce me a headache but a nice remembrance of a passionate and involved chemist, *Gānbēi!* Xunhua, your commitment is an example to follow for a successful career. Matthias, man thanks for showing that theoreticians are not always at the PC but can have an enjoyable way of seeing life. And my shy a pretty Nhan, I really wish to had share more with you but unfortunately chemistry made you disappear, hope you will keep doing great! Also all the other people from different batches, especially the latin mafia Lauris, Maria, Javier, and Ines, it was always nice to have a moment for Spanish refreshment out of all the other languages, *gracias* ;)

This thesis would not have been successful with all the support from the people who always were sending the best energy from the distance. All my university colleagues from the Universidad Nacional de Colombia with their constant support made me possible to represent them with all my best. Especially to Lina, Ingrid, Julio Cesar, Patron, Mikel with their supporting words during the tough times. And my brother and partner Edwin with his humble character of seeing chemistry as a *hobby* and enjoying every single second of life.

Pelao, you taught me to be serious at work and laugh at the rest; to be generous with everyone who needs it and being there supporting other ones, even when you are not in the best situation. *Hermano*, I hope that our dream to create a collaborative research group in organometallic chemistry and homogeneous catalysis, one day will become for real, starting a new wave of research in our adorable country Colombia!

I thank deeply from my heart to Andrea, my girlfriend, for being the star in the darkness; for being the balance we all need in love; for her constant support and trust on my capacity not just as chemist but as human being. *Ma petite Ciel*, you are one of the reasons to go beyond the goal. The distance has been hard but every single piece of time with you I have enjoyed till the eternity. *Te adoro desde lo más profundo de mi corazón!*

Last but not least, I am and I will be always in debt to my family for its support in every single situation, either sad or happy, they are always there. My sister Maria del Mar with her commitment for each task she is involved; her passion is unique comprising happiness and respect to people. Maria, you are an inspiration for me to work always with passion, enjoying the simple things of life…*la quiero muchisimo!* My brother Diego who is a role model with his commitment on understanding science with constructive criticism and for his worry about divulgation of science to non-scientific people. *Hermanin, usted es un teso, lo quiero muchisimo!* Checita *y los sobrinos mas locos y lindos* Arielin y Nima*, gracias por hacer de la vida una recocha sabrosa y mostrarme que con sonrisas tan simples y sinceras cualquier dificultad se puede afrontar con calma y sabiduría, los quiero muchisisimo y les doy un abrazote de OSO gigante!!!* Y finalmente, a mi Ma y Pa, *gracias a ustedes estoy en esta aventura de la ciencia, conociendo y entendiendo el mundo desde lo más micro hasta lo macro. Es mas que un orgullo formar parte de la familia que ustedes han sacado adelante con tanto esmero, amor y recocha. Siempre están presentes en cada acción que llevo a cabo y gracias por una de las más importantes enseñanzas "si de verdad lo quieres hacer, da lo mejor de ti, si no, no lo hagas". Los adoro y siempre los llevo en mi corazón!*

Daniel,

Berlin, 3rd February 2015

Publications during the PhD studies

1. B. Blom, M. Driess, **D. Gallego**, S. Inoue
   "Facile Access to Silicon-Functionalized Bis-Silylene Titanium (II) Complexes"
   Chem. Eur. J. **2012**, *18*, 13355–13360.
2. A. Brück, **D. Gallego**, W. Wang, E. Irran, M. Driess, J.F. Hartwig
   "Pushing the σ-Donor Strength in Iridium Pincer Complexes: Bis-(silylene) and Bis(germylene) Ligands Are Stronger Donors than Bis(phosphorus(III)) Ligands"
   Angew. Chem., Int. Ed. **2012**, *51*, 11478–11482.
3. **D. Gallego**, A. Brück, E. Irran, F. Meier, M. Kaupp, M. Driess, J.F. Hartwig
   "From Bis(silylene) and Bis(germylene) Pincer-Type Nickel(II) Complexes to Isolable Intermediates of the Nickel-Catalyzed Sonogashira Cross-Coupling Reaction"
   J. Am. Chem. Soc. **2013**, *135*, 15617–15626.
4. N. C. Breit, T. Szilvási, T. Suzuki, **D. Gallego**, S. Inoue
   "From a Zwitterionic Phosphasilene to Base Stabilized Silyliumylidene-Phosphide and Bis(silylene) Complexes"
   J. Am. Chem. Soc. **2013**, *135*, 17958–17968.
5. B. Blom, **D. Gallego**, M. Driess
   "N-heterocyclic silylene complexes in catalysis: new frontiers in an emerging field"
   Inorg. Chem. Front. **2014**, *1*, 134–148.
6. G. Tan, B. Blom, **D Gallego**, M. Driess
   "Facile Access to Mono- and Dinuclear Heteroleptic N-Heterocyclic Silylene Copper Complexes"
   Organometallics **2014**, *33*, 363–369.
7. G. Tan, B. Blom, **D. Gallego**, E. Irran, M. Driess:
   "Elucidating the Effect of the Nucleophilicity of the Silyl Group in the Reduction of CO_2 to CO Mediated by Silyl-Copper(I) Complexes"
   Chem. Eur. J. **2014**, *20*, 9400–9408.
8. B. Blom, M. Pohl, G. Tan, **D. Gallego**, M. Driess
   "From Unsymmetrically Substituted Benzamidinato and Guanidinato Dichlorohydridosilanes to Novel Hydrido N-Heterocyclic Silylene Iron Complexes"
   Organometallics **2014**, *33*, 5272–5282.

9. **D. Gallego**, S. Inoue, B. Blom, M. Driess
   "Highly Electron-Rich Pincer-Type Iron Complexes Bearing Innocent Bis(metallylene)pyridine Ligands: Syntheses, Structures, and Catalytic Activity"
   Organometallics **2014**, *33*, 6885−6897. *ASC Editor's Choice. 3rd Most Read Article of the Year 2014.*
10. B. Blom, G. Klatt, **D. Gallego**, G. Tan, M. Driess
    "Unprecedented silicon(II)→ calcium complexes with N-heterocyclic silylenes"
    Dalton Trans. **2015**, 44, 639−644.
11. **D. Gallego**, M. Driess, T. Szilvási, T. T. Metsänen, M. Oestreich
    "Unconventional Mechanism of a Carbonyl Hydrosilylation Catalyzed by an SiNSi Iron Pincer Complex"
    Submitted for publication.
12. **D. Gallego**, B. Blom, G. Tan, M. Driess
    "Chelating N-Heterocyclic Silylenes as Steering Ligands in Catalysis"
    Book chapter in *Reference Module in Chemistry, Molecular Sciences and Chemical Engineering*, Elsevier, **2015**. DOI:10.1016/B978-0-12-409547-2.11449-0

Participation in Conferences and Workshops

1. UniCat Workshop – Challenges in molecular catalysis, 25th-26th April, **2012**, Technical University Berlin, Berlin, Germany.
   Assistant with Poster entitled
   *"*Bis(silylene) and -germylene pincer ligands as novel scaffolds in catalysis"
2. 27th Tag der Chemie, 28th June, **2012**, Technical University Berlin, Berlin, Germany.
   Assistant with Poster entitled
   *"*The First Bis(silylene) SiCSi and Bis(germylene) GeCGe Pincer-Like Ligands and Their Catalytic Applications".
3. 28th Tag der Chemie, 27th June, **2013**, Potsdam University, Potsdam, Germany. *Assistant with Poster.*
4. ICIQ-UniCat Summer School, June 30th – July 4th, **2013**, Tarragona, Spain.
   Assistant with Poster entitled
   *"*Pushing the σ-Donor Strength in Iridium Pincer Complexes: Bis-(silylene) and Bis(germylene) Ligands Are Stronger Donors than Bis(phosphorus(III)) Ligands".
5. SILQCOM-POLYMAT 2013, 13-17th October, **2013**, Huatulco, Mexico.
   Oral presentation entitled
   "Introducing Bis(silylene) and Bis(germylene) Pincer Type Ligands in Catalysis".
6. XVII International Conference on Organometallic Chemistry, 13-18th July, **2014**, Sapporo, Japan.
   Assistant with Poster entitled
   *"*Bis(silylenes) and Bis(germylenes) Scaffolds on Pincer Backbones as Novel Ligands in Late Transition Metal-Based Catalysts".
7. ISOS XVII BERLIN 2014, The 17th International Symposium on Silicon Chemistry, 3rd-8th August, 2014, Berlin, Germany.
   Assistant with Si&Me Poster entitled
   "Bis(Silylene) Pincer Type Ligands: A Silicon System to Explore in the Universe of Catalysis". **Si&Me Poster prize.**
   www.scienceopen.com DOI:10.14293/P2199-8442.1.SOP-CHEM.PZOODJ.v1

Table of contents

List of abbreviations

Γ_{FWHM}	Full Width at Half Maximum
135DEPT	Distortionless Enhancement by Polarization Transfer with 135° pulse
J	Coupling constant (NMR)
Ad	Adamantyl
APCI	Atmospheric-Presure Chemical Ionization
COA	Cyclooctane
cod	Coordinated 1,5-cyclooctadiene
COD	1,5-cyclooctadiene
coe	Coordinated cyclooctene
COE	Cyclooctene
COSY	Correlation Spectroscopy
DFT	Density Functional Theory
Dipp	2,6-*i*Pr_2-C_6H_3
dme	Coordinated dimethoxyethane
DME	Dimethoxyethane
DOSY	Diffusion-ordered spectroscopy
equiv	Equivalent
ESI	Electrospray ionization
GC	Gas chromatography
Ge_2	Bis-germylene
HBPin	Pinacolborane
HMBC	Heteronuclear Multiple Bond Correlation
HOMO	Highest Occupied Molecular Orbital
HRMS	High Resolution Mass Spectrometry
HSQC	Heteronuclear Single Quantum Coherence
INEPT	Insensitive nuclei enhanced by polarization transfer
***i*Pr**	Isopropyl ($CH(CH_3)_2$)
IR	Infrared
KHMDS	$K[N(TMS)_2]$
LAH	$LiAlH_4$
LDA	$Li[N(iPr)_2]$
LiHMDS	$Li[N(TMS)_2]$
LUMO	Lowest Unoccupied Molecular Orbital
Mes	2,4,6-$(CH_3)_3$-C_6H_2
MS	Mass Spectrometry
NaHMDS	$Na[N(TMS)_2]$
NBO	natural bond orbital
***n*-BuLi**	n-Butyl Lithium
NHC	N-heterocyclic carbene
NHGe	N-heterocyclic germylene
$NHGe_2$	Bis-NHGe
NHSi	N-heterocyclic silylene
$NHSi_2$	Bis-NHSi
NHSn	N-heterocyclic stannylene
$NHSn_2$	Bis-NHSn
NMR	Nuclear Magnetic Resonance
Ph	Phenyl (C_6H_5)
ppm	Parts per million
PSQP	Pseudo-Square Pyramidal
SET	Single Electron Transfer
Si_2	Bis-silylene
Sn_2	Bis-stannylene
TBP	Trigonal Bipyramidal
***t*Bu**	*tert*-butyl
***t*-BuLi**	*tert*-butyl Lithium
***ter*Ph**	Terphenyl
THF	tetrahydrofurane
TM	Transition Metal
TMS	Trimethylsilyl
TON	Turnover number
VT-NMR	Variable Temperature NMR
WBI	Wiberg bond index
XRD	X-ray diffraction
δ	isomer shift or chemical shift
ΔE_Q	quadrupole splitting
μ_{eff}	Magnetic moment

ABSTRACT

Inspired by the application of pincer ligands in catalysis and the coordination abilities of N-heterocyclic silylenes and germylenes toward late transition metals, a combination of these systems was investigated for the synthesis of novel bis(silylene) and bis(germylene) pincer ligands. The coordination abilities toward late transition metals such as iridium, nickel and iron was studied and applied as precatalysts in different chemical reactions depending on the metal involved. Interestingly, the novel metal complexes presented good catalytic performances in C–H activation, cross-coupling, and hydrosilylation reactions. Most importantly, stoichiometric reactions allowed revealing important elementary reaction steps in the reaction mechanisms. These studies probed the innocent behavior of these ligand systems during the catalytic reaction, in addition to their potential application in the catalytic field as strong σ-donor ligands.

First, the novel pincer ligands based on N-heterocyclic silylenes and germylenes (**LE–X–EL**, E = Si^{II}, Ge^{II}; L = *N,N'*-di-*tert*-butyl(phenylamidinate); X = 4,6-di-*tert*-butyl-resorcinolate, 2-bromo-4,6-di-*tert*-butylresorcinolate, *N,N'*-diethylpyridine-2,6-diamido), denominated as **GeCHGe**, **GeCBrGe**, **SiNSi**, and **GeNGe** were synthesized and accessed in high and gram scale yields (> 70 %). Their chemical properties were compared with traditional phosphine pincer ligands ***t*Bu-PCHP** and ***i*PrN-PCHP** (CH = 4,6-di-*tert*-butylresorcinolate, *t*Bu-P = P(*t*Bu)$_2$, *i*PrN-P = P(*i*Pr-N(CH_2)$_2$N*i*Pr)), the latter being more electronic related with the bis(metallylene) pincer ligands. The coordination toward late transition metals was evaluated with the synthesis of the iridium(III) complexes of type **[ECE]IrHCl(coe)**; nickel(II) complexes of type **[ECE]NiBr**; and iron(II) and iron(0) complexes of type ***κ*^{2}*E,E'*-[ENE]FeCl$_2$** and **[ENE]Fe(PMe$_3$)$_2$**, respectively. The novel ligands and their complexes were fully characterized by spectroscopic methods such as ^{1}H, ^{13}C{^{1}H}, ^{29}Si{^{1}H}, ^{31}P{^{1}H} NMR, 2D NMR correlation ^{1}H-^{1}H COSY, ^{1}H-^{13}C HSQC, ^{1}H-^{13}C HMBC, single crystal X-ray diffraction analysis, ^{57}Fe Mössbauer, IR, ESI or APCI mass spectrometry, and elemental analysis.

With the series of iridium complexes **[ECE]IrHCl(coe)** the striking σ-donor capacity of these novel pincer ligand systems versus the phosphine ligands was demonstrated. An increase in the σ-donor strength was determined by spectroscopic means in the following

order: **[*t*Bu-PCP]** < **[*i*PrN-PCP]** < **[GeCGe]** < **[SiCSi]**. The iridium complexes **[ECE]IrHCl(coe)** also served as precatalysts in the borylation of arenes, possessing higher activity to the phosphine-based complexes. These results showed that the N-heterocyclic metallylenes are not only better σ-donors in these systems but also can be used in catalysis as substituents of the commonly used ligands.

The nickel complexes **[ECE]NiBr** were evaluated as precatalyst in the Sonogashira cross-coupling reaction between phenylacetylene and (*E*)-1-octenyl iodide. The reaction yields for the coupling products were moderate and an excess of the organic halide was required. However, evaluation of the elementary reaction steps in a sequence transmetallation-oxidative addition-reductive elimination process led to remarkable results. First, the transmetallation reaction between the nickel complexes and copper acetylides was demonstrated by single crystal XRD structure analysis of reactions intermediates. These intermediates involve both metal centers bridged by one of the pendant arms of the bis(metallylene) pincer ligands. These adducts **{[ECE]Ni–C≡C–R→CuBr}** (E = Si^{II}, Ge^{II}; R = Ph, *ter*Ph, respectively) were evaluated by DFT calculations finding a three-center two-electrons bonding situation between Ni–E–Cu. Further reaction with the (*E*)-1-octenyl iodide led to the formation of the coupling product and the expected **[ECE]NiI** complex. These studies allowed drawing a general mechanistic landscape for the rare Ni-catalyzed Sonogashira cross-coupling reaction, normally catalyzed by palladium complexes.

The iron(0) complexes **[ENE]Fe(PMe$_3$)$_2$** (E = Si^{II}, Ge^{II}) showed unprecendented stable pseudo square-pyrimidal structures at the iron(0) center over a wide range of temperature. Evaluation by ^{57}Fe Mössbauer spectroscopy, DFT calculations and IR spectroscopy for their carbonyl derivatives **[ENE]Fe(CO)$_2$** demostrated the innocent behavior of the pincer ligands **[ENE]**. Additionally, evaluation by single crystal XRD structure analysis demonstrated that the stability of the pseudo square-pyramidal structures is intrinsically based on steric effects and not on the electronic structure in the iron center. Further evaluation of the iron(0) complex **[SiNSi]Fe(PMe$_3$)$_2$** in catalysis showed a good activity as precatalyst in the hydrosilylation of ketones. Elucidation of the reaction mechanism revealed that the actual catalyst is formed by an oxidative addition of the hydrosilane to the iron(0) center forming an iron-hydrido-silyl complex **[SiNSi]FeH(SiR$_3$)(PMe$_3$)** as determined by XRD structure analysis. Surprisingly, it was found that neither the hydride

nor the silyl groups in the iron(II) center participate in the hydrosilylation process. Crossover experiments with a chiral silane showed retention of stereochemistry at the silicon center after hydrosilylation, indicating a concerted mechanism. Combination with DFT calculations showed the most likely intermediate where the ketone is activated by the silyl group bound to the iron center acting as a Lewis acid. Remarkably, these results exhibited a new reaction mechanism for the hydrosilylation of ketones mediated by this iron pincer complex, where the iron does not participate for the hydrosilylation process but its peripheral ligands. This result highlights a new paradigm in the catalytic arena for metal-based catalysis since the metal center acts merely as a spectator ligand.

1. INTRODUCTION

The introduction is divided in four main parts. The first is about the chemistry of pincer ligands, covering the general aspects as their nomenclature, importance in catalysis, and some selected examples of breakthroughs in bond activation and catalytic applications. The second focusses on the chemistry of metallylenes, especially N-heterocyclic metallylenes, covering their synthetic methods, reactivity toward inorganic and organic molecules, along with their behavior as ligands in transition metal complexes. Due to the fact that the main goal of this dissertation is related with the introduction of two N-heterocyclic metallylenes in a pincer backbone, the third part is related with the existing bis(metallylenes) and their synthetic methods which are not trivial. Additionally, the few existing chelate bis(metallylenes) metal complexes are addressed. In the fourth part, the catalytic application of these metal complexes is highlighted presenting the scarce examples in this field when compare with the N-heterocyclic carbene (NHC) metal complexes in catalysis.

1.1. Pincer ligands

Since the seminal work of Shaw and co-workers in the mid 1970's,[1] pincer-type ligands have become a central area in inorganic chemistry. Due to their versatile nature and facile entry of different functional groups into the ligand backbone, their use has been instrumental in the development of organometallic chemistry, and in particular homogeneous catalysis. The first reports on cyclometallated bis(phosphine) pincer-type complexes were based on the ligands **L1** and **L2** (Figure 1.1.1). The stabilization of metal centers of group 9, employing these novel ligand systems, and their interesting chemical properties was reported.[1]

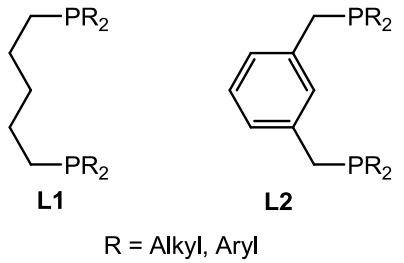

Figure 1.1.1. First pincer-type ligands introduced by Shaw and co-workers.[1]

The introduction of novel σ-donor atoms, i.e., N-heterocyclic silylenes and germylenes (NHSis and NHGes) from the group of metallylenes, in pincer backbones is of a great interest for tuning the electron density at the metal center. NHSis and NHGes possess strong σ-donor abilities, increasing the electron density at the metal center in metal complexes. Experimentally[2,3] and theoretically[4] NHSis have been demonstrated to be within the range of σ-donor strength of phosphines and carbenes, and in some cases even stronger than these well-known systems. Hence, the interest of working with the pincer ligands backbones for the novel ligands proposed herein.

1.1.1. Nomenclature

The term "pincer ligand" was first used by van Koten in his review article titled *Tuning the reactivity of metals held in a rigid ligand environment*[5] in 1989. Together with Albrecht, this term was used throughout their review article about the relevance of these ligands in chemical sensors and switches, and catalysis.[6] The name "pincer" originates from the singular coordination mode these ligands show toward a metal center. Pincer ligands are terdentate which normally coordinate to a metal center in a meridional fashion reminiscent of a trident and/or a pincer holding the dam, hence the term. The coordinating atoms are separated by non coordinating chemical spacers forming two metalacycles, sharing the M–D bond (M = Metal; D = Donor, Figure 1.1.2). Normally, for simplicity a short representation is used, depicting exclusively the donor atoms **[EDE]** employed in coordination or with their spacers, when they are worth mentioning, e.g., **POCOP**.

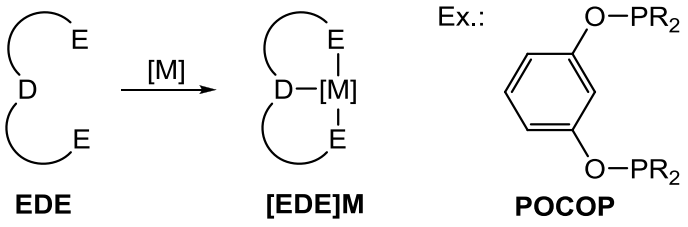

Figure 1.1.2. Schematic representation of pincer-type ligands and pincer complexes.

Generally, the arms (E) of a pincer ligand consist of neutral, two-electron Lewis donor moieties (e.g., E = PR_2, NR_2, or SR), which are connected via a linker group (often CH_2 or O) to the neutral or mono-anionic anchoring site (D; e.g., a pyridine or phenyl/alkyl group).

Henceforth, the referenced pincer ligands in this dissertation will be described according to their donor atoms. Thus, when the pincer ligand is coordinated to a metal, its nomenclature will be in the form of **[EDE]ML$_n$**, where **L$_n$** represents the coligands present at the metal center, **E** the donor atoms from the pendant arms, and **D** the central donor atom.

1.1.2. Chemical relevance

The versatility of pincer ligand permits their introduction in many chemistry research areas.[6–8] The facile entry of different functional groups in the ligand backbone enables tuning the reactivity on the metal center as well as improving desired physical properties (e.g., solubility). Figure 1.1.3 depicts the general structure of a pincer metal complex with the specific variable sites on the ligand backbone. This facile manipulation in the chemical structure renders pincer ligands a very attractive ligand framework for synthetic chemists since it offers a myriad of possibilities for a systematic study on structure and reactivity relationships. For instance, how the physical and chemical properties of pincer metal complexes vary by (i) the nature of the metal center (i.e., group in the periodic table, oxidation state), (ii) substituents on positions **D** and **Y** (e.g., chirality, bulkiness, electron-withdrawing or donating), (iii) ancillary ligands, and (iv) coordination geometry (e.g., open reaction sites).

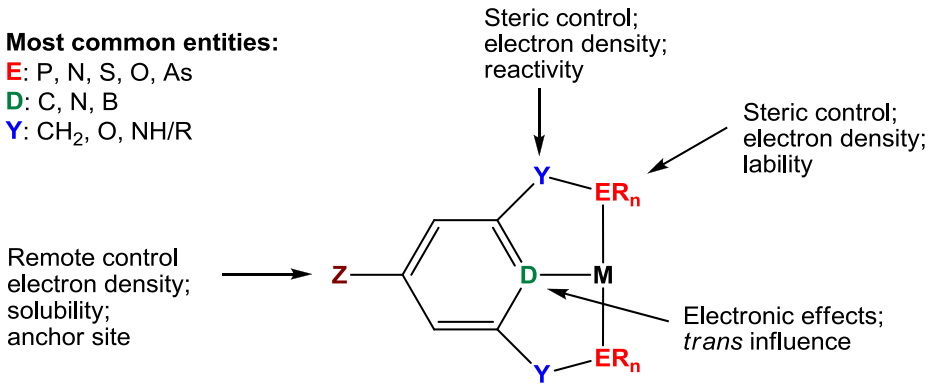

Figure 1.1.3. General structure of pincer complexes highlighting the potential modification sites in the ligand backbone and their effects on the properties of the metal center. Adapted from refs. 6, 9.

Upon coordination to a metal center the pincer ligand provides a unique balance between stability and reactivity. Especially the rigidity on aromatic-based pincer ligands improves the thermal stability of the metallic complexes even when they are coordinatively unsaturated (i.e., open reactive sites). This stability is very important for the application as catalyst in endothermic reactions without losing reactivity and selectivity.[9] Moreover, the planarity on the coordination mode has different consequences on the reactivity at the metal center, acting as a constraint on its coordination environment.[10] Additionally, the tuning on the steric properties has shown to enhance the catalytic activity increasing the turn over number (TON). This shows that not only varying the electronic properties at the metal center but the steric effects on the pincer ligand facilitates tuning the reactivity in the metal complex. This is very interesting since its modification might facilitate different reactivity and selectivity without changing the metal center.[11]

1.1.3. Breakthroughs in catalysis and bond activation based on pincer ligands

Several research groups have become attracted by the potential application of pincer ligands for stabilization of reactive species as well as improvement of reactivity along the first row transition metals. Important breakthroughs have been achieved during the last decade such dehydrogenation of alkanes using [PCP]Ir and [PCP]Rh complexes; cross-coupling reactions mediated by Ni complexes bearing nitrogen-based pincer ligands; coordination of N_2 by Ru, Rh and Ir complexes bearing PCP pincer-type ligands; activation of N–H in NH_3 by a [PCP]Ir^I complex; and activation of H_2 and CO_2 mediated by a [PNP]$Fe(H)_2(CO)$ complex.[6,9,11] This has shown the great potential of these complexes in the synthesis of valuable products from small entities, as well as, the exploitation of new energy sources with high energy barriers (e.g., activation of H_2). Herein some selected and key examples are described based on the importance and similarities on the systems studied in this dissertation. For a full review see references 7–9, 11 and references therein.

Activation of ammonia: Using an iridium pincer complex [PCP]Ir^I Hartwig and co-workers demonstrated the activation of a heteroatom–H bond. For the first time it was shown that the commonly used ancillary ligand ammonia (NH_3) can be activated by a high

electron rich Ir^{I} pincer complex (Scheme 1.1.1).[12] This started a new era in the coordination chemistry of the ancillary ligands previously heralded as "unreactive". The activation of the N–H bond occurs as a result of the high electron density on the Ir^{I} center; promoting the oxidative addition on the N–H bond resulting in an Ir^{III}-hydrido-amido complex.

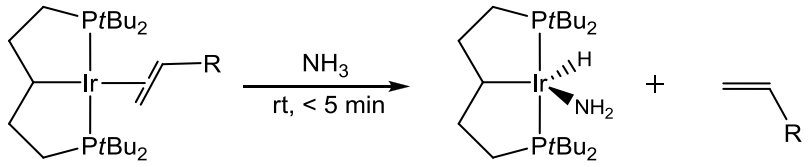

Scheme 1.1.1. Activation of N–H from the no longer ancillary ligand NH_3 reported by Hartwig *et al*.[12]

A methane complex: Using the pincer complex [PCP]Rh^{I} Brookhart and co-workers were able to characterize, in solution, a σ-C–H methane Rh^{I} complex (Scheme 1.1.2).[13] This showed the potential of using these pincer complexes in the activation of a relatively inert molecule. This came in addition to a report by Kaska and Jensen in the late 1990's with their application of Ir and Rh pincer complexes as catalysts in the dehydrogenation of alkanes.[14]

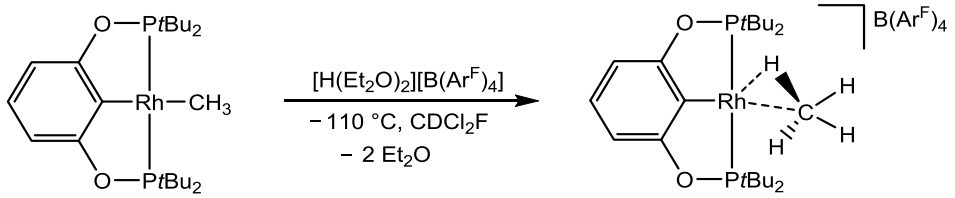

Scheme 1.1.2. Formation of a rhodium(I) σ-methane complex in solution ($B(Ar^{F})_4$ = $[B\{3,5\text{-}(CF_3)_2C_6H_3\}_4]^-$) reported by Brookhart *et al*.[13]

Activation of CO_2 and H_2: More recently, other research groups have explored the pincer complexes of the first row late transition metals (TM) due to their abundance in the Earth crust, lower toxicity and cost. Milstein and co-workers demonstrated the possibility of using H_2 and CO_2 as a feedstock for the production of formic acid mediated by a Fe^{II} pincer complex (Scheme 1.1.3).[15] In this report the use of a pyridine-based pincer heralded a relatively new concept in pincer ligand chemistry known as metal-ligand cooperation. In the proposed mechanism, the loss of aromaticity of the pyridine is a key elementary step

while the metal center remained with its formal oxidation state +2 throughout the catalytic cycle. Concurrently, Chirik and co-workers have been instrumental in the development of a variety of iron-based pincer type catalyst systems. Remarkable chemistry on low-valent pincer-type iron complexes and their potential use as hydrogenation and hydrosilylation catalysts has been reported (Scheme 1.1.4).[16] The redox non-innocence behavior of the pincer ligands employed by Chirik have been a topic of several subsequent studies.[17,18] This opened up a new type of chemistry in this field where the redox active center is the ligand and not the metal. Since then many other applications, mainly with first row TMs, appeared showing single electron transfer processes between the metal center and the ligand.[19]

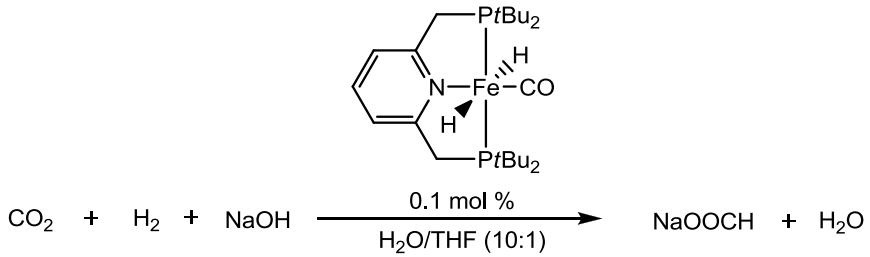

Scheme 1.1.3. Hydrogenation of carbon dioxide catalyzed by [PNP]Fe(H)$_2$CO pincer complex reported by Milstein *et al*.[15]

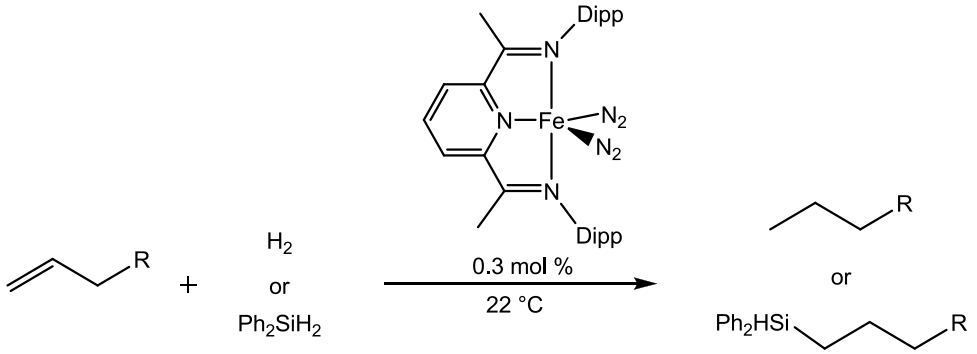

Scheme 1.1.4. Hydrogenation and hydrosilylation of olefins catalyzed by [NNN]Fe(N$_2$)$_2$ pincer complex (Dipp = 2,6-*i*Pr$_2$-C$_6$H$_3$) reported by Chirik *et al*.[16]

Cross-coupling reactions: Several groups have focused on the use of pincer-type systems for nickel-based catalysts.[20] The seminal work by Vicic[21] and Fu[22] demonstrated the use of Ni pincer complexes as catalysts in the Negishi C–C coupling reactions (Scheme 1.1.5). In the former a radical on the terpyridine ligand was shown to be a key factor for the activity of such a complex. Moreover, the research groups of Hu[23,24] and Inamoto[25] showed the potential application of Ni pincer complexes in Kumada–Corriu–Tamao and Suzuki

coupling reactions, respectively. In addition, Hu *et al.* have extended the application of their robust catalyst Nikamine® for the Sonogashira coupling reaction[26] to access alkyl coupling products with a broad functional group tolerance in high yields (Scheme 1.1.6).

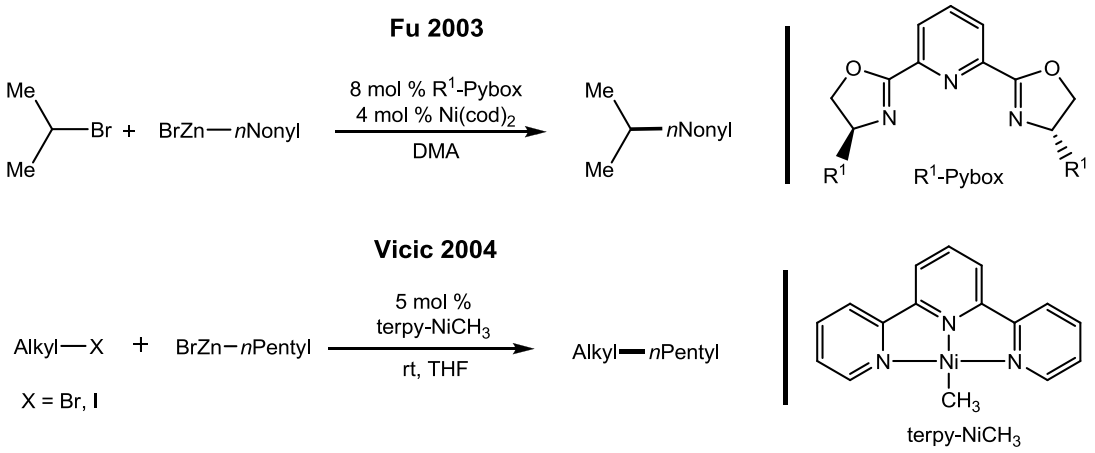

Scheme 1.1.5. Seminal work on nickel-based pincer complexes catalyzed Negishi cross-coupling reactions.[21,22]

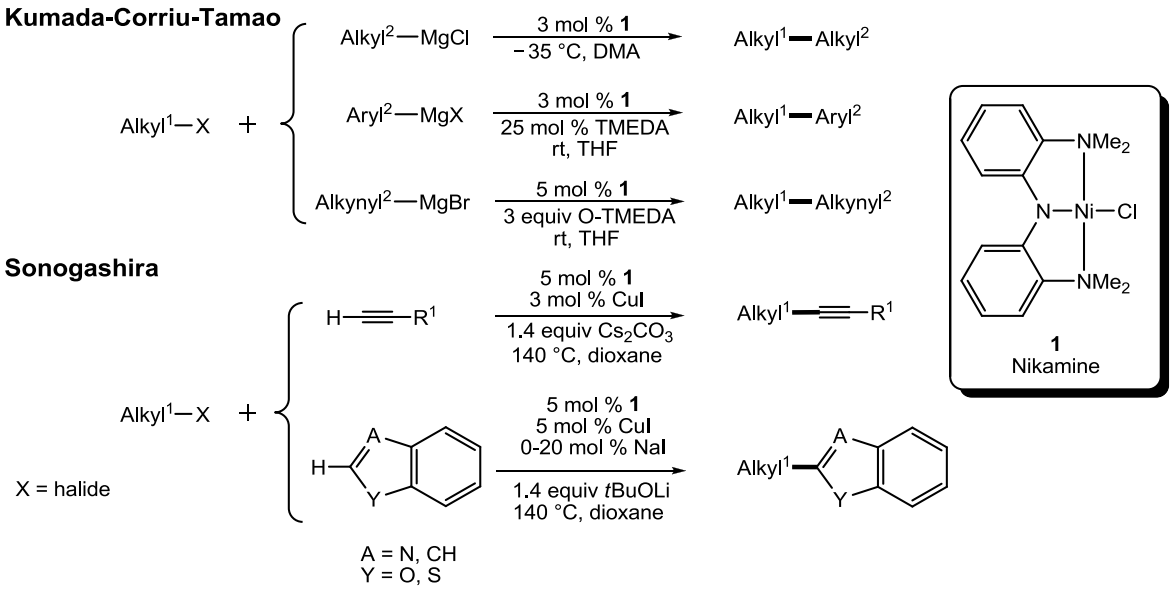

Scheme 1.1.6. Catalytic applications of the Nikamine® complex in Kumada–Corriu–Tamao and Sonogashira cross-coupling reactions reported by Hu *et al*.[23,24,26]

This brief summary on some key highlights, concerning the application of pincer ligands in homogeneous catalysis, shows the high importance and impact these ligand systems offer in the development of novel catalytic systems. Commonly, the increase of the electron density on the metal center has been shown to be critical for the activation of strong bonds

and the catalytic activity. Thus, the exploration of novel and stronger electron donor systems in pincer ligands is of high impact for the creation of highly electron rich metal pincer complexes that might lead to an improved and/or an unexplored reactivity.

Therefore, the introduction of NHSi and NHGe as strong donors in pincer backbones is an attractive idea. Hence, a short description about this class of compounds is presented addressing their synthetic methods, reactivity, and their coordination abilities toward transition metals.

1.2. Divalent group 14 compounds

1.2.1. General characteristics

Within the group 14 low-valent complexes, the well-known N-heterocyclic carbenes (NHCs) are widely studied. They have emerged as an important family of compounds with broad applications in organometallic chemistry, organic synthesis, and homogeneous catalysis.[27–31] Normally, low-valent group 14 compounds are difficult to isolate, being more challenging when moving up in the group (i.e., Pb→C). The same as with carbon, the heavier homologues of NHCs based on Si and Ge, required expertise for their synthesis and isolation.[32,33]

Contrary to the carbon-based compounds, heavier homologues exhibit a low propensity to undergo hybridization. This is due to the difference in geometrical sizes of the **ns** and **np** orbitals when n > 2. Therefore the divalent Si and Ge species would rather prefer the $(\mathbf{ns})^2(\mathbf{np})^2$ valence electron configurations.[32] In this case the electrons located at the **np** orbital are involved in the covalent bonds with the substituents and the **ns** electrons remain as a non-bonding electron pair. This electronic configuration is also found in the NHCs where a thermodynamic stabilization, through the N-based substituents, is present. Thus, the ground state of divalent R_2M: (M = Si, Ge, Sn, Pb; R = alkyl, aryl, heteroatom substituents) and NHCs is a singlet, contrary to the case of other carbenes of type R_2C: (R = H, alkyl, aryl), where the ground state is a triplet (Figure 1.2.1).[32,34] Specifically for NHCs the electron pair is located in an hybridized sp^2 orbital and the electronic configuration is alike to its heavier homologues NHSis and NHGes, where an electron pair is located in a **ns** orbital which is partially hybridized with a **np** orbital, sometimes called σ orbital.

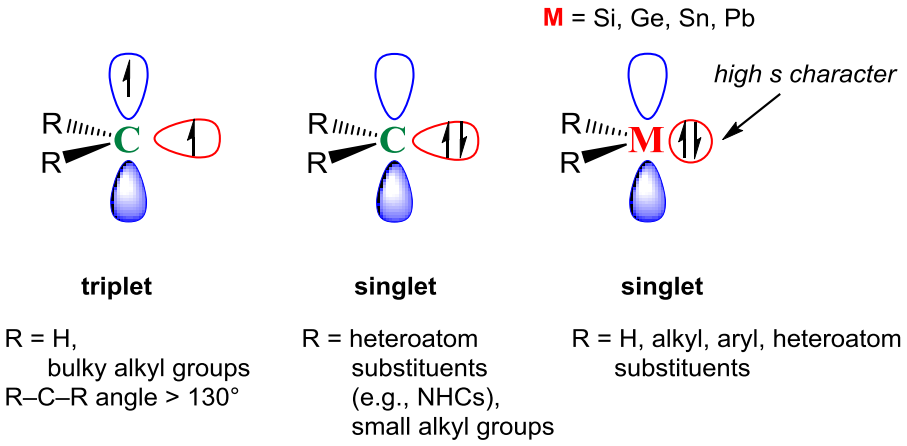

Figure 1.2.1. Difference between the ground states of carbenes and metallylenes. Adapted from refs. 32, 34.

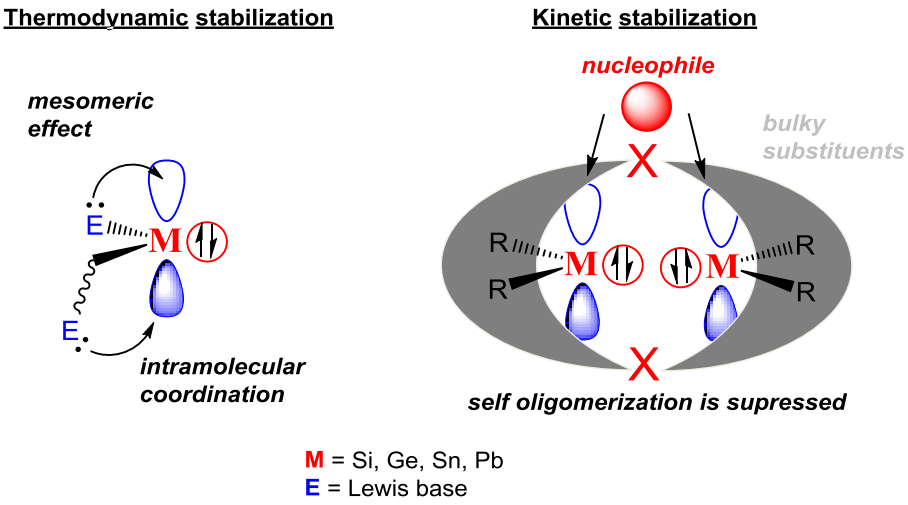

Figure 1.2.2. Thermodynamic and kinetic stabilization of metallylenes using either Lewis base or bulky alkyl/aryl as substituents in the ligand backbone, respectively. Adapted from ref. 32.

Owing to the ambiphilic character of metallylenes, with a vacant p-orbital and a lone electron pair in the s-orbital, they tend to be very reactive toward different molecules such as Lewis bases and acids. Therefore, their isolation as single molecules sometimes can be a difficult task. Thus, a stabilization of metallylenes is required either by thermodynamic and/or kinetic stabilization of these two reactive sites (Figure 1.2.2).[32] The thermodynamic stabilization is based on electronic effects on the divalent atom. Heteroatom-containing substituents are normally used to increase the electronic density in the p-orbital by

mesomeric effect or intramolecular coordination. The kinetic stabilization is based on steric effects, using bulky substituents around the divalent atom prevents their self oligomerization and/or reaction with external nucleophiles.

Before the 1990's, calculations and experiments showed that carbenes and silylenes were very reactive and eluded isolation. Characterization of some of these transient species was, however, successful under special conditions.[35] Only one example, reported by Jutzi in 1986, existed featuring a stable divalent Si center stabilized by π-interactions: decamethylsilocene.[36] In contrast, germylenes, stannylenes, and plumbylenes were more prone to be isolable, even as early as 1956,[37] as dimers and in some cases as monomers in the solid state.[32] The situation changed dramatically when Arduengo and co-workers reported the isolation of the first stable carbene **1-NHC**[38] (Figure 1.2.3) at room temperature in 1991, combining both stabilization strategies: thermodynamic stabilization by an N-heterocycle and kinetic stabilization by the adamantyl substituents at the N atoms. A few years later, in 1994, Denk and West reported the isolation of the first stable N-heterocyclic silylene **1-NHSi**[39] (Figure 1.2.3). The successful isolation of these two compounds represents a milestone in contemporary inorganic chemistry, and since then the chemistry of NHCs has been rigorously explored.[27–31,40] Their heavier homologues NHGe,[41] NHSn[42] were also isolated but for the case of the germylene *i*Pr was used as substituent instead of *t*Bu. The Pb^{II} analogue with unsaturated bonds in the 5-membered C_2N_2Pb ring has not been reported. But, with a saturated backbone using mesityl or Dipp substituents (mesityl = 2,4,6-Me_3-C_6H_3; Dipp = 2,6-*i*Pr_2-C_6H_3) a NHPb could be isolated.[43]

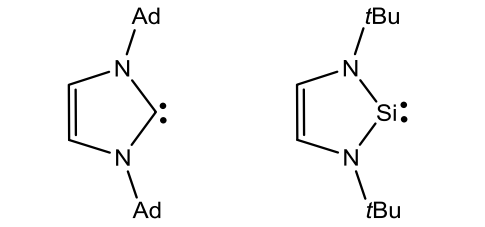

1-NHC Arduengo **1991** **1-NHSi** West & Denk **1994**

Figure 1.2.3. First isolated examples of an N-heterocyclic carbene (NHC) and an N-heterocyclic silylene (NHSi).

1.2.2. Synthetic methods

Other NHSis have been isolated using the push-pull stabilization method used for **1-NHSi** (Figure 1.2.4). However, the isolation of the first cyclic silylene **1-Si** without any N-based substituent was affordable by the kinetic stabilization using the large TMS substituents at the α carbon to the silicon center by Kira and co-workers.[44] West and Denk demonstrated that even under the absence of a π-conjugated system the isolation of the stable **2-NHSi** was possible. The synthesis of the **1-5-NHSis** is based on similar synthetic methods starting from the Si^{IV} dihalide precursors with reduction of the silicon center by suitable reducing agents (Scheme 1.2.1).[32,33,45] Another synthetic methodology is based on thermal or photochemical reduction of suitable M^{IV} precursors. For instance, the photochemical reductive elimination of a disilane from a bis-silyl precursor of type $R_2M(SiR'_3)_2$ produces the corresponding metallylene R_2M:. Similarly, the thermal and/or photochemical reductive elimination of an olefin or an alkyne from three-membered ring systems, metalliranes or metallirenes, affords the corresponding metallylenes (Scheme 1.2.1).

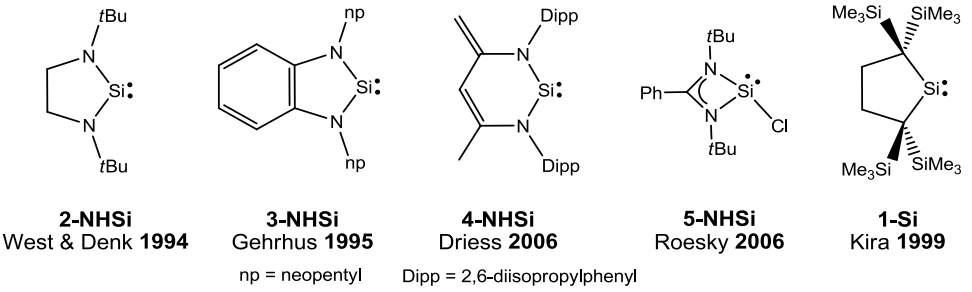

Figure 1.2.4. Selected examples of isolable N-heterocyclic silylenes.

The synthesis of heavier carbene analogues depends on suitable starting materials with oxidation state +2. Normally, due to the inert-pair effect, moving down in the group the oxidation state +2 is more stable. Thus for the case of tin and lead, their halides, $SnCl_2$ and $PbCl_2$, are stable starting materials for the synthesis of stannylenes and plumbylenes by a simple metathesis reaction, respectively. For the case of germylenes a commercially available and easily accessible polymeric starting material, $GeCl_2 \cdot$1,4-dioxane,[46] is used for their synthesis. For the case of silicon, up to date only two stable "SiX_2" (X = halide) complexes have been isolated, **NHC→$SiCl_2$** and **NHC→$SiBr_2$**, synthesized by Roesky[47]

and Filippou,[48] respectively. These compounds represent a facile entry of a Si^{II} center directly to the desired substituents by further metathesis reaction. However, the NHC coordinated to the Si center hampers the purification of the desired product.

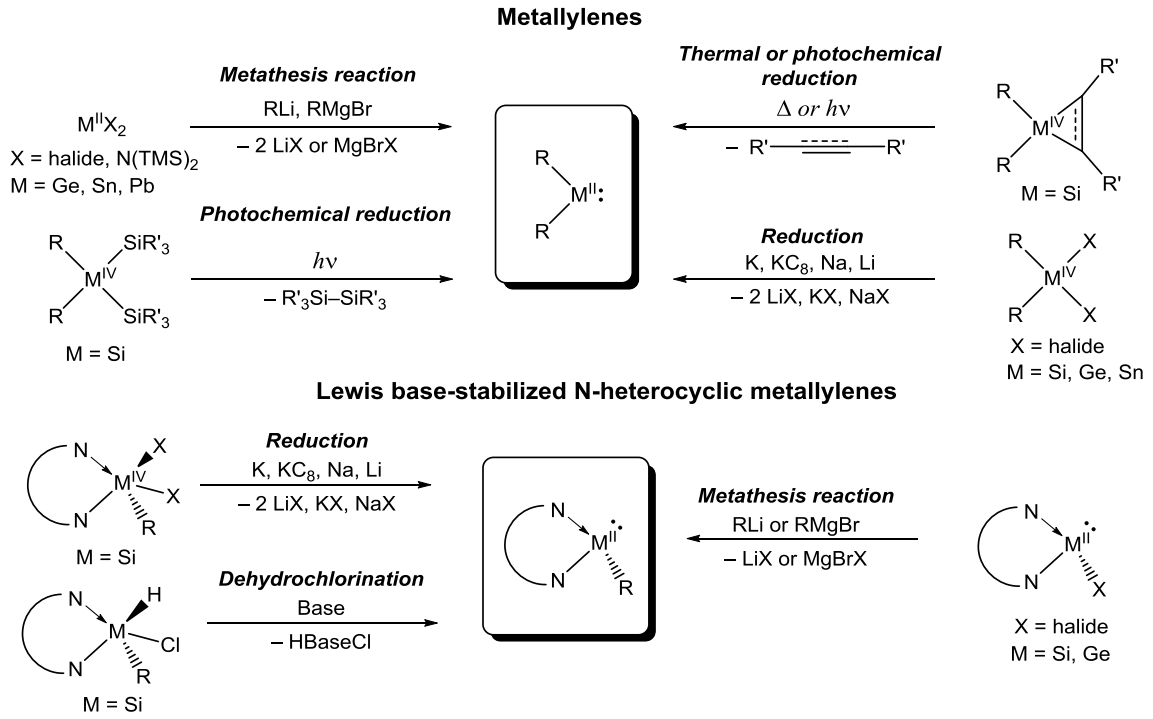

Scheme 1.2.1. Synthetic strategies for the isolation of metallylenes. Each methodology only works in certain cases which are shown.

In addition to the divalent N-heterocyclic group 14 compounds, another family of compounds exist which is accessible *via* intra or intermolecular coordination of a Lewis base into the empty valence p-orbital. These compounds are known as Lewis base-stabilized N-heterocyclic metallylenes and their synthesis can be accessed using a different methodology (e.g., dehydrochlorination or substitution). A summary of these synthetic strategies to access metallylenes is depicted in Scheme 1.2.1. Additionally, Roesky and co-workers could improve the synthesis of their previously reported base-stabilized chlorosilylene **5-NHSi**[49] by a dehydrochlorination reaction using a strong base (e.g., NHC or LiHMDS).[50] Normally, the reduction methods are carried out under harsh reaction conditions and the reaction yields are moderate. In contrast, the dehydrochlorination method is presented as a good synthetic strategy to obtain base-stabilized NHSis in quantitative yields.

In this dissertation the **5-NHSi** and its germanium homologue **1-NHGe** will be used as starting materials for the synthesis of the proposed pincer ligands. The synthesis of the **5-NHSi** implies dehydrochlorination of the $LSiHCl_2$ precursor (L = *N,N'*-bis-(*tert*-butyl)-phenylamidinato, Scheme 1.2.2). In contrast, the **1-NHGe** is afforded by a direct metathesis reaction of $GeCl_2$·1,4-dioxane with the ligand L lithiated species (Scheme 1.2.2).

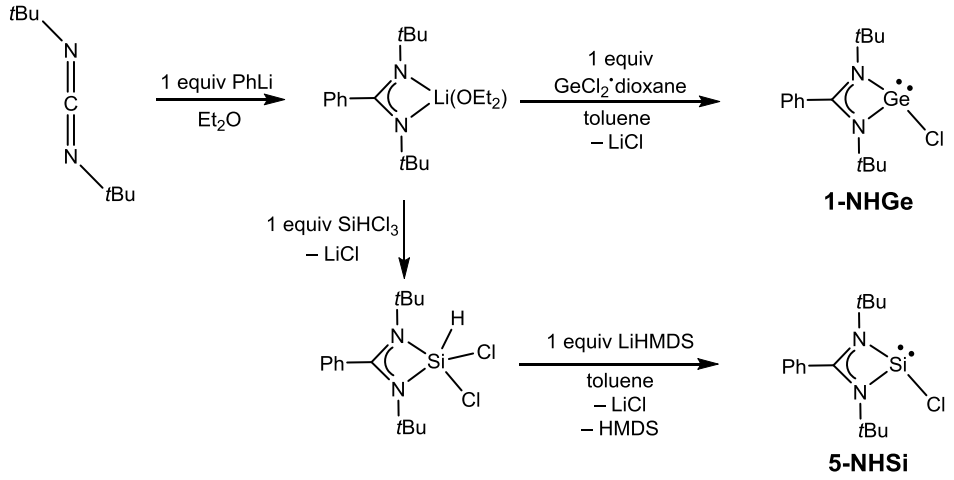

Scheme 1.2.2. Reported syntheses for the Lewis base-stabilized **5-NHSi** and **1-NHGe** used in the present work.[50,51]

1.2.3. Reactivity of metallylenes toward activation of strong bonds

Owing to the electronic properties of metallylenes, their lone electron pair can be use in activation of strong bonds. Important reviews about the reactivity of metallylenes toward different chemical bonds have been reported during the last decade.[32,33,45,52,53] The different variety of reactivities of the stable metallylenes can be categorized into five main groups: (i) insertion, (ii) cycloaddition, (iii) reduction, (iv) oxidation, and (v) coordination reactions. Herein, selected examples are described related mainly with NHSis and NHGes due to their higher reactivity as well as their relation with the main topic of this dissertation.

Main group elements. The five-membered silylenes **1-NHSi** and **3-NHSi** undergo facile reactions with chalcogens to form the corresponding spirocyclic dimers (Scheme 1.2.3). The reaction intermediate possesses a Si–E double bond which is not stable in solution affording the dimeric species.[52] In contrast, the carbene stabilized silylene **4-NHSi←NHC** can activate elemental sulfur, selenium, and tellurium to give the corresponding donor-

stabilized heavier silanone or silanoic silyl ester congeners. The reaction with the respective elemental chalcogens forms the expected NHC-supported silanechalcogenones.[53] Similar reactivity has been observed when the Lewis base-stabilized **2-NHGe** and **3-NHGe** were reacted either with elemental sulfur or selenium forming the germanechalcogenones. These species are very interesting when comparing the structural parameters and reactivity with the carbon homologous ketones, due to their low propensity to produce multiple bonds with main group elements. Therefore, it is expected to observe higher reactivity along these multiple bonds. Even the formation of other functional groups was observed. When the hydroxyl **3-NHGe** reacts with elemental sulphur and selenium, the thiogermanoic and seleniogermanoic acids are formed, respectively. These are very rare species even in the carbon chemistry, since the thiocarboxylic acid [RC(S)OH] does not exist in the free state and undergoes tautomerization to the carboxylic sulfide [RC(O)SH].[45]

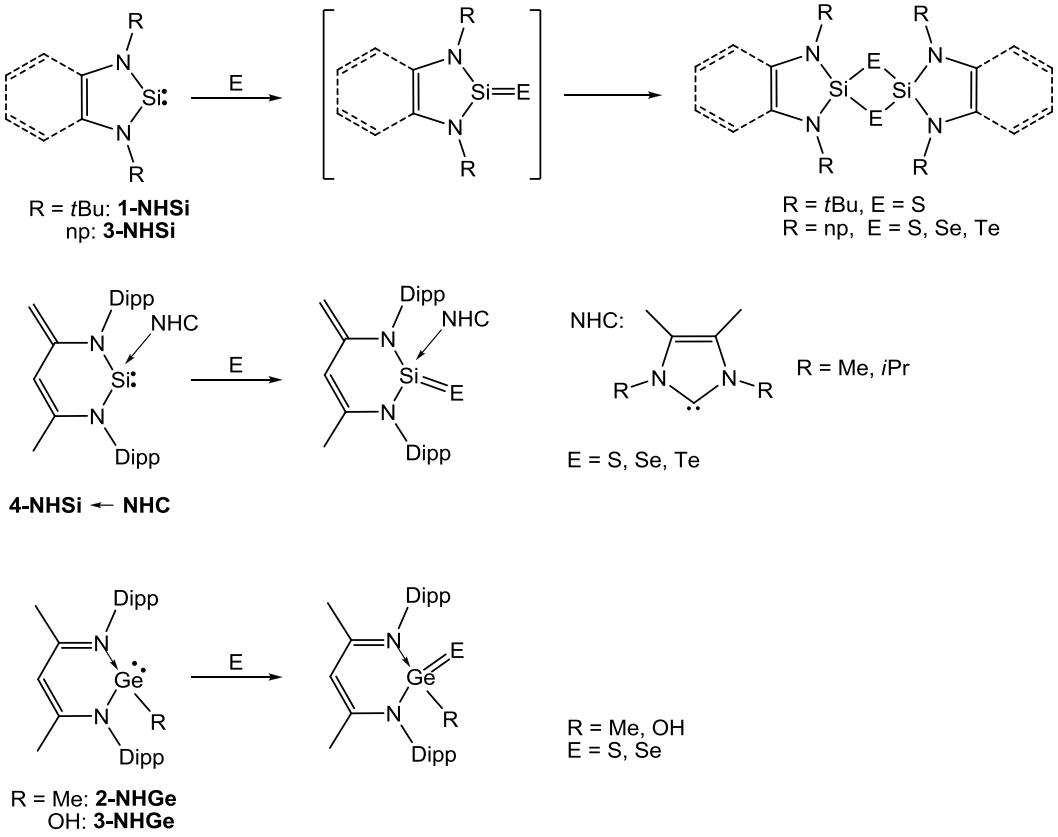

Scheme 1.2.3. Activation of elemental chalcogens by NHSis and NHGes.

Apart from the chalcogens, the activation of white phosphorus is also possible by the reaction with silylene **4-NHSi** at room temperature. The reaction produces two main products in contrast to the activation of P_4 by an NHC. One product is the 1:1 adduct, resulting from Si^{II} atom insertion of 1 equiv of **4-NHSi** into a P–P bond of the P_4 tetrahedron. A second equivalent of **4-NHSi** could also be inserted into another P–P bond of the 1:1 adduct to give the isolable 2:1 adduct with a Si_2P_4 skeleton (Scheme 1.2.4).[54]

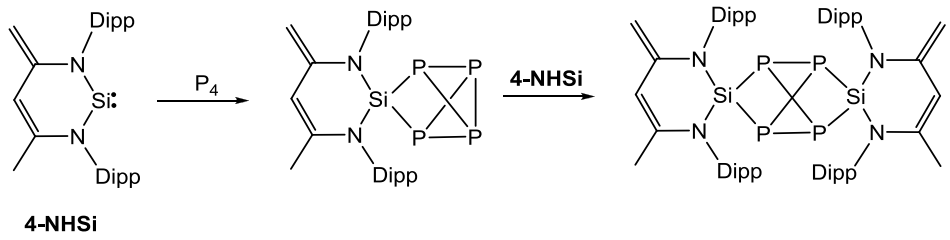

4-NHSi

Scheme 1.2.4. Activation of white phosphorus by **4-NHSi**. Adapted from ref. 54.

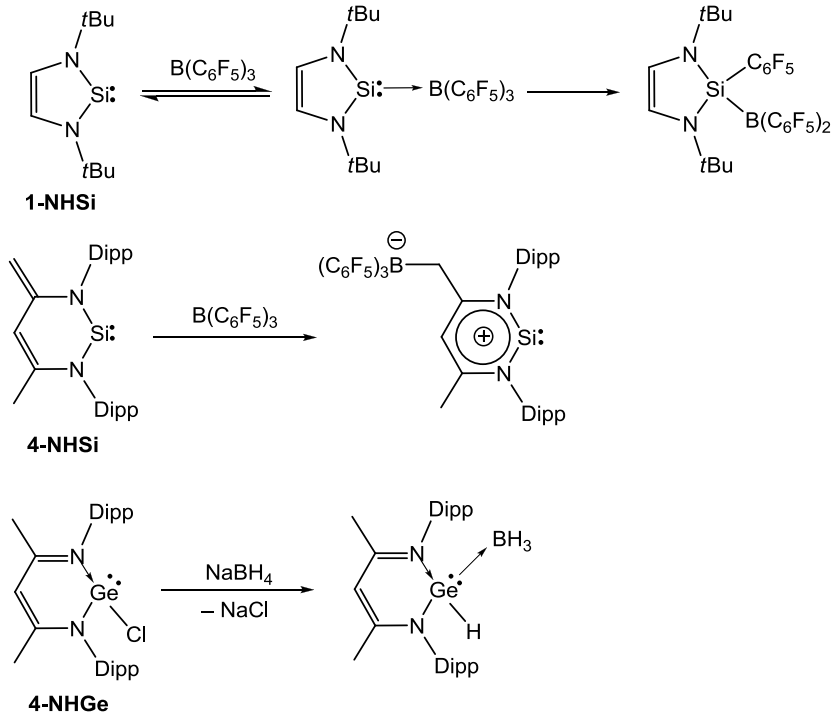

1-NHSi

4-NHSi

4-NHGe

Scheme 1.2.5. Selected reactivity of NHSis and NHGes toward Lewis acids.

Lewis acids. The lone pair located in the orbital with s-like character in metallylenes makes them react as Lewis bases. Accordingly, the reaction of **1-NHSi** with $B(C_6F_5)_3$ produces the Lewis acid-base adduct, however, unexpectedly, a concomitant insertion in a

C–B bond occurs producing as a sole product the silylborane over a period of two weeks[55] (Scheme 1.2.5). In contrast, the silylene **4-NHSi** reacts differently with $B(C_6F_5)_3$ due to the ylide-like character of this silylene. The reaction does not occur by the electron pair at the silicon atom but at the methylene in the ligand backbone.[56] Additionally, the reaction of the Lewis base-stabilized **4-NHGe** with $NaBH_4$ produces the germylene→borane adduct after the metathesis reaction of the hydride with the chloride anions.[57]

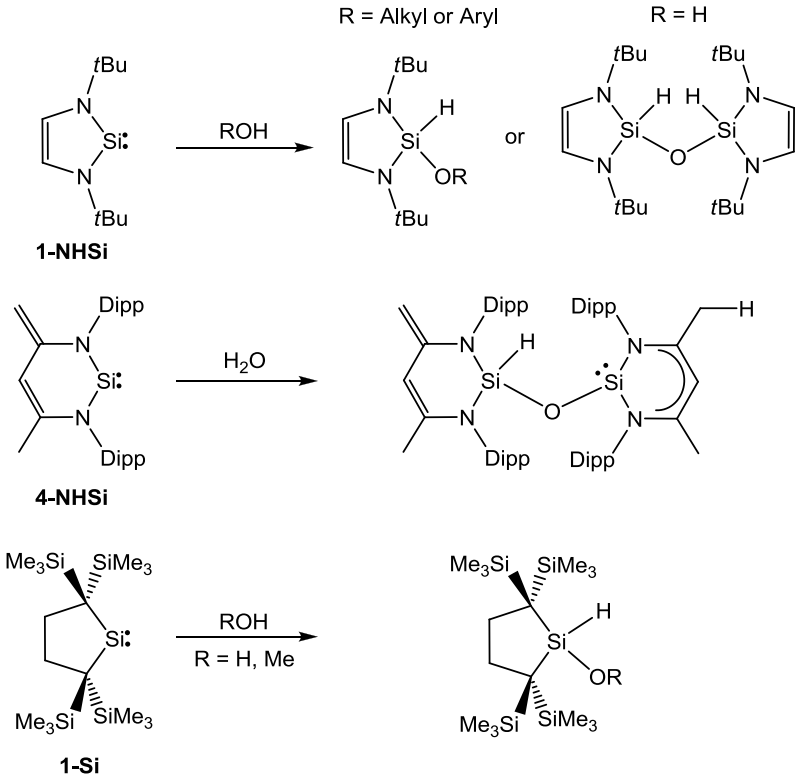

Scheme 1.2.6. Reactivity of NHSis and the cyclic silylene **1-Si** toward O–H bonds.

Heteroatom–H bonds. The vacant p-orbital on the NHSi tends to be the most reactive site when compared to the lone electron pair at the silicon center. Therefore, it is proposed that the activation of heteroatom–H occurs first *via* the coordination of the heteroatom to this vacant p-orbital. Subsequently, the nucleophilicity of the silicon center is enhanced by this coordination, a nucleophillic attack ocurrs to the H atom forming the Si^{IV} species. For example, most of the silylenes are moisture sensitive due to their facile reaction with H_2O forming the silanol and silyl ethers as decomposition products (Scheme 1.2.6).[32,58,59] For the case where the **1-NHSi** and **4-NHSi** are involved, the product (Si–OH) continue being

prone to react with another **NHSi**; indeed, these products react further to produce the silyl–silyl ethers. Due to the ylide-like character of **4-NHSi** a 1,4-H-migration occurred producing a mixed silane-silylene compound. But, in the case of **1-Si** this reaction is blocked most likely due to the steric hindrance around the OH function.

When evaluating other types of heteroatom–H bond the reactivity is likely the same. For instance, reaction of **4-NHSi** with the group 15 hydrides (YH_3, Y = N, P, As) forms the insertion products on the Y–H bond (Scheme 1.2.7).[60] Additionally, the reaction with H_2S forms the same product but due to the acidity of the thiol, it can react intramolecularly to produce a heavier homologue of formyl group with a Si–S double bond. The more reactive **1-Si** can activate even a stronger bond such as Si–H.[32] As suggested, this reaction must occur with direct insertion on the Si–H due to the lack of an electron pair, from the substrate, to attack as a nucleophile the vacant p-orbital.

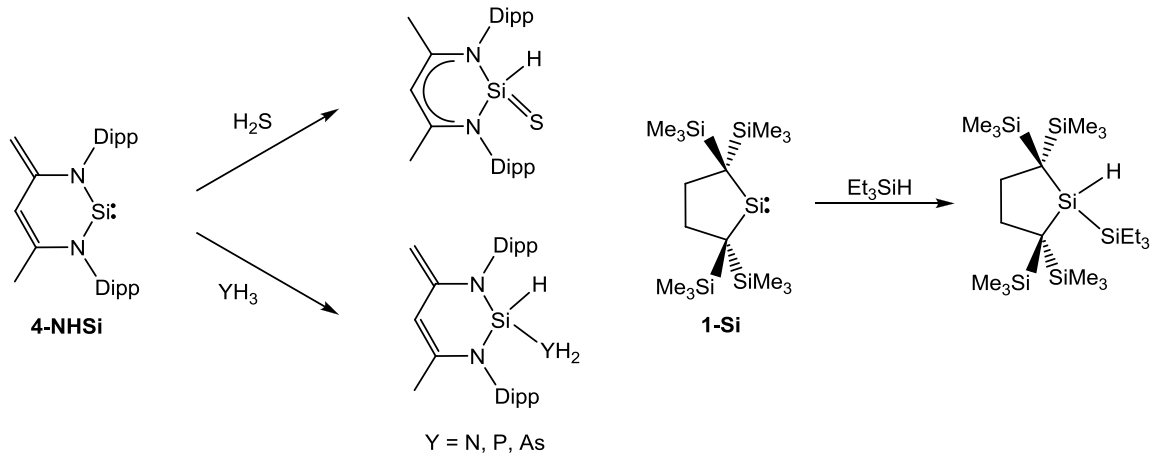

Scheme 1.2.7. Activation of heteroatom–H bonds by silylenes **4-NHSi** and **1-Si**.

Multiple bonds. Unsaturated molecules can also act as nucleophiles towards the vacant p-orbital of the silicon center. Depending on the degree of unsaturation the reaction might proceed either through [1+2]- or [1+4]-cycloaddition.[32,33] For instance **4-NHSi** reacts with benzophenone to produce the [1+4]-cycloaddition product, however, by a concomitant 1,3-H-migration produces the more stable product (Scheme 1.2.8).[61] This is in contrast when **4-NHSi** reacts with acetylenes which leads to the [1+2]-cycloaddition product, with formation of a silicon 3-membered cycle.[62] The reactivity also varies according to the silylene involved. For example, using the **5-NHSi** with the same type of molecules affords

different products. Reacting **5-NHSi** with benzophenone produced exclusively the [1+2]-cycloaddition product.[63] Additionally, the reaction of **5-NHSi** with diphenylacetylene forms the [1+2]-cycloaddition product as a transient species. This 3-membered ring is not stable and reacts further with another molecule of **5-NHSi** to produce the insertion product on the C(sp^2)–Si bond.[50]

This brief overview on reactivity of NHSis and NHGes toward organic molecules evidences that at the moment of studying their coordination toward TMs they cannot be consider as the isoelectronic phosphine ligands. Therefore, careful synthetic methodologies should be conducted to avoid possible side reaction either with solvent molecules or ancillary ligands on the metal precursor.

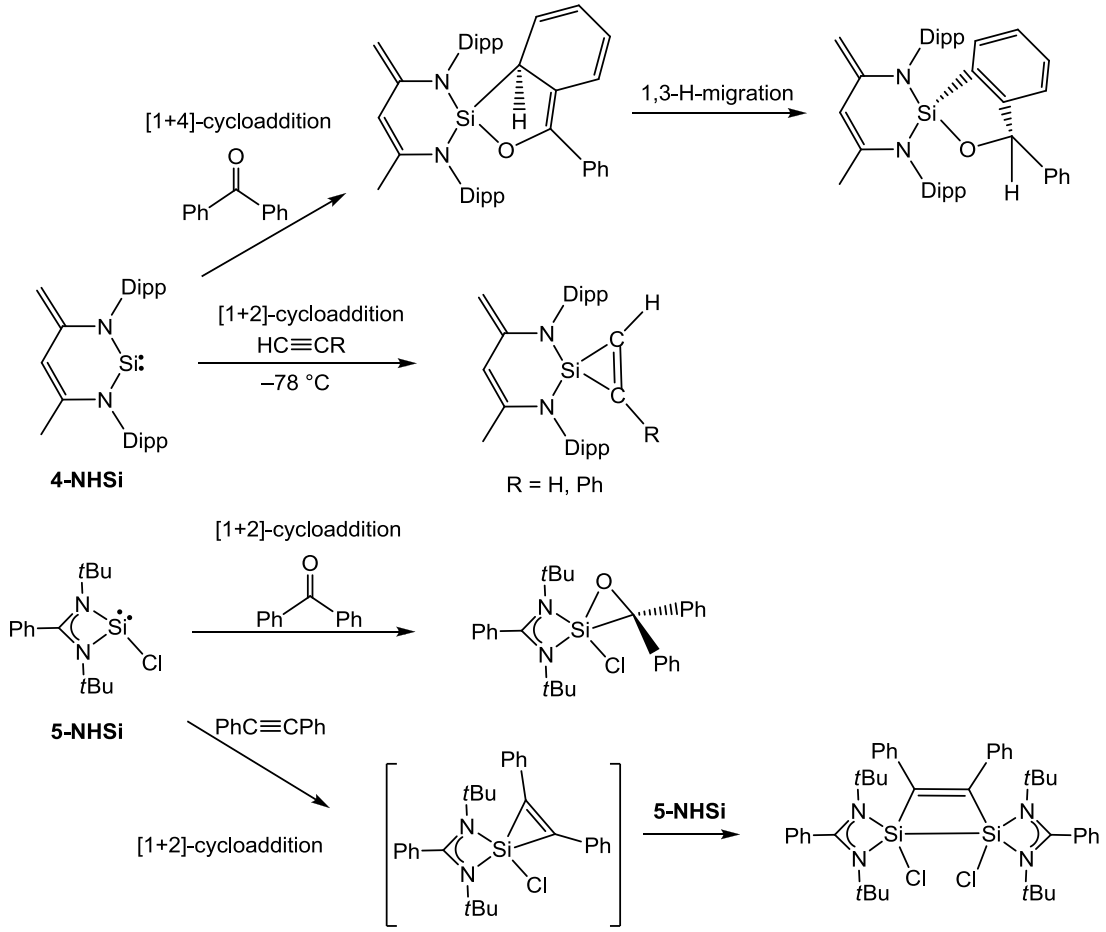

Scheme 1.2.8. Selected examples for the reactivity of NHSis toward multiple bonds in organic substrates.

1.2.4. Coordination toward transition metals

Apart from the reactivity toward chemical bonds, the electron pair located at the s-like orbital in N-heterocyclic metallylenes can act as ligand on different transition metals. A great variety of metal complexes have been isolated using metallylenes as ligands[64,65] and a superb review on the existing NHSis metal complexes has been reported recently.[3] Herein selected examples based on the NHSis and NHGes are introduced. For comparison purposes the silylene and germylene metal complexes more related with this dissertation, are left for further discussion in the section 3.2. Normally the existing metal complexes bearing silylenes and germylenes contain a metal center in low oxidation state and mainly with carbonyl as coligands, making their further application a difficult task. Several TM complexes using **5-NHSi** have been reported (Scheme 1.2.9).[3,66,67] Commonly their

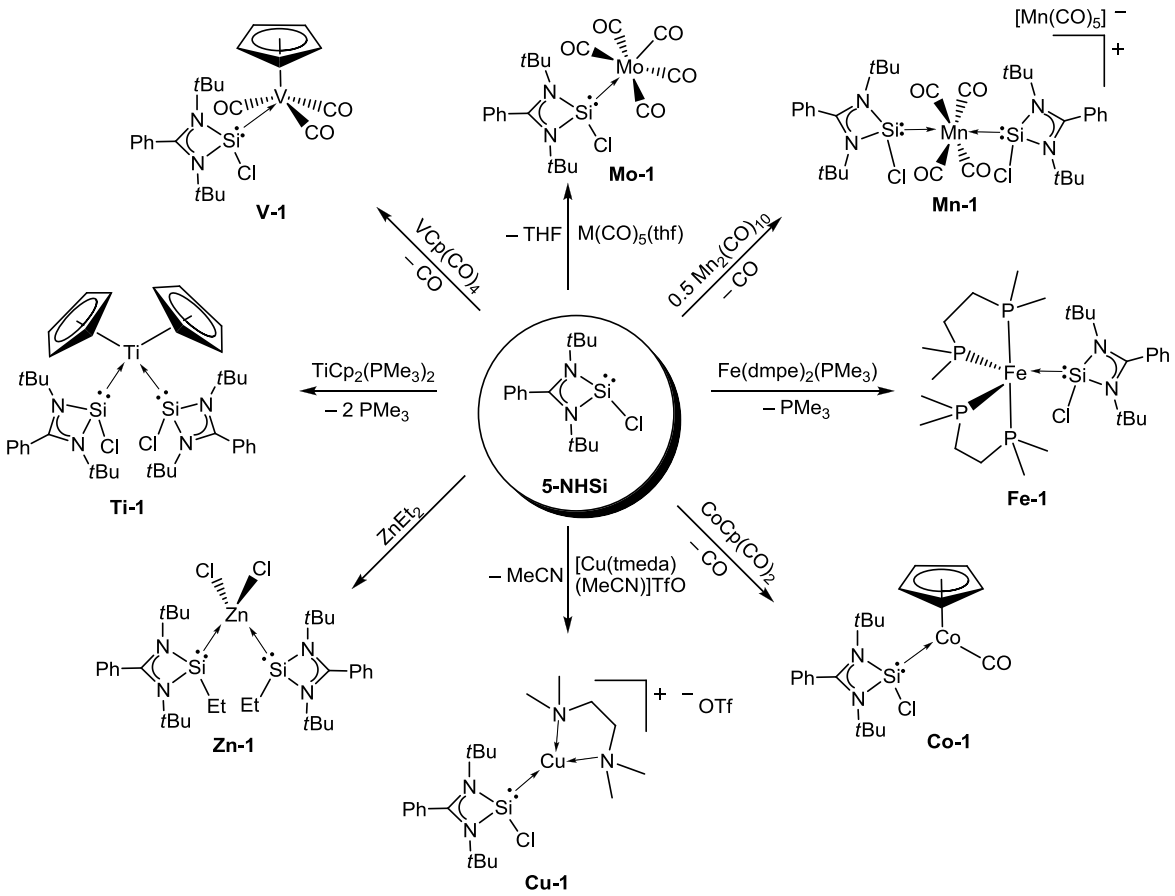

Scheme 1.2.9. Representative examples of transition metal complexes using **5-NHSi** as ligand.

synthesis is based on substitution reactions by a facile entry of the silylene replacing one of the coordinating ligands. Although, a recent report showed a salt metathesis reaction when diethyl zinc was used as metal substrate.[68]

A complete systematic study on the σ-donor strength was conducted in the Driess' group based on carbonyl nickel complexes bearing **4-NHSi** and its derivatives as ligands. The evaluation on the stretching frequency on the C–O bond by IR spectroscopy showed these silylenes within the range of σ-donor strength of the well-known NHCs and phosphine ligands (Figure 1.2.5).[2,69] This result shows the potential application of NHSis as chemical substitutes of phosphines and NHCs in catalysis (see section 1.4). Other metal complexes have been isolated using different NHSis and NHGes obtaining different substitution pattern depending on the metal precursor used. For instance, reaction of **1-NHSi** with $Ni(CO)_4$ and $Ni(cod)_2$ as Ni^0 precursors led to the different substitution pattern in the products **Ni-3** and **Ni-4**, respectively (Scheme 1.2.10).

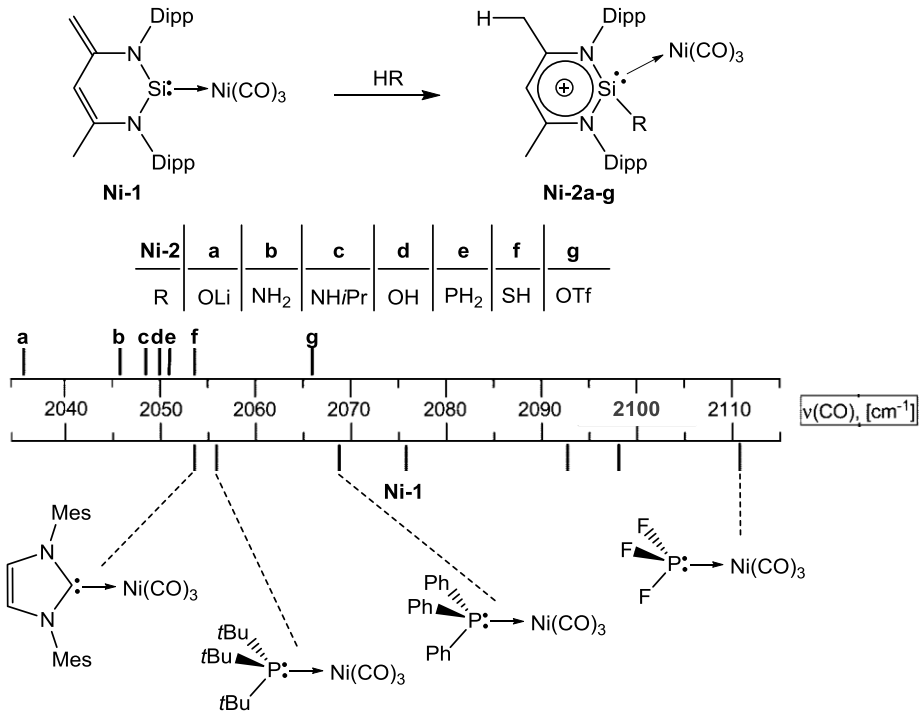

Figure 1.2.5. Relation of the σ-donor strength between silylenes, carbenes and phosphines when compared with their $Ni(CO)_3$ metal complexes by the C–O stretching frequency. Adapted from ref. 33.

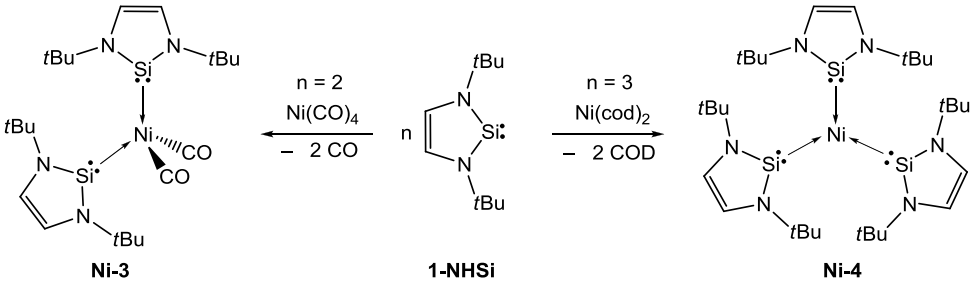

Scheme 1.2.10. Reactivity of **1-NHSi** toward different Ni^0 precursors.

For the case of NHGes similar reactivity has been observed substituting ligands at the metal center. A substitution reaction is obtained between **5-NHGe** and $W(CO)_5(thf)$[70] (Scheme 1.2.11). However, an unexpected reactivity was recently reported where the amidinato ligand, used for stabilization of the Ge^{II} center in **6-NHGe**, also participates in the ligand substitution reaction with $Co_2(CO)_8$ or $Ru_3(CO)_{12}$ as metal precursors.[71]

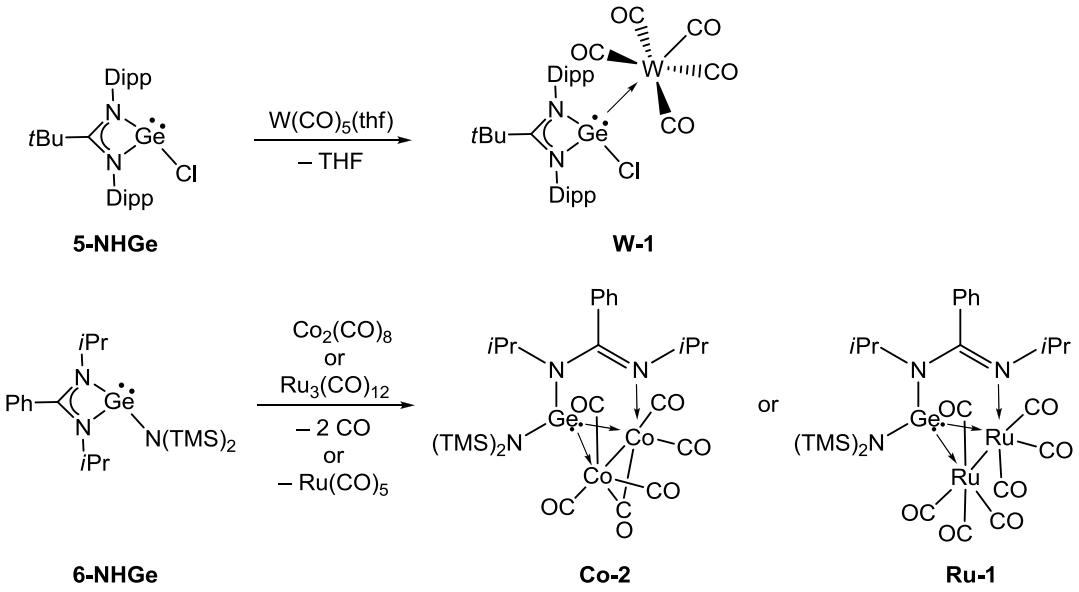

Scheme 1.2.11. Reactivity of base-stabilized NHGes toward carbonyl metal complexes.

1.3. Bis-metallylenes

1.3.1. Synthetic challenge

The synthesis of pincer ligands bearing two metallylene units as pendant arms is proposed for the present work. However, according to the synthetic methods and the intrinsic reactivity of metallylenes, the formation of a predesigned compound with two

metallylene moieties is experimentally challenging. The tendency of metallylenes to oligomerize renders the isolation of bis(metallylene) difficult as polymerization might result. Some rare examples are found *via* direct synthesis and most of bis(metallylenes) that exist are synthesized by reactions of organic substrates with the heavier homologues of alkenes and alkynes (i.e., $R_2E{=}ER_2$ RE≡ER, E = Ge, Sn).[32,72] Depending on the linkage between both moieties, all known bis(metallylenes) can be discriminated in two different types: i) "interconnected bis(metallylenes)", in which two $\mathbf{E^{II}}$ atoms are directly connected by a chemical bond, and ii) "spacer-separated bis(metallylenes)" which both $\mathbf{E^{II}}$ atoms are separated by linker moiety which normally does not interact with the metallylene centers.[72] Herein, a summary of selected spacer separated bis(metallylenes) is given due to their relation with the proposed pincer ligands in the present work.

1.3.2. Examples known in the literature

Late in the 1980's the synthesis of spacer separated bis(metallylenes) became an interesting research area since the seminal work by Veith and co-workers. The spacer separated bis(germylene) **1-NHGe$_2$** and bis(stannylene) **1-NHSn$_2$**[73] (Figure 1.3.1) were afforded by a metathesis reaction between the tetralithium amide and the available E^{II} starting substrates, $GeCl_2$·1,4-dioxane or $SnCl_2$. In a synthetic effort to obtain a heavier homologue of isonitrile (R–N≡C), the research groups of Lappert and Roesky isolated what it can be considered as dimeric species with two Ge^{II} centers **2-NHGe$_2$**[74] and **3-NHGe$_3$**.[75] A silicon homologue of these species **1-NHSi$_2$** appeared later in 2011 reported by Roesky *et al.*[76] through attempts to synthesize a silaisonitrile (R–N≡Si) which at the moment seems an unreachable target in main group chemistry. However, the bis(silylene) **1-NHSi$_2$** is very interesting from the synthetic point of view, but its low yield (21 %) reduced considerably its applicability. Additionally, Lappert and co-workers reported two bis(stannylenes) linked by two chlorido bridges with amides as coligands **1-Sn$_2$** and **2-Sn$_2$**.[77] In contrast, the bis(stannylene) **2-NHSn$_2$** was found to possess two bridged nitrogen atoms.[78] Continuing with the search of multiple bonding between main group elements Veith and co-workers isolated a bis-germylene **4-NHGe$_2$** bridged by two N atoms of the azide groups forming a planar four-membered Ge_2N_2 ring.[79] In this example, an extra stabilization through dative bonds was observed from the O*t*Bu terminal groups in the ligand backbone. Remarkably,

Lappert and co-workers demonstrated that the synthesis of a bis(silylene) can be obtained by dehalogenation with KC_8 forming **2-NHSi$_2$**.[80] Though, its coordination chemistry continue being like monodentate due to the rigidity of the ligand backbone.

Other common synthetic methodology used for spacer separated bis(metallylenes) is the reaction of the highly reactive heavier homologues of alkynes RE≡ER (E = Ge, Sn; R = very bulky substituents) with the desired spacer. N-separated bis(stannylene) **3-Sn$_2$**[81] and bis(germylene) **1-Ge$_2$**[82] have been afforded *via* the reaction with the respectively azide (R–N_3). Additionally, reaction with azobenzene (PhN=NPh) afforded the bis(germylene) **2-Ge$_2$**[81] and bis(stannylene) **4-Sn$_2$**[81] with the spacer unit PhN–NPh. Using a similar synthetic strategy the amidinato bis(germylene) **5-NHGe$_2$**[83] and bis(silylene) **3-NHSi$_2$** (using phenylacetylene)[84] were obtained with cleavage of the E–E bond in both cases (E = Si, Ge).

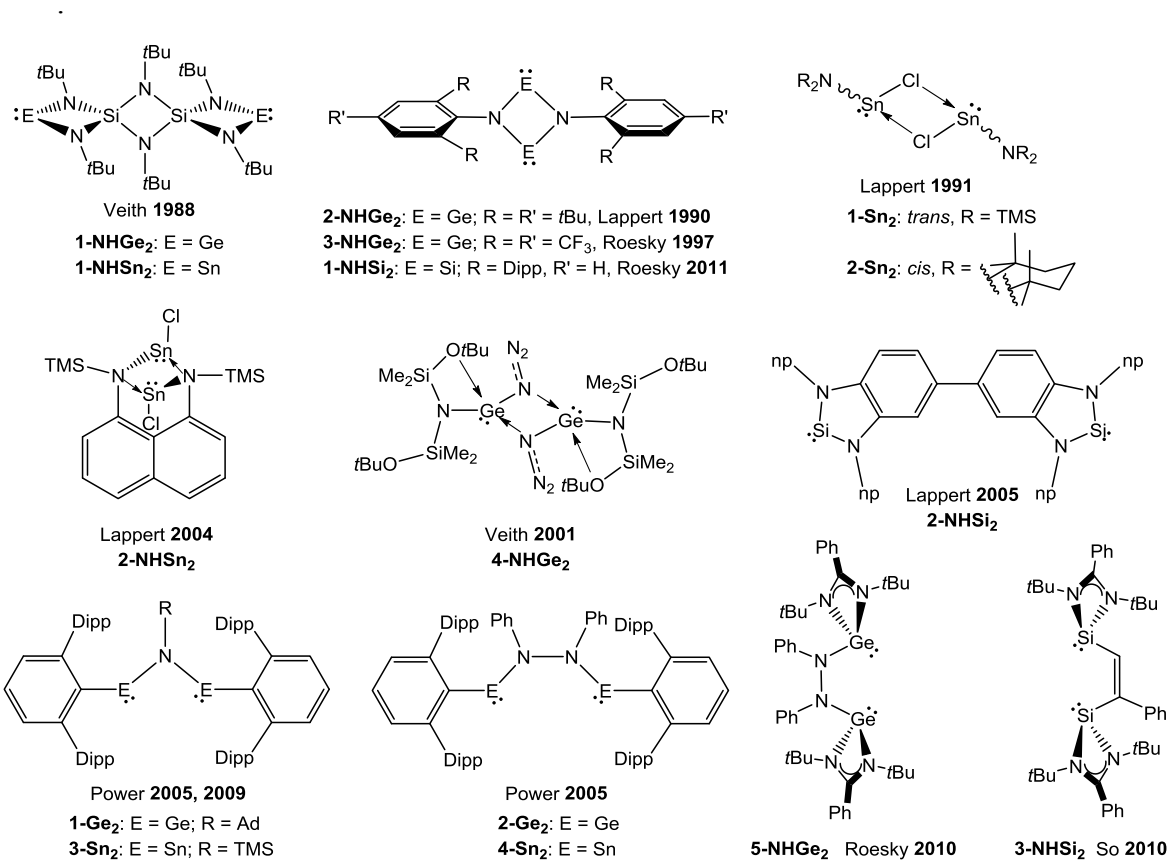

Figure 1.3.1. Selected examples of spacer separated bis(metallylenes).

Additionally to the work by Lappert *et al.* with the bis(silylene) **2-NHSi$_2$**, Hahn and co-workers reported the synthesis of a series of spacer separated chelating bis(germylenes) and bis(stannylenes) by a direct method based on salt metathesis reactions (Figure 1.3.2).[85,86] They demonstrated the chelating behavior by the preparation of some metallic complexes, however, the pincer-type bis(germylenes) **9-NHGe$_2$** and **10-NHGe$_2$** did not show a terdentate coordination fashion (cf. section 1.3.3). Recently the oxo- and sulfido-bridged bis(metallylenes) **4-NHSi$_2$**,[87] **13-NHGe$_2$**,[88] **14-NHGe$_2$**,[88] **3-Ge$_2$**,[89] and **5-Sn$_2$**[89] have been reported by different working groups and the synthetic approaches were different in each case. The synthesis of **4-NHSi$_2$** was achieved by double dehydrochlorination on the Si^{IV} precursors, whereas the **13-NHGe$_2$** and **14-NHGe$_2$** were synthesized *via* reduction with KC_8 of the respective Lewis base-stabilized chlorogermylene with concomitant oxidation with trimethylamine N-oxide (Me_3NO) or with elemental sulfur, respectively.

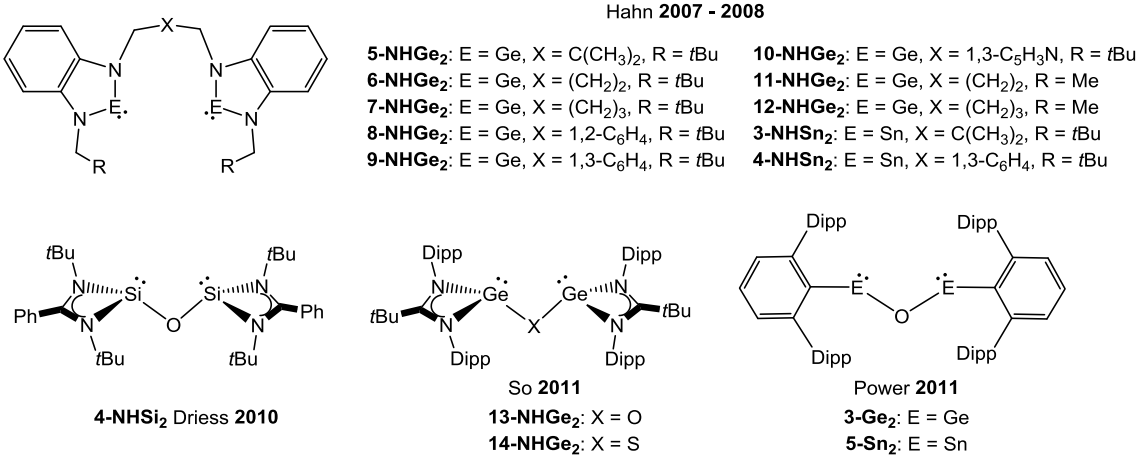

Figure 1.3.2. Selected examples of spacer separated bis(metallylenes) including pincer moiety (**9-NHGe$_2$**, **10-NHGe$_2$** and **4-NHSn$_2$**) and the single atom bridged (**4-NHSi$_2$**, **13–14-NHGe$_2$**, **3-Ge$_2$**, **5-Sn$_2$**).

Due to the versatility of the base-stabilized chlorosilylene **5-NHSi** in the formation of heteroleptic silylenes[90] Driess *et al.* reported the functionalized bis(metallylenes) using different bridges enhancing their potential application as ligands in catalysis. The first ferrocenyl bridged **5-NHSi$_2$** and **15-NHGe$_2$** were obtained by a metathesis reaction with the dilithiated ferrocene species in high yields (Figure 1.3.3).[91] Moreover, using the same synthetic approach the resorcinolate bis(silylene) **SiCHSi** pincer ligand was affordable in

high gram scale yields.[92] These latter species opened a new frontier in the **NHSi** and **NHGe** chemistry due to the similarities of the well-known phosphine ligands, normally applicable in catalytic reactions.

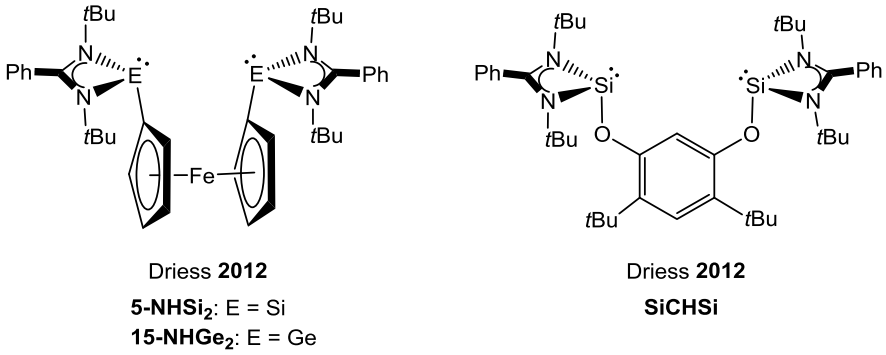

Figure 1.3.3. Novel functionalized spacer separated bis(metallylenes) bearing a ferrocenyl (**5-NHSi$_2$**, **15-NHGe$_2$**) and arene backbones (**SiCHSi**) with potential pincer behavior.

1.3.3. Examples of metal complexes using bis(metallylenes) as chelating ligands

For metallylene metal complexes, scarce examples exist to date with bis(metallylenes) acting as chelating ligands. Most likely it is because of the fact that many of existing bis(metallylenes) are either too close to each other, like the interconnected type (i), or they are far away separated acting as isolated monodentate ligands. The isolation of more spacer separated bis(metallylenes) enabled the synthesis of metalacycles bearing both metallylenes units as chelating ligand. Even though Hahn *et al.* had synthesized bis(germylenes) with pincer backbone they either could not obtain the terdentate coordination on a metal center and/or did not follow up this chemistry. However, using the bis(germylenes) **5-NHGe$_2$** and **7-NHGe$_2$**, with an aliphatic spacer, they afforded octahedral carbonyl molybdenum complexes **Mo-2** and **Mo-3** bearing both germylenes in a *cis* configuration (Figure 1.3.4).[86,93] The exploration of chelating ligands introducing NHSis and NHGes by the Driess' group have contributed profoundly to the study on these metal complexes. First, the coordination of the oxo-bridged bis(silylene) **4-NHSi$_2$** toward a Ni^0 center was studied forming the complex **Ni-5**.[87] In this example, the ligand acted as chelate stabilizing the

nickel center in solution when compared with the $Ni(cod)_2$ precursor. This stabilization occurred by a strong coordination by the NHSis moieties showing π-backbonding interaction as well. Additionally, using the chelating ligands **5-NHSi$_2$** and **15-NHGe$_2$** was possible to isolate Co^I complexes **Co-3** and **Co-4** bearing Cp as coligand (Figure 1.3.4).[91] In this case, a strong σ coordination to the metal center was observed by the high stability of these complexes in solution.

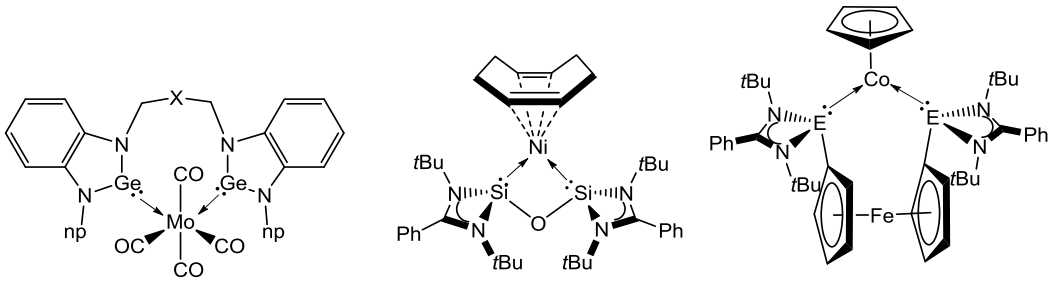

Figure 1.3.4. Selected chelate bis-metallylenes metal complexes.

When evaluating the metallation in the novel **SiCHSi** pincer ligand an unexpected reactivity was observed. Contrary to the behavior of the bis(phosphine) pincer ligands,[†] after metallation with the Pd^0 precursor $Pd(PPh_3)_4$ a hydride migration to the ligand ocurred. This happened *via* a hydride intermediate species **[SiCSi]PdH**[‡] which is very reactive toward the Si^{II} center. Nucleophilic attack to the p-orbital at the silicon center formed the mixed silylene-silyl-palladium complex ***κ^{1}Si*-[SiCHSi][Si^{IV}CSi^{II}]Pd** (Scheme 1.3.1).[92] This result proved that metallation on these novel pincer ligands is not trivial and a careful selection of the synthetic methodology for the metallation studies must be carried out.

[†]the formation of a hydride species does not alter the phosphine ligands **PCP**

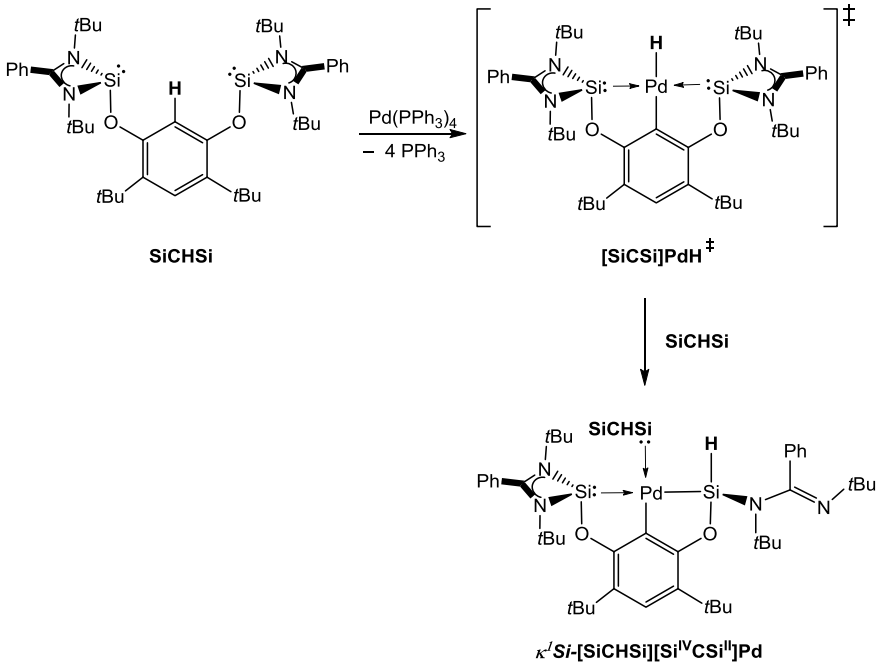

Scheme 1.3.1. Reactivity of pincer ligand **SiCHSi** toward the palladium(0) precursor $Pd(PPh_3)_4$ and its unexpected 1,2-hydride migration.

1.4. Metallylenes in catalysis: At their infancy

Surprisingly, NHCs have been applied broadly in catalytic reactions while only a few examples with their heavier homologues can be found in the literature. Most likely the reason for this is related to the robustness shown by NHCs for catalytic reactions whereas the stabilization of N-heterocyclic metallylenes still being a challenge. This research area is rather new with the first report on the application of NHSis as ligands at the early 2000's. Fürstner and co-workers reported in 2001 a dinuclear palladium(0) complex **Pd-1** bearing two **1-NHSi** ligands as bridging units and its potential application as catalyst in Suzuki cross-coupling reactions (Scheme 1.4.1).[94] This work revealed the potential application of NHSis as novel ligands in catalysis. Quite interesting, these studies did not have the success in the catalytic arena as their carbon counterparts and just seven years later the second report appeared. Roesky and co-workers showed the application of a palladium(II) complex **Pd-2**, bearing **1-NHSi** as ligand, as catalyst in the Heck cross-coupling between styrene and 4-bromoacetophenone (Scheme 1.4.1).[95]

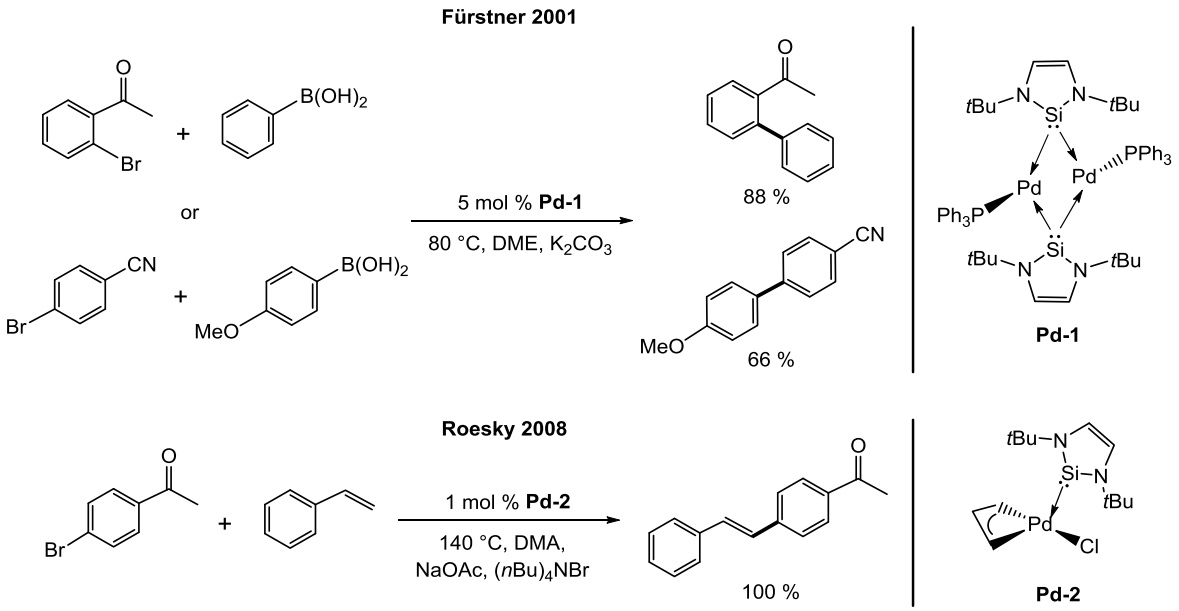

Scheme 1.4.1. Seminal examples of NHSi complexes **Pd-**1 and **Pd-2** as catalyst for the Suzuki and Heck cross-coupling reactions.

After the seminal work by Fürstner and Roesky, the Driess' group became attracted with the catalytic applications of the novel chelate as well as the monodentate silylene complexes synthesized during the last years.[96] Parallel to the work in catalysis reported in this dissertation other systems have been developed in the group. First, the cobalt complex **Co-3** was tested as catalyst for the [2+2+2] cyclotrimerization of phenylacetylene (Scheme 1.4.2).[91] A good activity was found producing quantitative yield in the reaction. Moreover, the catalytic system showed a potential application on the production of pyridines when acetonitrile was used as the solvent (Scheme 1.4.2).

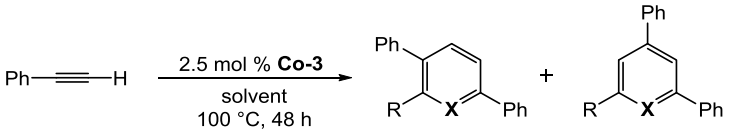

Solvent	Yield (%)	
toluene (X = CH; R = Ph)	72	28
CH_3CN (X = N; R = Me)	14	39

Scheme 1.4.2. Catalytic activity of the bis-NHSi cobalt(I) complex **Co-3** in cycloaddition reactions.

Continuing the exploration on the NHSi first row TM complexes, it was found that the hydrido-silylene iron(0) complex **Fe-2** catalyzes the hydrosilylation of ketones in a cooperative manner between the silicon and iron centers (Scheme 1.4.3a).[66] It is postulated that the system likely goes through a 1,2-hydride migration forming an iron-hydrido complex as the key intermediate of the reaction. Additionally, reduction of an organic amide could be afforded using the NHSi iridium(I) **Ir-1** and rhodium(I) **Rh-1** complexes as precatalysts using phenylsilane as reducing agent (Scheme 1.4.3b).[97]

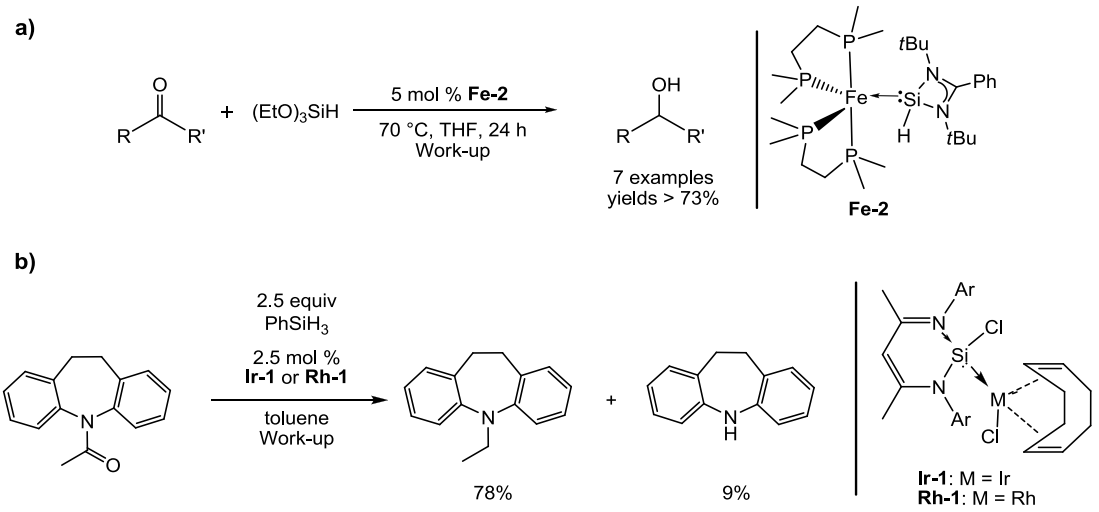

Scheme 1.4.3. Application of NHSi transition metal complexes in reduction reactions.

In extension to the catalytic application of the chelate ligands Enthaler, Inoue and co-workers applied the bis-NHSi nickel complex **Ni-5** as catalyst in cross-coupling reactions using zinc and Grignard reagents (Scheme 1.4.4).[98] Aryl halides were coupled with the aryl/alkyl organometallic substrates from moderate to good yields.

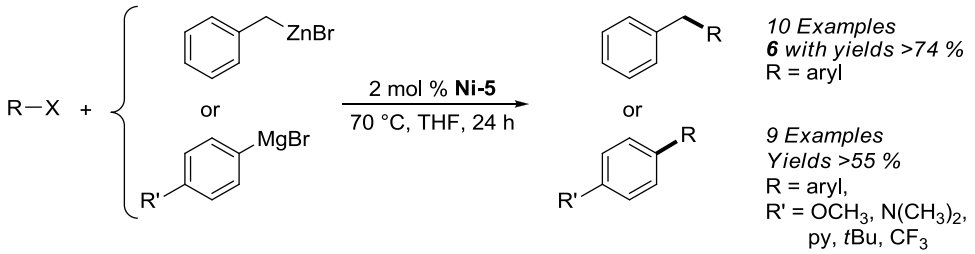

Scheme 1.4.4. Cross-coupling reactions with zinc and Grignard reagents using the bis-NHSi nickel(0) complex **Ni-5**.

Additionally to these efforts, Zaitsev and Karlov have explored the application of metallylene metal complexes in catalysis. Palladium(0) complexes bearing NHGe **Pd-3** and NHSn **Pd-4** were applied in Suzuki and Heck cross-coupling reactions (Scheme 1.4.5).[99] It was observed a high activity with moderate to good reaction yields and comparable to the yields obtained previously by Fürstner and Roesky in their seminal work in this area.

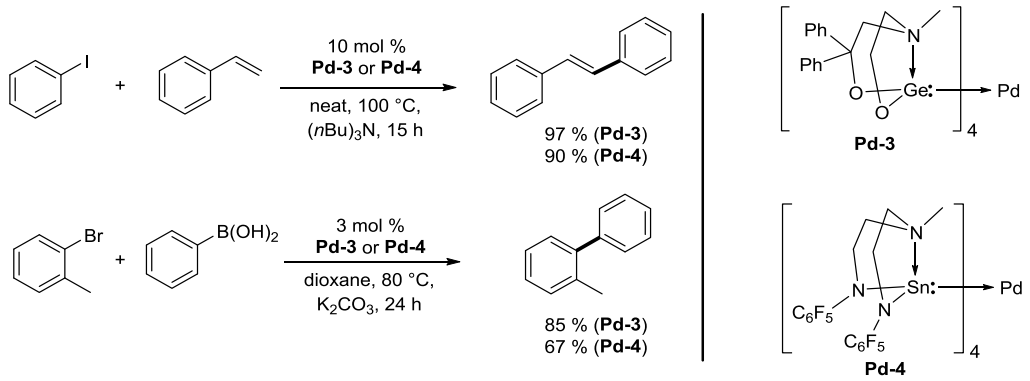

Scheme 1.4.5. Heck and Suzuki cross-coupling reactions using the NHGe and NHSn palladium(0) complexes **Pd-3** and **Pd-4**.

Finally, a recent report from the Driess' group demonstrated the application of a mixed bidentate donor system based on an NHC and NHSi as donor moieties. The nickel complex **Ni-6** proved to be a good precatalyst for the Kumada-Corriu-Tamao type coupling reaction between Grignard reagents and aryl/alkyl halides (Scheme 1.4.6).[100]

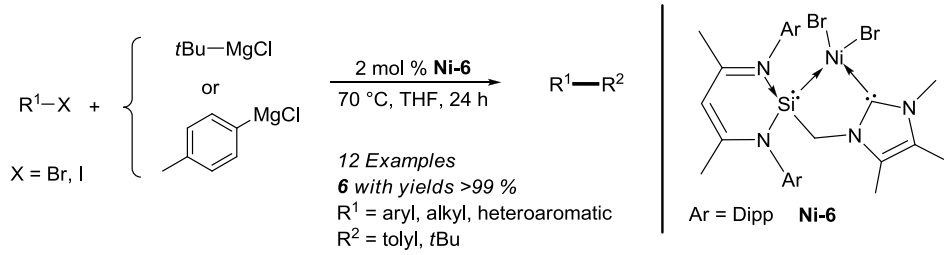

Scheme 1.4.6. Kumada-Corriu-Tamao type coupling reaction using NHC-NHSi complex **Ni-6** as precatalyst.

So far these examples are the only ones to date, apart from the reported in this dissertation, for the application of metal complexes with N-heterocyclic metallylenes as anchoring ligands in catalysis. It is very unusual that even when the synthetic methods and isolation of free metallylenes have improved during the last two decades, almost no scientific interest has been focused in their application in this field. Particularly silylenes represent a suitable family of ligands due to the abundance of silicon in the Earth crust, in addition to the coordination abilities toward transition metals. This shows that at the moment this research area is almost entirely unexplored, and represents a new frontier in contemporary inorganic chemistry. The potential application of these novel systems in homogenous catalysis might lead to unknown reactivities strengthening their introduction in the catalytic arena.

2. MOTIVATION AND OBJECTIVES

2.1. Motivation

It is evident the need of a systematic study on the application of NHSis and NHGes in catalysis. Therefore, the use of two units of NHSis and NHGes in pincer backbones is proposed as a starting point for the introduction of these novel ligand systems in catalysis (Figure 2.1). Based on the synthetic approach for the formation of the bis(silylene) **SiCHSi** pincer ligand (Figure 1.3.3, p. 29),[92] the synthesis of its germylene homologue is envisioned. Moreover, the synthesis of bis(phosphine) pincer ligands will be addressed for comparison purposes. Additionally, the synthesis of a neutral pincer ligand with a pyridine backbone is proposed for stabilization of highly electron rich zero-valent transition metal centers.

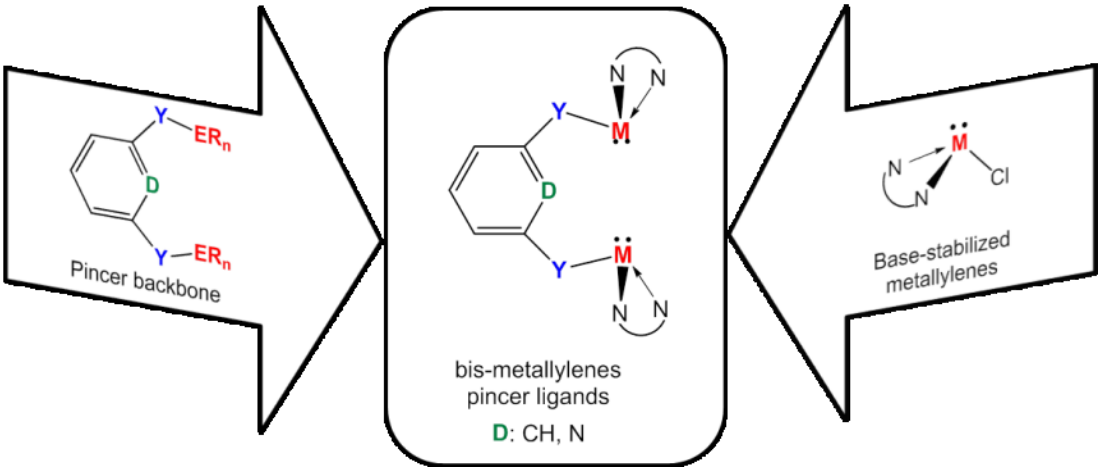

Figure 2.1. Combination of the σ-donor abilities of N-heterocyclic metallylenes and the robustness of pincer ligands for novel bis(metallylenes) pincer ligands.

With these novel ligands, the coordination abilities toward late transition metals will be explored focusing mainly on first row transition metals. A comparative study in the σ-donor strength will be studied based on the electronic structure of the metal complexes. More important, the application of these pincer complexes as catalysts will be evaluated in C–H activation, C–C cross-coupling, and hydrosilylation reactions. In addition, mechanistic studies will be addressed by conducting stoichiometric reactions to find possible reaction

intermediates, and show structurally that the fundamental reaction steps occur at the metal center and not at the metallylenes (Figure 2.2). This will illustrate that metallylenes might serve as spectator ligands during catalytic transformations enhancing the electronic properties at the metal centers.

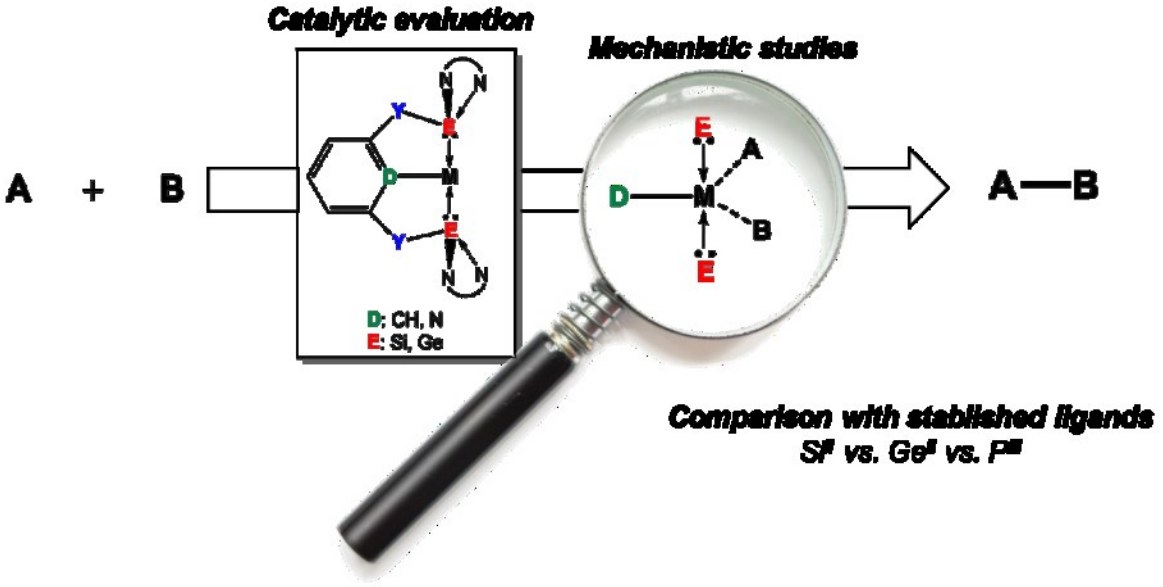

Figure 2.2. General scheme for the motivation of the present dissertation.

2.2. Objectives

2.2.1. General

Based on the σ-donor strength the N-heterocyclic silylenes and germylenes bearing the *N,N'*-bis-(*tert*-butyl)-phenylamidinato and chlorido ligands (**5-NHSi** and **1-NHGe**), their incorporation as novel scaffolds in pincer ligand backbones is proposed. Their reactivity as steering ligands for metal-based catalysis will be addressed and a direct comparison with the well-known bis(phosphine) pincer ligands will be evaluated. Isolation and characterization of the metal complexes will allow studying the electronic structures at the metal centers. Stoichiometric reactions between the metal complexes, acting as precatalyst, and the organic substrates will address the understanding of the possible reaction mechanisms.

2.2.2. Specific

1. Based on the synthesis of the bis(silylene) **SiCHSi** pincer ligand synthesized by the Driess' group, I will explore the synthesis of related novel ligands based on the **5-NHSi** and **1-NHGe**, reported by the Roesky group (Figure 2.3):

   i. Synthesis of the germanium homologue of the previously reported monoanionic **SiCHSi** pincer ligand based on an arene backbone.

   ii. Synthesis of the arene bromide centered **ECBrE** pincer ligands (E = Si^{II}, Ge^{II}).

   iii. Access to the neutral **ENE** pincer ligands (E = Si^{II}, Ge^{II}) based on a pyridine backbone.

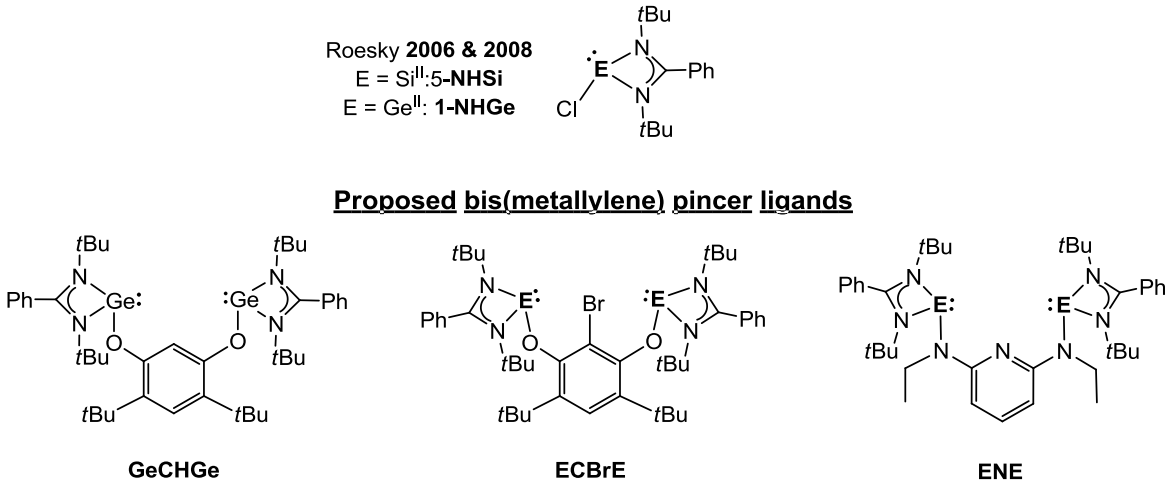

Figure 2.3. Structures of the **5-NHSi** and **1-NHGe** as starting material for proposed pincer ligands **GeCHGe**, **ECBrE**, and **ENE** (E = Si^{II}, Ge^{II}).

2. With the pincer ligands fully characterized, I will focuss the metallation studies on late transition metals of groups 8, 9 and 10:
    i. Synthesis and characterization of iridium and rhodium complexes with the monoanionic **ECHE** ligands (E = Si^{II}, Ge^{II}).
    ii. Synthesis and characterization of nickel complexes with the monoanionic **ECXE** ligands (E = Si^{II}, Ge^{II}; X = H, Br).
    iii. Synthesis and characterization of iron complexes with the neutral **ENE** pincer ligands (E = Si^{II}, Ge^{II}).

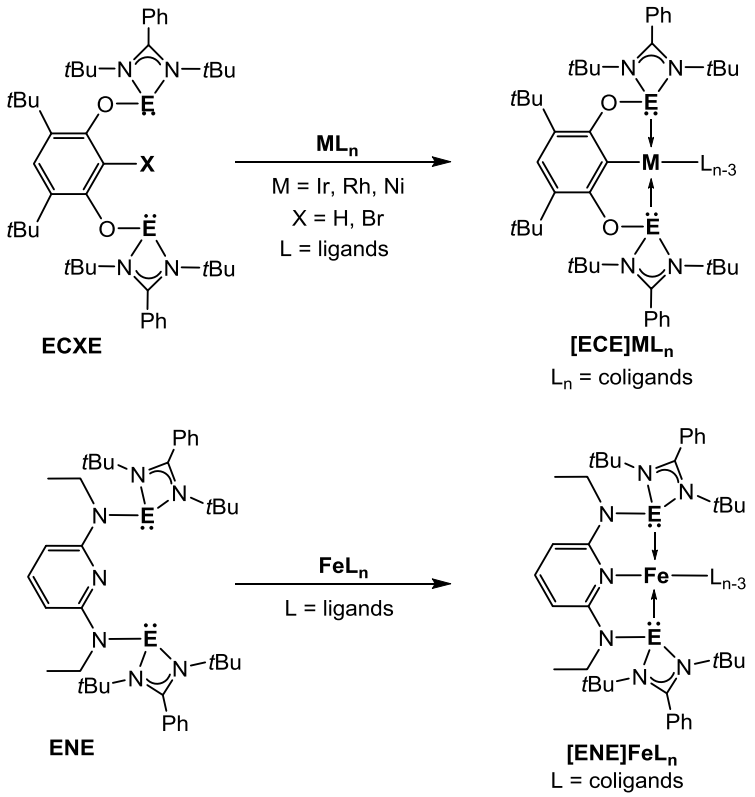

Figure 2.4. Proposed metallation studies with the **ECXE** and **ENE** pincer ligands (E = Si^{II}, Ge^{II}; X = H, Br).

3. With the well defined bis(metallylene) metal pincer complexes, I will study their potential application as precatalysts in different chemical transformations. In addition, I will carry out stoichiometric reactions for a deep understanding of the reaction mechanisms.

   i. Apply the iridium pincer **[ECE]IrL$_n$** complexes as precatalysts for the borylation of arenes.

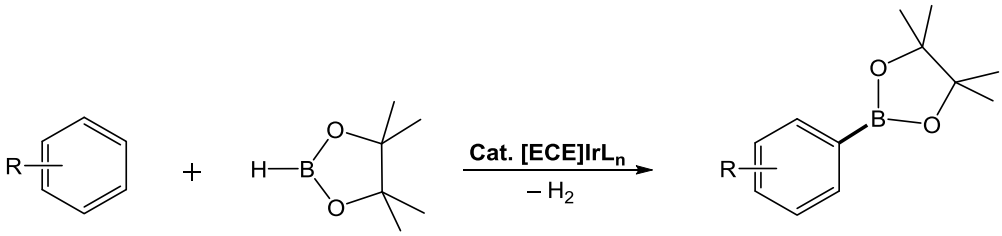

   ii. Apply the nickel pincer **[ECE]NiL$_n$** complexes as precatalysts for the Sonogashira cross-coupling reaction.

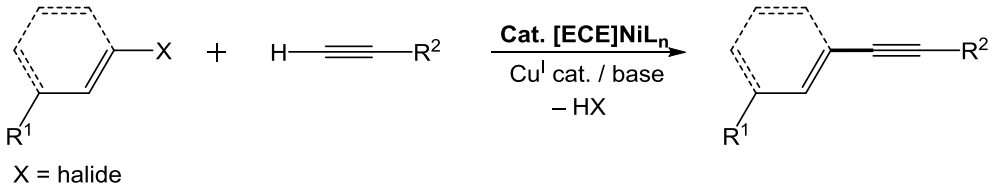

   iii. Apply the iron pincer **[ENE]FeL$_n$** complexes as precatalyst for the hydrosilylation of ketones.

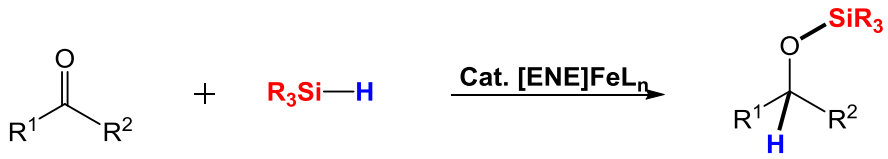

3. RESULTS AND DISCUSSION

3.1. Synthesis of pincer ligands bearing silylenes, germylenes and phosphinites as pendant arms

Owing to the versatile nature of pincer ligands (cf. section 1.1), their synthetic routes differ according to the substrates used to prepare them. Based on the similar reactivity shown by the {*N,N'*-bis-(*tert*-butyl)-phenylamidinato}chloro–silylene (**5-NHSi**)[49] and –germylene (**1-NHGe**)[51] to the chloro dialkyl/diaryl phosphanes (**R_2PCl**), the synthesis of the desired pincer ligands can be achieved *via* metathesis reactions. Pincer ligands can be synthesized either in a one-pot reaction or step-wise with the *in-situ* formation of the alkoxide and/or resorcinolate salt using a strong base (Scheme 3.1.1).[7,101] Scant examples are found in the literature for the synthesis of spacer separated bis(metallylenes) due to their difficult manipulation and isolation (cf. section 1.3).[72] In the Driess' group an elegant and relatively simple synthetic route afforded the bis(silylene) pincer type ligand **SiCHSi** *via* a metathesis reaction (Figure 1.3.3, p. 29).[92,102] This novel synthetic strategy to obtain bis(metallylene) ligands has been taken as the starting point for the synthesis of the ligands reported in this dissertation.

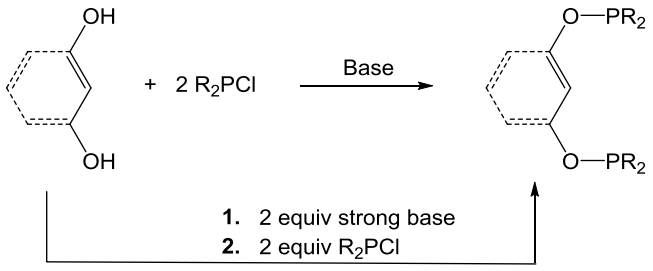

Scheme 3.1.1. General synthetic strategy for the synthesis of bis(phosphinite) pincer ligands.

Herein, the synthesis of the first monoanionic bis(germylene) **GeCHGe** and **GeCBrGe** pincer ligands is reported and discussed. Additionally, the synthesis of the related bis(phosphinite) ***t*Bu-PCHP** and ***i*PrN-PCHP** pincer ligands using the same ligand backbone, 4,6-di-*tert*-butyl-resorcinolate, for comparison studies is also described.

Moreover, the synthesis of the first neutral bis(metallylene) **SiNSi** and **GeNGe** pincer type ligands with a pyridine backbone is described and discussed.

3.1.1. Synthesis of the GeCHGe pincer ligand

The interesting reactivity exhibited by the first bis(silylene) **SiCHSi**[92] pincer ligand and its facile synthetic procedure were used as the starting point. For a systematic study, evaluating the σ-donor strength of the silylenes and germylenes versus the phosphine pincer ligands, the synthesis of the NHGe homologue was undertaken. The bis(germylene) **GeCHGe** pincer ligand was synthesized following the same synthetic strategy as for **SiCHSi**. Deprotonation of 4,6-di-*tert*-butylresorcinol with 2 equiv of *n*-BuLi and subsequent reaction with **1-NHGe**[51] afforded the expected product in quantitative yield (Scheme 3.1.2).

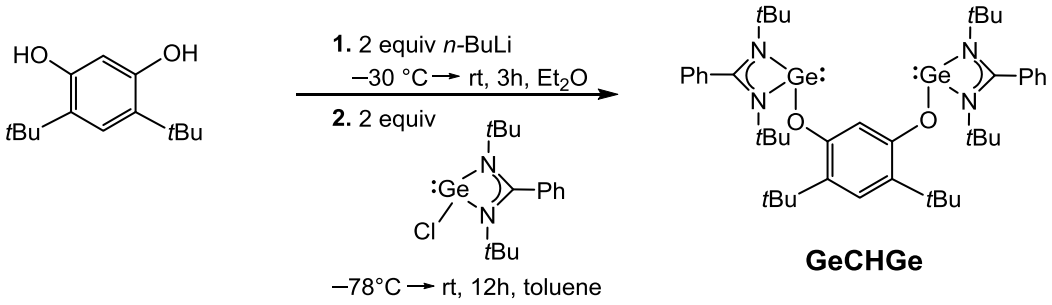

Scheme 3.1.2. Synthesis of the bis(germylene) pincer ligand **GeCHGe**.

The crude reaction mixture showed a major product with C_{2v} symmetry in the ^{1}H NMR spectrum, where two singlet signals are observed for the *t*Bu groups in the aliphatic region at δ = 1.10 and 1.86 ppm for the N-*t*Bu and Ar-*t*Bu, respectively. Isolation by recrystallization in *n*-hexane afforded the air sensitive product **GeCHGe** in 83% yield. Correlation NMR spectroscopy (HMQC and HMBC), in addition to the ^{13}C{^{1}H} NMR spectra (DEPT and 135DEPT) allowed the full assignment of the resonance signals. The characteristic signals for the aryl group are observed at δ = 7.62 and 7.68 ppm as singlets, for the 5-C*H* and 2-C*H* on the resorcinolato backbone, respectively.

The structure of the **GeCHGe** ligand was unambiguously determined by single crystal XRD structure analysis of crystals grown in a concentrated *n*-hexane solution. Contrary to the crystals obtained for **SiCHSi**,[92] the crystallographic data were of high quality, confirming the structure of the novel bis(metallylene) pincer ligand system bearing an arene as linker unit. The molecular structure in the solid state shows both germanium atoms in a distorted pseudo-tetrahedral structure with the electron pairs pointing to the center of the arene backbone (Figure 3.1.1). This is in contrast to the structure and dynamic behavior of the **SiCHSi** homologue, where the pendant NHSi arms are pointing out at the same direction, with a low energy difference between both structures in accordance to the DFT calculations.[92] Since the structural parameters are akin on the amidinato ligand, this difference can be correlated with the radii of the Si and Ge centers as well as the atomic weight which plays a role in this dynamic behavior. The angles around each Ge site changed slightly upon formation of the new covalent O–Ge bonds (Table 3.1).

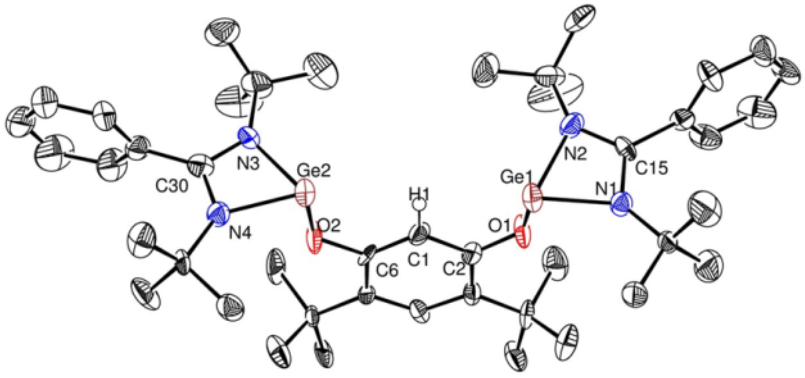

Figure 3.1.1. ORTEP representation of the bis(germylene) **GeCHGe** pincer ligand in the solid state. Thermal ellipsoids are drawn at the 50% probability level; hydrogen atoms are omitted for clarity, except H1.

It is noteworthy that in the crystal structure there are neither inter nor intra Lewis-type molecular interactions. The NHGe could act as Lewis acid by the p-like acceptor orbital and the amino and/or the germylene centers might act as Lewis bases by the non-bonding electron pair at the N or at the Ge centers. This in contrast to the previous observations on the less sterically congested bis(germylenes) synthesized by Hanh and co-workers (Figure 1.3.2, p. 28).[86,93]

Table 3.1.1. Selected bonds [Å] and angles [°] for **GeCHGe** and **1-NHGe**

Bond	GeCHGe	1-NHGe[51]
Ge–X (X = O, Cl)	1.850 ± 0.011(6)	2.2572(13)
Ge–N	2.008 ± 0.003(7)	2.060 ± 0.012(2)
N–C(15) or N–C(30)	1.330 ± 0.014(10)	1.330(3)
N–Ge–N	64.8 ± 0.5(3)	63.22(11)
N–Ge–X (X = O, Cl)	92.7 ± 0.9(3)	92.10(8)
N–C–N	108.1 ± 1.1(7)	108.6(3)
N–C–C_{ipso}Ph	126.0 ± 1.5(7)	125.72(13)
C–O–Ge	124.5 ± 0.1(5)	–

3.1.2. Synthesis of the GeCBrGe pincer ligand and attempts to prepare the elusive SiCBrSi analogue

The synthesis of the bromide-centered **ECBrE** pincer ligands (E = Si^{II}, Ge^{II}) was proposed based on the unprecedented reactivity observed by the **SiCHSi** pincer ligand towards the palladium precursor $Pd(PPh_3)_4$. The formation of a mixed silylene(Si^{II})-silyl(Si^{IV})-Pd^{II} pincer complex was obtained (Scheme 1.3.1, p. 31).[92] This occurred through a hydride migration from the [SiCSi]Pd^{II}–H transient species to one of the silylene pendant arms. This result suggested that the hydrido ligand has a higher reactivity toward the silylenes, ending in a redox process where one of the pendant arms is oxidized to a Si^{IV} center. Therefore, the idea to have a halogen on the carbon was first to reduce the reactivity of the coligand formed after metallation (i.e., halide), and second to have a more prone C(sp^2)–X bond to metallate through an oxidative addition reaction using low-valent metal precursors (Scheme 3.1.3). However, the synthesis of the **ECBrE** pincer-type ligands was challenging, and successful results can only be obtained for the **GeCBrGe** ligand.

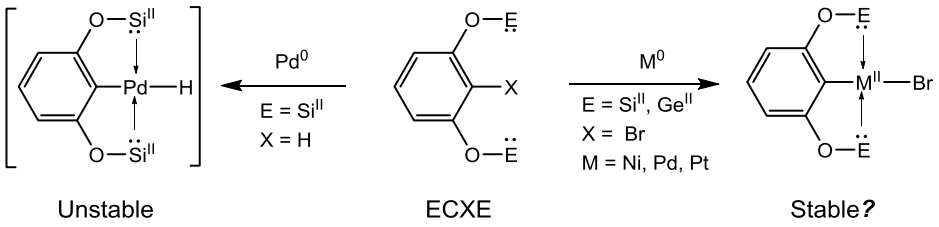

Scheme 3.1.3. Previous reactivity for the **SiCHSi** ligand with $Pd(PPh_3)_4$ and proposed metallation of bis(metallylene) pincer-type ligands with group 10 metals.

Initially, a deprotonation reaction of the 2-bromo-4,6-di-*tert*-butylresorcinol with different bases (LiHMDS, KHMDS, LDA, KH) produced purple intractable reaction mixtures of undefined composition. Following the reported procedure for the synthesis of the iodide centered ***t*Bu-PCIP** pincer ligand, where NaHMDS was premixed with tBu$_2$PCl in THF with concomitant addition of the 2-iodoresorcinol,[103] did not afford the desired product using **5-NHSi** or **1-NHGe** and 2-bromo-4,6-di-*tert*-butylresorcinol as reagents. Instead, in the case of **5-NHSi** a salt metathesis reaction occurred before addition of the resorcinol derivative. Moreover, an oxidative addition of the O–H bond to the Si^{II} center was obtained using the (dimethylamido)silylene **LSiNMe$_2$** (Scheme 3.1.4) as observed in the ^{1}H NMR spectrum.

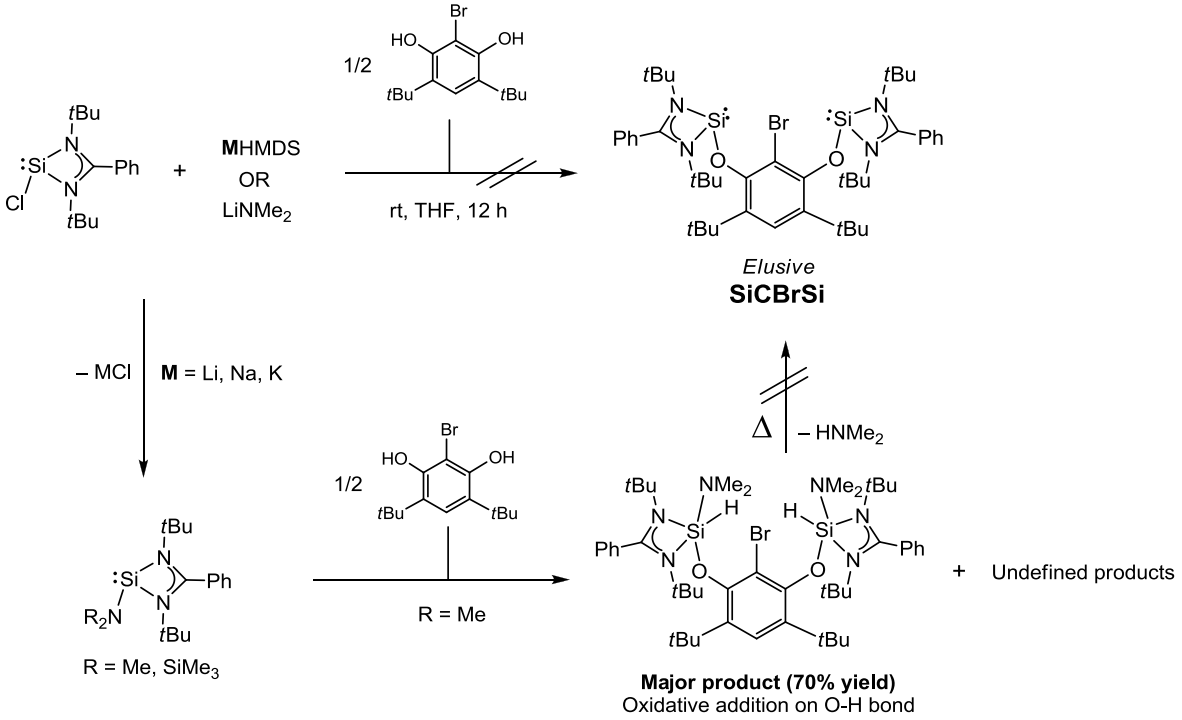

Scheme 3.1.4. Attempts to synthesize the **SiCBrSi** pincer ligand.

Combination of ^{1}H and ^{29}Si{^{1}H} NMR spectra suggested that the oxidative addition to the Si^{II} occurs. In the ^{1}H NMR spectrum two signals for the protons on the silicon center were observed at δ = 4.81 and 4.84 ppm. Additionally, in the ^{29}Si NMR INEPT spectrum two signals were observed at δ = –84.3 and –84.9 ppm, correlating to a pentacoordinated Si^{IV} species having an amidinato as ligand backbone.[49] This reactivity has been observed for a five-membered[58,104] and a six-membered[59] but not in a four-membered NHSi.

However, having the dimethylamide group and a proton bound to the silicon atom, it was tempting to see whether the elimination of dimethylamine (bp: 7 °C) would be possible. Heating the reaction mixture at 60 °C produced several decomposition products and neither the formation of $HNMe_2$ nor the **SiCBrSi** pincer ligand was observed. Other synthetic approach can be considered reducing a bis(silane) precursor. However, this synthetic approach has been proven to be unsuccessful in the Driess' group by Wang in an attempt to synthesize the **SiCHSi** pincer ligand.[102] The double dehydrochlorination of a bis(silane) (Si^{IV} centers) on a 1,3-resorcinolate backbone was proved to be ineffective. Unfortunately, these attempts showed that **SiCBrSi** pincer ligand remains elusive due to the intrinsic reactivity of the NHSi toward heteroatom–H bonds.

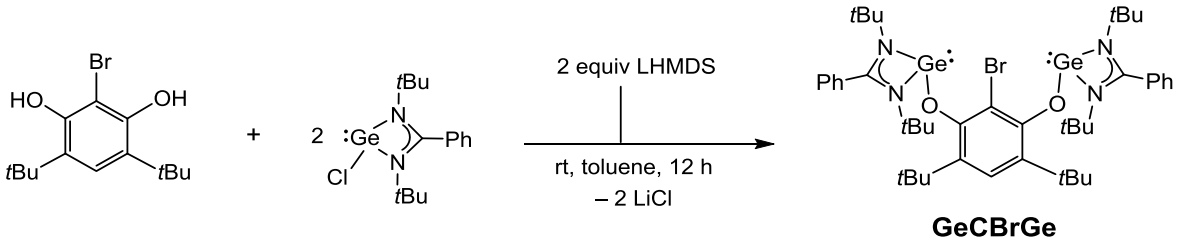

Scheme 3.1.5. Synthesis of the bromo-centered bis(germylene) **GeCBrGe** pincer-type ligand.

In the case of **5-NHGe** after mixing it with the resorcinol, the ^{1}H NMR spectrum showed that the reagents remained unreacted, indicating that the germylene center (Ge^{II}) is much less reactive towards the O–H bond than the silylene (Si^{II}) analogue. Therefore, the reverse addition of the reactants to the reaction flask was planned for the synthesis of the **GeCBrGe** ligand in a one-pot reaction. Slow addition of 2 molar equiv of LiHMDS in toluene to a mixture of 2-bromo-4,6-di-*tert*-butylresorcinol and 2 equiv of **5-NHGe** at room temperature produced the envisioned **GeCBrGe** ligand (Scheme 3.1.5). The ^{1}H NMR spectrum for the reaction mixture showed two major singlet resonance signals for the *t*Bu groups with a relative ratio of 1:2. Purification by extraction with *n*-hexane and recrystallization afforded the **GeCBrGe** ligand in 68 % yield as a colorless solid. The **GeCBrGe** ligand was fully characterized by ^{1}H and ^{13}C{^{1}H} NMR spectroscopy, mass spectrometry and single crystal XRD structure analysis. The ^{1}H NMR spectrum presented the C_{2v} symmetry for the ligand where the two singlet resonance signals for the *t*Bu groups were observed at δ = 1.07 and 1.83 ppm for N-*t*Bu and Ar-*t*Bu, respectively. Additionally,

the characteristic signal 5-C*H* for the resorcinolato backbone was observed at δ = 7.61 ppm. Other aromatic signals for the phenyl groups were observed as broad multiplets in two ranges, one at δ = 6.90–7.04 ppm and the other one at δ = 7.29–7.32 ppm with a total integration of 10 protons. Additionally, the high resolution mass spectrum APCI-MS ($M^{\cdot+}$: calcd. 908.26975, found: 908.26978) confirmed the ligand composition.

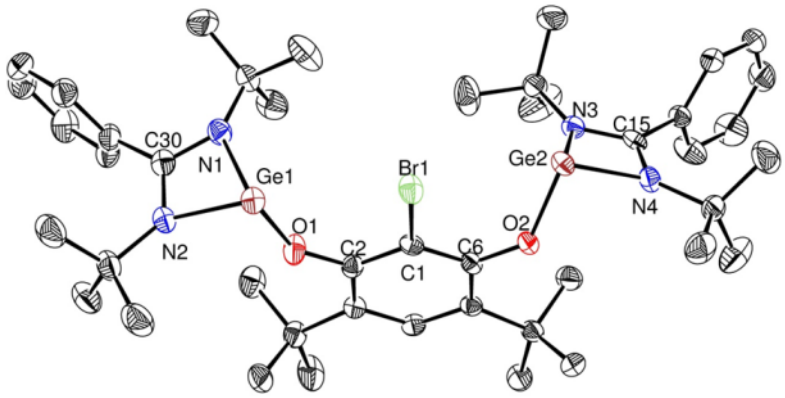

Figure 3.1.2. ORTEP representation of the **GeCBrGe** pincer ligand in the solid state. Selected distances [Å] and angles [°]: C1–Br1 1.905(3), O1–Ge1 1.862(2), O2–Ge2 1.868(2), C2–O1 1.347(3), C6–O2 1.355(3), Ge1–N1 2.031(3), Ge2–N4 2.021(2), C2–O1–Ge1 142.6(2), C6–O2–Ge2 136.3(2), N1–Ge1–N2 64.8(1), N3–Ge2–N4 64.8(1). Thermal ellipsoids are drawn at a 50% probability level; hydrogen atoms are omitted for clarity.

The structure of the **GeCBrGe** ligand (Figure 3.1.2) was unambiguously determined by single crystal XRD structure analysis of crystals grown in a concentrated *n*-hexane solution. The main structural features are akin to those of **GeCHGe**, however, the presence of the bromide on the C1 makes the C2–O1–Ge1 and C6–O2–Ge2 angles wider (**GeCHGe**: 124.4(5)°, 124.5(5)°; **GeCBrGe**: 142.6(2)°, 136.3(2)°); and longer Ge1–Ge2 interatomic distances (**GeCHGe**: 5.123(5) Å, **GeCBrGe**: 6.379(5) Å) due to the additional steric effect of the Br atom.

3.1.3. Synthesis of the phosphinite based *t*Bu-PCHP and *i*PrN-PCHP pincer ligands

Due to the novelty of these pincer ligand systems based on N-heterocyclic metallylenes, a direct comparison with well-established ligands was carried out. The P^{III}-based ligands were selected as isoelectronic donor systems. In the literature there are several pincer-type ligands with phosphine as donor systems, however, there are no reports with *t*Bu groups on the arene backbone with the standard dialkyl and/or diaryl phosphinite ligands (R_2P-OAr, R = alkyl, aryl) which might vary their properties. Additionally, a ligand system, more related to the amidinato ligand, based on *N,N'*-di-*iso*-propyl-ethylendiamido is already reported in the literature and taken as reference system. With this in mind, the ***t*Bu-PCHP** and ***i*PrN-PCHP** ligands were chosen as reference (Figure 3.1.3) and their synthesis is described below.

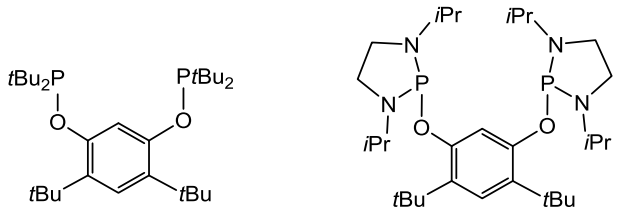

Figure 3.1.3. Selected phosphinite pincer ligands as references for the present work.

Normally the synthesis of PCP pincer-type ligands can be achieved using several synthetic approaches and conditions.[7,101] However, due to the electronic properties on the 4,6-*tert*-butylresorcinol, deprotonation of OH groups was only affordable using KH as a base in refluxing THF (Scheme 3.1.6). The ***t*Bu-PCHP** and ***i*PrN-PCHP** ligands were afforded by concomitant addition of the chloro or bromo substituted phosphine after deprotonation. The synthesis of the ***i*PrN-PCHP** pincer ligand was previously reported, although, using this straightforward fashion the yields were improved. The ***t*Bu-PCHP** and ***i*PrN-PCHP** ligands were fully characterized by ^{1}H, $^{13}C\{^{1}H\}$, $^{31}P\{^{1}H\}$ NMR spectroscopy and single crystal XRD structure analysis for the ***t*Bu-PCHP**.

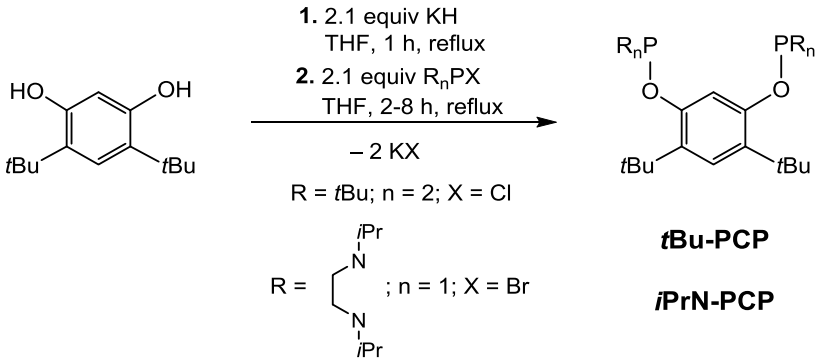

Scheme 3.1.6. Synthesis of the bis(phosphinite) ***t*Bu-PCHP** and ***i*PrN-PCHP** pincer ligands.

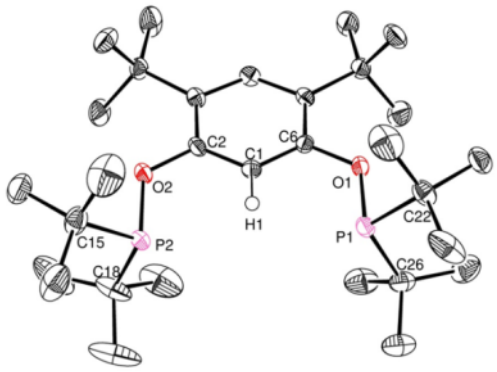

Figure 3.1.4. ORTEP representation of the ***t*Bu-PCHP** pincer ligand in the solid state. Selected distances [Å] and angles [°]: P1–O1 1.6826(18), P2–O2 1.6792(18), C2–O2 1.398(3), C6-O1 1.403(3), P1–C22 1.871(3), P1–C26 1.874(3), P2–C15 1.862(3), P2–C18 1.868(3) C2–O2–P2 122.18(15), C6–O1–P1 121.77(15), O1–P1–C22 97.24(11), O1–P1–C26 99.90(11), O2–P2–C15 97.32(11), O2–P2–C18 100.68(12), C15–P2–C18 111.28(15), C22–P1–C26 110.86(13). Thermal ellipsoids are drawn at a 50% probability level; hydrogen atoms are omitted for clarity, except H1.

The ^{1}H, $^{13}C\{^{1}H\}$, and $^{31}P\{^{1}H\}$ NMR spectra of the synthesized ***i*PrN-PCHP** ligand matches with the previously reported values.[105] The ^{1}H NMR spectrum of the ***t*Bu-PCHP** ligand reveals a C_{2v} symmetry with two signals at the aliphatic region: a doublet resonance signal for the P-*t*Bu at δ = 1.21 ($^{3}J_{P\text{-}H}$ = 11.8 Hz) and a singlet resonance at δ = 1.59 ppm for the Ar-*t*Bu groups. In the aromatic region there are two resonance signals, one as singlet at δ = 7.51 ppm, for the proton at the 5-C*H*, and the other as triplet at δ = 8.98 ppm ($^{4}J_{P\text{-}H}$ = 9.6 Hz), for the proton at the 2-C*H* on the aromatic ring. The $^{31}P\{^{1}H\}$ NMR depicts a

singlet resonance signal at δ = 146.5 ppm in the range of phosphinites ligands ($P(OR)R'_2$ with R' = alkyl or aryl).[101] The structural features for ***t*Bu-PCHP** were unambiguously determined by XRD structure analysis from of single crystals grown in a concentrated *n*-hexane solution (Figure 3.1.4). It is worth mentioning that only scant examples of bis(phosphinites) ligands exist which have been structurally characterized due to the high mobility of the side arms; normally they are isolated as oils or amorphous solids.[7,106] The P atoms possess a pseudo-tetrahedral structure as the Ge atoms in the described **GeCXGe** ligands (X = H, Br). The non-bonding electron pair is located in a sp^3 hybridized orbital of the P atom, showing similar structural and electronic features with the bis(metallylenes) pincer ligands.

3.1.4. Synthesis of SiNSi and GeNGe pincer ligands

The synthesis of neutral tridentate ligands based on bis(silylene) and bis(germylene) as σ-donors was envisaged with a view to expand their coordination chemistry toward low-valent TMs. Based on the synthetic approach for the synthesis of **ECHE**, the synthesis of the pyridine-based pincer ligand was envisaged through a salt metathesis route starting from 2,6-diamine-*N,N'*-diethylpyridine as a backbone. The synthesis of this disubstituted pyridine was carried out following the reported procedures for alkylation of amines.[107] Acetylation of the 2,6-diaminepyridine with concomitant reduction with LAH produced the desired 2,6-diamine-*N,N'*-diethylpyridine (Scheme 3.1.7).

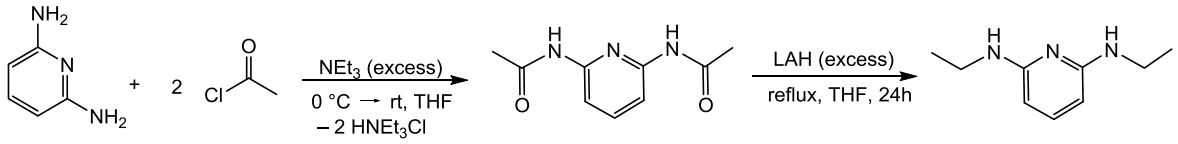

Scheme 3.1.7. Synthesis of the 2,6-diamine-*N,N'*-diethylpyridine

Deprotonation of 2,6-diamine-*N,N'*-diethylpyridine with 2 molar equiv. of *n*-BuLi under reflux in diethyl ether, followed by the dropwise addition of 2 molar equiv. of **5-NHSi** or **1-NHGe** in toluene solutions at –78 °C afforded a new product after warming up to room temperature overnight (Scheme 3.1.8). The ^{1}H NMR spectra for **SiNSi** and **GeNGe** showed a major product containing a singlet resonance signal for the *t*Bu, a triplet for the

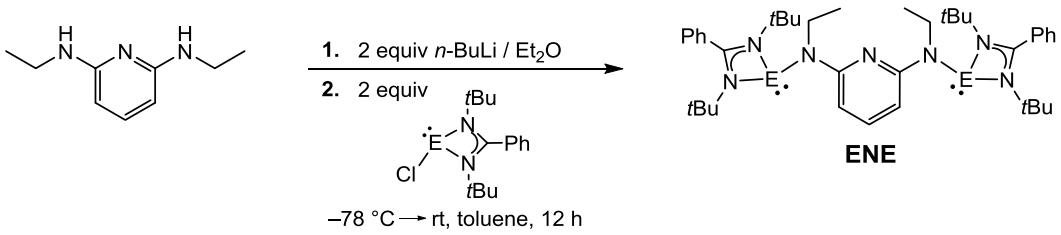

Scheme 3.1.8. Synthesis of the neutral bis(metallylene) **ENE** (E = Si^{II}, Ge^{II}) pincer ligands.

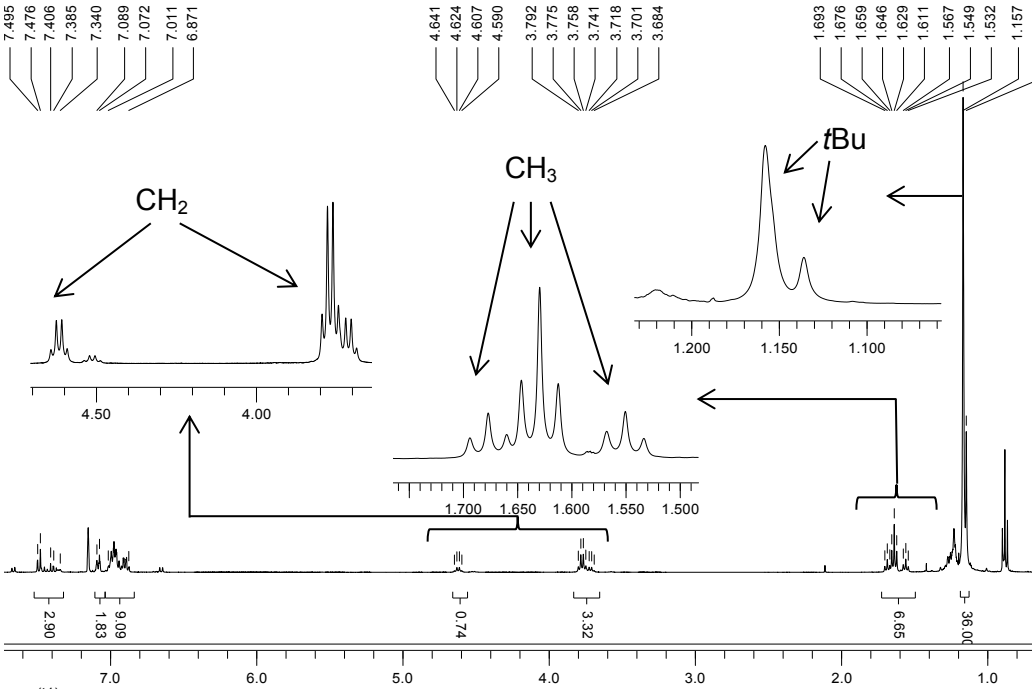

Figure 3.1.5. ^{1}H NMR spectrum (δ/ppm) of the bis(silylene) **SiNSi** pincer ligand in C_6D_6 at 25 °C (see structure in Scheme 3.1.8 for assignment).

methyl and a quartet for the methylene moieties with the relative intensity of 18:3:2, respectively. Purification by extraction with *n*-hexane and recrystallization produced the desired ligand **SiNSi**. Somewhat noteworthy is that the **GeNGe** ligand exhibits a much higher solubility in organic solvents than its silicon homologue and thus its crystallization failed. However, removal of the solvent *in vacuo* produced the desired **GeNGe** ligand in high purity (>95%). Both ligands were fully characterized by ^{1}H, $^{13}C\{^{1}H\}$ and $^{29}Si\{^{1}H\}$ NMR spectroscopy, high resolution mass spectrometry, elemental analysis, and single crystal XRD structure analysis for **SiNSi**. The ^{1}H NMR spectra for both ligands are alike to each other showing the aliphatic signals for the *t*Bu, CH_3, and CH_2 groups at δ = 1.16, 1.63,

and 3.77 ppm and δ = 1.11, 1.57, and 3.76 ppm for **SiNSi** and **GeNGe** respectively. In the ^{1}H NMR spectrum, the aromatic region is more complex and multiplets for the phenyl groups of the amidinato and the pyridine moieties are located separately. Interestingly, the ^{1}H, ^{13}C{^{1}H} and ^{29}Si{^{1}H} NMR spectra of isolated crystals of **SiNSi** showed two sets of signals related with two rotational conformers in the pendant arms (Figure 3.1.5). For instance, the ^{29}Si{^{1}H} NMR spectrum revealed three signals: one major signal at δ = –14.9 ppm and two other resonance signals at δ = –13.8 and –17.1 ppm, showing the inequivalency of the two silylene moieties (Figure 3.1.6). The set of signals were unambiguously assigned to the same chemical species through a DOSY NMR experiment showing the same diffusion coefficient for all signals in the ^{1}H NMR spectrum.

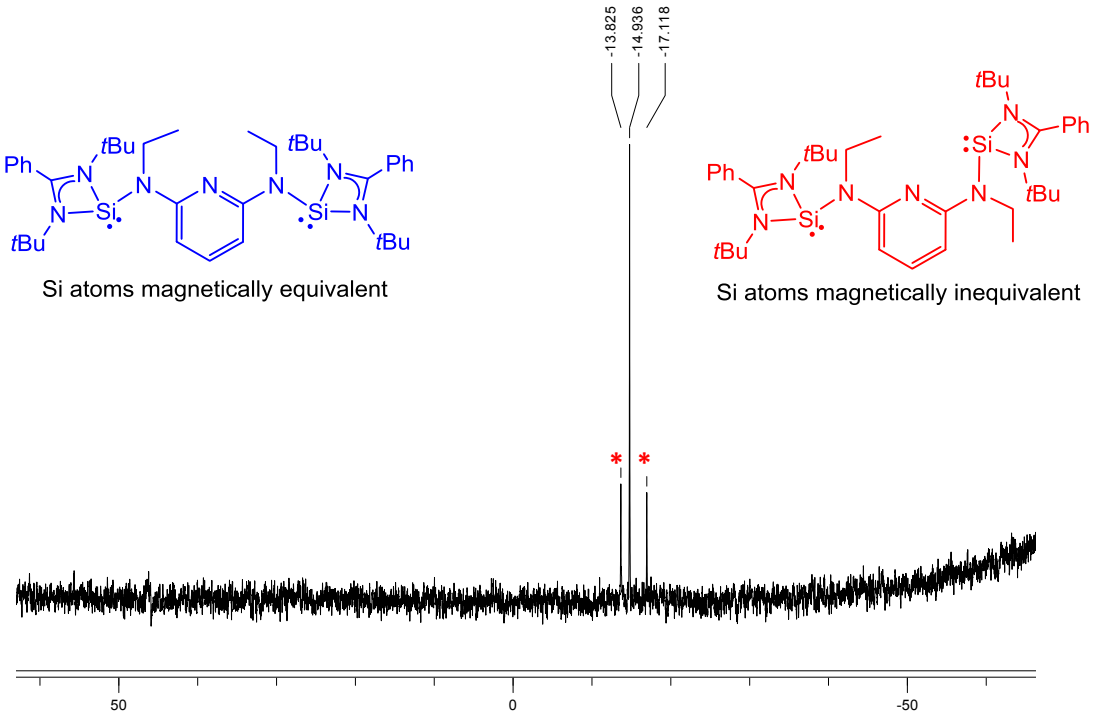

Figure 3.1.6. ^{29}Si{^{1}H} NMR spectrum (δ/ppm) of the bis(silylene) **SiNSi** pincer ligand in C_6D_6 at 25 °C.The signals marked with * are related with the asymmetric conformer.

Single crystals of the **SiNSi** ligand suitable for XRD structure analysis were grown in a concentrated *n*-hexane solution. The structural features for the **SiNSi** ligand (Figure 3.1.7) shows that in the solid state just one of the conformers is in the crystal lattice. The bond distances in the ligand backbone are almost unaltered after the new N–Si covalent bonds

were formed. The Si atoms are located in a pseudo-tetrahedral structure as presented in the precursor **5-NHSi**[49] (Table 3.2). It is also observable that the non-bonding electron pair for both NHSi moieties are pointing out from the pyridine moiety. This might alter its coordination abilities as terdentate ligand. However, the fluxional behavior observed by NMR spectroscopy suggested the possibility to have it as a potential pincer ligand, in a meridional tridentate coordination fashion (see section 3.2.3).

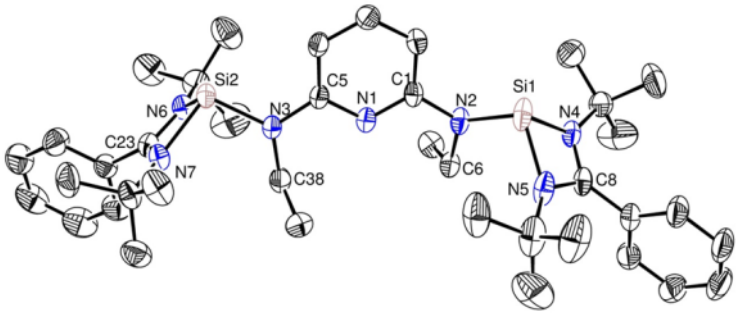

Figure 3.1.7. ORTEP representation of the **SiNSi** ligand in the solid state. Thermal ellipsoids are drawn at the 50% probability level; hydrogen and solvent atoms are omitted for clarity.

Table 3.2. Selected bonds [Å] and angles [°] of **SiNSi** and **5-NHSi**

Bond	**SiNSi**	**5-NHSi**[49]
Si–X (X = N(2-3), Cl)	1.7791± 0.0103(19)	2.156(1)
Si–N(4-7)	1.882 ± 0.009(2)	1.894 ±0.023(2)
N–C(8) or N–C(23)	1.336 ± 0.006(3)	1.333 ± 0.000(2)
N(4/6)–Si–N(5/7)	68.83± 0.00(9)	68.35(8)
N(4-7)–Si–X (X = N(2-3), Cl)	101.02 ± 1.76(10)	96.19 ± 0.37(6)
N(4/6)–C–N(5/7)	105.5 ± 0.2(2)	105.94(18)
N–C–C_{ipso}Ph	127.2 ± 1.6(2)	126.8(5)
C(1/5)–N–Si	119.65 ± 0.54(15)	–

3.2. Coordination ability of the ECXE and ENE pincer ligands (E = Si^{II}, Ge^{II}; X = H, Br) toward late transition metals

The intrinsic reactivity of metallylenes has shown potential applications towards activation of strong bonds (cf.section 1.2).[32,33,53] However, the coordination abilities as normal σ-donor ligands toward late TMs is still in its infancy compared to the corresponding carbon homologues: NHCs.[3] Some reports have shown that the use of these systems is not as straightforward as the existing and more classical σ-donor ligands (i.e. P^{III}, O^{II}, N^{III}, C^{II}). Redox reactions can occur during their synthesis including oxidative addition to the metal-halide bonds (Scheme 3.2.1),[108,109] in addition to their synthesis by

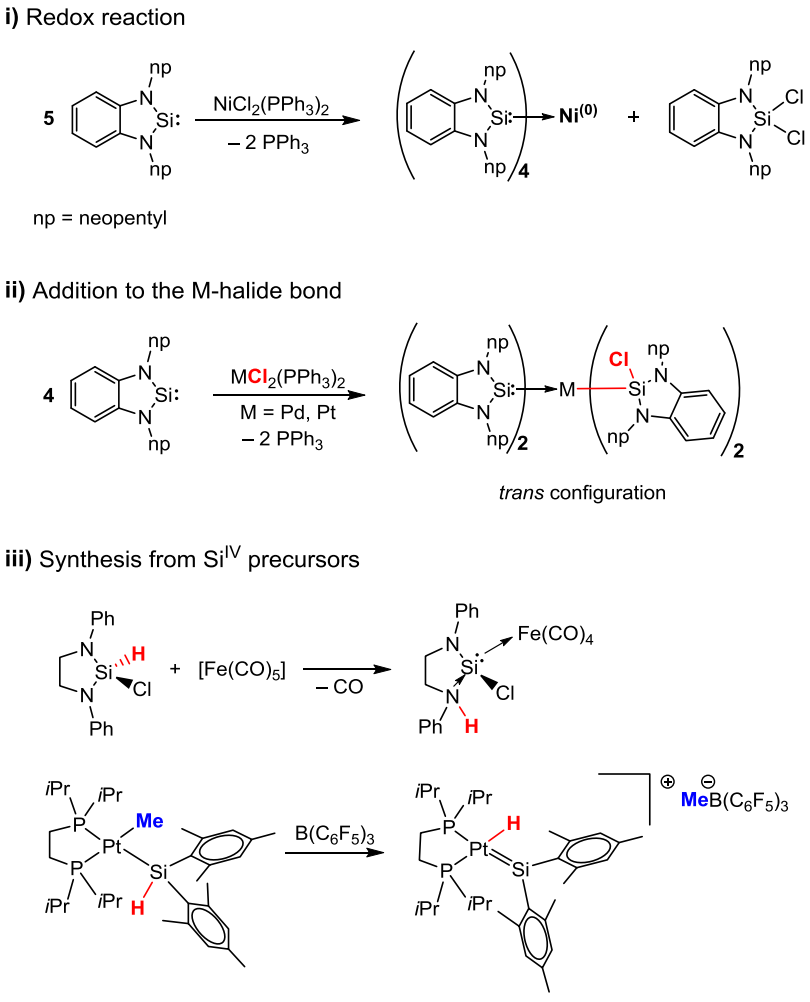

Scheme 3.2.1. Selected examples for the reactivity of NHSis toward late TMs (**i** and **ii**) and the synthesis of metal complexes through H-migration reactions (**iii**).

non-conventional reactions for their metal complexes starting from the E^{IV} precursors (E = Si, Ge).[110] Hence, a synthetic strategy avoiding such potential side reactions must be envisaged for the metallation on **ECXE** and **ENE** novel pincer ligands.

The reported methodologies for the metallation on more traditional monoanionic pincer ligands are based on the following four reaction types (Scheme 3.2.2):[7,11,111]

a) Oxidative addition on the centered C_{ipso}–X (X= H, Cl, Br) bond: In this instance, a low-valent TM precursor with weak coordinating ligands is employed. The highly electron rich metal center M^{n+} is oxiddative added to the C–X bond affording a $M^{(n+2)+}$ oxidation state with formation of a new C–M–X bond.
b) C–H activation with metal salts MX_2L_2: The coordinating ligands L are substituted by the chelate ECHE pincer ligand forming the κ^2E,E'-[ECHE]MX_2 intermediate. The C–H bond is activated by an agostic interaction. In the presence of a external agent such as a base (B), the proton is released as a HB adduct, and the desired pincer complex [ECE]MX is formed.
c) Lithiation and transmetallation: Selective lithiation (e.g., *n*-BuLi, *t*-BuLi, etc…) is carried out on the C_{ipso}–X bond (X = H, Br) from the ECXE pincer ligand. A transmetallation with a metal salt MX_2L_n (n = 2, 3, 4) affords the expected pincer complex [ECE]MXL_m ($0 = m < (n–2)$).
d) Metal complex as template of pincer ligand: Also known as ligand introduction route,[7,112] for this method the C–M bond is formed before the introduction of the very bulky σ-donor pendant arms. Normally the synthesis for these ligands is not possible by the common synthetic methods described in section 1.1. Firstly, the oxidative addition of the C_{ipso}–X on the TM center is carried out. Once the new C_{ipso}–M bond is formed, the precursors for the pendant arms react with this complex to form the tridentate ligand in a meridional coordination fashion *via* precoordination to the metal center.[112,113]

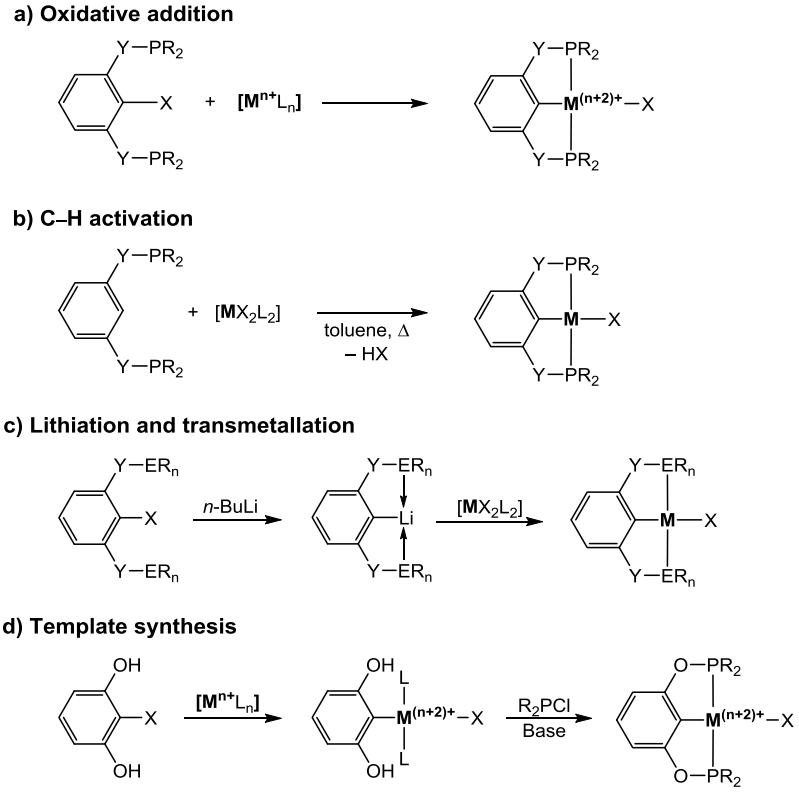

Scheme 3.2.2. Synthetic methodologies for metallation of monoanionic pincer-type ligands (E = P, O, N, C; Y = O, CH_2; X = H, halide; M = late TM; L = neutral ligand).

Some of these synthetic methods either employ a strong base (Scheme 3.2.2c) or a strong acid is formed during the reaction (Scheme 3.2.2b). The latter reaction conditions are not suitable while working with NHSis and NHGes as pendant arms due their intrinsic reactivity. In addition, the use of a template synthesis (Scheme 3.2.2d) is inconvenient for the NHSis and NHGes due to their reactivity toward Y–H and M–X bonds (Y = heteroatom; X = halide; M = metal). Therefore, the oxidative addition of a low-valent TM on the C_{ipso}–X bond of the pincer ligand is the milder synthetic method for its metallation. However, the stability of these ligands also depends on the reactivity of the product formed, as shown in the case of the reaction of **SiCHSi** with $Pd(PPh_3)_4$ (see section 1.3.3, Scheme 1.3.1, p. 31). Thus, more stable species as products must be envisaged for a better stability. Additionally, the use of an excess of a non-nucleophillic base with a metal salt (Scheme 3.2.2b) could be a useful strategy for the synthesis of the targeted pincer metal complexes.

In this chapter the metallation of the pincer ligands **ECXE** with Ir, Rh and Ni is presented and discussed as well as the coordination of the neutral pincer ligands **ENE** toward Fe as metal center.

3.2.1. Coodination of Iridium and Rhodium

3.2.1.1. Synthesis of [ECE]IrHCl(coe), [*i*PrN-PCP]IrHCl(coe) and [*t*Bu-PCP]IrHCl complexes

With the **ECHE** pincer-type ligands fully characterized and considering the reactivity of **SiCHSi** towards $Pd(PPh_3)_4$, previously unravelled,[92] more stable hydride species were targeted for the stability of the pendant arms. The group 9 TMs was selected owing their higher electron density to form stable hydride species, to apply them as precatalysts in chemical transformations.

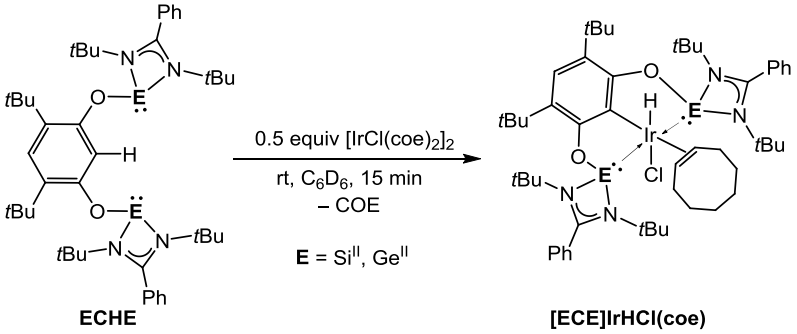

Scheme 3.2.3. Synthesis of the bis(metallylene) **[ECE]IrHCl(coe)** (E = Si^{II}, Ge^{II}) complexes by oxidative addition of Ir^{I} to the C_{ipso}–H bond using the dimer $[IrCl(coe)_2]_2$ as Ir^{I} precursor.

Addition of 1.0 mL of C_6D_6 to a mixture of **SiCHSi** and $[IrCl(coe)_2]_2$ led to the immediate and quantitative formation of a new compound reflected by a hydride resonance signal in the ^{1}H NMR spectrum at δ = –25.6 ppm. After purification by removal of volatiles *in vacuo* and washing thoroughly with *n*-hexane, the ^{1}H NMR spectrum of the white solid revealed three sets of singlet resonance signals for the *t*Bu groups at δ = 0.99, 1.31, and 1.43 ppm with equal integration for each corresponding to the $NC(CH_3)_3$, $NC(CH'_3)_3$, and $Ar\text{-}C(CH_3)_3$ groups, respectively. This shows the inequivalency of the *t*Bu groups on the amidinato backbone revealing the C_s symmetry of the complex by oxidative addition on the C_{ipso}–H bond (Scheme 3.2.3). Moreover, the $^{29}Si\{^1H\}$ NMR spectrum shows a singlet at δ = 54.9 ppm, which is considerably shifted from the signal for the free **SiCHSi** ligand at δ =

–24.0 ppm,[92] indicating coordination of the Si atoms to the Ir center in the **[SiCSi]IrHCl(coe)** product. In a similar fashion, the reaction of $[IrCl(coe)_2]_2$ with **GeCHGe** afforded a metal hydride complex, according to its ^{1}H NMR spectrum, with a singlet resonance signal at δ = –26.8 ppm. The other proton signals are observed in the same range of its bis(silylene) homologue featuring a C_s symmetric complex. Another characteristic signal, located through the 2D NMR correlation spectroscopy, is the one for the olefinic protons from the *coe* coligand, apart from the resonces of the aromatic protons at lower field. These signals are located for the **[ECE]IrHCl(coe)** complexes at δ = 3.37 and 4.06 ppm for E = Si^{II} and Ge^{II}, respectively. The difference in chemical shift is a consequence of the σ-donor strength of the ligands and will be discussed later together with the bis(phosphinite) complexes (see page 63).

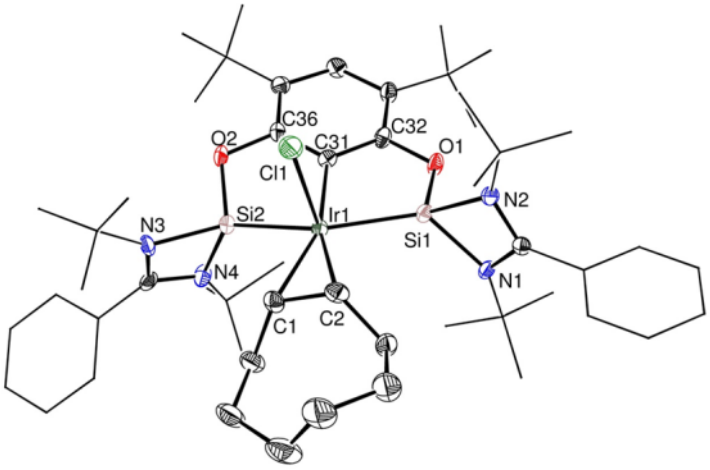

Figure 3.2.1. ORTEP representation of the **[SiCSi]IrHCl(coe)** complex in the solid state. Selected distances [Å] and angles [°]: Ir1–Si1 2.301(1), Ir1–Cl1 2.514(1), Ir1–Si2 2.305(1), Ir1–C31 2.127(4), Ir1–C45 2.222(4), Ir1–C52 2.232(4); N1-Si1-N2 70.4(1), N2-Si1-Ir1 134.3(1), N3–Si2–Ir1 137.4(1), Ir1–Si2–N4 126.1(1), N4–Si2–N3 71.3(2), N1–Si1–Ir1 129.7(1). Thermal ellipsoids are drawn at the 50% probability level; hydrogen and solvent atoms are omitted, and Ph and *t*Bu groups are drawn in wireframe fashion for clarity.

The molecular structure of the **[SiCSi]IrHCl(coe)** complex was unambiguously determined by single crystal XRD structure analysis (Figure 3.2.1). The structure depicts, for the first time, the terdentate coordination mode of this novel pincer ligand in a meridional fashion. It exhibits a distorted octahedral Ir center bearing a chlorido and

hydrido ligand, the latter undetectable by the Fourier electron density map, *trans* with respect to each other. Comparing to previously reported Ir–silyl and Ir–silylene complexes, the Ir–Si bond lengths in **[SiCSi]IrHCl(coe)** (Ir–Si: 2.305(1) and 2.301(1) Å) are between the reported values for Ir^{III}–Si^{IV} and Ir^{III}–Si^{II} distances. For instance the octahedral Ir–silyl complexes posses Si–Ir bond distances in the range of 2.36–2.42 Å[114] and the base- and *non*-base-stabilized silylene→Ir complexes amount values in the range of 2.21–2.26 Å (Figure 3.2.2).[115–118] For the case of the silyl complexes (**Ir-1**: 2.418(3) and 2.394(3) Å;[119] **Ir-2**: 2.361(3) Å;[120] and **Ir-3**: 2.414(2) Å[121]) a high covalent character has been described for the Ir–Si bonds. In the case of the NHSi complex **Ir-4** (Ir–Si: 2.2328(9) Å)[118] a Ir→Si π-backbonding was proposed as the effect for this short bond length. In contrast, the silylene complexes **Ir-5** and **Ir-6** have bond lengths of 2.260(3)[115,116] and 2.210(2) Å[117] respectively, with a described double bond for the Ir–Si bond *via* a Ir→Si π-backbonding interaction. Therefore, a coodinative bond (covalent single bond) is defined for the Ir–Si in the **[SiCSi]IrHCl(coe)** complex with the base-stabilized NHSis on the pendant arms.

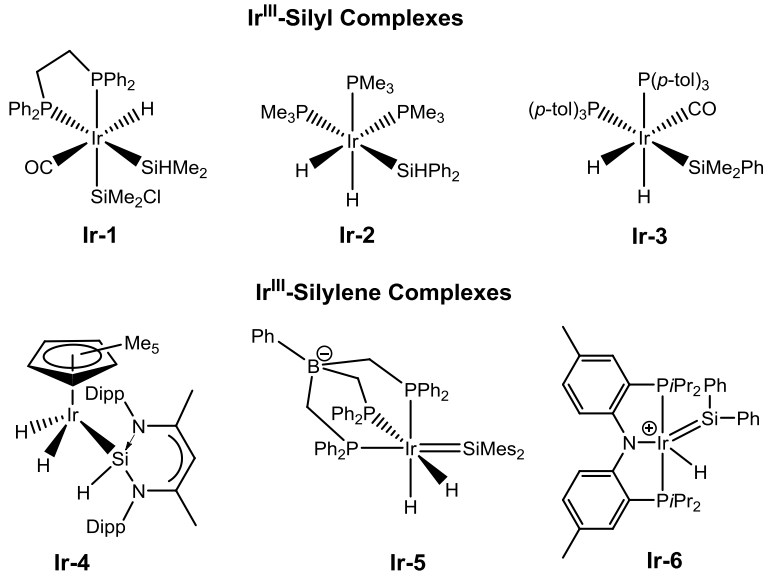

Figure 3.2.2. Selected examples for Ir^{III}–silyl and Ir^{III}–silylene complexes (Dipp = 2,6-diisopropylphenyl; Mes = 2,4,6-trimethylphenyl; *p*-tol = 4-methylphenyl).

Remarkably, the C–C distance of 1.409(9) Å of the olefinic *coe* group in the **[SiCSi]IrHCl(coe)** complex is one of the longest reported to date for a C=C bond.[122] It resembles the high electron density observed at the Ir center through Si^{II}→Ir σ-donation.

This difference in σ-donor strength is explained together with the bis(phosphinite) complexes later on in this section (see below).

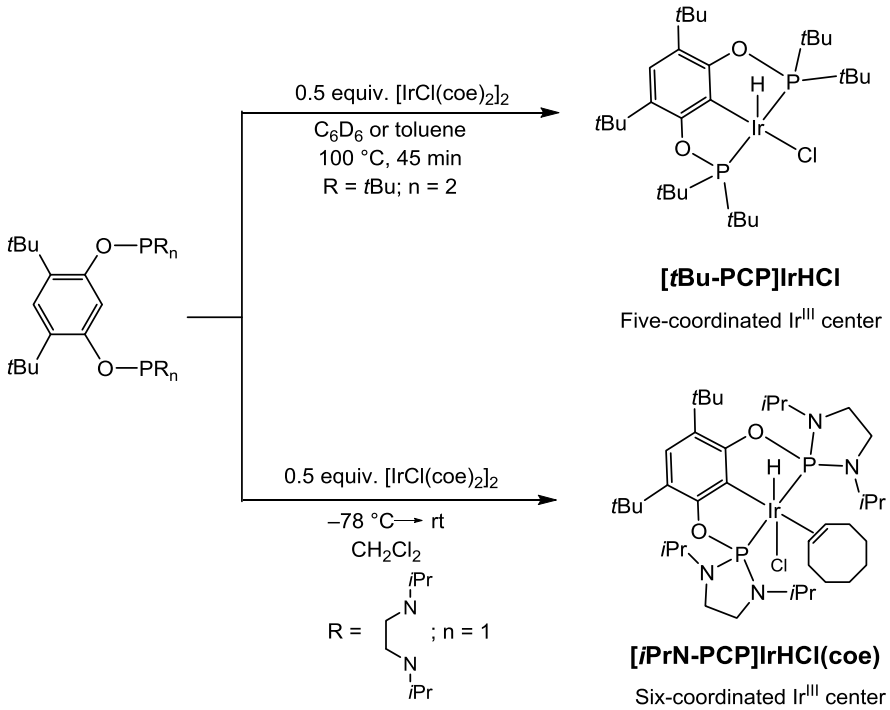

Scheme 3.2.4. Syntheses for the bis(phosphinite) **[*t*Bu-PCP]IrHCl** and **[*i*PrN-PCP]IrHCl(coe)** pincer complexes through an oxidative addition on the C–H bond using the dimer $[IrCl(coe)_2]_2$ as Ir^I precursor.

Comparing these novel ligands with the well-established P^{III} ligand systems, Ir^{III} complexes were targeted using the synthesized ***t*Bu-PCHP** and ***i*PrN-PCHP** pincer ligands (see section 3.1.3). Complexation of both ligands with $[IrCl(coe)_2]_2$ proceeded in a similar fashion as bis(metallylene) ligands, but with slight modifications on the synthetic protocol (Scheme 3.2.4). For ***t*Bu-PCHP** a higher temperature was required to overcome the barrier for C_{ipso}–H oxidative addition. Most probably this difference is related with lower σ-donor strength of the tBu_2P–OAr pendant arms; with lower electron density on the Ir center. This would require more energy for C–H oxidative addition on the Ir center. Not surprisingly, this reaction afforded the five-coordinated **[*t*Bu-PCP]IrHCl** complex as reported for other bis(phosphinite) pincer ligands with a resorcinolate backbone.[9,106,123,124] This preference for a five- over a six-coordination is explained by a more electron deficient metal center, which in the case of **[ECE],** as chelate agent, requires an additional π-acceptor ligand (*coe*) for

stabilization of the metal center (see below for further discussion). The ^{1}H NMR spectrum shows a triplet resonance signal for the metal hydride proton at δ = –41.6 ppm ($^{2}J_{H–P}$ = 13.1 Hz) together with two virtual triplets at δ = 1.39 and 1.42 ppm for the *t*Bu groups on the phosphorous atoms, showing the C_s symmetry of the molecule bearing a mirror plane passing through the C_{ipso}–Ir–Cl atoms. The other resonance signal for the *t*Bu groups, on the aromatic ring, is observed at δ = 1.42 ppm overlapping with the virtual triplet at the same chemical shift. Moreover, the ^{31}P{^{1}H} NMR spectrum shows a single resonance signal at a higher chemical shift value of δ = 176.6 ppm compared to the free ligand in solution at δ = 146.5 ppm, indicating coordination to the metal center.

The bis(amido)phosphinite ***i*PrN-PCHP** pincer ligand was also tested in the reaction with the Ir^{I} precursor. Reacting ***i*PrN-PCHP** with $[IrCl(coe)_2]_2$ at room temperature led to a mixture of products, but addition at –78°C and slow warming to room temperature (Scheme 3.2.4) showed clean conversion to a new hydride species with a triplet resonance signal at δ = –24.6 ppm ($^{2}J_{H–P}$ = 15.1 Hz) in the ^{1}H NMR spectrum along with the signals for the ligand backbone and the coligand *coe*. The ^{1}H and ^{13}C{^{1}H} NMR spectra show a C_s symmetry on the product with four proton signals for the *i*Pr groups and one signal for the *t*Bu groups. The resonance signal corresponding to the olefinic group was located by ^{1}H-^{13}C HSQC NMR correlation spectroscopy revealing that its chemical shift is at δ = 4.31 ppm, somewhat deshielded in comparison to the **[ECE]IrHCl(coe)** (E=Si^{II},Ge^{II}) complexes.

The structures of the **[*t*Bu-PCP]IrHCl** and **[*i*PrN-PCP]IrHCl(coe)** complexes were unambiguously determined by single crystal XRD structure analyses (Figure 3.2.3). Hence, the coordination of the *coe* as coligand on the distorted octahedral Ir center of the **[*i*PrN-PCP]IrHCl(coe)** complex and the square pyramidal coordination of the Ir center in the **[*t*Bu-PCP]IrHCl** complex (Σ<Ir = 360.0(4)°) were determined. The hydrides could not be located on the difference Fourier electron density map in the structure solution. However, the results obtained by ^{1}H NMR and IR spectrocopies ($\nu_{Ir–H}$ (cm^{-1}): **[*i*PrN-PCP]** 2220; **[*t*BuPCP]** 2014), suggest that the H atom is most likely located at the apical position for the pyramidal Ir center in the latter and *trans* to the chloride ligand in the former. The molecular structure of **[*i*PrN-PCP]IrHCl(coe)** shows disordering at the periphery of the coordinated *coe*, while the olefinic group is not disordered. The P–Ir bond distances are within the range of P^{III}–Ir^{III} distances observed for other phosphorous based iridium pincer

complexes (2.28–2.30 Å). In addition, in the reported bis(phosphane) and bis(phosphinite) [PCP]Ir complexes regardless of the steric bulk around the P atom, the preferred coordination number is five and the coordination geometry is square-pyramidal around the metal center.[9,106,124,125] The difference with the **[*i*PrN-PCP]** ligand, where a six coordinated Ir center is found, is related with the higher donor capacity of the P atom enhanced by mesomeric effect from the amido substituents on the ligand backbone. The longer Ir–Cl bond distance, in the **[*i*PrN-PCP]IrHCl(coe)** complex, is due to the *trans* effect of the hydride ligand producing an elongation in the Ir–Cl bond.

Inspection of the structural parameters for the coligand *coe*, in **[*i*PrN-PCP]IrHCl(coe)** complex, reveals that the C–C double bond is 1.35(1) Å. This bond length is slightly longer than the values for uncoordinated olefins (ca. 1.32 Å)[126] and remarkably shorter than the

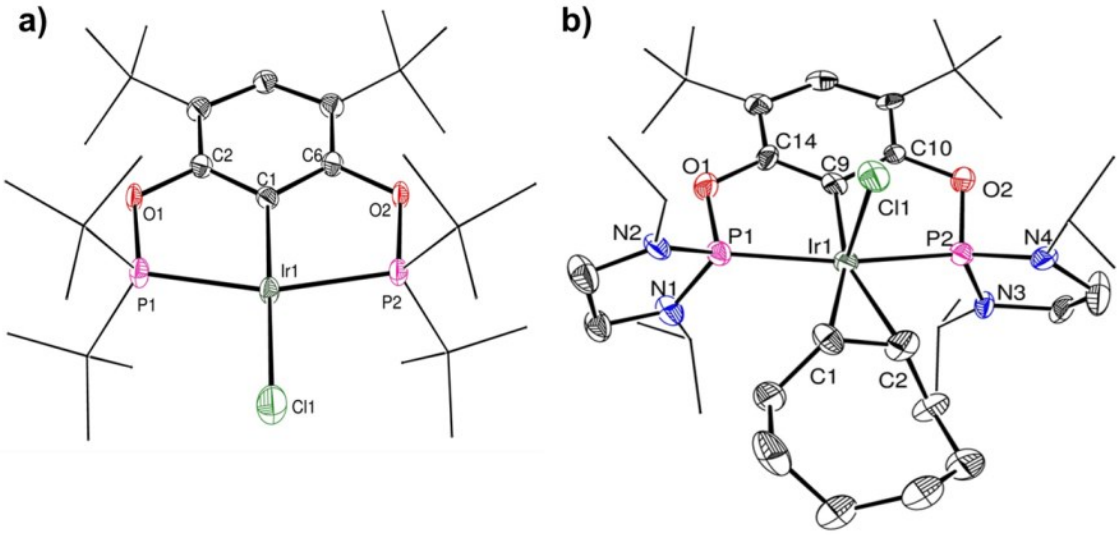

Figure 3.2.3. ORTEP representation of a) **[*t*Bu-PCP]IrHCl** and b) **[*i*PrN-PCP]IrHCl(coe)** complexes in the solid state. Selected distances [Å] and angles [°]: **a)** Ir1–C1 2.014(5), Ir1–Cl1 2.412(2), Ir1–P2 2.293(1), Ir1–P1 2.294(1), Cl1–Ir1–P2 99.44(4), Cl1–Ir1–P1 99.43(4), P1–Ir1–C1 80.4(1), P2–Ir1–C1 80.7(1). **b)** P1–Ir1 2.290(2), Ir1–Cl1 2.506(2), Ir1–P2 2.282(2), C9–Ir1 2.053(6), Ir1–C9 2.053(6), Ir1–C1 2.285(7), Ir1–C2 2.307(7), Ir1–P1–N2 126.9(2), Ir1–P1–N1 121.1(2), Ir1–P2–N4 128.9(2), Ir1–P2–N3 119.3(2), N1–P1–N2 93.2(3), N4–P2–N3 92.9(3). Thermal ellipsoids are drawn at the 50% probability level; hydrogen and solvent atoms are omitted, and *i*Pr and *t*Bu groups are drawn in wireframe fashion for clarity.

C–C double bond length in **[SiCSi]IrHCl(coe)** complex (1.409(9) Å) described above. The spectroscopic features on the olefinic groups, such as NMR chemical shifts and structural parameters, can serve as a probe for evaluating the electron density on a metal center. According to the Dewar–Chatt–Duncanson bonding model (Figure 3.2.4), a more electron-rich metal center leads to stronger π-backbonding to the olefin, resulting in a lengthening of the C–C double bond; and in the ^{1}H and ^{13}C{^{1}H} NMR spectra a high-field shift for the chemical shifts corresponding to the olefinic protons and carbon atoms.[127,128] A summary of the chemical shifts (^{1}H NMR spectra are depicted in Figure 3.2.5) and the bond lengths for the olefinic group is reported in Table 3.2.1. Looking at the NMR data, the most shielded values are for the iridium complex bearing the **[SiCSi]** pincer ligand followed by the **[GeCGe]** and **[*i*PrN-PCP]** ligands. Therefore, the σ-donor strength decreases in the following order: **[SiCSi]** > **[GeCGe]** > **[*i*PrN-PCP]** > **[*t*Bu-PCP]**.[†] This result shows the strikingly σ-donor capacity of NHSis and NHGes when compared with phosphine ligands. This led to higher electron rich iridium centers which can be applied in activation of strong bonds (see section 3.3).

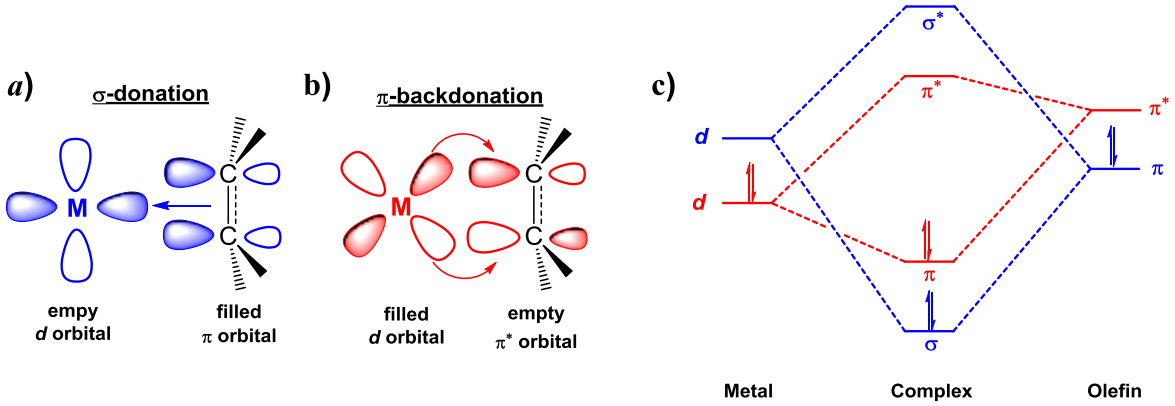

Figure 3.2.4. Dewar-Chatt-Duncanson model for olefin coordination through σ-bonding (*a*) and π-backbonding (b) interactions and the molecular orbital diagram representation (c).[127,128]

[†]The ligand **[*t*Bu-PCP]** is included in this series due to the lack of coordinated *coe* in its complex; it is inferred that the electronic density is not high enough to have a strong π-backbond interaction with the COE.

Table 3.2.1. NMR and XRD selected data for the olefinic group in the *coe* coligand in the **[ECE]IrHCl(coe)** (E = Si^{II}, Ge^{II}) and **[*i*PrN-PCP]IrHCl(coe)** complexes.

Ligand	**[SiCSi]**	**[GeCGe]**	**[*i*PrN-PCP]**
^{1}H NMR (δ, ppm)	3.38	4.06	4.31
$^{13}C\{^{1}H\}$ NMR (δ, ppm)	55.8	65.1	81.6
C–C double bond length (Å)	1.409(9)	N. A.*	1.35(1)

*Not Available.

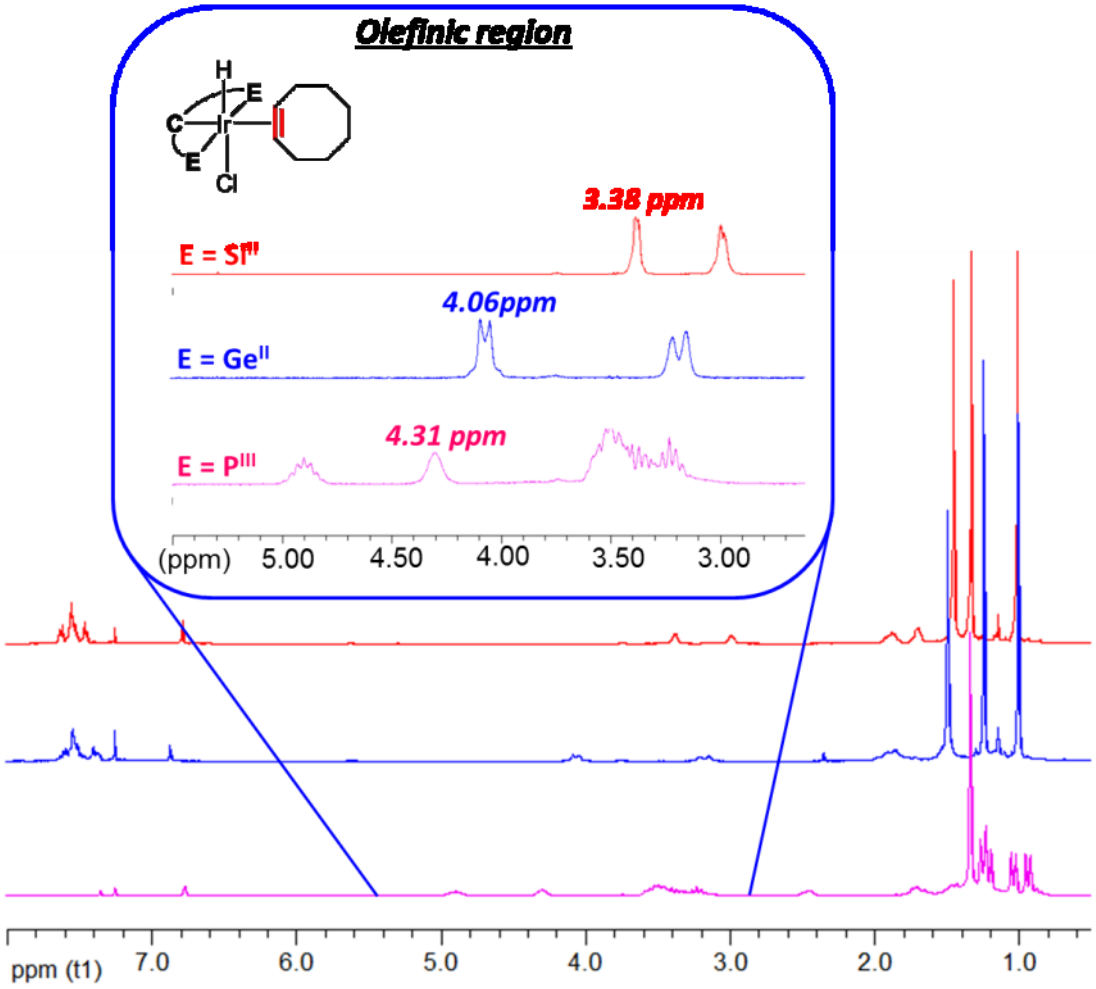

Figure 3.2.5. Stacked ^{1}H NMR spectra for the **[ECE]IrHCl(coe)** (E = Si^{II}: red-top, Ge^{II}: blue-medium) and **[*i*PrN-PCP]IrHCl(coe)** complexes (pink-bottom) in $CDCl_3$. The olefinic region is depited in the inset.

3.2.1.2. Synthesis of the [SiCSi]Ir(H)$_2$(CO) and [SiCSi]Rh(Cl)(H)(PPh$_3$) complexes

With the aim to expand the chemistry and to learn more about the coordination and reactivity of these novel pincer ligands, the reactions with Vaska's [IrCl(CO)(PPh$_3$)$_2$] and [IrH(CO)(PPh$_3$)$_3$] complexes as metal precursors were tested. Reaction of both **ECHE** ligands (E= Si^{II}, Ge^{II}) with [IrCl(CO)(PPh$_3$)$_2$] led to a mixture of undefined products. However, a mixture of **SiCHSi** with [IrH(CO)(PPh$_3$)$_3$] in C_6D_6 at 100 °C for 1 h led to a clean conversion of the starting material to a new hydride species, which exhibit a singlet resonance signal at δ = –10.2 ppm in the ^{1}H NMR spectrum (Scheme 3.2.4). Moreover, in the $^{31}P\{^1H\}$ NMR spectrum the characteristic signal for "free" PPh$_3$ was observed at δ = –5.0 ppm indicating displacement of the PPh$_3$ by the tridentate **[SiCSi]** ligand. After purification, in addition to the hydride signal with a relative integral of two, the signals for the *t*Bu groups were located at δ = 1.34 and 1.82 ppm with relative integration to the hydride of 36:18, respectively.

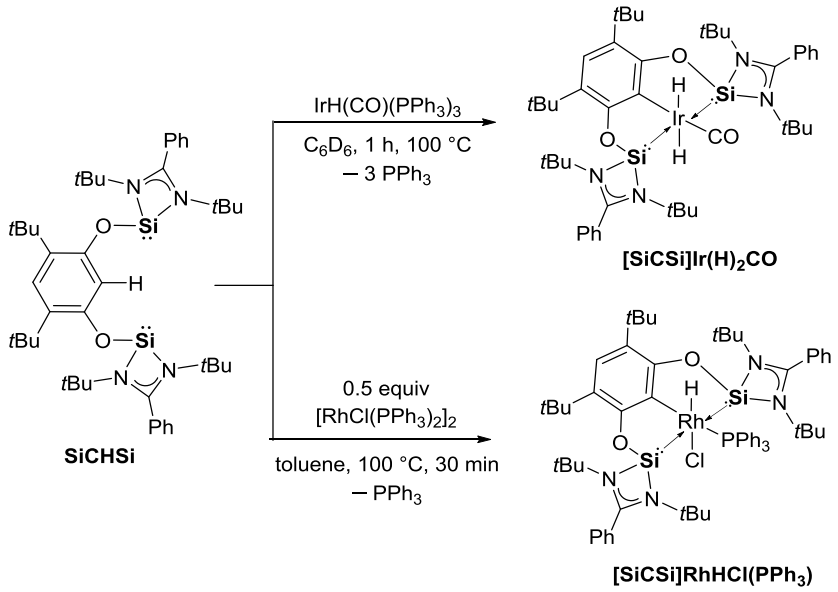

Scheme 3.2.4. Syntheses for the bis(silylene) **[SiCSi]Ir(H)$_2$CO** and **[SiCSi]RhHCl(PPh$_3$)** pincer complexes through an oxidative addition on the C–H bond using IrH(CO)(PPh$_3$)$_3$ and the dimer [RhCl(PPh$_3$)$_2$]$_2$ as Ir^I and Rh^I precursors, respectively.

Additionally, the IR spectrum showed the CO stretching vibration at ν_{C-O} = 1968 cm^{-1} and another weak absorption band for the hydrides at ν_{Ir-H} = 2251 cm^{-1}. These data are in agreement to the postulated **[SiCSi]Ir(H)$_2$(CO)** product which would feature local C_{2v} symmetry (Scheme 3.2.4). The C–O stretching frequency for this complex is close to the range for the Ir^{I} complexes with bis(phosphinite) pincer ligands (1947-1955 cm^{-1}).[129] This is somewhat remarkable due to the electron density of this Ir^{III} center is akin the known Ir^{I} complexes of this type. This shows the higher electron donor properties of these ligands, increasing the electron density in the Ir^{III} center.

Contrary to the reactivity observed for the **SiCHSi**, the NHGe analogue slowly decomposed when heated in solution with [IrH(CO)(PPh$_3$)$_3$] at 100 °C for a prolonged period of time. None of the decomposition products showed any new hydride signals in the hydridic region in the ^{1}H NMR spectrum, indicating that the oxidative addition of the Ir^{I} center to the C–H bond did not occur. This outcome is explained by the lower electron-donating properties of **GeCHGe** compared to **SiCHSi** (see above). That is, initial substitution of two PPh$_3$ ligands by the chelate bis(metallylene) ligand would lead to an intermediate κ^2*E,E'*-[ECHE]IrH(CO)(PPh$_3$) complex, which in the case of **GeCHGe** might not be electron-rich enough to undergo an irreversible C–H oxidative addition reaction to form the expected **[GeCGe]Ir(H)$_2$(CO)** complex.

In contrast to iridium, complexes of rhodium with these novel **ECHE** pincer ligands proved to be more challenging. Reactions conducted with [RhCl(coe)$_2$]$_2$ or [RhCl(CO)$_2$]$_2$ as metal precursors produced undefined reaction mixtures, but Wilkinson's catalyst [RhCl(PPh$_3$)$_2$]$_2$ (generated *in situ*) reacted with the **SiCHSi** ligand to form cleanly a new hydride species. The ^{1}H NMR spectrum showed the C_s symmetry of the expected complex with a doublet of doublets at δ = –17.2 ppm ($^2J_{H-P}$ = 11.0 Hz, $^2J_{H-Rh}$ = 22.1 Hz) for the metal hydride protons and three singlet resonance signals for the *t*Bu groups at δ = 0.90, 1.34 and 1.88 ppm with the same integration each. Moreover, a doublet resonance signal at δ = 36.6 ppm ($^1J_{P-Rh}$ = 97.6 Hz) in the ^{31}P{^{1}H} NMR spectrum, and a doublet of doublets at δ = 66.4 ppm ($^2J_{Si-P}$ = 20.6 Hz, $^1J_{Si-Rh}$ = 59.4 Hz) in the ^{29}Si{^{1}H} NMR spectrum were observed. The ^{29}Si NMR chemical shift to lower field, when compared with "free" ligand (δ = –24.0 ppm) in solution,[92] in addition to the ^{29}Si–^{31}P and ^{29}Si–^{103}Rh coupling, with the P atom from the PPh$_3$ and the Rh center, confirmed the formation of the expected product

(Scheme 3.2.4). Unfortunately, single crystals of this **[SiCSi]RhHCl(PPh$_3$)** product suitable for XRD structure analysis could not be obtained. However, based on the chemical shift for the hydride and the coupling constants $^2J_{H–P}$ and $^1J_{P–Rh}$, sensitive to the TM coordination environment, a structure can be suggested: comparing the values for the coupling constants with the values for the similar **[PCP]RhHCl(PPh$_3$)** complex ($^2J_{H–P}$ = 12.8 Hz, 12.3 Hz; and $^1J_{P–Rh}$ = 111.3 Hz, 82.5 Hz)[130] indicates that the structure of **[SiCSi]RhHCl(PPh$_3$)** is most likely as depicted in Scheme 3.2.4.

3.2.2. Synthesis of the [ECE]NiBr and [*i*PrN-PCP]NiBr complexes

Despite the reactivity of the **SiCHSi** ligand towards Pd(PPh$_3$)$_4$ where a 1,2-hydrogen migration led to a modification of the ligand, alternative synthetic routes were explored for the synthesis of group 10 TM complexes employing these novel ligand systems. Two possible synthetic strategies can be selected with the **ECHE** and **GeCBrGe** ligands. For the former, the use of an excess of a non-nucleophilic base might help in the formation of the envisaged complexes by the C_{ipso}–H bond activation on the arene. For the latter, an oxidative addition of a low-valent TM precursor to the C_{ipso}–Br bond (see Scheme 3.2.2, p. 59) on **GeCBrGe** has been probed.

Reacting [Ni(cod)$_2$] with **GeCBrGe** at room temperature produced immediately a color change from yellow to dark red. However, the ^{1}H NMR spectrum of this mixture showed broad signals indicating the presence of paramagnetic species in the reaction. These undefined species could be formed by a rapid ligand substitution of the the olefin by the NHGe donors. Indeed, controlling the reaction temperature at –30 °C for longer reaction time (8 h) the color changed gradually from yellow to red affording a new diamagnetic species, as determined by ^{1}H NMR spectroscopy. Isolation by extraction and crystallization from *n*-hexane showed the formation of a sole product in quantitative yield. The C_{2v} symmetry determined by the two singlets for the *t*Bu groups at δ = 1.21 and 1.83 ppm with the relative integral ratio of 2:1 and its mass spectrum ($M^{\bullet+}$: exp. 966.20721; calcd. 966.20510) showed unambiguously the formation of the desired **[GeCGe]NiBr** complex (Scheme 3.2.5).

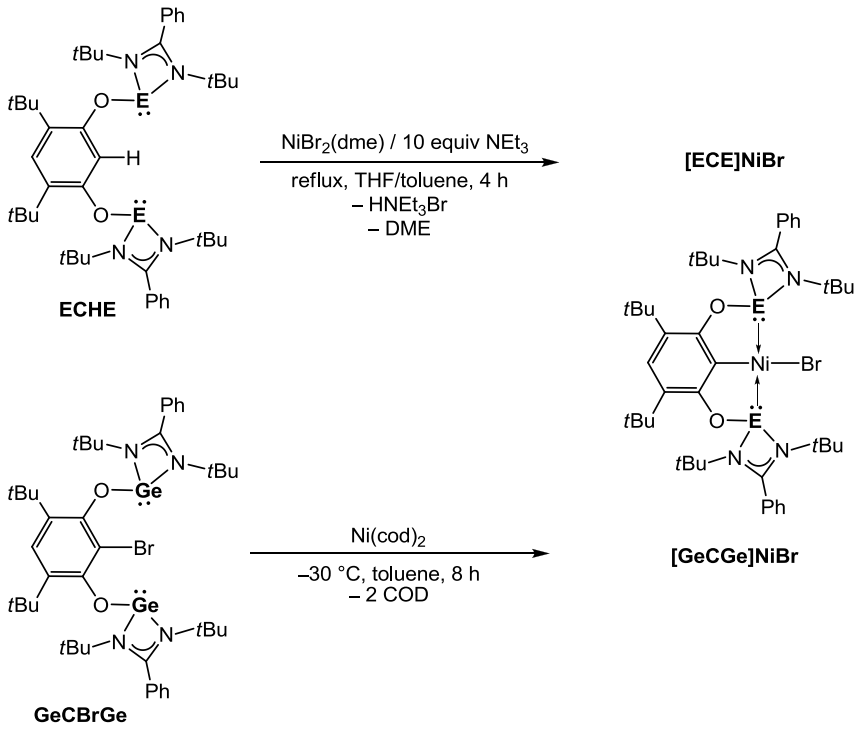

Scheme 3.2.5. Synthesis of the bis(metallylene) **[ECE]NiBr** pincer complexes (E = Si^{II}, Ge^{II}) *via* C–H activation and oxidative addition of nickel to the C–Br bond (cod = 1,5-cyclooctadiene; dme = 1,2-dimethoxyethane).

Due to the elusive preparation of the NHSi homologue of **GeCBrGe**, the C–H activation on the arene was tested for the preparation of the corresponding bis(silylene) nickel complex (Scheme 3.2.5). The reaction between $NiBr_2$(dme) and **SiCHSi** in a solvent mixture THF:toluene (1:1) under reflux and an excess of NEt_3 afforded a color change from dark blue to yellow within 4 h. The ^{1}H NMR spectrum of the isolated Ni complex features the same signal pattern for the **[GeCGe]NiBr** complex obtained by oxidative addition of the C(sp^2)–Br bond described above. The absence of the signal in the ^{1}H NMR spectrum for the aromatic proton between the silylene donor arms, and the sole resonance at δ = 20.2 ppm in the ^{29}Si{^{1}H} NMR spectrum of **[SiCSi]NiBr** are consistent with the formation of the desired pincer complex in addition to its APCI-HRMS ($M^{\bullet+}$: exp. 874.31805; calcd. 874.31774). Moreover, the already described complex **[GeCGe]NiBr** could be synthesized by this method, albeit in lower yield.

The structures of these complexes in the solid state were unambiguously determined by their single crystal XRD structure analysis from single crystals obtained at ambient temperature in concentrated *n*-hexane solutions or by layering toluene solutions of **[SiCSi]NiBr** and **[GeCGe]NiBr** with *n*-hexane, respectively (Figure 3.2.6). Their molecular structures reveal a Ni center in a square planar coordination mode typical for known Ni^{II} pincer complexes bearing phosphorous, carbon or nitrogen as σ-donor atoms.[131] For direct comparison with the well known phosphine pincer ligands, the analogous nickel complex containing the sterically and isoelectronically related ***i*PrN-PCHP** pincer ligand was prepared. Following the nickel metallation procedure for the ligands **ECHE** using [$NiBr_2$(dme)] (Scheme 3.2.5), the **[*i*PrN-PCP]NiBr** complex was obtained in quantitative yield (Figure 3.2.6c). Its ^{1}H NMR spectrum shows the C_{2v} symmetry of the product. It depicts one doublet resonance and one multiplet for the *i*Pr groups at δ = 1.32 and 3.28 ppm, and a singlet resonance for the *t*Bu groups at δ = 1.31 ppm with a relative ratio of 12:2:9. Moreover the ^{31}P{^{1}H} NMR spectrum depicts a single signal at δ = 134.6 ppm, significantly shifted from the free ligand (δ = 118.4 ppm) in solution, indicating its coordination to the Ni^{II} center.

Comparing the structural features for the three Ni complexes **[ECE]NiBr** (E = Si^{II}, Ge^{II}), and **[*i*PrN-PCP]NiBr** all possess a Ni^{II} center in a square planar coordination sphere (Figure 3.2.6). The E–Ni interatomic distances vary in accordance with the covalent radii of the donor atom. This affects the C_{ipso}–Ni bond length owing to the less steric constrain for the bigger donor atom, being in this series the Ge atom (Table 3.2.2). Whereas the difference in the Ni–Br bond length depends on the σ-donor strength of the pincer ligands **[ECE],** being longer for the strongest donating ligand **[SiCSi]** (Table 3.2.2). This is in accordance with the previously established order for the same ligand series on the Ir^{III} olefinic complexes **[ECE]IrHCl(coe)** (E = P^{III} < Ge^{II} ≤ Si^{II}, see section 3.2.1). In addition, in the ^{13}C{^{1}H} NMR spectra the signal for the C_{ipso} nuclei varies accordingly with the electron density on the Ni^{II} center. Then, the more shielded ^{13}C nucleus is the bonded to the higher electron-rich metal center, in this case, in the bis(silylene) complex followed by the bis(germylene) and bis(phosphine) complexes.

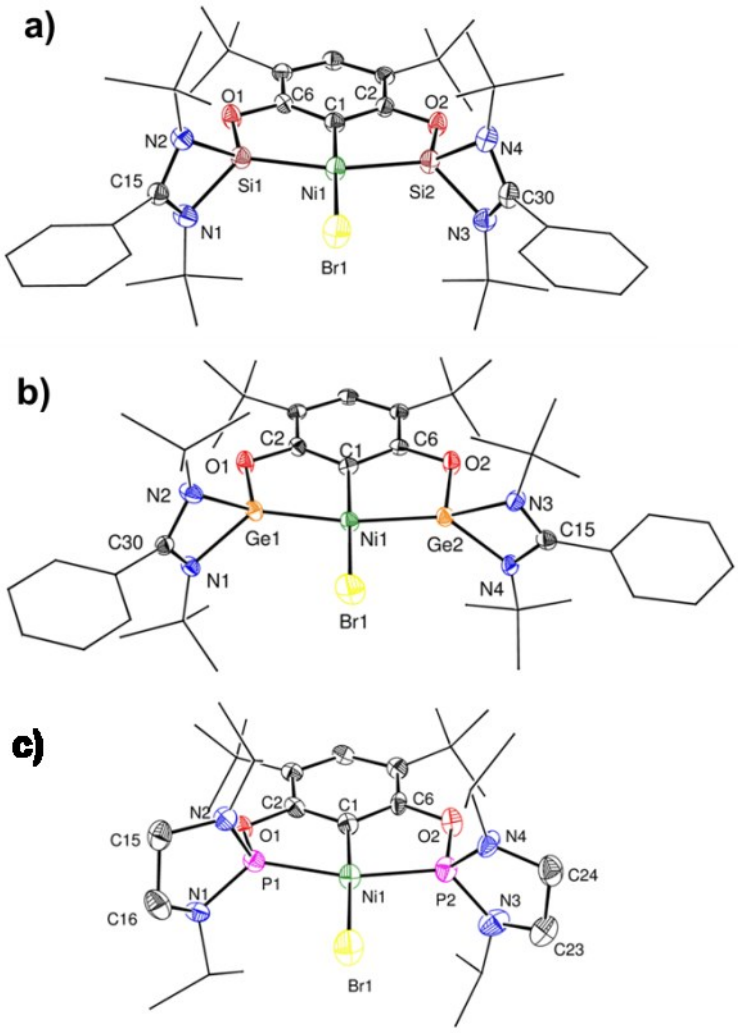

Figure 3.2.6. ORTEP representation in the solid state with selected distances [Å] and angles [°] of a) **[SiCSi]NiBr**: C1–Ni1 1.927(2), Br1–Ni1 2.3410(5), Si1–Ni1 2.1737(7), Si2–Ni1 2.1716(7), C1–Ni1–Br1 178.51(7), Si1–Ni1–Si2 161.75(3), C6–O1–Si1 110.8(1), C2–O2–Si2 110.5(1), Σ<Ni1 360.02(7); b) **[GeCGe]NiBr**: C1–Ni1 1.961(3), Br1–Ni1 2.3351(5), Ge1–Ni1 2.2113(6), Ge2–Ni1 2.2190(6), C1–Ni1–Br1 178.5(1), Ge1–Ni1–Ge2 165.42(2), C2–O1–Ge1 109.9(2), C6–O2–Ge2 110.7(2), Σ<Ni1 360.0(1); c) **[PCP]NiBr**: C1–Ni1 1.881(4), Br1–Ni1 2.3297(7), P1–Ni1 2.136(2), P2–Ni1 2.151(2), C1–Ni1–Br1 178.0(2), P1–Ni1–P2 165.36(5), C2–O1–P1 111.6(3), C6–O2–P2 113.5(3), Σ<Ni1 360.1(1). Thermal ellipsoids are drawn at a 50% probability level; Ph, *t*Bu and *i*Pr groups are drawn in wire frame and hydrogen and solvent atoms are omitted for clarity.

Table 3.2.2. Selected ^{13}C NMR values and bond distances of the donor atoms to the Ni center in the **[ECE]NiBr** complexes.

Complex	**[SiCSi]NiBr**	**[GeCGe]NiBr**	**[*i*PrN-PCP]NiBr**
Ni–E [Å]	2.1737(7), 2.1716(7)	2.2113(6), 2.2190(6)	2.136(2), 2.151(2)
Ni–C_{ipso} [Å]	1.927(2)	1.961(3)	1.881(4)
Ni–Br [Å]	2.3410(5)	2.3351(5)	2.3297(7)
$^{13}C\{^{1}H\}$ NMR δ C_{ipso} [ppm]	131.3	132.3	134.3

These novel complexes are the first examples of bis(metallylenes)-Ni^{II} complexes having a Ni center in oxidation state +2. All reported nickel complexes with either silylenes or germylenes as ligands posses low-valent Ni center (Figure 3.2.7) due to the coexistence of the couple E^{II}–Ni^{II} is not thermodynamically favoured (E = Si, Ge) as demonstrated by Lappert[108] and Heinicke[132] when reacting NHSis and NHGes with group 10 metal salts. Here, it is shown that the C_{ipso}–Ni bond in **[ECE]NiBr** permits the stabilization of the Ni center in the oxidation state +2. This is in contrast with the reported Ni complexes synthesized from the Ni^{II} salts undergoing redox reactions with a silylene (Si^{II}) to produce Ni^{0} and Si^{IV} species[108] (see Scheme 3.2.1, p. 57). Although, the stability in solution of these complexes is medium as observed after more than two weeks a nickel mirror started to be visible in the flask's wall. But in the solid state their stability has been proven for more than a year without any observable decomposition.

The Si–Ni bond distances of 2.1737(7) Å and 2.1716(7) Å in **[SiCSi]NiBr** are slightly shorter than those in the **Ni-3** (2.207(2) Å and 2.216(2) Å)[133] and **Ni-5** complexes (2.1908(7) Å and 2.1969(7) Å, Figure 3.2.7)[87] due to the higher electrophillic character in the Ni^{II} center. Moreover, the Si–Ni bond lengths are in the range of the **Ni-7** complex (2.165(2) Å)[108] but longer than in complex **Ni-9** (2.0597(10) Å).[134] This large difference for the latter is related with the increased π-backdonation from the metal to the ylide-like NHSi.

On the other hand, in the **[GeCGe]NiBr** complex the Ge–Ni bond lengths (2.2113(6) Å and 2.2190(6) Å) are in the range for the germylene→Ni^{0} complexes **Ni-8** (2.2343(4) Å)[132] and **Ni-10-13** (**Ni-10**: 2.283(2) Å;[135] **Ni-11**: 2.2400(16) Å[136]). Only for **Ni-12** and **Ni-13** the Ni–Ge bond length is shorter (2.206(1) and 2.1814(7) Å), respectively.[137] This is mainly

due to the higher π-backdonation from the metal center to the germylene. Suprisingly, the Ni–Ge bond lengths in the **Ni-8** (2.2443(4) Å)[132] and **Ni-11** complexes (2.2400(16) Å)[136] are longer than in the **[GeCGe]NiBr** complex being unexpected for these *non*-base-stabilized germylenes; steric hindrance of the larger substituents on the ligand is most probably the influence for these bond lengths.

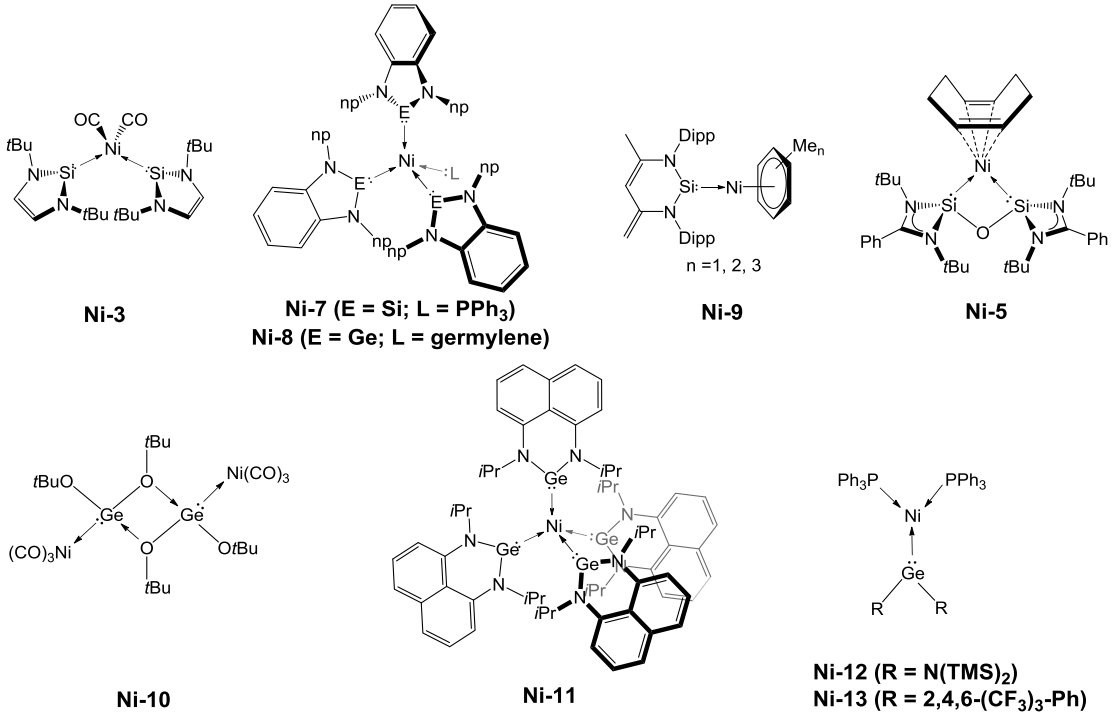

Figure 3.2.7. Reported nickel complexes bearing E–Ni bonds (E = Si^{II}, Ge^{II}).

3.2.3. Synthesis of iron complexes

3.2.3.1. Synthesis of the [ENE]$FeCl_2$ complexes

The syntheses of the neutral pincer ligands of type **ENE** were targeted with the aim to explore the stabilization of low-valent TM centers especially iron as nontoxic, abundant and economical TM. Reaction of the **ENE** pincer ligands (E = Si^{II}, Ge^{II}) with the *in-situ* prepared $FeCl_2$•$(thf)_{1.5}$ adduct afforded yellow solutions at room temperature (Scheme 3.2.6). As expected, the ^1H NMR spectra of the reaction mixtures showed paramagnetism with broad signals at chemical shifts within the δ = –5 to +30 ppm range. Integration of the

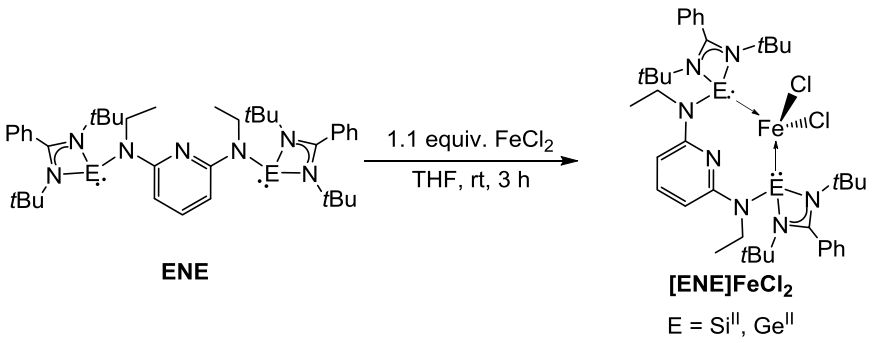

Scheme 3.2.6. Synthesis of the ***κ²E,E'*-[ENE]FeCl₂** complexes (E = Si^{II}, Ge^{II})

paramagnetically shifted signals, however, correlated with all the protons in the desired complexes. Extraction and crystallization in toluene afforded yellow crystals in high yields (> 70%). Their mass spectra (APCI-MS) unambiguously showed the coordination of the iron dichloride to the tridentate ligands forming the **[ENE]FeCl₂** complexes ($M^{\bullet+}$, E = Si^{II}: exp. 807.30914; calcd. 807.30915, E = Ge^{II}: exp. 899.19928; calcd. 899.19765). Surprisingly, after growing suitable crystals for XRD structure analysis, the structure in the solid state showed that the pyridine moiety most likely does not coordinate to the iron center (Figure 3.2.8) with N1–Fe interatomic distances of 3.304 and 3.543 Å, for the bis(silylene) and bis(germylene) complexes, respectively. These distances are larger than the sum of covalent radii for nitrogen and iron, and the complexes are hence better described by ***κ²E,E'*-[ENE]FeCl₂**. This result contrasts to existing Fe^{II} complexes with pyridine-based pincer ligands of type PNP, NNN, CNC, NNP (Figure 3.2.9),[138–140] in which a pentacoordinated iron center is present. This difference might be related to the enhanced σ-donor strength of the **ENE** ligands: first, the stronger σ-donor properties of the metallylenes (cf., section 3.2.1, p. 60) make the iron center more electron rich, possibly impeding 5-fold coordination and preferential tetrahedral coordination. Second, the high *trans* effect for the metallylenes might play a role in favoring the tetrahedral structure at the iron center.

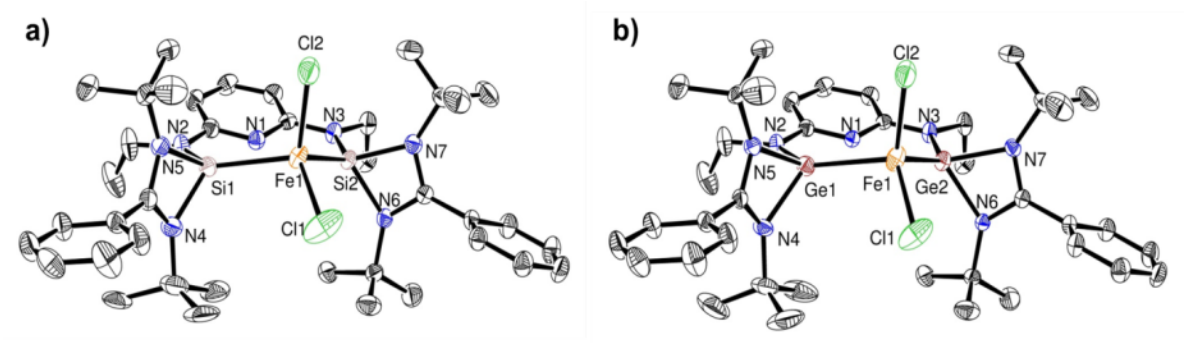

Figure 3.2.8. ORTEP representation of the ***κ²E,E'*-[ENE]FeCl₂** complexes in the solid state. Selected distances [Å] and angles [°]. (a) **E = Si^{II}**: Fe(1)–Si(1) 2.5256(7), Fe(1)–Si(2) 2.5110(7), Fe(1)–Cl(1) 2.2621(8), Fe(1)–Cl(2) 2.2819(8), Si(1)–N(2) 1.761(2), Si(1)–N(4) 1.855(2), Si(2)–N(3) 1.7608(19), Si(2)–Fe(1)–Si(1) 110.04(2), Cl(1)–Fe(1)–Cl(2) 113.23(4), Cl(1)–Fe(1)–Si(1) 110.09(4), Cl(2)–Fe(1)–Si(1) 107.39(3), Cl(1)–Fe(1)–Si(2) 108.82(3), Cl(2)–Fe(1)–Si(2) 107.22(3), N(2)–Si(1)–N(4) 104.93(10), N(4)–Si(1)–N(5) 70.22(9). (b) **E = Ge^{II}**: Fe(1)–Ge(1) 2.5670(4), Fe(1)–Ge(2) 2.5509(4), Fe(1)–Cl(1) 2.2268(7), Fe(1)–Cl(2) 2.2358(7), Ge(1)–N(2) 1.8739(18), Ge(1)–N(4) 1.9795(18), Ge(2)–N(3) 1.8661(16), Ge(2)–Fe(1)–Ge(1) 102.434(13), Cl(1)–Fe(1)–Cl(2) 120.17(3), Cl(1)–Fe(1)–Ge(1) 108.88(3), Cl(2)–Fe(1)–Ge(1) 107.34(2), Cl(1)–Fe(1)–Ge(2) 108.52(2), Cl(2)–Fe(1)–Ge(2) 108.06(2), N(2)–Ge(1)–N(4) 102.00(8), N(4)–Ge(1)–N(5) 65.95(7). Thermal ellipsoids are drawn at the 50% probability level; hydrogen and solvent atoms are omitted for clarity.

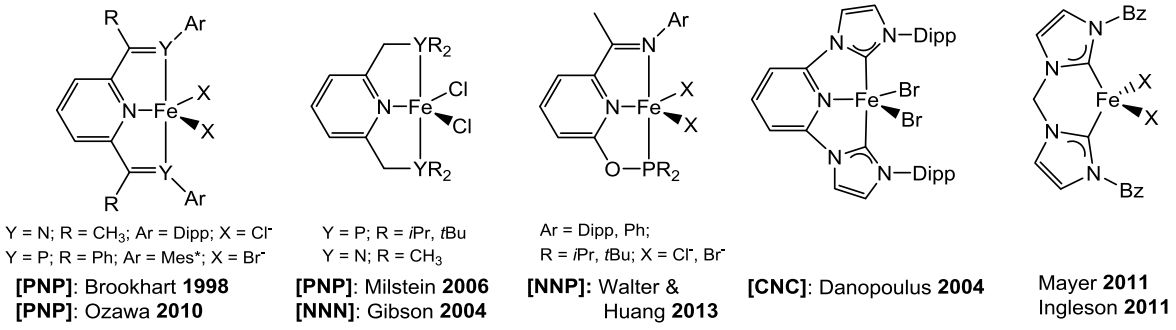

Figure 3.2.9. Some examples for Fe^{II} complexes bearing pincer ligand moieties as well as a chelate bis-carbene ligand for comparison.

The molecular structures depicted in Figure 3.2.8 show that the iron center exhibits a distorted tetrahedral coordination sphere in both complexes, being more similar to the literature examples where bidentate ligands such as bis-carbene (Figure 3.2.9)[139–141] or bis-phosphine[142] are employed. Both complexes crystallized in the monoclinic space group $P2_1/n$ having a C_{2v} symmetry where the vertical plane crosses the iron and chloro atoms. The Fe–Cl bond lengths are within the range of the $FeCl_2$ complexes in a tetrahedral structure, but comparing the ***κ²E,E'*-[ENE]FeCl₂** (E = Si^{II}, Ge^{II}) complexes, there is an elongation in the bond distance of about 3.5-4.6 pm with the silylene as the σ-donor atom. Both structures are equivalent in their coordination sphere; therefore, this elongation is mainly due to the intrinsically higher σ-donor ability of the silylene versus the germylene subunit. This increases the electronic density on the Fe^{II} center decreasing the interaction with the chlorido ligands which is in accord with the previous observations on the iridium and nickel complexes with the monoanionic **[ECE]** ligand (see sections 3.2.1 and 3.2.2).

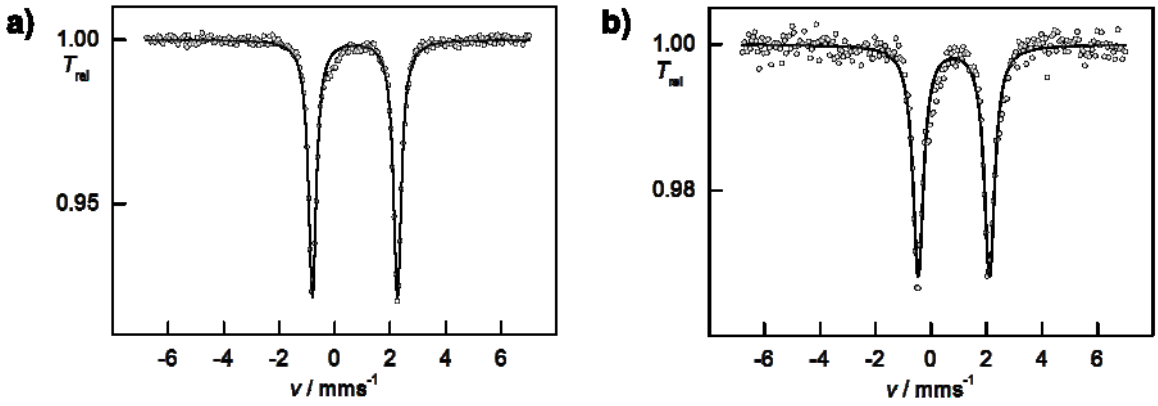

Figure 3.2.10. Zero field ^{57}Fe Mössbauer spectra of complexes ***κ²E,E'*-[ENE]FeCl₂** at 77 K. The circles are experimental data and the lines are the simulated Lorentzian curves. (a) **E = Si^{II}**: δ = 0.73(1) mm s^{-1}, ΔE_Q = 3.06(1) mm s^{-1}, Γ_{FWHM} = 0.34(1) mm s^{-1}. (b) **E = Ge^{II}**: δ = 0.82(1) mm s^{-1}, ΔE_Q = 2.57(1) mm s^{-1}, Γ_{FWHM} = 0.46(1) mm s^{-1}.

The electronic structures of the ***κ²E,E'*-[ENE]FeCl₂** complexes were in addition studied by ^{57}Fe Mössbauer spectroscopy and solution magnetic moment studies (Evans method). From the ^{57}Fe Mössbauer spectra (Figure 3.2.10) the isomer shift (δ) and quadrupole splitting (ΔE_Q) values for these complexes are in accordance with the expected values for

distorted tetrahedral high-spin Fe^{II} complexes, δ = 0.73 mm s^{-1}, 0.82 mm s^{-1} and ΔE_Q = 3.06 mm s^{-1}, 2.57 mm s^{-1}, for E = Si^{II} and Ge^{II}.[139,140,142] This is in agreement with the experimentally determined magnetic moment in solution of μ_{eff} = 4.6 and 4.7 μB for E = Si^{II} and Ge^{II}, respectively, which also correspond to a high-spin S = 2 ground state.[139,143]

3.2.3.2. Synthesis of the [ENE]Fe(PMe$_3$)$_2$ complexes

The reduction of the iron complexes under a nitrogen atmosphere was envisaged to afford homologues of the bis(dinitrogen) iron pincer complexes [NNN]Fe(N_2)$_2$ and [CNC]Fe(N_2)$_2$ (Figure 3.2.11) synthesized by Chirik[16] and Danopoulos.[144] Recently, an arene iron(0) complex stabilized by the bis-carbene ligand [bis-NHC]Fe(η^6-C_7H_8) (bis-NHC = bis-(*N*-Dipp-imidazole-2-ylidene)methylene) was reported in Driess' group[141] and its comparison with its heavier homologues bis(silylene) and bis(germylene) would be also of interest, if isolable. Reduction of the ***κ²E,E'*-[ENE]FeCl$_2$** complexes with KC_8 in

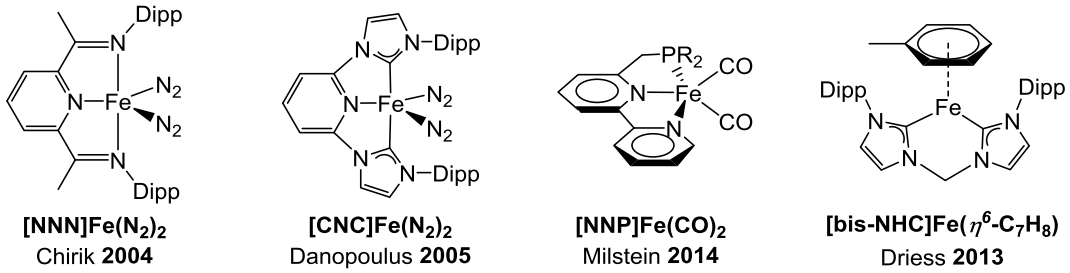

Figure 3.2.11. Examples of isolable iron(0) complexes bearing chelate ligands of type NNN, CNC, NNP and bis-NHC.[16,141,144,152]

toluene/THF produced intense red solutions, although, after work up and several unsuccessful attempts to crystallize a product, a red oil as crude product was obtained. The ^{1}H NMR data suggested a ligand reduction as the major product along with other undefined side products but gave no hint for the formation of neither the desired arene nor the bis-N_2 complex. Based on this result an alternative synthetic route was proposed. The use of a coligand which would possibly better stabilize the expected highly electron-rich iron(0) center after reduction was envisaged. Hence, the use of trimethylphosphane was planned as: i) stabilizing ligand for the expected highly electron-rich Fe^0 complex (assuming innocence of the ligand), and ii) a labile ligand for further reactivity studies, possibly by elimination reaction.

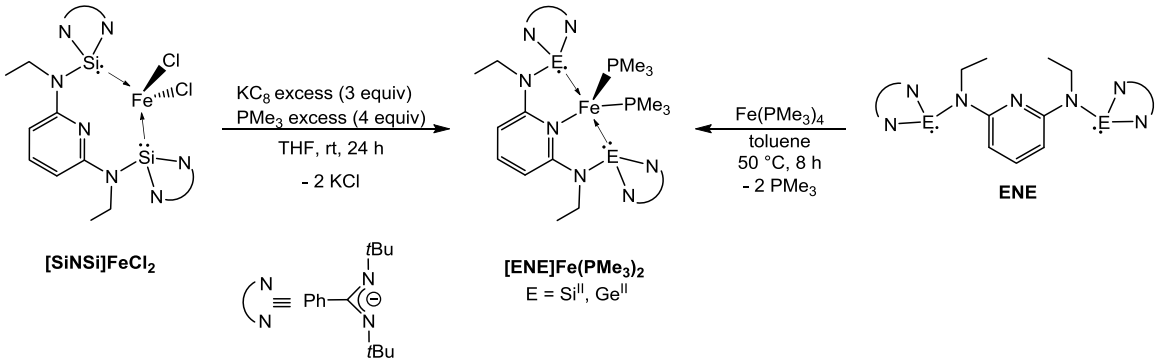

Scheme 3.2.7. Synthesis of the **[ENE]Fe(PMe$_3$)$_2$** pincer complexes (E = Si^{II}, Ge^{II})

Indeed, reduction of ***κ^{2}Si,Si'*-[SiNSi]FeCl$_2$** with KC_8 in THF in the presence of excess of PMe_3 selectively afforded a new diamagnetic species with the tridentate **SiNSi** ligand and two phosphines as coligands: **[SiNSi]Fe(PMe$_3$)$_2$**. The C_s symmetry in solution was revealed collectively by the ^{1}H, ^{29}Si and ^{31}P NMR spectra, all showing the inequivalency of the phosphorus atoms at the iron center (Scheme 3.2.7). The ^{1}H NMR spectrum exhibits two singlet resonance signals at δ = 1.09 and 1.52 ppm, two doublet signals at δ = 1.29 and 1.89 ppm ($^2J_{H–P}$ = 4.0 Hz) and a triplet at δ = 1.58 ppm ($^3J_{H–H}$ = 7.0 Hz) with a relative ratio of 18:18:9:9:6, respectively. These signals were unambiguously assigned by 2D NMR (^{1}H-^{1}H COSY; ^{1}H-^{13}C HMQC; ^{1}H-^{13}C HMBC) correlation spectroscopy in the following order: the non-equivalent *tert*-butyl groups, the PMe_3 coligands and the methyl group from the bound ethyl to the amine. Other aliphatic signals were observed at δ = 3.49 and 3.70 ppm which at the first sight resembled sextets integrating for two protons each. These signals reflect the diastereotopic nature of the protons on the methylene units in the backbone. ^{1}H-^{1}H COSY NMR showed a correlation between both signals as well as in the HSQC ^{1}H-^{13}C only one correlation with the methylene carbon was observed confirming the assignment. The virtual sextet is basically a doublet of quartets with roof effect $\left(\Delta\nu/J = 6,\right.$ $\left.400\ \text{MHz}\right)$,[145] and arises from the value for the $^2J_{H–H}$ coupling (14.0 Hz), being in this case, exactly twice the value for the $^3J_{H–H}$ coupling (7.0 Hz). Moreover, the C_s symmetry for the **[SiNSi]Fe(PMe$_3$)$_2$** complex is also observed at the ^{31}P{^{1}H} and ^{29}Si{^{1}H} NMR spectra. In the former two broad signals at δ = 7.2 and 20.8 ppm highlight the inequivalency of both phosphorus atoms and for the latter a doublet of doublets ($^2J_{Si–P}$ = 22.4 Hz, 91.9 Hz)

centered at δ = 68.3 ppm showed the equivalency for both silicon atoms but with different metric coupling constants to each phosphine.

The reduction of ***κ²Ge,Ge'*-[GeNGe]FeCl₂** by the same synthetic strategy afforded only unwanted side products also observed during the reduction without the presence of PMe_3 in the reaction mixture. As an alternative, employing the iron(0) precursor $Fe(PMe_3)_4$, in a PMe_3 substitution reaction with the **SiNSi** ligand at 50 °C, a species with identical NMR spectra of the **[SiNSi]Fe(PMe₃)₂** complex was observed. This result showed the possibility to form the iron(0) complex bearing NHGes directly from the pincer **GeNGe** ligand. Then, the reaction between the **GeNGe** ligand and $Fe(PMe_3)_4$ at 50 °C also afforded a new diamagnetic dark red species in quantitative yield after 8 h. Extraction with pentane and removal of the solvent by three freeze–pump–thaw cycles afforded a red foamy solid in high purity. Unfortunately, given the high solubility of the **[GeNGe]Fe(PMe₃)₂** complex in aprotic organic solvents such as pentane, hexane, diethyl ether, toluene and THF, its crystallization was unfruitful. The NMR spectra exhibit signals in close analogy to the **[SiNSi]Fe(PMe₃)₂** complex. However, in the $^{31}P\{^1H\}$ NMR spectrum two doublets at δ = 10.2 ppm and 27.2 ppm ($^2J_{P\text{-}P}$ = 20.9 Hz) are observed instead of the broad signals for the **[SiNSi]Fe(PMe₃)₂** complex. This fact might be related to the Berry pseudorotation rate of the phosphines on the iron center (see below VT-NMR studies) as well as the P–Fe–P angle, as it has been previously shown in other bis(phosphine) metal complexes.[146]

Single crystals of **[SiNSi]Fe(PMe₃)₂** suitable for XRD structure analysis were obtained in a *n*-pentane solution at 0 °C after a week. The structural analysis confirms the C_s symmetry of the molecule deduced from the NMR spectra. The geometric features of **[SiNSi]Fe(PMe₃)₂** depict the iron center in a slightly distorted pseudo-square pyramidal (PSQP) coordination environment with τ = 0.18,* with a trimethylphosphane ligand occupying the apical position (Figure 3.2.12). To note, this geometry is unusual for Fe^0 low-spin complexes,[16,148] therefore a careful study was carried out to define its electronic structure by its spectroscopic analysis with ^{57}Fe Mössbauer spectroscopy and DFT calculations (see below). The apical phosphorous atom features a slightly larger bond

*The parameter τ is a relation between the angles in a pentacoordinated metal complex to define its geometry. τ = (β – α)/60, where β is the greatest of the basal angles. For a perfect trigonal bpyramidal geometry β = 180°, α = 60°, then τ = 1. For a perfect square-pyramidal β = 90°, α = 90°, then τ = 0.[147]

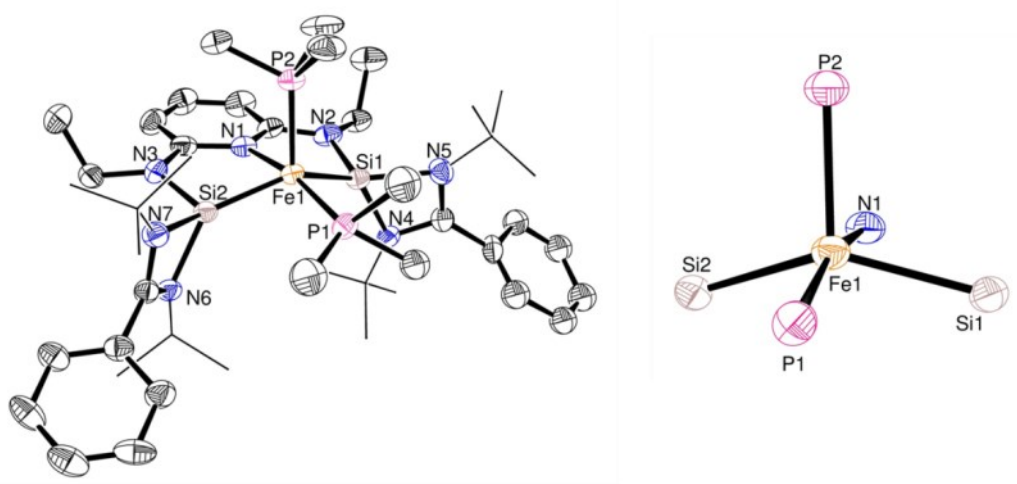

Figure 3.2.12. ORTEP representation of the **[SiNSi]Fe(PMe$_3$)$_2$** complex in the solid state. Selected distances [Å] and angles [deg]. Fe(1)–N(1) 2.059(3), Fe(1)–Si(1) 2.1637(15), Fe(1)–Si(2) 2.1695(13), Fe(1)–P(1) 2.1455(11), Fe(1)–P(2) 2.1881(10), Si(1)–N(2) 1.790(4), Si(2)–N(3) 1.779(3), Si(1)–N(4) 1.927(4), N(1)–Fe(1)–P(1) 165.48(9), N(1)–Fe(1)–Si(1) 80.63(11), N(1)–Fe(1)–Si(2) 80.83(11), N(1)–Fe(1)–P(2) 86.80(9), P(1)–Fe(1)–Si(1) 94.19(5), P(1)–Fe(1)–Si(2) 95.38(5), P(1)–Fe(1)–P(2) 107.71(4), Si(1)–Fe(1)–P(2) 106.23(5), Si(2)–Fe(1)–P(2) 106.31(5), Si(1)–Fe(1)–Si(2) 141.28(5). Thermal ellipsoids are drawn at the 50% probability level; *t*Bu groups are drawn with wireframe and hydrogen atoms are omitted for clarity.

distance to the iron center by 4.26(1) pm compared with the phosphorous atom situated at the equatorial position, and the Fe–P distances are comparable to the Fe^0 complexes with silylene as coligand of type [(dmpe)$_2$Fe(←:Si(X)L)] (L = *N,N'*-di-*tert*-butyl(phenylamidinato), X = Cl, Me, H).[66] Moreover, the Si–Fe bond lengths are within the range with the latter complexes (2.1634–2.200 Å) and shorter when compared with the silylene→Fe(CO)$_4$ complexes reported by West (:Si(N*t*BuCH)$_2$: 2.196 Å)[149] and Roesky ([:Si(O*t*Bu){(N*t*Bu)$_2$CPh}], 2.237(7) Å).[150] Additionally, the bond distances are in fact comparable to the silylene→Fe complex [Cp*Fe(CO)(SiMe$_3$)SiMes$_2$] reported by Tobita and coworkers where a formal double bond was described between the Si and Fe centers,[151] which indicate a potential multiple bond character which will be discussed further during the DFT calculations analysis (see below). The non-innocent behavior of the bis(imino)pyridine ligand used by Chirik and coworkers in the [NNN]Fe(N$_2$)$_2$ complex

(Figure 3.2.11) has been demonstrated and it is best described as an Fe^{II} complex with a dianionic ligand having a radical located on each imino subunit.[17,18] This effect was previously shown to play a role in the bond distances between the metal center with the donor atoms.[17] The N–Fe bond distances in [NNN]Fe$(N_2)_2$ can therefore be thought as a N–Fe^{II} bonding situation changing the nature of the expected N–Fe^0 bond. Recently, Milstein and coworkers[152] reported a series of dicarbonyl iron complexes stabilized by a bipyridine phosphine pincer ligand [NNP]Fe$(CO)_2$ (Figure 3.2.11), where the innocent behavior of their ligand systems was demonstrated. For their examples the $N_{centered}$–Fe bond distance is shorter within a difference of 11–13 pm than in the **[SiNSi]Fe$(PMe_3)_2$** complex. This difference is related with the strong Fe→CO π-backbond. Comparisons to these well-defined complexes showed the **[SiNSi]** and **[GeNGe]** ligand systems most likely as innocent since bond distances are within narrow limits of actual Fe^0 complexes.

The low symmetry of the molecule in the solid state and in solution led to explore the possibility whether the C_s symmetry of the unusual PSQP iron complex is simply a conformer in equilibrium with the higher (C_{2v}) symmetric system in a trigonal bipyramidal (TBP) conformation. For this purpose, variable temperature ^1H and $^{31}P\{^1H\}$ NMR (VT-NMR) experiments were carried out for both iron **[ENE]Fe$(PMe_3)_2$** complexes (E = Si^{II}, Ge^{II}). Remarkably the C_s symmetry remains for the entire temperature range without observing any Berry pseudorotation on the ligand system, even at rather high temperatures! (Figure 3.2.13). Along the literature reported iron complexes, the complexes reported here represent the first examples of configurationally stable PSQP Fe^0 complexes: even after heating at 70 °C for > 7 days, no changes were observed in the ^1H and $^{31}P\{^1H\}$ NMR spectra. The remarkable stability of the PSQP over the TBP conformer is likely controlled by sterics: the high steric demand on the substituents on the pincer backbone, likely play a role in the stabilization of this iron center thereby freezing out the trimethylphosphane coligands in the molecule.

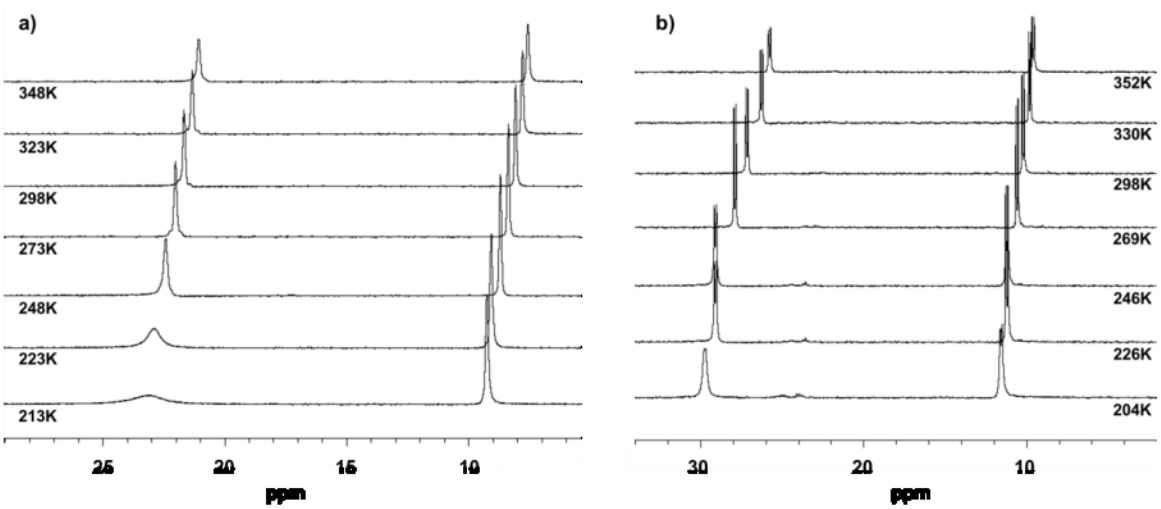

Figure 3.2.13. Stacked variable temperature $^{31}P\{^{1}H\}$ NMR in d_8-toluene for (a) **[SiNSi]Fe(PMe$_3$)$_2$,** and (b) **[GeNGe]Fe(PMe$_3$)$_2$.**

3.2.3.3. Electronic structure of the [ENE]Fe(PMe$_3$)$_2$ complexes

The diamagnetic ^{1}H NMR spectrum of **[SiNSi]Fe(PMe$_3$)$_2$** in C_7D_8 (Figure 3.2.14) reveals exclusively signals in the diamagnetic spectral window. A doublet resonance at δ = 5.95 ppm ($^{3}J_{H\text{-}P}$ = 8.0 Hz) corresponding to the proton at the *meta* position on the pyridine moiety and a triplet of doublets at δ = 7.18 ppm ($^{3}J_{H\text{-}P}$ = 8.0 Hz, and long range coupling $^{6}J_{H\text{-}P}$ = 1.8 Hz) which corresponds to the proton at the *para* position of the pyridine backbone are observed. This is in close agreement with the signals observed by Danopolous on pyridine in the [CNC]Fe$(N_2)_2$ complex[144] but not with the reduced bis(imino)pyridine ligand used by Chirik in [NNN]Fe$(N_2)_2$[16] (Figure 3.2.11) where large isotropic shifts were observed. This result points to the innocent behavior of the **ENE** ligands; which was additionally confirmed by ^{57}Fe Mössbauer spectroscopy and DFT studies (see below).

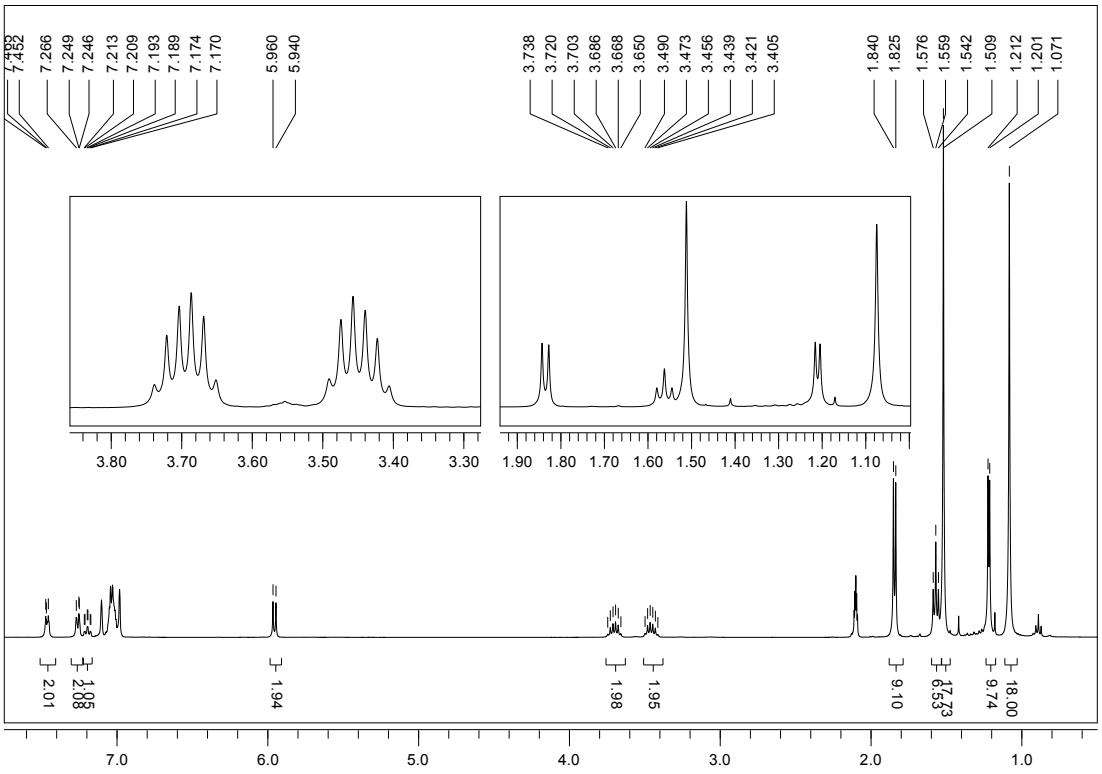

Figure 3.2.14. ^{1}H NMR spectrum of the **[SiNSi]Fe(PMe$_3$)$_2$** complex in C_7D_8 at 298 K with the aliphatic region depicted in the insets (for the signals assignment see discussion in p. 80 and Scheme 3.2.7).

The isomer shifts and quadrupole splitting found for **[ENE]Fe(PMe$_3$)$_2$** in the ^{57}Fe Mössbauer spectra at 77 K (E = Si^{II}: δ = 0.24(1) mm s^{-1}, ΔE_Q = 1.66(1) mm s^{-1}; E = Ge^{II}: δ = 0.36(1) mm s^{-1}, ΔE_Q = 1.87(1) mm s^{-1}) are in the range expected for iron(0) complexes in a pentacoordinated environment (Figure 3.2.15). It is worth mentioning that these values are strongly dependent on the nature of the donor atoms and on the coordination symmetry around the iron center. Thus, a meaningful comparison can only be carried out with those iron complexes having similar structural environment (e.g. pincer moiety, pentacoordinated systems) and donor atoms (i.e. σ-donors). Table 3.2.3 shows a comparison with some reported five-coordinate iron(0) complexes with similar features to these novel complexes. Comparing the **[ENE]Fe(PMe$_3$)$_2$** complexes with those with PSQP structure, i.e., [PDI]Fe(N_2)$_2$ and [PDI]Fe(depe), the ΔE_Q is somewhat similar to the latter since the electronic structure and donor atoms are closely related to the evaluated complexes. The compounds (dmpe)$_2$Fe(:SnClAr), (depe)$_2$FeN_2 bearing a TBP structure have more

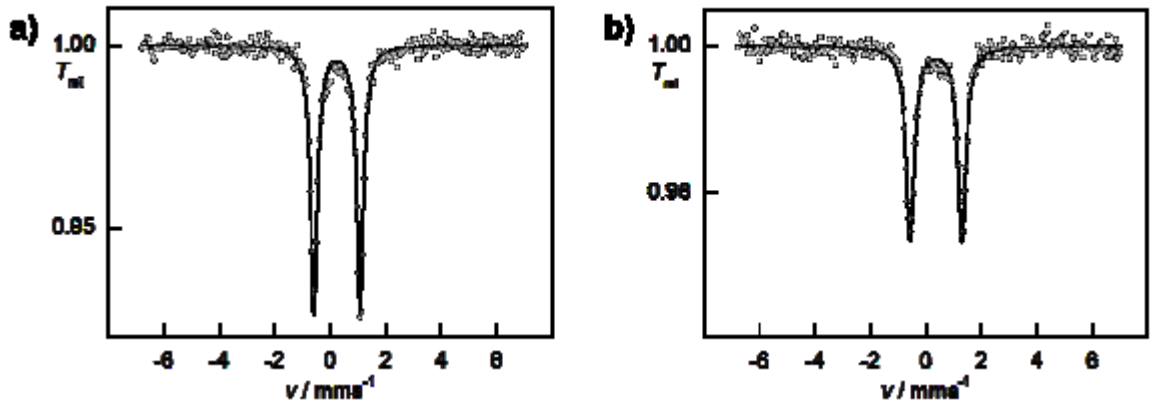

Figure 3.2.15. Zero field ^{57}Fe Mössbauer spectra of **[ENE]Fe(PMe$_3$)$_2$** complexes at 77K. The circles are experimental data and the lines the simulated Lorentzian curves. a) **E = Si^{II}**: δ = 0.24(1) mm s^{-1}, ΔE_Q = 1.66(1) mm s^{-1}, Γ_{fwhm} = 0.30 (1) mm s^{-1}. b) **E = Ge^{II}**: δ = 0.36(1) mm s^{-1}, ΔE_Q = 1.87(1) mm s^{-1}, Γ_{fwhm} = 0.35(1) mm s^{-1}.

Table 3.2.3. Zero field Mössbauer parameters for iron(0) complexes bearing pincer-like phosphane and metallylene arms.

compound	δ (mm s^{-1})	ΔE_Q (mm s^{-1})	ref
[SiNSi]Fe(PMe$_3$)$_2$	0.24(1)	1.66(1)	this work
[GeNGe]Fe(PMe$_3$)$_2$	0.36(1)	1.87(1)	this work
[PDI]Fe(N$_2$)$_2$[a]	0.39	0.53	17
[PDI]Fe(depe)[b]	0.33	1.43	154
[PDI]Fe(PEt$_3$)N$_2$	0.30	1.04	154
(dmpe)$_2$Fe(:SnClAr)[c]	0.31	1.00	155
(depe)$_2$FeN$_2$	0.24	2.14	155
[PNN]Fe(CO)$_2$	0.02 (P(*t*Bu)$_2$) 0.04 (P(Ph)$_2$)	1.49 1.93	152
[CNC]Fe(N$_2$)$_2$[d]	0.27	0.69	153
[CNC]Fe(CO)$_2$[d]	– 0.10	0.62	153

[a]Intermediate state Fe^{II} with diradical ligand PDI*. [b]depe = bis(diethylphosphino)ethane. [c]dmpe = bis(dimethylphosphino)ethane. [d]Mixed state Fe^{II}↔Fe^0 with anion centered at the pyridine.

differentiated ΔE_Q values depending on the type of chelate ligands and donor atoms. Moreover, the dinitrogen complex [PDI]Fe(PEt$_3$)N$_2$ with a PSQP structure shows a strong effect from the dinitrogen as coligand since its value is lower than the [PDI]Fe(depe). Very recently, Chirik and co-workers extended the understanding on the electronic structure of

[CNC]Fe$(N_2)_2$ (Figure 3.2.11, Table 3.2.3), synthesized by Danopoulous *et al*.[144] observing a redox non-innocent behavior for this bis(carbene)pyridine ligand. Therefore, the electronic structure for this complex is better described as a mixed oxidation state on the Fe center (+2 and 0) with a radical located on the pyridine backbone [CNC]$Fe^0(N_2)_2$ ↔ [CNC]$Fe^{II}(N_2)_2$.[153] Table 3.2.3 shows the Mössbauer values for this complex as well as its biscarbonyl [CNC]Fe$(CO)_2$ complex. Comparing the ΔE_Q values for the **[ENE]Fe(PMe$_3$)$_2$** and these bis(carbene)pyridine iron complexes there is a large difference but not with the well-defined biscarbonyl Fe^0 complexes [NNP]Fe$(CO)_2$[152] (Figure 3.2.11) bearing the innocent phosphine-bipyridine PNN ligand. This points out that the electronic structures for the novel Fe^0 complexes, reported here, are more related with Fe^0 center rather than a mixed $Fe^{II} \overset{2e^-}{\longleftrightarrow} Fe^0$ oxidation states.

The δ value can be directly related to the s-electron density, thus giving insights into the oxidation state of the Fe center. For the examples shown in Table 3.2.3, the complexes bearing CO as coligands show a major influence on the isomer shifts due to the strong π-back-bonding interaction, which affects dramatically the s-electron density at the iron centers, and lower value for δ (0.02, 0.04 mm s^{-1}). For the other complexes the δ values are within the same range as for the bis(metallylene)pyridine iron complexes showing their similarities on the electronic structure at the Fe center. In particular, **[SiNSi]Fe(PMe$_3$)$_2$** exhibits the same δ value (0.24 mm s^{-1}) as that of (depe)$_2$Fe(N_2), which is a good reference of a pentacoordinate Fe^0 complex. The **[GeNGe]Fe(PMe$_3$)$_2$** complex has a notably higher δ value (0.36 mm s^{-1}) which is related to the reduced σ-donor strength of Ge vs. Si (see section 3.2.1) resulting in a lower effective s-electron density at the iron center and a concomitant increase in δ, as observed. Hence, there appears to be some correlation of the δ values for **[ENE]Fe(PMe$_3$)$_2$** (E = Si^{II}, Ge^{II}) and other Fe^0 complexes with comparable ligand arrangements. In conclusion, the comparison of the ^{57}Fe Mössbauer parameters with reported values for isolated and isostructural Fe^0 and Fe^{II} complexes clearly supports that the **[ENE]Fe(PMe$_3$)$_2$** (E = Si^{II}, Ge^{II}) complexes show similar features with other pentacooordinate Fe^0 complexes, again pointing to the innocent nature of the **ENE** ligands.

To further elucidate the electronic structure of the metal center detailed density functional theory (DFT) calculations were conducted at the B3LYP/6-31G(d)/LANL2DZ [Fe] level of theory, to conclusively define the redox innocence/non-innocence of the ligand. The calculations were focused mostly on atomic charges from natural bond orbital (NBO) analysis and the Wiberg bond index (WBI) to define the bonding situation within a complex. A summary of the theoretical values is presented in Table 3.2.4.

Table 3.2.4. NBO Charge and Wiber Bond Index Analyses for [SiNSi]Fe(PMe_3)$_2$

NBO Charge		Wiberg Bond Index	
Fe1	–1.897	Fe-Si	1.102
Si1	+1.617		1.115
Si2	+1.606	Fe-N	0.456
P1	+1.276		
P2	+1.249	Fe-P	0.808
N1	–0.458		0.857

The bonds with the Fe center are heavily polarized according to the NBO charges on each donor atom which is indicative of low valence (zero valence) at the Fe center. Moreover, the WBIs differ for each donor atom with the Fe center. The WBI can be considered as an underestimation of bond order in polar bonds, and the values for the Fe–Si bonds (WBI >1) therefore indicate some multiple-bonding character.[156] The molecular orbitals (MOs) HOMO and HOMO–1, show the multiple bonding character for the Fe–Si bond through a π-back-donation between the distorted $d_{x^2-y^2}$ and d_{yz} from the Fe center to the 3p orbitals from the Si^{II} atoms (Figure 3.2.16). This is in agreement with the short Fe–Si bond distance in the crystal structure and comparable to the previously reported [(dmpe)$_2$Fe(←:Si(X)L)] (L = *N,N'*-di-*tert*-butyl(phenylamidinato), X = Cl, Me, H) complexes, where a related multiple-bonding character between the Fe and Si was observed.[66] The other filled MOs, HOMO–2 and HOMO–3, are metal centered (d_{xy} and d_{xz} orbitals). The σ-donation from Si→Fe is observed but at lower energy (HOMO–9) showing the stability of this bond, mediated by the d_{z^2} orbital from the metal center and the s-like orbital from the silylene. The DFT calculations highlight that none of the frontier orbitals show any buildup of electron density on the ligands and, thus, convincingly show that the

ENE ligands are innocent. This is in accord with the ^{57}Fe Mössbauer spectra, the X-ray structural data, and the observed diamagnetic NMR spectra (see above).

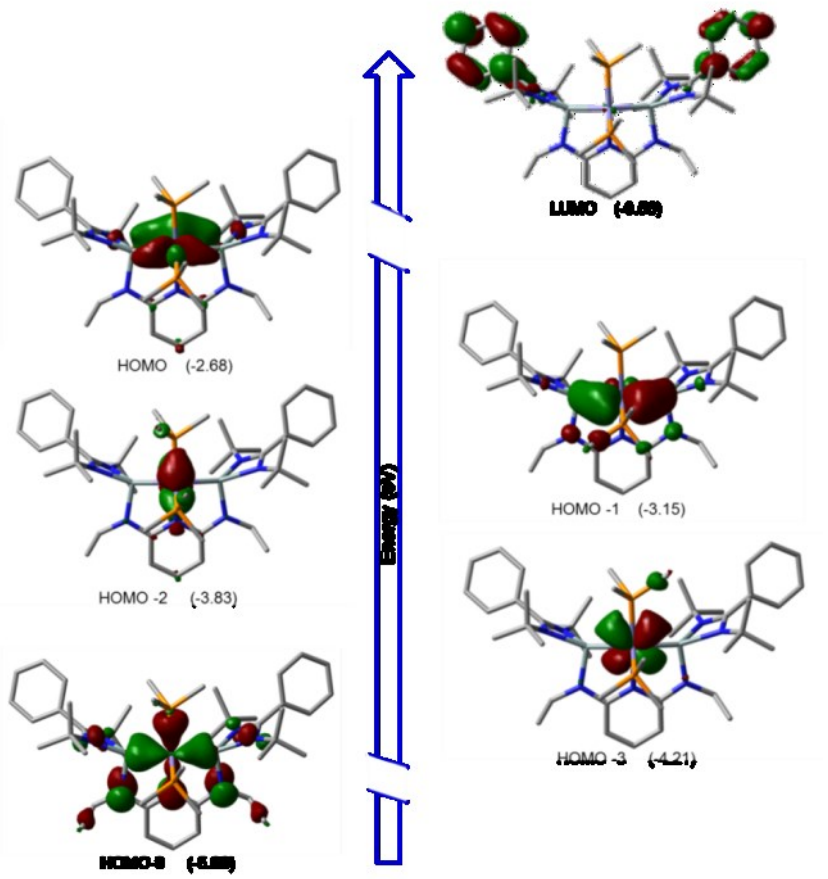

Figure 3.2.16. Selected molecular orbitals for the **[SiNSi]Fe(PMe$_3$)$_2$** calculated at the B3LYP/6-31G(d)/LANL2DZ [Fe] level of theory.

To gain further insights into the electronic nature at the Fe^0 center in the complexes described above, ligand substitution reactions of the **[ENE]Fe(PMe$_3$)$_2$** complexes with CO (Scheme 3.2.8) to use it as a probe in the IR spectrum. Stirring pentane solutions overnight of the iron complexes under CO atmosphere afforded substitution of the PMe$_3$ ligands by CO. However, the reaction consistently produced a mixture of two compounds: the disubstituted **[ENE]Fe(CO)$_2$** as major product and trisubstituted ***κ^{2}E,E'*-[ENE]Fe(CO)$_3$**, as observed in the single crystal XRD analysis (Figures 3.2.17 and 3.2.18). For the case of E = Ge^{II} another complex having one phosphine ***κ^{2}Ge,Ge'*-[GeNGe]Fe(CO)$_2$PMe$_3$**, could also be isolated as a side product cocrystallized with **[GeNGe]Fe(CO)$_2$** (Figure 3.2.19).

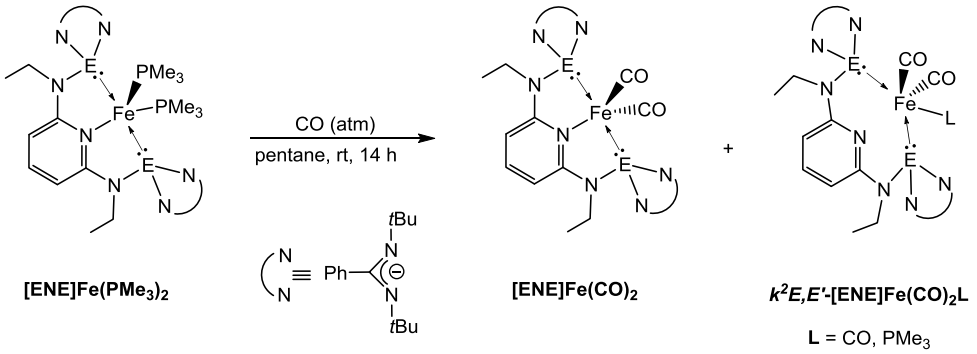

Scheme 3.2.8. Phosphine substitution reaction of **[ENE]Fe(PMe$_3$)$_2$** (E = Si^{II}, Ge^{II}) by CO

Along the different families of pincer ligands of type **PNP**, **CNC** and **NNN** this reactivity of coordination lability on the N-pyridine has not been observed before. This might be consequence of the strong σ-donor capacity on these novel **ENE** ligand systems. Therefore, in this case the higher electron density at the iron center is stabilized by the extra π-acceptor ligand CO. The high *trans* effect from the metallylenes, discussed previously for the Fe^{II} complexes, might favor the formation of the TBP configuration with both metallylenes in a *cis* configuration at an equatorial and an apical positions on the five-coordinate Fe^0 center (Figures 3.2.18 and 3.2.19). These complexes, moreover, are thermally robust without observing decomposition in solutions at 70 °C after 7 days. However, after heating for one day, solutions containing ***κ^{2}Ge,Ge'*-[GeNGe]Fe(CO)$_2$PMe$_3$** liberate PMe$_3$, through intramolecular coordination of the N atom at the pyridine backbone to iron, to give **[GeNGe]Fe(CO)$_2$**. This result suggests that the formation of the disubstituted carbonyl complex most likely does not proceed through the intermediate ***κ^{2}E,E'*-[ENE]Fe(CO)$_3$** but it does through the κ^2 intermediate ***κ^{2}E,E'*-[ENE]Fe(CO)$_2$(PMe$_3$)** possessing a phosphine ligand as represented in Scheme 3.2.9.

The **[ENE]Fe(CO)$_2$** complexes (E = Si^{II} and Ge^{II}) exhibit a C_{2v} symmetry in solution according to their NMR spectra, which is consistent with a TBP structure, contrary to the PSQP structure in the precursor **[ENE]Fe(PMe$_3$)$_2$** complexes. Single crystal XRD structural analyses revealed that both **[ENE]Fe(CO)$_2$** complexes (E = Si^{II} and Ge^{II}) possess a TBP structure in the solid state. The Fe–Si and Fe–N bond distances are largely invariant with the CO substitution (Fe1–N1 2.059(3) vs. 2.089(4) Å, Fe1–Si1 2.1637(15) vs. 2.1579(15) Å, Fe1–Si2 2.1695(13) vs. 2.1664(15) Å), and the electronic structure is comparable

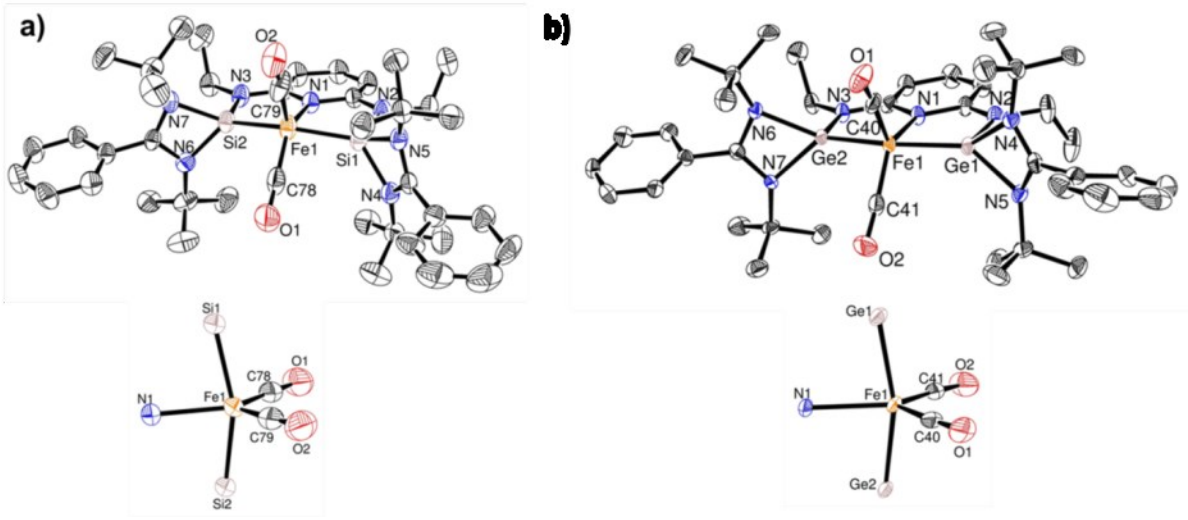

Figure 3.2.17. ORTEP representation of the **[ENE]Fe(CO)$_2$** complexes in the solid state. Selected distances [Å] and angles [°]: **a) E = Si^{II}**: Fe(1)–C(78) 1.701(6), Fe(1)–C(79) 1.759(7), Fe(1)–N(1) 2.089(4), Fe(1)–Si(1) 2.1579(15), Fe(1)–Si(2) 2.1664(15), Si(1)–N(2) 1.757(4), Si(1)–N(4) 1.865(5), Si(2)–N(3) 1.747(4), O(1)–C(78) 1.192(7), O(2)–C(79) 1.168(8), C(78)–Fe(1)–C(79) 114.7(3), C(78)–Fe(1)–N(1) 131.8(3), C(79)–Fe(1)–N(1) 113.5(3), C(78)–Fe(1)–Si(1) 90.85(19), C(79)–Fe(1)–Si(1) 98.33(19), N(1)–Fe(1)–Si(1) 81.36(12), C(78)–Fe(1)–Si(2) 91.82(19), C(79)–Fe(1)–Si(2) 99.49(19), N(1)–Fe(1)–Si(2) 81.33(11), Si(1)–Fe(1)–Si(2) 158.95(7). **b) E = Ge^{II}**: Fe(1)–C(41) 1.718(5), Fe(1)–C(40) 1.750(6), Fe(1)–N(1) 2.156(4), Fe(1)–Ge(1) 2.2086(9), Fe(1)–Ge(2) 2.2092(9), Ge(1)–N(2) 1.880(4), Ge(1)–N(4) 1.994(4), Ge(2)–N(3) 1.870(4), O(1)–C(40) 1.164(7), O(2)–C(41) 1.189(7), C(41)–Fe(1)–C(40) 113.8(3), C(41)–Fe(1)–N(1) 126.8(2), C(40)–Fe(1)–N(1) 119.35(19), C(41)–Fe(1)–Ge(1) 97.06(17), C(40)–Fe(1)–Ge(1) 93.56(16), N(1)–Fe(1)–Ge(1) 82.06(11), C(41)–Fe(1)–Ge(2) 90.51(17), C(40)–Fe(1)–Ge(2) 96.20(16), N(1)–Fe(1)–Ge(2) 82.15(11), Ge(1)–Fe(1)–Ge(2) 164.04(4). Thermal ellipsoids are drawn at the 50% probability level; hydrogen and solvent atoms are omitted for clarity.

to the **[ENE]Fe(PMe$_3$)$_2$** complexes calculated by DFT (Figure 3.2.20); this confirms that the high stability of the PSQP structure for the **[ENE]Fe(PMe$_3$)$_2$** is dominated by sterics and not by electronics at the Fe center. A summary of the bond distances and the IR stretching frequencies for the **[ENE]Fe(CO)$_2$** and similar reported pincer complexes is

presented in Table 3.2.5. Comparing the values for the CO stretching frequencies, lower frequencies were observed for the novel **[ENE]Fe(CO)$_2$** (E = Si^{II} and Ge^{II}) complexes as well as an elongation of the C–O bond distance, indicating the higher σ-electron donor abilities for Si^{II} and Ge^{II} due to the strong Fe → CO π-back-bonding interactions. This is consistent with a more electron-rich Fe^0 center for E = Si^{II} and Ge^{II} as compared to the analogous complexes with E = C^{II}, P^{III}, and N^{III} donor atoms, once more pointing out the innocent behavior of these novel ligands.

Table 3.2.5. Comparison for the CO ligands in pincer complexes by structural and spectroscopic means.

Compound	IR υ_{CO} (cm^{-1})	XRD C–O (Å)	ref
[SiNSi]Fe(CO)$_2$	1830, 1778	1.192(7), 1.168(8)	this work
[GeNGe]Fe(CO)$_2$	1855, 1805	1.189(7), 1.164(7)	this work
[CNC]Fe(CO)$_2$	1928, 1865	1.161	144
[NNN]Fe(CO)$_2$	1974, 1914	1.147(2)	16,157
[PNP]Fe(CO)$_2$	1950, 1894	1.1734(11)	157
[*i*Pr-PNN]Fe(CO)$_2$	1895, 1838	1.1580(17), 1.1615(15)	152

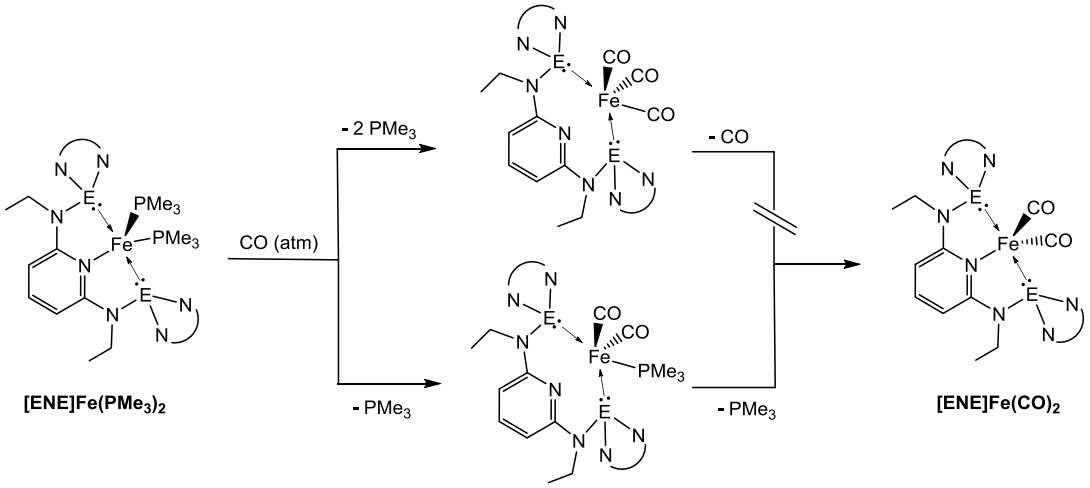

Scheme 3.2.9. Competitive pathways in the PMe$_3$ substitution reaction showing that ***κ*^{2}*E,E'*-[ENE]Fe(CO)$_2$PMe$_3$** is the most likely intermediate for the formation of the **[ENE]Fe(CO)$_2$** complexes.

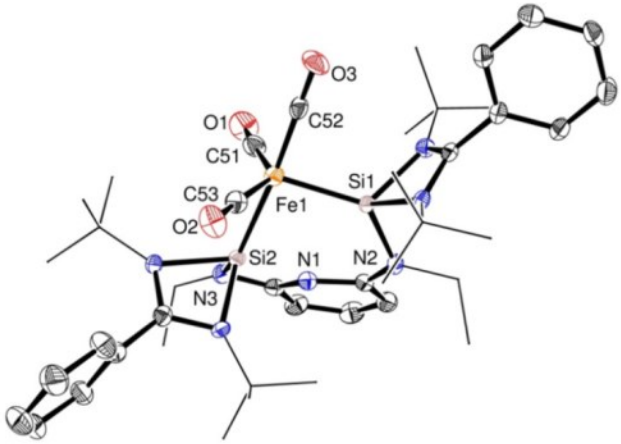

Figure 3.2.18. ORTEP representation of the **[SiNSi]Fe(CO)$_3$** complex in the solid state. Selected distances [Å] and angles [°]: Fe(1)–C(51) 1.751(4), Fe(1)–C(52) 1.757(4), Fe(1)–C(53) 1.762(4), Fe(1)–Si(1) 2.1963(12), Fe(1)–Si(2) 2.2945(12), O(1)–C(51) 1.164(5), O(2)–C(53) 1.168(5), O(3)–C(52) 1.162(5), Si(1)–N(2) 1.791(3), Si(2)–N(3) 1.825(3), C(51)–Fe(1)–C(52) 96.38(19), C(51)–Fe(1)–C(53) 136.5(2), C(62)–Fe(1)–C(61) 94.45(18), C(51)–Fe(1)–Si(1) 109.80(15), C(52)–Fe(1)–Si(1) 87.97(13), C(53)–Fe(1)–Si(1) 112.56(13), C(51)–Fe(1)–Si(2) 81.90(14), C(52)–Fe(1)–Si(2) 176.10(13), C(53)–Fe(1)–Si(2) 84.50(13), Si(1)–Fe(1)–Si(2) 95.90(4). Thermal ellipsoids are drawn at the 50% probability level; hydrogen and solvent atoms are omitted and, *t*Bu and Et groups are drawn in wireframe for clarity.

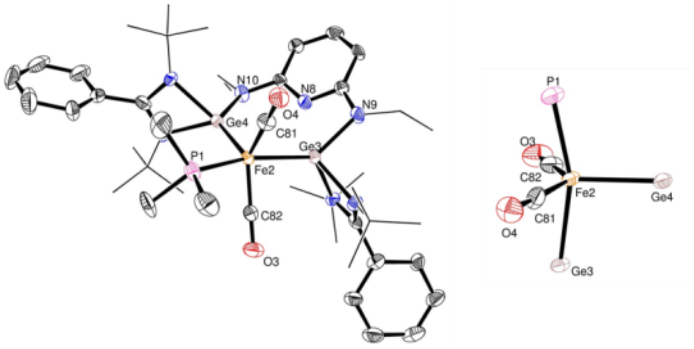

Figure 3.2.19. ORTEP representation for the **[GeNGe]Fe(CO)$_2$PMe$_3$** complex in the solid state (co-crystallized in the same crystal with complex **[GeNGe]Fe(CO)$_2$**). Selected distances [Å] and angles [°]: Fe(2)–C(81) 1.755(5), Fe(2)–C(82) 1.754(5), Fe(2)–P(1) 2.1381(15), Fe(2)–Ge(3) 2.2767(9), Fe(2)–Ge(4) 2.2956(9), Ge(3)–N(9) 1.918(4), Ge(4)–N(10) 1.948(4), O(4)–C(81) 1.166(7), C(82)–O(3) 1.164(7), C(81)–Fe(2)–C(82) 135.1(3), C(81)–Fe(2)–P(1) 87.46(18), C(82)–Fe(2)–P(1) 87.43(17), C(81)–Fe(2)–Ge(3) 86.30(18), C(82)–Fe(2)–Ge(3) 84.40(17), P(1)–Fe(2)–Ge(3) 161.03(6), C(81)–Fe(2)–Ge(4) 110.10(16), C(82)–Fe(2)–Ge(4) 114.7(2), P(1)–Fe(2)–Ge(4) 101.18(5), Ge(3)–Fe(2)–Ge(4) 97.78(3). Thermal ellipsoids are drawn at the 50% probability level; hydrogen and solvent atoms are omitted and, *t*Bu and Et groups are drawn in wireframe for clarity.

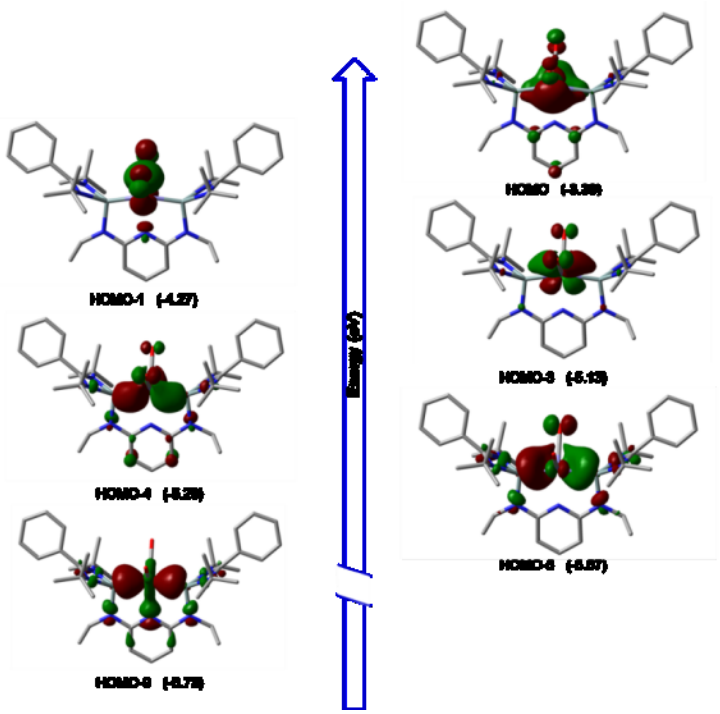

Figure 3.2.20. Selected molecular orbitals for the **[SiNSi]Fe(CO)$_2$** calculated at the B3LYP/6-31G(d)/LANL2DZ [Fe] level of theory.

3.3. Reactivity and catalytic applications of metal pincer complexes of the type [EXE]MX_nL_m

3.3.1. Borylation of arenes by the iridium complexes

3.3.1.1. Catalytic evaluation

Catalytic C–H borylation[158,159] of arenes with pinacolborane (HBPin) was chosen to probe the novel iridium complexes in C–H functionalization reactions. The **[ECE]IrHCl(coe)** complexes are coordinatively saturated, however, a substitution reaction of the chlorido ligand by a hydride source to form the **[ECE]Ir(H)$_2$(coe)** complex was envisaged. This complex could be conceived by a metathesis reaction with HBPin. Then, *via* an intramolecular hydrogenation reaction, cyclooctane (COA) might release and produce the coordinatively unsaturated **[ECE]Ir^I** active species. Initially, a reaction between **[SiCSi]IrHCl(coe)** with 20 equiv of HBPin in C_6D_6 was tested. After heating for 2 h at 100 °C, the formation of C_6D_5BPin and COA was observed by NMR and GC-MS. Continued heating for several hours did not show any increase of the product peaks by NMR spectroscopy over a prolonged period of time. However, addition of cyclooctene (COE) to the same sample led to a rapid formation of the products. This shows the beneficial effect of a hydrogen acceptor being present in the reaction medium. Based on this preliminary result, the comparison between the ligand systems was carried out and followed by GC-MS using neat benzene (Scheme 3.3.1)

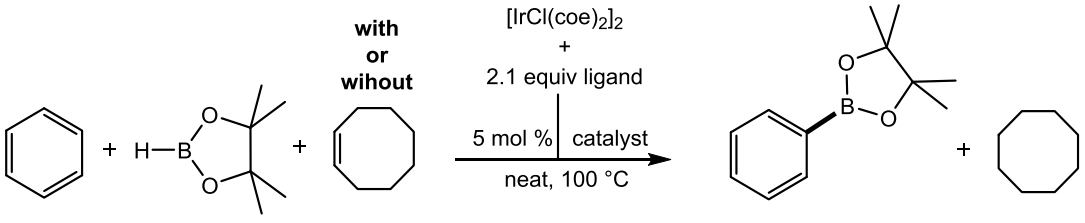

Scheme 3.3.1. Borylation of benzene using the *in situ* prepared **[ECE]IrHCl(coe)** (E = Si^{II}, Ge^{II}), **[*t*Bu-PCP]IrHCl**, and **[iPr-PCP]IrHCl(coe)** complexes as precatalysts.

Figure 3.3.1 depicts the reaction profiles using 5 mol % of the *in situ* generated **[ECE]IrHCl(coe)]** and **[*t*Bu-PCP]IrHCl** complexes (see section 3.2.1) with and without one equivalent of COE. Remarkably, the reaction proceeded significantly faster using the

ECHE ligands when an additional equivalent of COE, as hydrogen acceptor, was used. Moreover, the catalytic yield was improved when the additional hydrogen acceptor was present: 90 vs. 53 % and 80 vs. 46 %, yield after 24 h for **SiCHSi** and **GeCHGe**, respectively. These results are in strong contrast to those with the well stablished P^{III}-based systems having alkyl and/or aryl substituents. For instance, the concentration of COE had little effect using ***t*Bu-PCHP** as a ligand having 64 vs. 60% yield of C_6H_5BPin after 24 h in the presence or absence of COE, respectively; whereas addition of COE in the case of ***i*PrN-PCHP** had a contrary effect altering the selectivity. Not only the yield of C_6H_5BPin varies significantly from 55 to 21% in the presence of additional COE, but also the selectivity is altered towards the hydroborylation of COE producing borylated cyclooctane (coaBPin) in ca. 35 % yield.

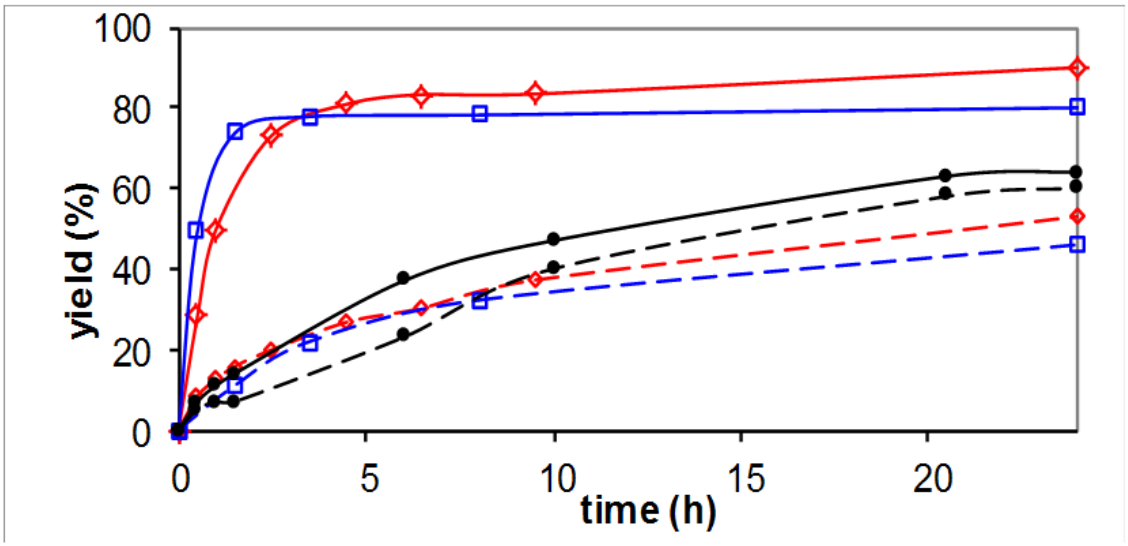

Figure 3.3.1. Reaction profile for the C–H borylation of benzene using HBPin and 5 mol% precatalyst generated *in situ* (**SiCHSi**: red/diamonds; **GeCHGe**: blue/squares; ***t*Bu-PCHP**: black/dots) in the presence (straight lines) and absence (dashed lines) of additional COE.

The substrate scope was evaluated for a range of aromatic substrates bearing different steric and electronic properties (Table 3.3.1). Steric effects seem to dictate the reaction yields. Employing toluene as substrate showed a good selectivity towards *meta* and *para* substitution products with no formation of the *ortho* substituted product. However, the reaction yields were lower with 91 % (*o*:*m*:*p* = 0:1.6:1) and 39 % (*o*:*m*:*p* = 0:1.5:1) yield for

SiCHSi and **GeCHGe**, respectively, while the bis(phosphinite) ligands showed 40 % and 6 % with the same isomeric ratio (*o*:*m*:*p* = 0:1.4:1) for ***t*Bu-PCHP** and ***i*PrN-PCHP,** respectively. Moreover, the sterically more demanding substrates like *o*-xylene and *m*-xylene showed only 3–15 % of ArBPin, and the main products originate from COE hydroborylation (coaBPin) and vinylic C–H borylation (1-coeBpin).

Table 3.3.1. Catalytic yields (%) for the borylation of arenes using the iridium pincer type complexes as precatalyst with the **ECHE**, ***t*Bu-PCHP** and ***i*PrN-PCHP** ligands. Yields in bold are without the presence of COE.

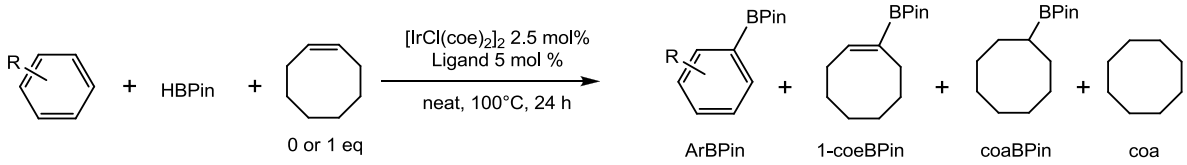

Ligand	SiCHSi	GeCHGe	*t*Bu-PCHP	*i*PrN-PCHP
	ArBPin: 90 coaBPin: 3 coeBPin: 1 **ArBPin: 53**	ArBPin: 80 coaBPin: 9 coeBPin: 8 **ArBPin: 46**	ArBPin: 64 coaBPin: 11 coeBPin: 7 **ArBPin: 60**	ArBPin: 21 coaBPin: 35 coeBPin: - **ArBPin: 55**
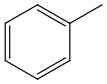	ArBPin: 91 (o:m:p = 0:1.6:1) coaBPin: 3 coeBPin: 3 **ArBPin: 16**	ArBPin: 39 (o:m:p = 0:1.5:1) coaBPin: 8 coeBPin: 7 **ArBPin: 12**	ArBPin: 40 (o:m:p = 0:1.4:1) coaBPin: 49 coeBPin: 10 **ArBPin: 9**	ArBPin: 9 (o:m:p = 0:1.4:1) coaBPin: 34 coeBPin: - **ArBPin: 20**
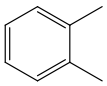	ArBPin: 15 coaBPin: 19 coeBPin: 26 **ArBPin: 11**	ArBPin: 4 coaBPin: < 3 coeBPin: < 3 **ArBPin: 5**	ArBPin: 10 coaBPin: < 3 coeBPin: < 3 **ArBPin: 8**	ArBPin: 11 coaBPin: 25 coeBPin: - **ArBPin: 23**
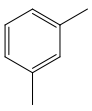	ArBPin: 11 coaBPin: 30 coeBPin: 50 **ArBPin: 10**	ArBPin: 6 coaBPin & coeBpin: < 5 **ArBPin: 3**	ArBPin: 17 coaBPin & coeBpin: < 5 **ArBPin: 4**	ArBPin: 5 coaBPin: 20 coeBpin: - **ArBPin: 19**
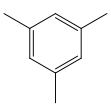	ArBPin: 0 - -	ArBPin: 0 - -	- - -	- - -

A comparison between the catalytic performance of the **[ECE]IrHCl(coe)** (E = Si^{II}, Ge^{II}) and bis(phosphinite) pincer systems used here, and the benchmark systems based on bidentate nitrogen ligands,[158] shows that these novel systems possess a significantly lower activity. This low activity is most likely due to the large sterically crowded ligands around the metal center due to the need of bulky substituents for stabilization of the metallylene moeities. However, the electronic properties in the metal center in pincer complexes, as discussed in section 3.2.1, are enhanced with metallylenes as pendant arms. This in conjuction to the difference in catalytic performance with the standard ***t*Bu-PCHP** ligand, shows that the metallylenes are not simply isoelectronic complexes of phosphines but they can alter the chemical properties on the metal center while acting as ligands.

3.3.1.2. Proposed mechanism for the borylation of arenes catalyzed by the [ECE]IrHCl(coe) pincer complexes

The difference in the catalytic performance with an additional hydrogen acceptor (COE) suggests that the active species might be stabilized by the COE during the catalytic cycle. Based on the reported results for the C–H borylation and alkane dehydrogenation,[9] a plausible catalytic mechanism is proposed for this chemical transformation using the novel catalysts (Scheme 3.3.2). First, the precatalyst is activated *via* a metathesis reaction with HBPin producing the dihydride species **A**. After the hydrogenation of COE, releasing COA, the unsaturated Ir^{I} reactive species **B** is formed. An oxidative addition of HBPin to the Ir^{I} center occurs subsequently affording **C**. This hydrido-boryl-Ir^{III} adduct then reacts with the arene by a C–H activation process forming the ArBPin product and the $Ir^{III}(H)_2$ species **D**, either *via* an oxidative addition/reductive elimination sequence or a σ-bond metathesis route. Due to the high σ-donor capacity for the **[ECE]** and **[*i*PrN-PCP]**, a highly electron rich Ir^{III} center is expected. Therefore, the presence of an additional equivalent of COE assists in the stabilization for these reactive species (pathway b) forming **A**. This is unlikely to occur when the **[*t*Bu-PCP]** ligand is used; due to the lower electron density on the metal center: the Ir^{III} center does not require any additional ligand for its stabilization. Then, the **[*t*Bu-PCP]Ir(H)$_2$** has to overcome the high energy barrier to release H_2 (pathway a) and produce the active Ir^{I} species **B**. In the literature, five-coordinate phosphinite-based [PCP]Ir$(H)_2$ complexes are used as starting materials in alkane dehydrogenation reactions

and have been proven to release H_2 at elevated temperatures.[9] In contrast, the Ir complexes bearing the ligands **[ECE]** and **[*i*PrN-PCP]** prefer a six-coordinate environment; and due to the stronger σ-donor properties, the release of H_2 through a reductive elimination is not energetically favoured. This is in agreement with the beneficial effect on the turnover frequency and number with an additional COE. In an alternative pathway (gray in color), an olefin could coordinate to the Ir^{III} species **C** to produce the octahedral species **E** which undergoes vinylic C–H borylation or hydroboration to produce 1-coeBPin or coaBPin, respectively.

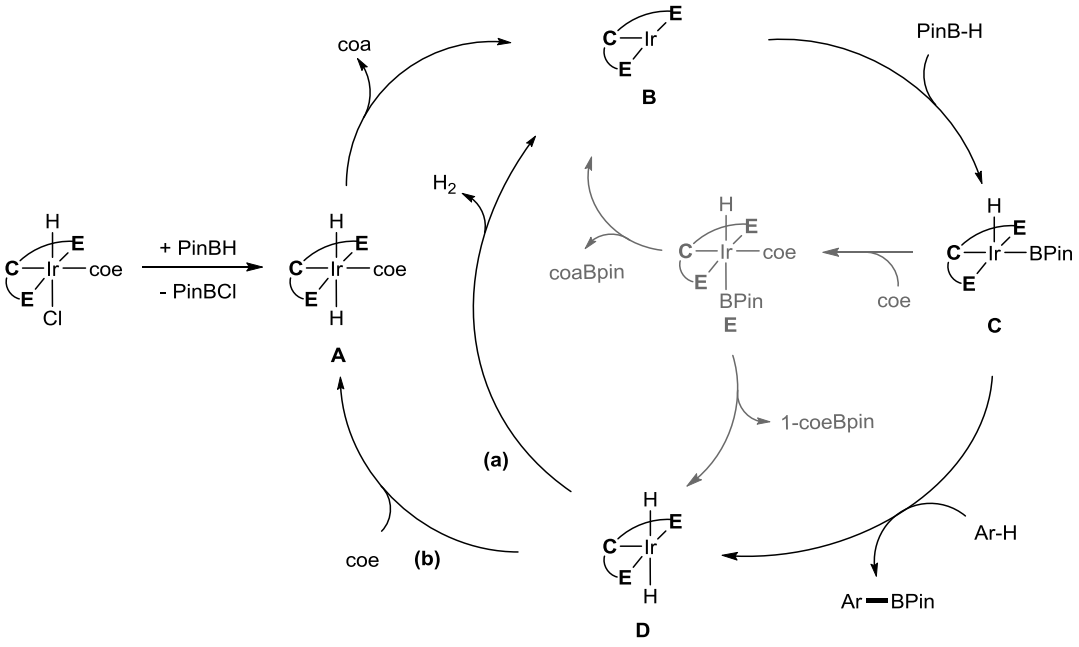

Scheme 3.3.2. Proposed mechanism for borylation of arenes catalyzed by pincer complexes of type [ECE]Ir (E = Si^{II}, Ge^{II}, P^{III}).

3.3.2. Sonogashira cross-coupling reaction catalyzed by the [ECE]NiBr complexes

3.3.2.1. Catalytic evaluation

The ligands **[ECE]** have been proven to enhance the electron density at the metal center in the **[ECE]NiBr** complexes. To evaluate whether these Ni complexes may serve as metal abundant substitutes of their noble metal counterparts, a catalytic reaction commonly

catalyzed by Pd complexes was sought to study their reactivity. Initially, the **[ECE]NiBr** and **[*i*PrN-PCP]NiBr** pincer complexes were tested as catalysts for the Sonogashira cross-coupling reaction. The reaction between (*E*)-1-iodo-1-octene with phenylacetylene as test substrates was carried out using 5 mol % of the catalyst and different amounts of the halide substrate (Table 3.3.2). Only with stoichiometric amounts of the substrates the yields were poor, albeit meaningful, being at the same order of the P^{III} reference system, and additionally ca. 3-fold higher than in the case were the Ni catalyst was absent. This result suggests that the active species, during the catalytic cycle, are most likely unstable without the presence of one of the substrates in excess. Assuming that the first elementary reaction step is a transmetallation between the Ni complexes and the *in situ* formed copper acetylide, an excess of the organic halide should improved the yield. The latter might occur due to the transmetallation product will have more substrate to react for the next elementary reaction. Indeed, with partial increase in the molar equivalents of the organic halide the catalytic yields were considerably improved reaching 39, 53, and 40 % yield for **[SiCSi]NiBr**, **[GeCGe]NiBr,** and **[*i*PrN-PCP]NiBr,** respectively. However, the reaction yields indicate a moderate catalytic performance for these systems which might be related with a poor stability of the active species under the catalytic conditions. Nevertheless, the fact that these novel nickel species act as catalysts not only expands the application of NHSis and NHGes as potential ligands in catalysis but also inspired to study further the elementary reactions of the cross-coupling process.

Table 3.3.2. Evaluation of the **[ECE]NiBr** (E = Si, Ge, P) complexes as precatalysts in the Sonogashira cross-coupling reaction.

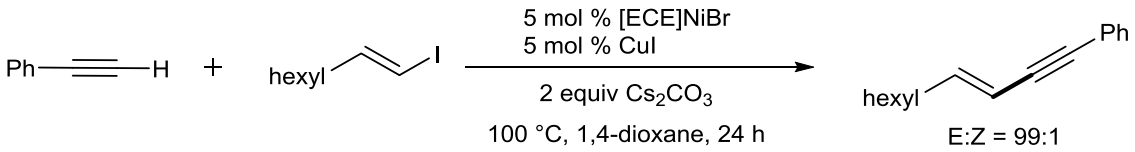

Equiv 1-iodo-1-octene	[SiCSi]NiBr	[GeCGe]NiBr	[*i*PrN-PCP]NiBr	-
1	21	12	18	7
2	23	46	17	-
3	26	54	32	-
5	39	53	40	5

A careful analysis of the product distribution after the catalysis showed the formation of a black residue, indicating most likely the formation of Ni^0. This observation raised the question of whether the metallylene moieties are stable under the reaction conditions and if the typical elementary steps of oxidative addition, transmetallation, and reductive elimination account for the catalytic activity. For existing metallylene→metal complexes,[3,64,65,132] a defined chemical transformation at a metal center coordinated with metallylene scaffolds has not been reported in the literature yet. This is of general interest since metallylenes are prone to undergo chemical reactions with several functional groups (see section 3.1.1).[32,33,53,160] Therefore, the possible elementary reaction steps for the catalytic cycle were followed by stoichiometric reactions; to learn whether some intermediates for the evaluated Sonogashira cross-coupling reaction could be identified. A plaussible reaction mechanism includes i) transmetallation on the Ni^{II} center with the copper phenylacetylide, ii) oxidative addition of the alkenyl iodide, and iii) reductive elimination to produce the coupling product and regenerate the Ni^{II} active species.

3.3.2.2. Mechanistic investigation: stepwise stoichiometric reactions with copper acetylides

First, the transmetallation was studied as elementary reaction step. Different copper acetylides were synthesized following reported procedures (Scheme 3.3.3).[161] Noteworthy, following the reported procedure for the synthesis of the copper acetylides, the synthesis of **Cu-4** with the steric demanding terphenyl group did not produce the expected product. Instead, direct deprotonation with *n*-BuLi and transmetallation with CuI afforded the product **Cu-4** in quantitative yield.

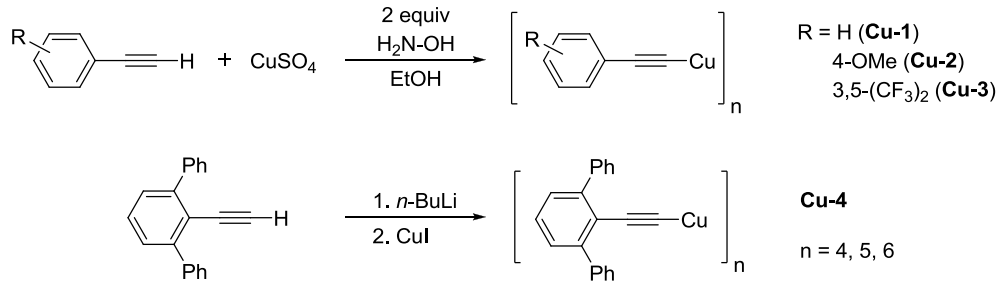

Scheme 3.3.3. Synthesis of copper acetylides for stoichiometric reactions with the nickel pincer complexes.

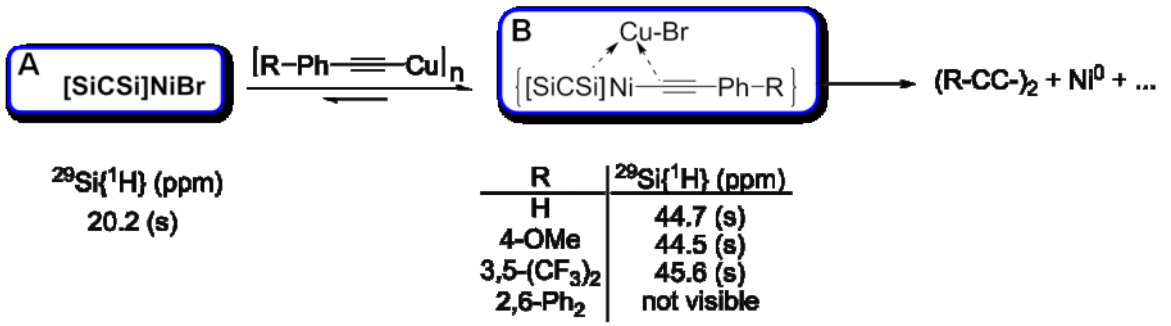

Scheme 3.3.4. Stoichiometric reaction between the **[SiCSi]NiBr** complex and copper acetylides and the corresponding $^{29}Si\{^{1}H\}$ NMR data.

Due to the cluster nature of the copper acetylides, their solubility is somewhat poor in non coordinating solvents such as benzene or toluene. However, this poor solubility permited a "controlled" reaction between the Cu-acetylides and the **[SiCSi]NiBr** complex by low concentration in solution. Two molar equiv. of **Cu-1** reacted as a slurry with **[SiCSi]NiBr** in C_6D_6 over 4 hours. Evaluation of the reaction mixture, after filtration through Celite, by ^{1}H and $^{29}Si\{^{1}H\}$ NMR spectroscopy showed that a new product with C_{2v} symmetry was formed selectively. This was confirmed by the shift of the singlet resonance signals corresponding to the *t*Bu groups in the ^{1}H NMR spectrum as well as one singlet resonance in the $^{29}Si\{^{1}H\}$ NMR spectrum (Scheme 3.3.4 and Figure 3.3.2).

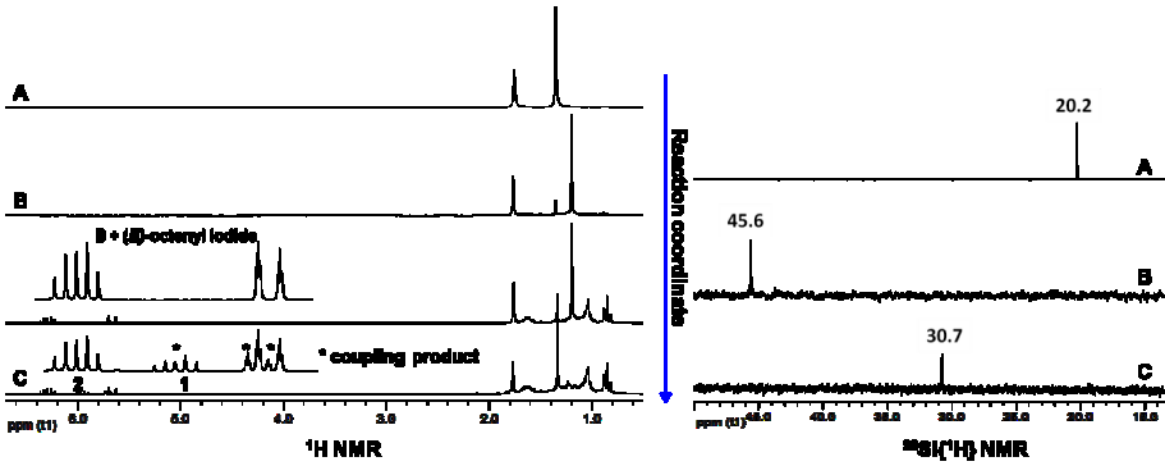

Figure 3.3.2. Sequential ^{1}H and $^{29}Si\{^{1}H\}$ NMR spectra for the course of the cross-coupling reaction in stoichiometric scale (**A** and **B**: see Scheme 3.3.4; **C**: see Scheme 3.3.5 page 110).

Unfortunately, even when the transmetallation occurred in quantitative yields and with high selectivity, the products were only moderately stable in solution for a few hours and afforded a black precipitate upon evaporation of the solvent. The original signals for **[SiCSi]NiBr** reappeared partially in the ^{1}H NMR spectra and the homocoupled phenylacetylenes $(C{\equiv}C{-}Ar)_2$ were observed in the GC-MS. These results collectively indicate that, i) not all of the CuBr formed in the transmetallation could be removed by simple filtration due to the recovery of the **[SiCSi]NiBr** complex; and ii) that the intermediate Ni-acetylides, if formed, reacted in a bimolecular reaction to form the observed homocoupled phenylacetylenes, Ni^0 and undefined organic products from the ligand.

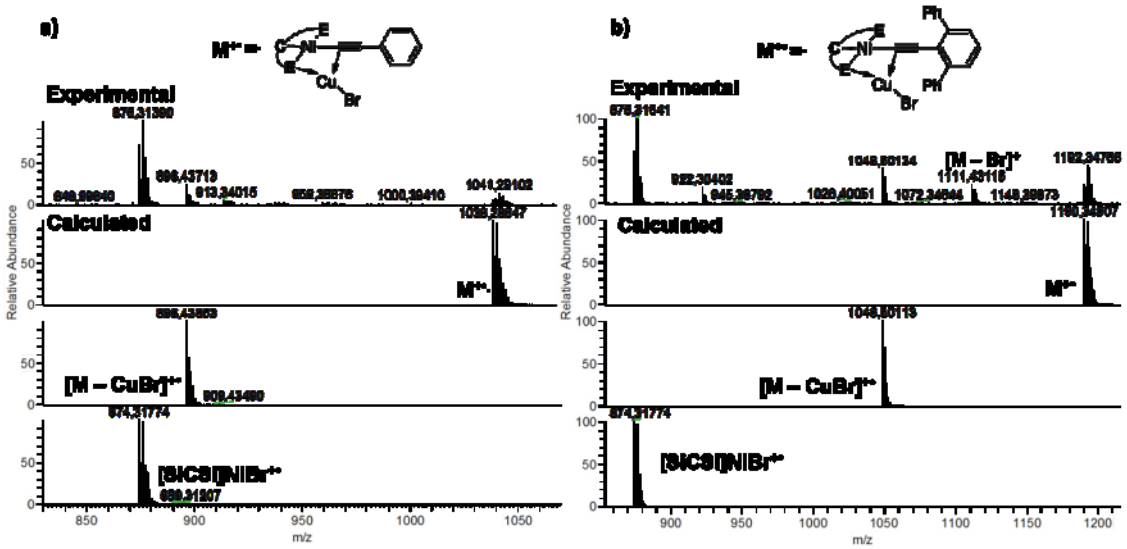

Figure 3.3.3. APCI-MS and calculated spectra for the transmetallation intermediates a) **{[SiCSi]Ni–C≡C–Ph→CuBr}** and b) {**[SiCSi]Ni–C≡C–*ter*Ph→CuBr}**

The formation of the homocoupling diyne product most probably occurs *via* a bimolecular decomposition pathway. To evaluate this hypothesis a cross-over experiment was carried out. Solutions generated by reaction of **[SiCSi]NiBr** with **Cu-1** and **Cu-3** were combined. Not surprising, the mixed diyne Ph–C≡C–C≡C–3,5-$(CF_3)_2C_6H_3$ was detected by CG-MS after standing for one day at room temperature. In this way, this reaction is considered as a side reaction which might deactivate the catalytically active species. Further characterization of the crude Ni-acetylides in solution by APCI-HRMS (Figure 3.3.3) showed three molecular ions in each case: **[SiCSi]NiBr** as the most intense signal,

one signal for the expected Ni-acetylides **[SiCSi]Ni–C≡C–Ph–R**, and strikingly one signal for the adduct **{[SiCSi]Ni–C≡C–Ph–R→CuBr}** (Figure 3.3.3a). The signals for the latter two species were approximately equal in intensity, indicating that they have the same concentration and/or their origin is from the same chemical species.

Fortunately, after several crystallization attempts single crystals were obtained from the reaction of **[SiCSi]NiBr** with $[Cu–C≡C–Ph]_4$. Several microfiltrations of the reaction mixture and storage in a mixture of *n*-pentane/toluene as solvent at –78 °C for approximately one week afforded yellow crystals suitable for single crystal XRD structure analysis. Interestingly, the structure of the product is the **{[SiCSi]Ni–C≡C–Ph→CuBr}** adduct (Figure 3.3.4a). This structure consists of a copper center in close proximity to the C–C triple bond and one of the silylene arms from the pincer ligand.

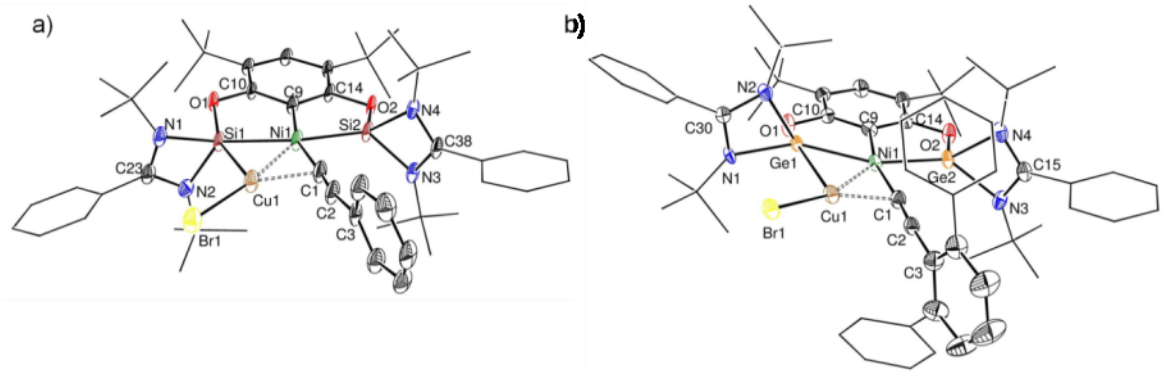

Figure 3.3.4. Molecular structures with selected bond lengths [Å] and angles [°] of a) **{[SiCSi]Ni–C≡C–Ph→CuBr}**: Ni1–Si1 2.296(1), Ni1–Si2 2.137(1), Ni1–C9 1.940(4), Ni1–C1 1.860(4), Ni1–Cu1 2.4628(9), Si1–Cu1 2.508(1), C1–Cu1 1.976(4), C2–Cu1 2.420(4), C1–C2 1.213(6), C2–C3 1.451(6), Cu1–Br1 2.2855(7), Si1–Ni1-Si2 160.93(5), C1–Ni1–C9 162.9(2), Ni1–Si1–Cu1 61.49(3), C10–O1–Si1 115.4(2), C14–O2–Si2 110.4(2), Σ<Ni1 360.1(1); b) **{[GeCGe]Ni–C≡C–*ter*Ph→CuBr}**: Ni1–Ge1 2.3254(6), Ni1–Ge2 2.1786(6), Ni1–C9 1.985(3), Ni1–C1 1.890(4), Ni1–Cu1 2.5208(7), Ge1–Cu1 2.5450(6), C1–Cu1 1.951(3), C2–Cu1 2.403(3), C1–C2 1.216(5), C2–C3 1.437(5), Cu1–Br1 2.2855(7), Ge1–Ni1–Ge2 161.09(3), C1–Ni1–C9 164.1(2), Ni1–Ge1–Cu1 62.15(2), C10–O1–Ge1 113.4(2), C14–O2–Ge2 109.0(2), Σ<Ni1 360.4(1). Thermal ellipsoids are drawn at a 50% probability level; hydrogen and solvent atoms are omitted for clarity.

Moreover, after re-dissolving the crystals in C_6D_6, the same mass spectrum with the three species and the symmetric NMR data, as described above, were obtained (see section 3.3.2.3 for a detailed discussion on the bonding situation).

Transmetallation reactions between the synthesized Cu-phenylacetylides and **[GeCGe]NiBr** occurred in a fashion similar to the reactions with **[SiCSi]NiBr**, but full conversion to the Ni-phenylacetylides intermediates were not observed. However, the products were less stable and decomposed in the presence of larger quantities of the Cu-phenylacetylides. The dependence of the stability for these transmetallation products on the amount of Cu-phenylacetylide implies that at least one of the decomposition pathways is bimolecular. Thus, a more sterically hindered Cu-phenylacetylide **Cu-4** was selected to block the Ni center and make its decomposition pathway kinetically less unfavoured (Scheme 3.3.4, p. 102).

Copper-terphenylacetylide **Cu-4** reacted cleanly with each of the metallylene pincer **[ECE]NiBr** (E = Si^{II}, Ge^{II}) complexes. As anticipated, the products were stable in solutions for several days without any decomposition. The ^{1}H NMR spectrum of the bis(germylene) derivative showed the same C_{2v} symmetry as described for the intermediates above, but the signals for the *t*Bu groups on the amidinate ligands in the bis(silylene) complex were as broad singlet resonances in addition to the absence of any signal in the $^{29}Si\{^1H\}$ NMR spectrum. These spectroscopic features might be related with i) steric interactions between the silylene moieties and the terphenyl group, or ii) the reversible coordination/decoordination with CuBr, thereby breaking the C_{2v} symmetry. The APCI-HRMS of the crude reaction contained three sets of signals for the **[ECE]NiBr** precursor, the **[ECE]Ni–C≡C–*ter*Ph** transmetallation product, and the CuBr adduct of the transmetallation product (the signal due to the adduct was more intense than it was for the non-sterically hindered acetylides; Figure 3.3.3b, p. 103). This kinetic stabilization of the transmetallation product by steric hindrance allowed the crystallization of the copper bromide adduct using the bis(germylene) **[GeCGe]** ligand at room temperature without any notable decomposition. The solved structure by XRD data analysis again revealed the formation of the **{[GeCGe]Ni–C≡C–*ter*Ph→CuBr}** adduct (Figure 3.3.4b).

Transmetallation experiments with the phosphine analogue **[*i*PrN-PCP]NiBr** with **Cu-1** and **Cu-4** showed similar reactivity to the **[ECE]NiBr** complexes. However, the equilibrium is significatly shifted to the starting nickel bromide complex and an isolable product could not be obtained. Reaction with 5 molar equiv of **Cu-1** at 60 °C for 12 h furnished the transmetallation product in 5 % conversion as determined by $^{31}P\{^{1}H\}$ NMR (Figure 3.3.5). Analysis by APCI-HRMS showed two molecular ions related with the **[*i*PrN-PCP]NiBr** and **[*i*PrN-PCP]Ni–C≡C–Ph** complexes, the latter with lower intensity (Figure 3.3.5 inset). The CuBr adduct was not observe in this case. This difference in reactivity can be related with the higher electron density on the Ni^{II} center in the **[ECE]NiBr** (E = Si^{II}, Ge^{II}) complexes in which the π-backbonding interaction with the C–C triple bond is expected to be stronger leading to a better stability of the transmetallation product.[162]

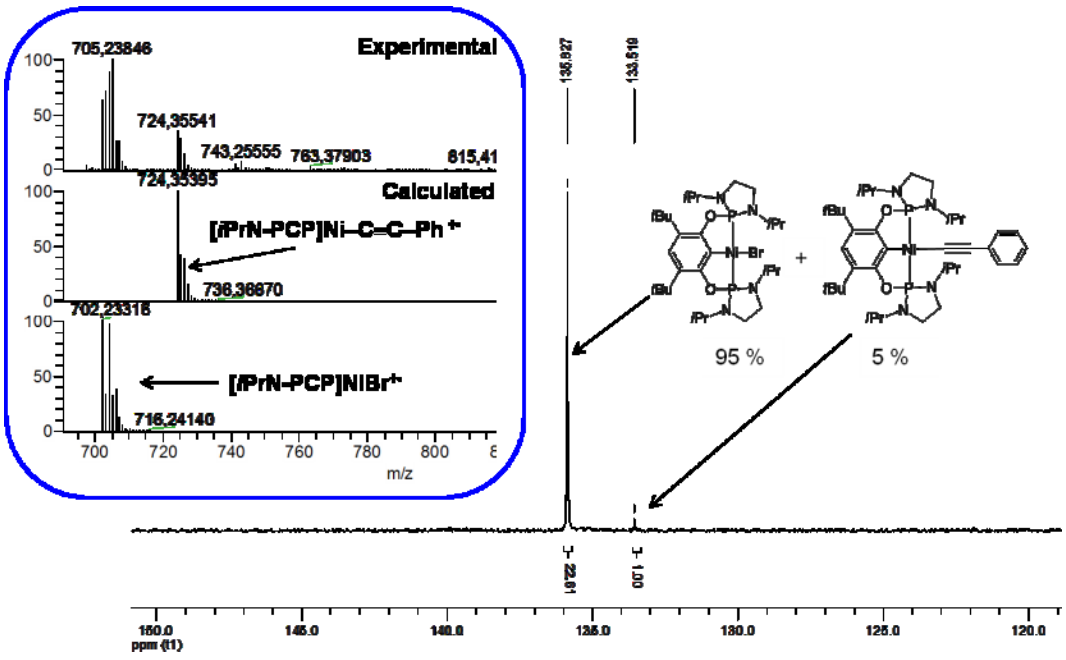

Figure 3.3.5. $^{31}P\{^{1}H\}$ NMR spectrum in C_6D_6 and APCI-HRMS (inset) after transmetallation reaction between **[*i*PrN-PCP]NiBr** and **Cu-1**.

3.3.2.3. Structural features and DFT calculations of the isolated intermediates

The coordination of copper bromide to the acetylide unit renders the structures in Figure 3.3.4 unsymmetrical. The **E–Ni** (E = Si^{II}, Ge^{II}) distances between the CuBr-coordinated side (d(Ni–Si1) = 2.296(1) Å, d(Ni–Ge1) = 2.3254(6) Å) and the non-coordinated side (d(Ni–Si2) = 2.137(1) Å, d(Ni–Ge2) = 2.1786(6) Å) are different in both **{[ECE]Ni–C≡C–Ph/*ter*Ph→CuBr}** complexes. In addition, the copper atom is much closer to the C1 atom (d(Cu–C1) = 1.976(4) Å, 1.951(3) Å for E = Si^{II}, Ge^{II}, respectively) of the acetylide ligand than to the remote C2 atom (d(Cu–C2) = 2.420(4) Å, 2.403(3) Å for E = Si^{II}, Ge^{II}, respectively). The unsymmetrical binding of the copper is different from a classical "side-on" coordination in which Δd(Cu–C1 vs. Cu–C2) is less than 0.150 Å.[24,163–167] † Additionally, the C1–C2–C3 and Ni–C1–C2 angles are indicative of a C≡C→Cu bond (side-on: ca. 156–165°; end-on: ca. 170°–180°[24,167]) and show, if at all, only minor perturbation of the C–C triple bond (Si: 170.5(5)° and 174.9(4)°; Ge: 171.5(4)° and 176.4(3)°). The arms of the pincer ligands open towards the Cu atom in accordance with a reduction of the O1–E1–N angles (average change: E1 = Si: 106.75°→99.45°; Ge: 106.41°→97.12°) and shortening of the Cu–E distances (d(Cu–Si) = 2.508(1) Å; d(Cu–Ge) = 2.5450(6) Å), indicating a E→Cu bond. Due to the complexity of the system having two metal centers bridged by a metallylene moiety, a theoretical study was carried out to evaluate these interatomic interactions.

The bonding situation in the four member ring (C1–Ni–Si1–Cu) was calculated and explained by detailed density functional theory (DFT) for both **{[ECE]Ni–C≡C–Ph/*ter*Ph→CuBr}** intermediates (E = Si^{II}, Ge^{II}) employing B3LYP-D3(BJ)/def2-TZVP level of theory.[168–173] For comparison, the corresponding **[ECE]Ni–C≡C–Ph/*ter*Ph** complexes lacking bound CuBr were also computed. Calculations were conducted on i) fully optimized structures (**fullopt**) and ii) the X-ray crystal structures after reoptimization of the hydrogen-atom positions (**crystal/H-opt**). The analysis was focused mostly on atomic charges from natural population analysis (NPA) and on a real space description by

† The C≡C triple bond distances are not very indicative of a side-on or end-on coordination mode: Si, 1.213 Å; Ge, 1.222 Å; side-on, 1.207 −1.239 Å; end-on, 1.193 Å.[24]

the electron localization function (ELF)[174–176] or the related electron localizability indicator (ELI-D).[177,178] The bond distances of the **fullopt** structures agree well with those of the **crystal/H-opt** structures (Table 3.3.3). The main effect of CuBr coordination in all cases is the lengthening for the **E1–Ni** bonds and concomitant shortening of the **E2–Ni** bond opposite to the CuBr fragment. Interestingly, the bending of the phenylacetylide ligand out of a linear C_{ipso}–Ni–C≡C arrangement in both complexes with CuBr is accompanied by a slight but significant lengthening of the alkyne C1–C2 triple bond and of the C2–C3 single bond.

Table 3.3.3. Selected bond lengths in **{[ECE]Ni–C≡C–R→CuBr}** and **{[ECE]Ni–C≡C–R}** complexes (E=Si, R=Ph / E=Ge, R=*ter*Ph)[a]

	bond length [Å]					
	{[ECE]Ni–C≡C–R→CuBr}				{[ECE]Ni–C≡C–R}	
	crystal/H-opt[b]		fullopt-D3[b]		fullopt-D3[b]	
Bond	E=Si	E=Ge	E=Si	E=Ge	E=Si	E=Ge
E1–Ni	2.296	2.317	2.319	2.329	2.181	2.199
E2–Ni	2.137	2.181	2.131	2.178	2.182	2.196
Ni–C1	1.861	1.881	1.866	1.885	1.848	1.858
C1–C2	1.212	1.219	1.233	1.232	1.222	1.224
C2–C3 (ipso,R[c])	1.452	1.444	1.420	1.423	1.413	1.414
Cu–C1	1.976	1.948	2.020	1.998		
Cu–C2	2.420	2.422	2.528	2.551		
Cu–E1	2.508	2.558	2.496	2.548		
Cu–Ni	2.462	2.526	2.485	2.531		
Cu–Br	2.286	2.285	2.318	2.306		

[a]For atom number assignment see Figure 3.3.4, p. 104.
[b]B3LYP/def2-TZVP results (cf. Computational details). [c]C_{ipso} of the phenylacetylide ligand.

The ELF plot displayed in Figure 3.3.6 shows that the Cu atom is involved in a three-center bond with **E1** and **Ni** (ELI-D gives a qualitatively similar bonding description, Table 7.2.2 in Appendix 7.2). While no interaction of Cu with the acetylide ligand is apparent in the ELF, an appreciable Cu–C1 Mayer bond order (Si: 0.963; Ge: 0.855) suggests that there are bonding interactions between Cu and the acetylide ligand (see Table 7.2.3 in Appendix 7.2). The reduced bond order in the C–C triple bond in the full optimized structures

containing the CuBr bound (Si: 0.728, Ge: 1.321), as compared to the bond order for C–C triple bond in the system lacking CuBr (Si: 1.737; Ge: 2.076) is in agreement with a bonding interaction between C1 and the Cu center. NPA charges (Tables 7.2.4 and 7.2.5 in appendix 7.2) show that CuBr receives about 0.2 electrons from the complex, and E1 becomes more negative by about 0.18 electrons for E = Si^{II} and by about 0.13 electrons for E = Ge^{II}. Closer examination shows that this charge results mainly from the Ni center and the E2 atom on the opposite side, with smaller contributions from other parts of the ligand framework. This charge distribution is consistent with a charge transfer towards the newly formed **E1–Cu–Ni** three-center bond (Figures 3.3.4 and 3.3.6). Overall, a pattern of delocalized interactions emerges that allows the CuBr fragment to bond to the combination of Ni, one metallylene arm from the pincer moiety, and the acetylide coligand.

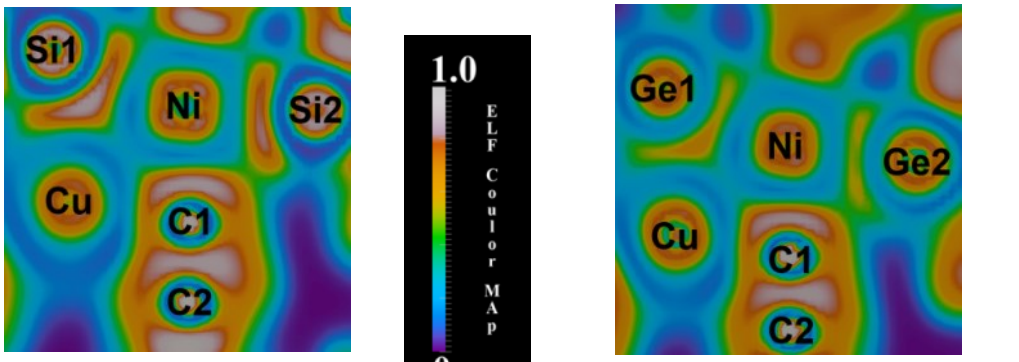

{[SiCSi]Ni–C≡C–Ph→CuBr} **{[GeCGe]Ni–C≡C–*ter*Ph→CuBr}**

Figure 3.3.6. ELF plot in the main Ni coordination plane of the **{[ECE]Ni–C≡C–Ph/*ter*Ph→CuBr}** complexes (E= Si^{II}, Ge^{II}). Calculations carried out at the B3LYP-D3/def2-TZVP level of theory.

After the complete analysis by the spectroscopic methods and DFT calculations of the **{[ECE]Ni–C≡C–Ph/*ter*Ph→CuBr}** complexes, it can be concluded that the first step of the catalytic reaction occurs *via* a transmetallation process forming the CuBr adduct in solution with a medium half-life time. Consequently, to study the next elementary step, the transmetallation products were generated *in situ* and used after microfiltration.

3.3.2.4. Mechanistic investigation: stepwise stoichiometric reaction with (E)-1-iodo-1-octene

A possible scenario for the observed Sonogashira cross-coupling is the sequence of transmetallation, oxidative addition, and reductive elimination. In this sequence, oxidative addition of the substrate containing a C(sp^2)–halide bond would occur at the nickel center from the phenylacetylide product. Indeed, addition of 3 equiv of (*E*)-1-iodo-1-octene to solutions of the *in situ* generated {[SiCSi]Ni-phenylacetylides→CuBr} in C_6D_6 formed the C(sp)–C(sp^2) coupling products in yields from 80-95% (determined by GC/MS and NMR) after a few hours at 50 °C, in combination with the **[SiCSi]NiI** complex (Scheme 3.3.5 and Figure 3.3.2). The spectroscopic features for the latter species were confirmed by the

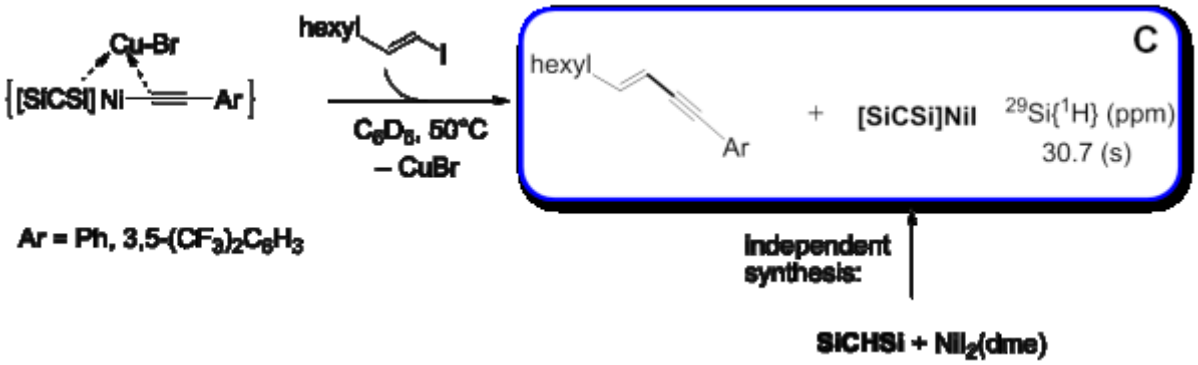

Scheme 3.3.5. Sequential reaction between the transmetallation product **{[SiCSi]Ni–C≡C–Ph→CuBr}** and the (*E*)-octenyl iodide (see Figure 3.3.2, p. 102 for NMR spectra), and independent synthesis of the iodide complex **[SiCSi]NiI**.

independent synthesis of the nickel iodide complex. This complex was prepared by the same procedure applied for the bromide analogue but using NiI_2(dme) as the metal precursor instead, and fully characterized by ^{1}H, ^{13}C{^{1}H} and ^{29}Si{^{1}H} NMR spectroscopy, APCI-HRMS and single crystal XRD structure analysis (Figure 3.3.7). The formation of the coupling product and the nickel iodide is consistent with a combination of oxidative addition and reductive elimination. The solved structure by XRD data analysis of **[SiCSi]NiI** resembles the structural features of **[SiCSi]NiBr** concluding that no alteration on the ligand backbone has occurred after closing the catalytic cycle. Moreover, a test reaction to probe the reversibility and stability of the system was carried out using the copper acetylide **Cu-3** (Scheme 3.3.6). Up to 3 TONs were followed by ^{1}H NMR (Figure

3.3.8) before the loss of the catalyst by microfiltrations and deactivation by side reactions, as discussed before. In the sequential ^{1}H NMR the formation of the **[SiCSi]NiI** can be seen clearly after reaction of (*E*)-1-iodo-1-octene with the adduct **{[ECE]Ni–C≡C–3,5-(CF$_3$)$_2$-C$_6$H$_3$→CuBr}**. In a close up to the olefinic region in the ^{1}H NMR spectrum (Figure 3.3.8, right), the formation of the coupling product could also be observed. At the end of the reaction time, it reached the stoichiometric amount (relative to **[SiCSi]NiBr**).

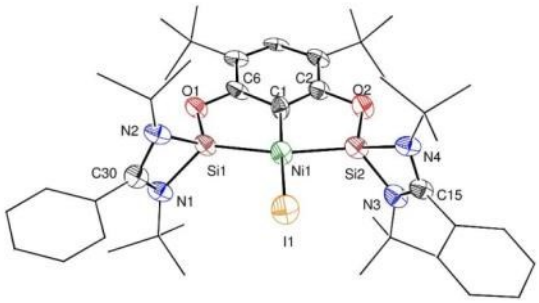

Figure 3.3.7. ORTEP representation of the of **[SiCSi]NiI** complex in the solid state with selected distances [Å] and angles [°]: C1–Ni1 1.928(8), I1–Ni1 2.5068(15), Si1–Ni1 2.159(3), Si2–Ni1 2.171(3), C1–Ni1–I1 175.0(3), Si1–Ni1–Si2 161.96(11), C6–O1–Si1 112.0(5), C2–O2–Si2 110.0(6), Σ<Ni1 360.3(3). Thermal ellipsoids are drawn at a 50% probability level; phenyl, *t*Bu and *i*Pr groups are drawn in wire frame and hydrogen and solvent atoms are omitted for clarity.

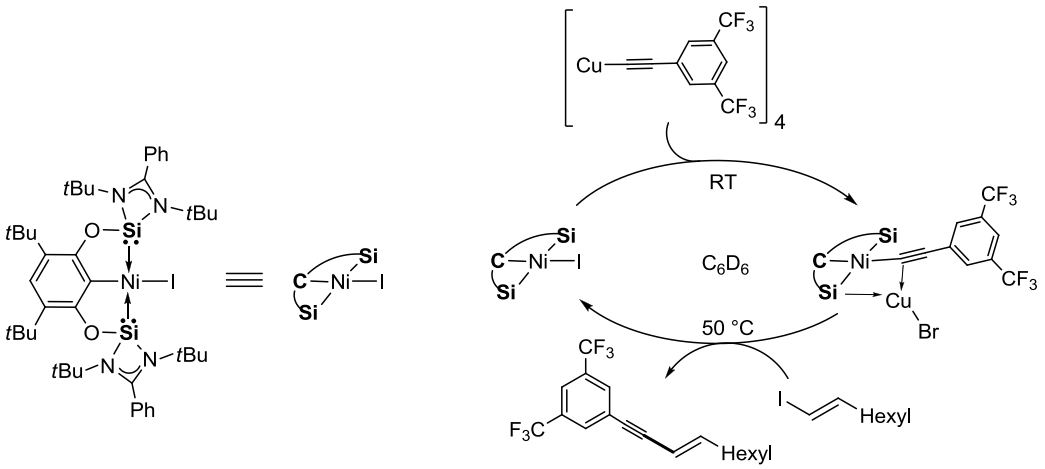

Scheme 3.3.6. Stoichiometric evaluation of the catalytic cycle using stoichiometric amounts of **[SiCSi]NiI**, **Cu-3** and (*E*)-octenyl iodide in C_6D_6.

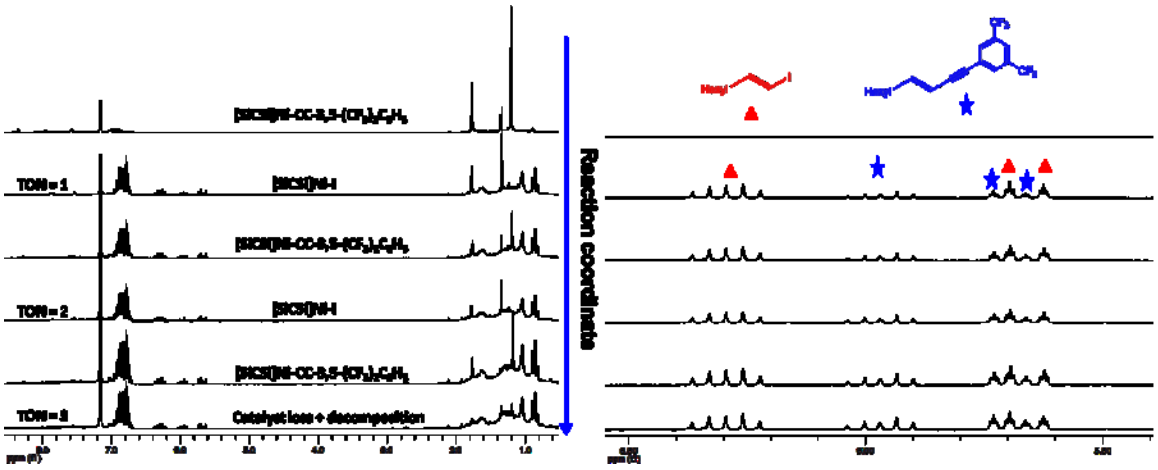

Figure 3.3.8. Sequential ^{1}H NMR for the catalytic cycle (3 TON) using stoichiometric amounts of substrates and catalyst from Scheme 3.3.6.

After evaluate the reactions with the organic halide, there is no evidence of the reaction intermediate for the hypothetical elementary step of oxidative addition on the Ni center. However, the evidence of the remaining *E* stereochemistry on the final product characterized by ^{1}H NMR spectroscopy suggested that two possible scenarios might occur. The first is based on the typical oxidative addition and subsequent reductive elimination passing through a Ni^{IV} intermediate. And the second might involve radicals in which the rate of recombination is faster than the isomerization on the vinylic radical. A test experiment with the radical clock (iodomethyl)cyclopropane and phenylacetylene was conducted, however, poor selectivity of the reaction was observed by GC-MS and ^{1}H NMR. The lost of the signals from the cyclopropane group in the ^{1}H NMR spectrum indicated full conversion. However, some undefined signals overlapping in the olefinic region suggest that radicals are involved because the cyclopropane ring opened to produce an aliphatic olefin. The double bond could isomerize along the aliphatic chain by the Ni^{0} species formed from the decomposition of catalyst,[‡] producing plenty of resonance signals in the olefinic region. This result is in agreement with the work by Hu and co-workers who demonstrated a radical mechanism of the Ni-catalyzed alkyl-alkyl[180] and alkyl-aryl[181] Kumada cross-coupling reactions. In their work a bimetallic oxidative addition was demonstrated for the coupling between the Ni-alkyl and organic halide species (Scheme 3.3.7). In the corresponding mechanism a single electron transfer (SET) is involved in the

[‡] Ni^{0} species have shown catalytic activity in isomerization of olefins, see ref. 179

activation of the organic halide by the alkyl-Ni^{II} species (**1**) forming a Ni^{III} species (**2**) and an alkyl radical. This radical recombines with another molecule of **1** to obtain the dialkyl-Ni^{III} species (**3**). Then, by a reductive elimination of **3** the coupling product and a Ni^{I} species (**4**) are formed. Finally, by a disproportionation reaction between species **2** and **4** the Ni^{II} species (**1** and **5**) are recovered. Additionally, the nickel halide **5** can react with the Grignard reagent to form **1**.

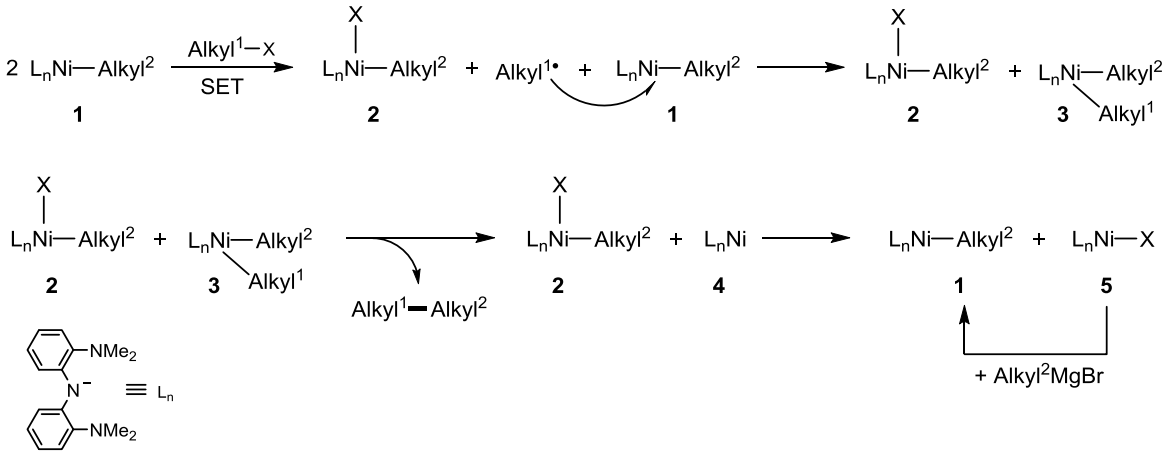

Scheme 3.3.7. Bimetallic oxidative addition involving a radical mechanism for the activation of alkyl halides by SET in the Kumada cross-coupling reaction catalyzed by a Ni^{II} pincer complex (adapted from X. Hu refs. 180,181).

Accordingly to the postulated hypotheses, the reaction mechanism most likely goes through a radical pathway by a single electron transfer (SET) mechanism in the activation of (*E*)-1-iodo-1-octene. Due to the similarity of the monoanionic pincer ligands [**NNN**] and [**SiCSi**], it is conceivable that the second elementary step goes through a similar mechanism as shown in Scheme 3.3.7. Noteworthy, in the reported mechanistic studies, Hu and co-workers[180] observed the presence of an adduct between the alkyl species **1** and the Grignard reagent as the key intermediate for the improvement in the catalytic performance with higher TOF numbers. This raised the question whether the adducts **{[ECE]Ni–C≡C–Ar→CuBr}** might play a synergistic role between both metal centers where the SET process would be thermodynamically more favoured. Due to the lability of these adducts a detailed study on the mechanism was unfruitful, although, these studies open a new door in Ni-catalyzed coupling reactions since a radical mechanism might be favoured in the presence of heterometallic species.

3.3.2.5. Proposed reaction mechanism for the Ni-catalyzed Sonogashira cross-coupling reaction

The results of the stoichiometric reactions and the reported studies on C–C coupling reactions collectively suggest a general mechanism for the Sonogashira cross-coupling between phenylacetylene and (*E*)-1-iodo-1-octene (Scheme 3.3.8). Firstly, The **[ECE]NiX** (E = Si^{II}, Ge^{II}; X = Br, I) complex reacts with the Cu-phenylacetylide which is generated *in situ* by the phenylacetylene, CuI and Cs_2CO_3. The product of this transmetallation binds to CuBr to form the adduct **B**. In a subsequent step, the (*E*)-1-iodo-1-octene is activated *via* a radical mechanism, where the alkenyl radical and the Ni^{III} species **C** are formed. The radical then reacts rapidly with species **B** to generate the key Ni^{III} intermediate **D**. Due to the absence of any racemization in the final product, the formation of **D** must be kinetically more favoured than the racemization on the olefin moiety. *Via* a reductive elimination from **D**, the coupling product (*E*)-dec-3-en-1-ynyl-benzene and a Ni^{I} species **E** are then formed. Finally, a comproportionation reaction between **C** and **E** occurs to produce the Ni^{II} species **A** and **B'**, the latter being **B** without the coordinated CuX.

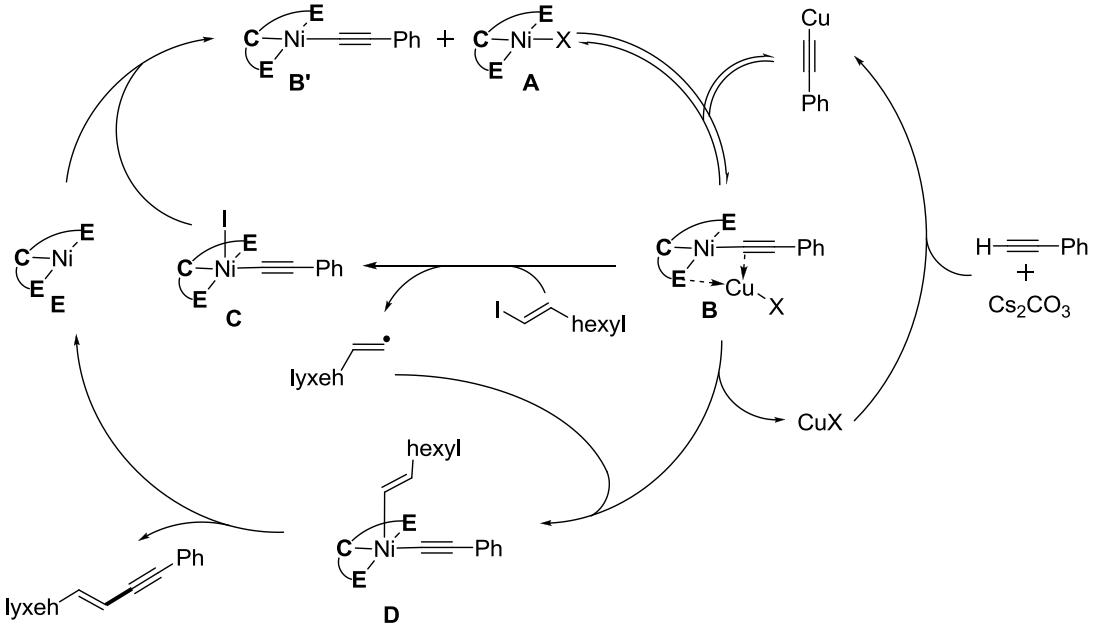

Scheme 3.3.8. Proposed catalytic cycle for the Sonogashira cross-coupling reaction catalyzed by the **[ECE]NiX** complexes (E = Si^{II}, Ge^{II}; X = Br, I).

3.3.3. Hydrosilylation of ketones by the [ENE]Fe(PMe$_3$)$_2$ complexes

3.3.3.1. Catalytic evaluation

During the last decade iron catalysts have become widespread in several chemical transformations (e.g. hydrogenation, hydrosilylation, coupling reactions)[182,183] having in some examples comparable activities to its noble metal counterparts (e.g. Rh, Ir, Ru). Several iron pincer complexes have shown to be very robust under different catalytic conditions as well as very active even under mild conditions.[184] Previously, the hydrosilylation of ketones by the [(dmpe)$_2$Fe(←:Si(H)L)] (L = *N,N'*-di-*tert*-butyl(phenylamidinato); dmpe = 1,2-bis(dimethylphosphino)ethane) complex was reported,[66] when a cooperative behavior was elucidated between the Si^{II} and Fe^0 centers. This result demonstrated that the NHSi can act as a co-operative ligand in catalytic systems. However, a spectator ligand would also be of interest when a robust catalyst is required. Thus, the application the **[ENE]Fe(PMe$_3$)$_2$** complexes for ketone hydrosilylation was envisaged; with the aim to elucidate whether the pincer moiety serves as an improved system for the catalytic performance. First, employing catalytic amounts (2 mol %) of the **[ENE]Fe(PMe$_3$)$_2$** (E = Si^{II}, Ge^{II}) complexes in the hydrosilylation of *p*-methoxyacetophenone with triethoxysilane, conversions up to 87% after 22 h at 70 °C in THF were obtained (Figure 3.3.9). Both catalysts showed good performance, but an induction period was required when E = Ge^{II} and at the end of the reaction decomposed material was the remaining residue from the catalyst. In contrast, when E = Si^{II} a clear orange solution was obtained after the catalytic run. This is likely due to the instability of the **[GeNGe]Fe(PMe$_3$)$_2$** under the catalytic conditions forming iron particles which might also be catalytically active.[185] Due to the **[SiNSi]Fe(PMe$_3$)$_2$** complex showed good stability and homogeneity, the catalytic optimization was carried out exclusively with this complex.

The catalytic reaction conditions were optimized using *p*-methoxyacetophenone as substrate (Table 3.3.4). The polarity of the reaction media has a little effect on catalytic performance (entries 1-5) which is contrary to the reported systems that commonly work better in polar solvents.[183] This might be a consequence of the high solubility of the catalyst which, due to its lipophilicity, is soluble in almost all tested aprotic solvent such as pentane, hexane, toluene, THF. Therefore, THF was selected as the optimal solvent due to

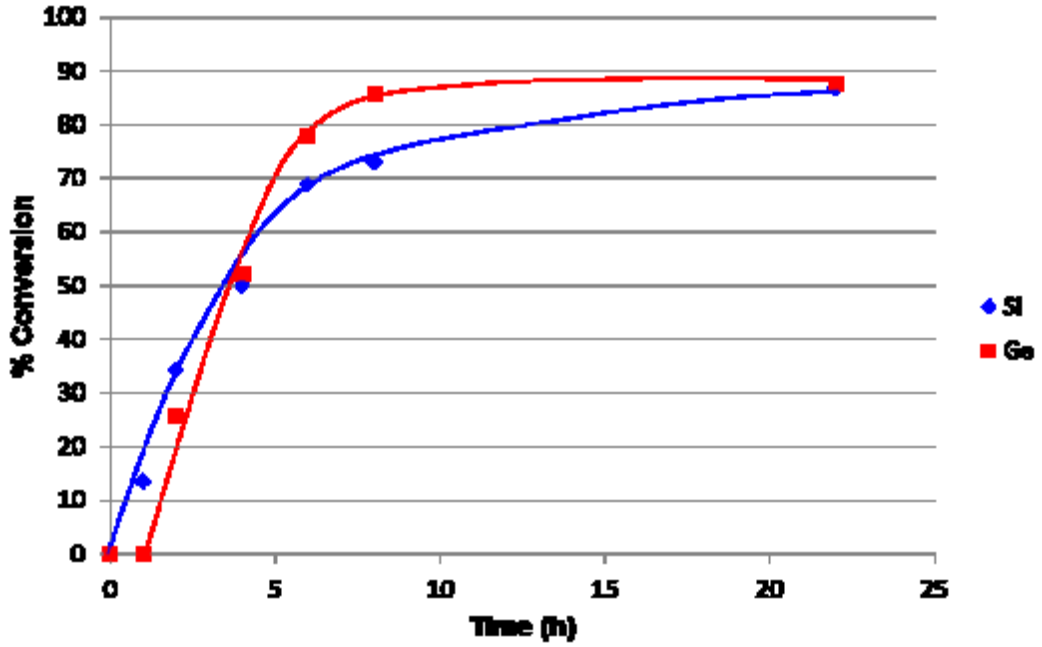

Figure 3.3.9. Catalytic hydrosilylation of *p*-methoxyacetophenone using triethoxysilane and 2 mol % of **[ENE]Fe(PMe$_3$)$_2$** (E = Si^{II}: diamonds/blue, Ge^{II}: squares/red) complexes as precatalyst.

the possibility to work a high temperatures and its ease post-reaction removal. Different temperatures were tested between a range of 40-80 °C (entries 3, 6-9) showing 70 °C as an optimal temperature for these reactions. Evaluating different silanes showed that the yield depends on the electronic nature of the silane used. Triethylsilane (entry 10) remained virtually unreacted whereas dimethylphenylsilane (entry 11) gave moderate yields, indicating that the steric effects around the hydrosilane play a role in this reaction. As expected, the more reactive di- and trihydrosilanes improved the yield further (entries 12-13). Finally, alkoxysilanes such as triethoxysilane and polymeric silane polymethylhydrosiloxane (PHMS) gave distinctly the best results at relatively mild conditions. The reaction with the commercially available and inexpensive polymeric silane PMHS highlights the possibility to apply this system in low cost ketone reduction processes. Unfortunately, increasing the reaction temperature from 40 °C to 70 °C (entry 15) results in a decrease in the yield, contrary to the reaction with the triethoxysilane where an improved reaction yield was observed (entries 3 and 6). Decreasing the quantity of the reducing agent resulted in an unaltered reaction yield; however, excess of 0.5 molar equiv

was required to maintain the maximum reaction yield (entries 16-20). Reduction on the catalyst loading revealed lower catalytic yields in the evaluation time of 22 h (entries 22-23) and no background activity was observed when the catalyst was absent (entry 21). This showed unambiguously the activity of the **[SiNSi]Fe(PMe$_3$)$_2$** complex as precatalyst in the hydrosilylation of ketones.

Table 3.3.4. Catalytic activity of **[SiNSi]Fe(PMe$_3$)$_2$** as precatalyst in the hydrosilylation of *p*-methoxyacetophenone.[a]

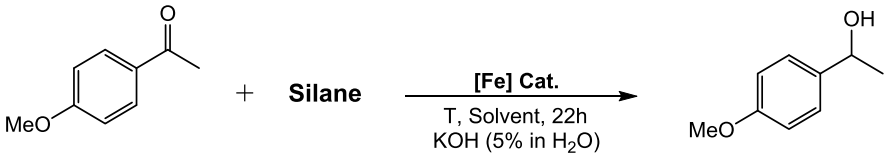

Entry	Solvent	T (°C)	Silane (equiv)	Cat. (mol %)	Yield (%)[b]
1	Hexanes	70	$(EtO)_3SiH$ (3)	2.5	89
2	Toluene	70	$(EtO)_3SiH$ (3)	2.5	92
3	THF	70	$(EtO)_3SiH$ (3)	2.5	96
4	Dioxane	70	$(EtO)_3SiH$ (3)	2.5	85
5	DMA	70	$(EtO)_3SiH$ (3)	2.5	95
6	THF	40	$(EtO)_3SiH$ (3)	2.5	68
7	THF	50	$(EtO)_3SiH$ (3)	2.5	86
8	THF	60	$(EtO)_3SiH$ (3)	2.5	91
9	THF	80	$(EtO)_3SiH$ (3)	2.5	99
10	THF	40	Et_3SiH (3)	2.5	1
11	THF	40	$Ph(CH_3)_2SiH$ (3)	2.5	26
12	THF	40	Ph_2SiH_2 (3)	2.5	40
13	THF	40	$PhSiH_3$ (3)	2.5	48
14	THF	40	PMHS (3)	2.5	62
15	THF	70	PMHS (3)	2.5	43
16	THF	70	$(EtO)_3SiH$ (1.1)	2.5	73
17	THF	70	$(EtO)_3SiH$ (1.5)	2.5	>99
18	THF	70	$(EtO)_3SiH$ (2)	2.5	>99
19	THF	70	$(EtO)_3SiH$ (2.5)	2.5	>99
20	THF	70	$(EtO)_3SiH$ (4)	2.5	98
21	THF	70	$(EtO)_3SiH$ (1.5)	0	0
22	THF	70	$(EtO)_3SiH$ (1.5)	0.5	77
23	THF	70	$(EtO)_3SiH$ (1.5)	1.0	88

[a]Reaction conditions: *p*-methoxyacetophenone (0.10 mmol). [b]Average yield from two runs determined by GC-MS and ^{1}H NMR using anisole as internal standard.

Once the reaction conditions were optimized, the substrate scope and limitations were tested with ketones bearing different steric and electronic properties (Table 3.3.5). Good functional group tolerance was observed from substrates bearing electron donating (entries

1-3) to those with electron withdrawing groups (entries 4, 6) on the aromatic ring. However, the reaction yield for the *p*-diethylaminoacetophenone was reduced considerably (entry 2). In general electronic effects were not observed for the substrate scope but steric effects seem to dominate. For instance, when a 2,6-disubstituted ketone was used the reaction yields decreased dramatically (entries 10 and 11). The reaction yields were significantly lowered when using either electron donating or electron withdrawing groups

Table 3.3.5. Substrate scope for the hydrosilylation of ketones using the **[SiNSi]Fe(PMe$_3$)$_2$** complex as precatalyst.[a]

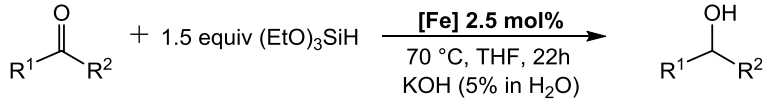

Entry	R^1		R^2	Yield[b] (%)	Ref.
1	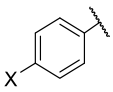	X = OMe	Me	>99	186
2		X = NEt_2	Me	40	187
3		X = Me	Me	82	188
4		X = Br	Me	>99	189
5		X = H	Me	93 95[c]	186
6		X = CF_3	Me	95	186
7		X = OMe	Me	70	188
8		X = Me	Me	70	190
9		X = Cl	Me	49	188
10	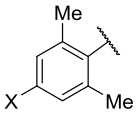	X = Me	Me	<1	188
11		X = *t*Bu	Me	3	188
12	Ph		Ph	60	190
13	Ph		Et	18	188
14	Ph		*i*Pr	16	188
15	4-Br-C_6H_4		Ph	92	191
16	2-Me-C_6H_4		Ph	41	188
17	4-py		Me	72	192
18	2-furanyl		Me	84	193
19	cyclopropyl		Me	>99	194
20	4-*t*Bu-cyclohexanone		-	25 (*cis*, d.r. > 20:1)	195

[a]Reaction conditions: precatalyst (0.0025 mmol), substrate (0.10 mmol), $(EtO)_3SiH$ (0.15 mmol). [b]Average yield from two runs determined by GC-MS and ^1H NMR using anisole as internal standard. [c]under the presence of 25 mol% of PMe_3.

at the *ortho* position (entries 7-9). Interestingly, benzophenone (entry 12) reacted readily while the substrates with larger aliphatic chains such as propiophenone (entry 13) and isobutyrophenone (entry 14) afforded yields of only 18 and 16 % yield, respectively. Substitution on the benzophenone also showed that steric effects control the catalytic perfomance since with 2-methylbenzophenone the reaction yield decreased considerably (entry 16) but with 4-bromobenzophenone the activity is comparable and even improved (entry 15) to the case when benzophenone was used as substrate (entry 12). Additionally, the reaction also tolerates ketones bearing heteroaromatic groups in good yields (entries 17, 18) which do not deactivate the catalyst. To see whether radicals are involved during the catalytic reaction, the cyclopropyl methyl ketone was evaluated (entry 19). Satisfying, the cyclorpopyl ring remained in the product suggesting that radicals are not involved in this reaction. Interestingly, when evaluating the 4-*tert*-butylcyclohexanone (entry 20) the predominance of the *cis*-4-*tert*-butylcyclohexanol in the product shows that the hydride transfer to the ketone is controlled by the steric effects (see further discussion in mechanistic studies).

3.3.3.2. Evaluation of the catalytic active species

After the catalytic reactions were conducted, the remaining solutions were homogeneous with orange color without any residue and/or precipitate. NMR spectroscopic evaluation of the remaining species in solution showed the selective formation of a new iron hydride species. The ^{1}H NMR spectrum revealed a hydride signal at $\delta = -14.84$ ppm while the $^{31}P\{^{1}H\}$ NMR spectrum showed a single resonance signal at $\delta = 16.8$ ppm. These data indicates that the resting state of the active species is most likely produced from the reaction between the **[SiNSi]Fe(PMe$_3$)$_2$** and the triethoxysilane. Thus, the reaction between **[SiNSi]Fe(PMe$_3$)$_2$** and different hydrosilanes was explored to gain insight into the mechanistic aspects. When a mixture of **[SiNSi]Fe(PMe$_3$)$_2$** and the hydrosilane was heated to 70 °C, new distinct signals appeared in the ^{1}H, $^{29}Si\{^{1}H\}$, and $^{31}P\{^{1}H\}$ NMR spectra respectively (Scheme 3.3.9). In particular, in the case of $(EtO)_3SiH$, the same characteristic signals were obtained as those of the remaining organometallic species after the catalytic reactions. The ^{1}H NMR spectrum clearly indicated the formation of the new iron hydride species **[SiCSi]FeH(SiR$_3$)(PMe$_3$)** by Si–H bond oxidative addition to the Fe^0 center.

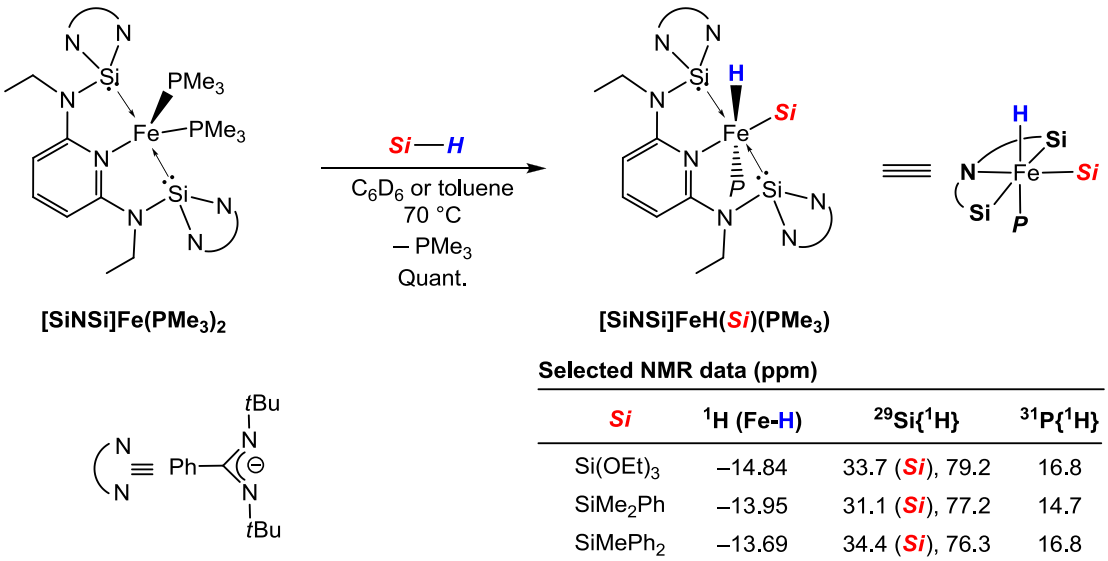

Selected NMR data (ppm)

Si	^{1}H (Fe-H)	^{29}Si{^{1}H}	^{31}P{^{1}H}
$Si(OEt)_3$	–14.84	33.7 (*Si*), 79.2	16.8
$SiMe_2Ph$	–13.95	31.1 (*Si*), 77.2	14.7
$SiMePh_2$	–13.69	34.4 (*Si*), 76.3	16.8

Scheme 3.3.9. Reaction of **[SiNSi]Fe(PMe$_3$)$_2$** with trisubstituted silanes affording the iron(II)-hydride-silyl complexes of type **[SiCSi]FeH(SiR$_3$)(PMe$_3$)**.

Detailed 2D NMR analysis revealed that the hydride is likely to be *trans* to the apical phosphine ligand. The silyl group was assigned by 2D NMR experiments to be at the equatorial position *trans* to the pyridine ligand. Single crystals suitable for XRD structure analysis of the **[SiCSi]FeH(SiMe$_2$Ph)(PMe$_3$)** complex were grown by layering *n*-pentane on a toluene solution at room temperature. The molecular structure of the **[SiCSi]FeH(SiMe$_2$Ph)(PMe$_3$)** complex was in accord with the spectroscopic findings, and confirmed the structure (Figure 3.3.10). The hydride could be located from the Fourier electron density map. The molecular structure depicts a distorted octahedral iron(II) center where the hydride is tilted towards one of the silylene donor arms and is deviated from the *trans* coordination to the trimethylphosphane, also observed in other iron(II)-hydride pincer complexes.[186] Moreover, the Si−Fe bond distances (Fe–Si^{II}: 2.1509(7), 2.1715(7) Å; Fe–Si^{IV}: 2.2986(8) Å) are within the range of silylene-iron complexes of type [(CO)$_4$Fe←:Si(O*t*Bu)L] (2.237(7) Å)[150] and [(dmpe)$_2$Fe←:Si(X)L] (X = Cl: 2.1634(9) Å; Me: 2.200(2) Å; H: 2.184(2) Å; L = *N,N'*-di-*tert*-butyl(phenylamidinato); dmpe = 1,2-bis(dimethylphosphino)ethane),[66] and silyl-iron pincer complexes of type [PNP]FeH(SiH$_2$Ph)(N$_2$) (2.2718(6) Å).[157] Noteworthy, the *t*Bu groups encage the hydride atom with an obtuse Si1−Fe−Si2 angle (144.54(3)°). This shows the poor accessibility for a substrate to react with the Fe–H bond. Therefore, reactivity along this bond was carried out

to study whether this is the reactive site within the complex or it is mearly a spectator group.

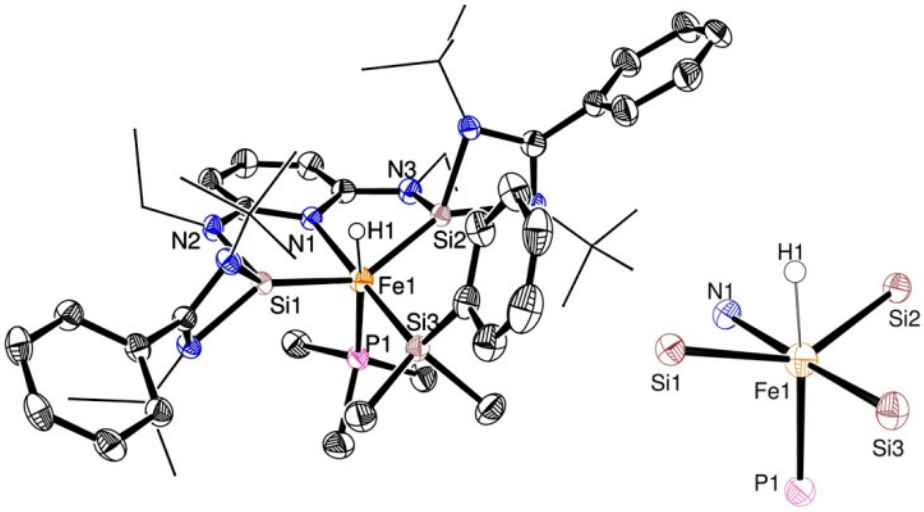

Figure 3.3.10. ORTEP representation of **[SiCSi]FeH(SiMe$_2$Ph)(PMe$_3$)** complex in the solid state with selected distances [Å] and angles [°]: Fe–N1 2.063(2), Fe–Si1 2.1509(7), Fe–S2 2.1715(7), Fe–Si3 2.2986(8), Fe–P 2.1975(8), Fe–H 1.430(5), Si1–Fe–Si2 144.54(3), N1–Fe–Si3 176.87(6), P–Fe–H 170.20(5), N1–Fe–Si1 82.72(6), Si1–Fe–Si3 95.53(3), Si1–Fe–H 66.53(5), Si2–Fe–H 85.43(5). Thermal ellipsoids are drawn at a 50% probability level; *t*Bu and Et groups are drawn in wire frame, and hydrogen and solvent atoms are omitted for clarity, except for H1.

3.3.3.3. Reaction between the iron(II)-hydride and acetophenone

Generally, metal hydrides react with the ketones *via* an insertion of the M–H bond into the C–O double bond.[196,197] Therefore, once the iron(II)-hydride complexes were characterized, a stoichiometric reaction with a ketone was carried out. Surprisingly, no reaction occurred between the **[SiCSi]FeH(SiMe$_2$Ph)(PMe$_3$)** complex and acetophenone (Scheme 3.3.10, right). Even at higher temperatures (70 °C) for prolongued times (> 2 days) no reaction occurred according to the ^{1}H and ^{31}P{^{1}H} NMR spectra. This "inert" reactivity of the Fe–H bond, rare within the metal hydrides, has been also observed in several examples with iron[186] and other transition metals.[198] However, theoretical studies have shown contradictory results to these experimental results. In the study from Guan and

co-workers[186] the Fe–H remained as spectator when the hydrosilylation reaction was carried out. But Wei and co-workers[199] showed that the ketone insertion on this Fe–H bond is the most energetically favoured pathway, and postulated it as the most likely reaction mechanism, which strongly contradicts the experimental results from Guan. Additionally, silyl insertion into the C–O double bond might be likely, in accordance with the Chalk-Harrod mechanism, however, this was also not observed (Scheme 3.3.10, left).

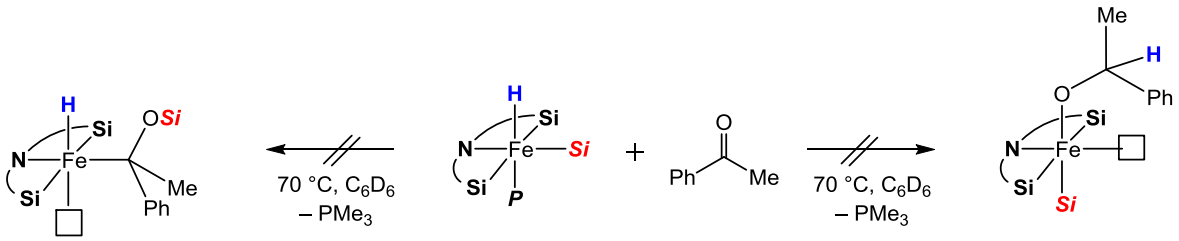

Scheme 3.3.10. Stoichiometric reaction between the **[SiCSi]FeH(SiR$_3$)(PMe$_3$)** complexes and acetophenone showing the inert behavior of the Fe–H and Fe–Si^{IV} bonds toward a carbonyl function (square means a vacant coordination site).

Due to this unexpected result, the study of the reaction mechanism had to be conducted based on the mechanism proposals reported in the literature. Therefore, a short description of the possible mechanisms involved in ketone hydrosilylation is described in the following section.

3.3.3.4. Reported mechanisms for ketone hydrosilylation[196,197,200]

In the pioneering work by Ojima and co-workers a modified Chalk-Harrod mechanism was postulated for the hydrosilylation of organic carbonyls (Scheme 3.3.11).[197,200] Firstly, the silane is oxidatively added over a metal center in the (pre)catalyst. Then, the formed metal-silyl-hydrido species can react with the ketone either by insertion into the M–H bond or into the M–Si bond. Both species can reductively eliminate the product forming a catalytic cycle depending on two oxidation states of the metal center M^n and $M^{(n+2)+}$. However, those metals which are not prone for reductive elimination, their alkoxide or alkyl complexes can react with another silane molecule (two silanes cycle). In the former, a σ-bond metathesis can occur with the "free" silane recovering the metal hydride species with the silyl group, of the first activated silane, remaining as spectator. In contrast, the

alkyl intermediate reacts *via* another oxidative addition forming a high valent metal complex $M^{(n+4)+}$ which then undergoes reductive elimination to produced the silyl ether product and the metal-silyl-hydride species. In these two mechanisms, depending on the reaction pathway the hydride and silyl source vary. Thus, the discrimination between both can be done evaluating the final products employing crossover experiments using two different silanes.

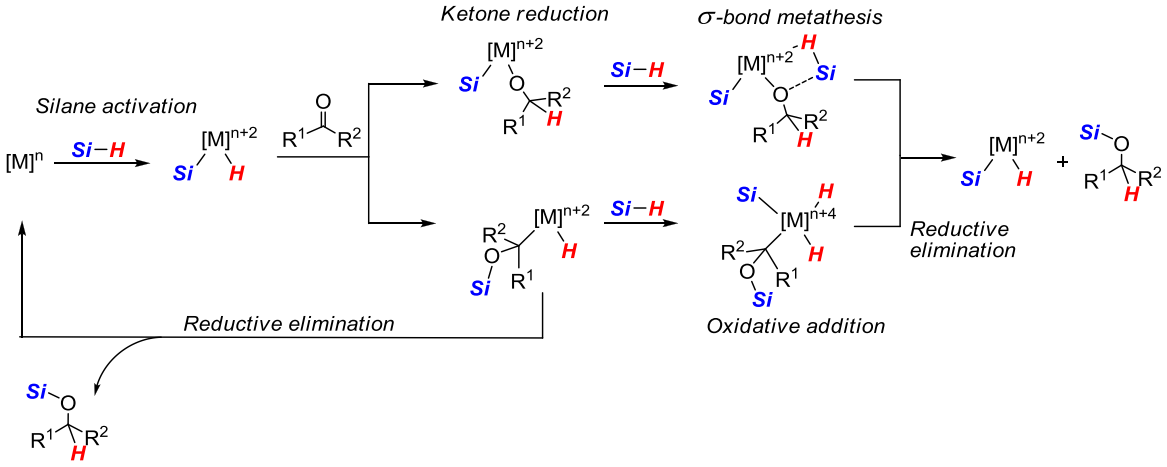

Scheme 3.3.11. Ojima mechanism (modified Chalk-Harrod) for ketone hydrosilylation by metal hydride species.

Recently, another plausible proposed mechanism for the metal-catalyzed hydrosilylation reactions was accounted based on the Lewis acid concept. Basically, the metal center can act as a Lewis acid to activate either the ketone or the silane (Scheme 3.3.12).[186,196] It is argued, and some mechanics studies have shown, that when the silane is activated a silylium cation is formed.[201,202] This cation is transferred immediately to the ketone to form the silyloxonium cation and a metal-hydride species. The silyloxonium cation is strongly polarized and has the carbonyl function activated. It reacts further by a nucleophillic attack from the hydride species to form the silyl ether product and without changing the oxidation state of the metal center. For the case when the ketone is activated, a hydrosilylation occurs without any interaction between the silane and the metal center. The major distinction between both reaction pathways is the formation of the silylium cation with a concomitant S_N2 type reaction. Therefore, the use of a chiral silane would distinguish between both reaction pathways.

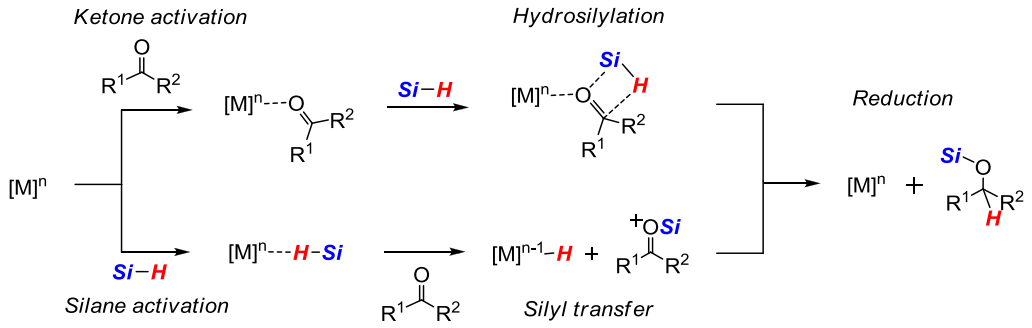

Scheme 3.3.12. Proposed mechanism for hydrosilylation of ketones involving a metal center acting as a Lewis acid.

3.3.3.5. Hydride scrambling

3.3.3.5.1. Silane *Si*–D/Fe–H scrambling using Me_2PhSiD

Firstly, the nature of the proton transfer to the carbonyl function was studied. For this purpose the possibility of a hydride scrambling was followed by a reaction between the **[SiCSi]FeH(SiMe$_2$Ph)(PMe$_3$)** complex and the deuterated silane Me_2PhSiD (>95% in D). A mixture of **[SiCSi]FeH(SiMe$_2$Ph)(PMe$_3$)** and Me_2PhSiD in THF at 70 °C presented a slow H/D exchange (Scheme 3.3.13, red curve) reaching a statistical ratio 50:50 after 24 h. This result shows that the Fe–H bond is not inert as previously seen with the unreacted mixture with acetophenone (see section 3.3.3.3). This is contrary to the other iron hydrido system where the Fe–H/Si–H exchange was not observed.[186] In addition, in the stoichiometric reaction between **[SiCSi]FeH(SiMe$_2$Ph)(PMe$_3$)**, Me_2PhSiD, and acetophenone (section 3.3.5.2) the kinetics for the exchange in the silane (Scheme 3.3.13, blue curve) is at the same order of magnitude than in the absence of the ketone. Therefore, this exchange has to be taken into account during the understanding of deuterated studies in the ketone hydrosilylation process (section 3.3.5.2).

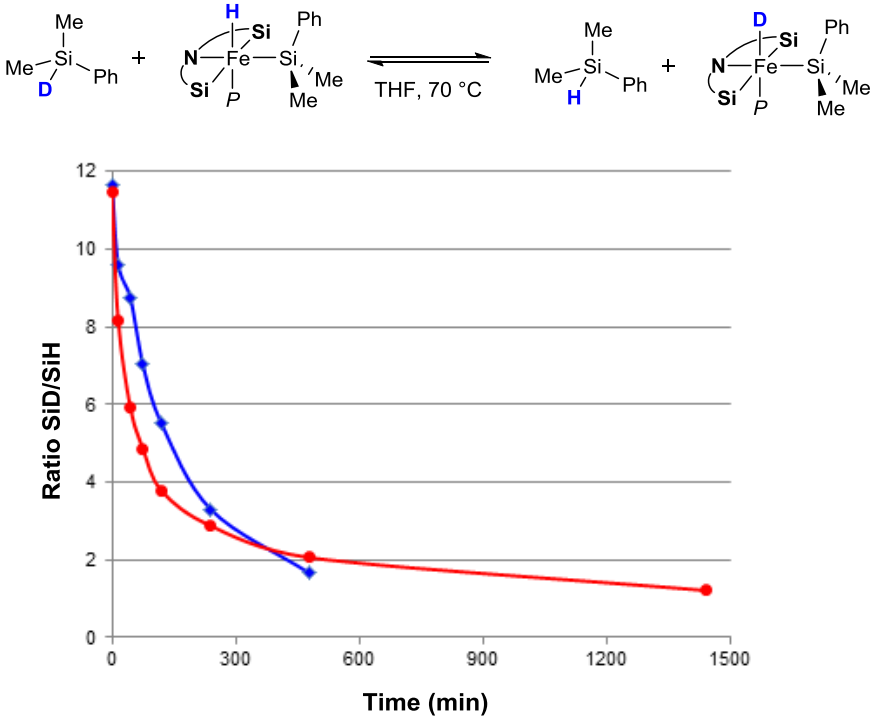

Scheme 3.3.13. Evaluation of the Fe−H/Si−D exchange in Me_2PhSiH under the catalytic conditions with (diamonds, blue curve) and without acetophenone (circles, red curve).

3.3.3.5.2. Deuteration studies with Me_2PhSiD

Once the Fe−H/Si−D exchange was determined (see previous section 3.3.3.5.1), the stoichiometric reaction between **[SiCSi]FeH(SiMe$_2$Ph)(PMe$_3$)** (1.0 equiv), Me_2PhSiD (1.1 equiv, >95% in D), and acetophenone (1.5 equiv) was carried out and analyzed periodically by GC-MS (Scheme 3.3.14). The D/H ratio in the product was calculated according to the intensity of the peaks 242/241 $[M–CH_3]^+$ in the mass spectrum for the GC peak corresponding to the silyl ether product **1*a***. Unexpectedly, the result was puzzling at the first and last regimes (Scheme 3.3.14, top figure). Initially, the D:H ratio at the methine position of the silyl ether is nearly 50:50. However, it quickly increases reaching a maximum of 64:36 at the first 6 hours with 25% of conversion. Then, unexpectedly it progressively decreases again, reaching the equilibrium at 50:50 at full conversion after a few days. Meanwhile, the corresponding reaction with partially deuterated Me_2PhSiD/H (~50% deuteration grade) yielded the silyl ether product with just a little deuterated ratio after 19% conversion (D/H = 10:90). This ratio rapidly increases further to 22:78, reaching

an equilibrium plateau after 4 hours. These results reveal that even though the hydride at the silicon atom in Me_2PhSiD is exchanging with the iron-bound hydride in **[SiCSi]FeH(SiMe$_2$Ph)(PMe$_3$)**, hydride transfer to the carbonyl carbon atom of acetophenone occurs from the hydrosilane and not from iron complex.[186,198] Moreover, the reaction with partially deuterated hydrosilane indicates that the kinetic isotope effect of that hydride transfer is significant since the non-deuterated product predominates at the first regime.

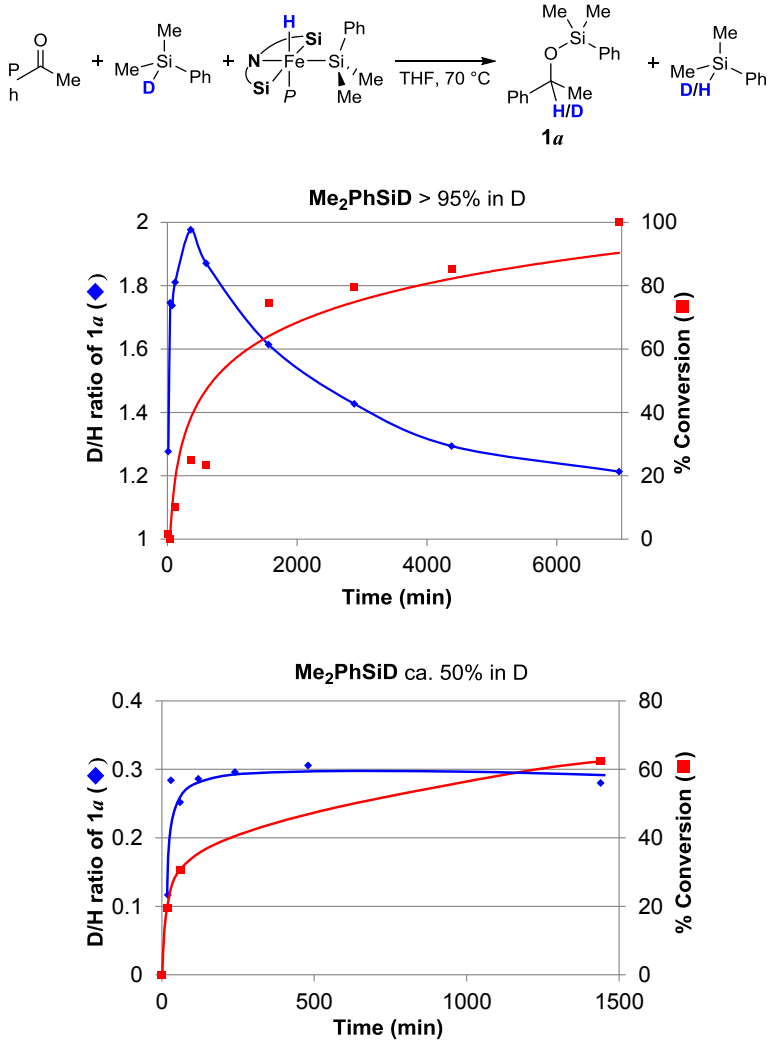

Scheme 3.3.14. Evaluation of the deuteration ratio in **1*a*** using the deuterated silane Me_2PhSiD with different deuteration grade (>95%: top, 50%: bottom). A high isotopic effect is observed by the predominance of the non-deuterated product at first regime and strong indication of "free" silane being transferred to the final product.

3.3.3.6. Scrambling at the C−H bond

3.3.3.6.1. Scrambling experiment with deuterated silyl ether

The constant decrease in the D/H ratio at the silyl ether product (see precious section 3.3.3.5), in the experiment with the deuterated hydrosilane Me_2PhSiD (>95% in D), even after 80% conversion suggests that the methine proton most likely exchange with the Fe–H from **[SiCSi]FeH(SiMe$_2$Ph)(PMe$_3$)**. Then a control experiment with a deuterated silyl ether **1*a*-*d*$_1$** (>98% in D) was conducted (Scheme 3.3.15). An equimolar reaction mixture of the **1*a*-*d*$_1$** and **[SiCSi]FeH(SiMe$_2$Ph)(PMe$_3$)** indeed led to a constant C–D/Fe–H scrambling, reaching a deuteration rate of 92% after 3 days.

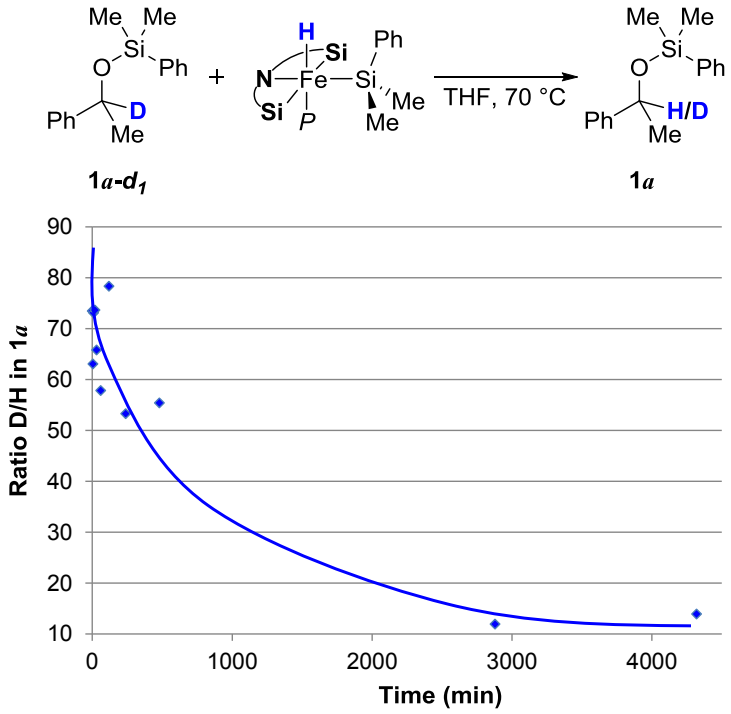

Scheme 3.3.15. C–D/Fe–H scrambling at the methine group in the silyl ether **1*a***. This scambling confirmed the decrease in the D:H ratio in the silyl ether **1*a*** with the time in the previously shown deuterated studies (section 3.3.3.5).

3.3.3.6.2. Racemization experiment with enantiopure silyl ether

Nevertheless, the previous experiment does not prove the mechanism for this C–D/Fe–H interchange and it is unclear whether the final step in the hydrosilylation is reversible. For this porpuse an enantiopure silyl ether **(*S*)-1*a*** was treated under the catalytic conditions (precatalyst **[SiCSi]Fe(PMe$_3$)$_2$** and Me_2PhSiH generate catalyst **[SiCSi]FeH(SiMe$_2$Ph)(PMe$_3$)**, Scheme 3.3.16). The reaction mixture was evaluated periodically by a chiral HPLC to see whether racemization occurs at the benzillic carbon. The different samples showed no erosion of the enantiomeric purity of the silyl ether **(*S*)-1*a*** even for a prolongued reaction time (> 6 days). The configurational stability of **(*S*)-1*a*** suggests that the last step in the formation of the product, involving hydride transfer, is irreversible. Consistently, a concerted mechanism involving frontside attack at the asymmetrically substituted carbon atom is needed to explain the hydrogen atom exchange between the catalyst and the product.

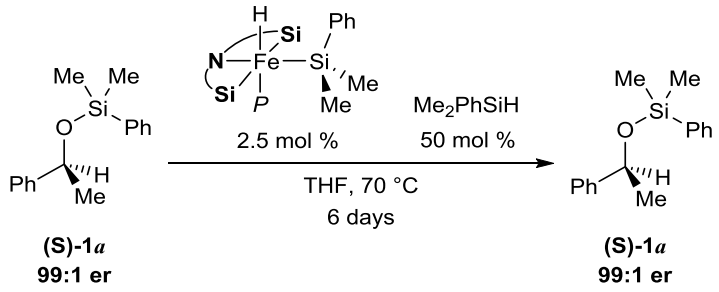

Scheme 3.3.16. Evaluation of the enantiomeric stability by a C–H/ Fe–H scrambling under the catalytic conditions.

3.3.3.7. Silyl scrambling

Before evaluating the fade of the silyl group transfer to the silyl ether product, a control experiment of silyl scrambling was realized. A mixture of **[SiCSi]FeH(SiMe$_2$Ph)(PMe$_3$)** with a different hydrosilane $MePh_2SiH$ in C_6D_6 was heated up at 70 °C and evaluated periodically by ^{1}H NMR spectroscopy (Scheme 3.3.17). Initially lot of decomposition was observed, however, with the time a partial scrambling up to 10% was observed. Nonetheless, it was visible that this type of scrambling is not involved within the evaluation of the stoichiometric reactions due to its slow kinetics.

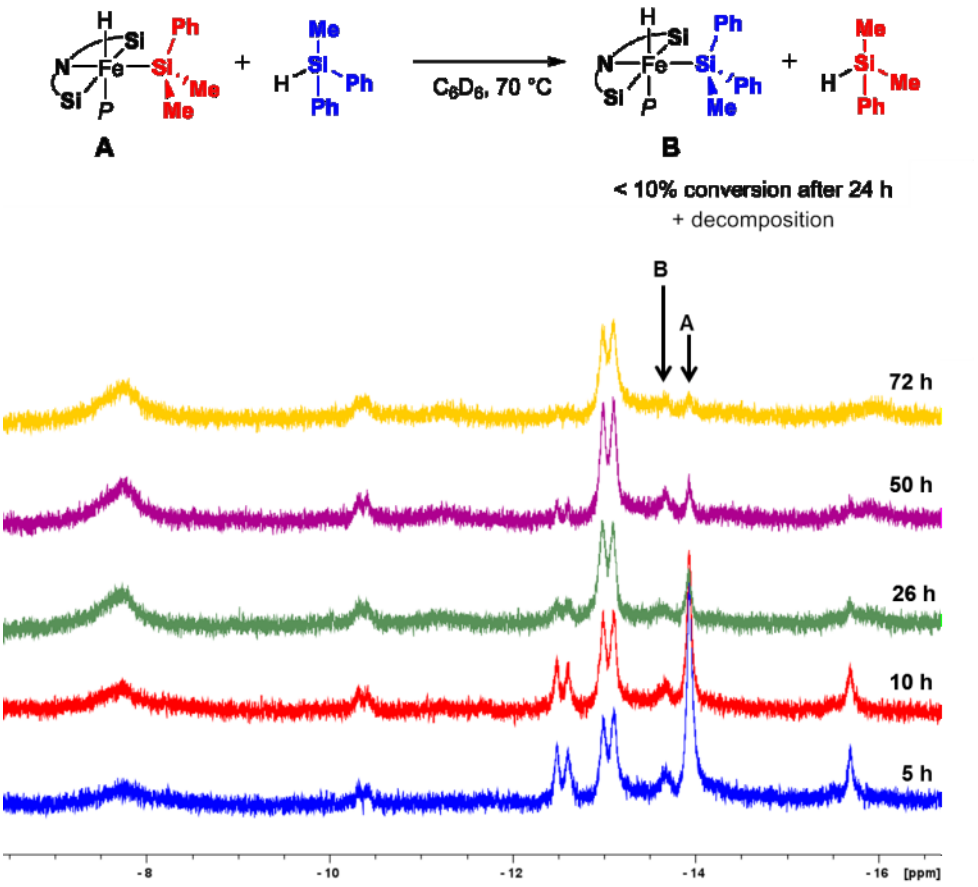

Scheme 3.3.17. Evaluation of the silyl scrambling in the **[SiCSi]FeH(SiMe$_2$Ph)(PMe$_3$)** complex and the stacked ^{1}H NMR spectra in the hydride region for different times.

3.3.3.8. Phosphine scrambling

The accessibility of the iron center in **[SiCSi]FeH(SiMe$_2$Ph)(PMe$_3$)** complex was also tested by a possible phosphine scrambling. A NMR experiement was carried out following the reaction mixture of this complex with PEt_3 at 70 °C. Along the evaluation time, just the $^{31}P\{^1H\}$ signals corresponding to the **[SiCSi]FeH(SiMe$_2$Ph)(PMe$_3$)** complex and free PEt3 were observed without the formation of the phosphine exchange product **[SiCSi]FeH(SiMe$_2$Ph)(PEt$_3$)** nor free PMe_3. Additionally, a catalytic test using acetophenone as substrate and an excess of PMe_3 (25 mol%) did not alter the catalytic yield

(Table 3.3.5, p. 118). These results suggest that the decoordination of the PMe_3 is quite unlikely for the formation of the catalytic active species

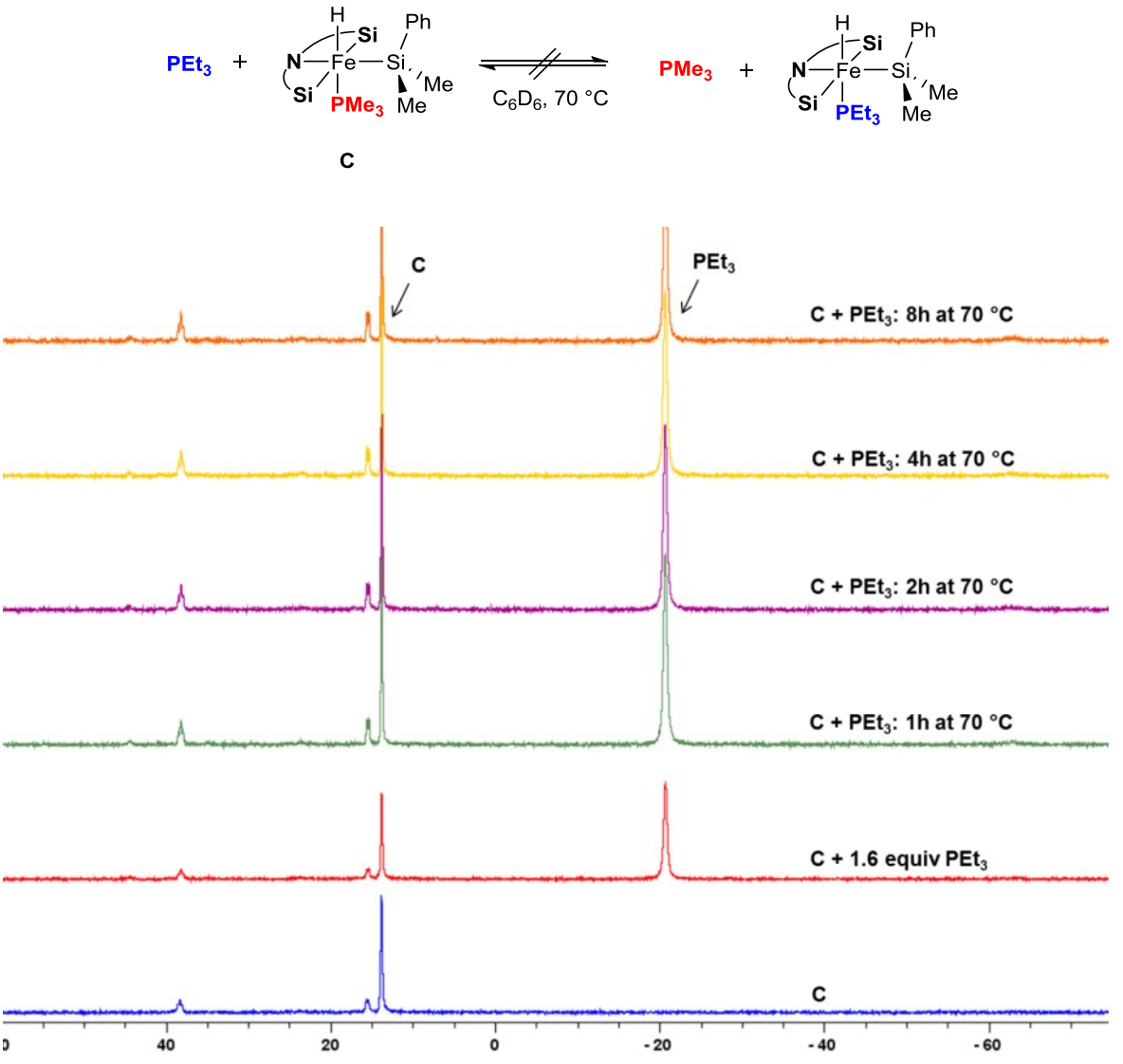

Scheme 3.3.18. Evaluation of the phosphine scrambling in the **[SiCSi]FeH(SiMe$_2$Ph)(PMe$_3$)** complex and the stacked $^{31}P\{^1H\}$ NMR spectra at different time.

3.3.3.9. Crossover experiment

To evaluate whether the silyl group is transferred either from the metal complex or from the hydrosilane to the carbonyl group, a crossover experiment was carried out. Using a mixture of stoichiometric amounts of **[SiCSi]FeH(SiMe$_2$Ph)(PMe$_3$)**, acetophenone and MePh$_2$SiH in THF at 70 °C the silyl transfer was studied (Scheme 3.3.19). Remarkably, the silyl ligand Fe–SiMe$_2$Ph at the metal complex remained as spectator ligand whereas the silyl at the hydrosilane is transferred to the carbonyl group producing exclusively **1*b***. During the reaction a partial silylation containing the silyl group from the metal complex was observed; related with the silyl scrambling described above (section 3.3.3.7).

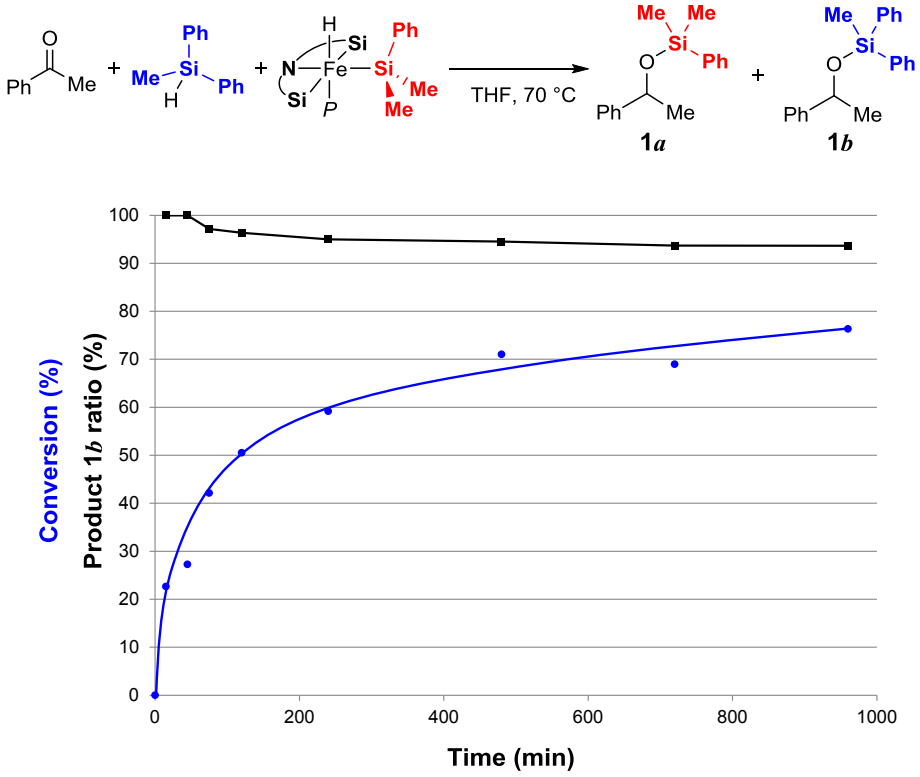

Scheme 3.3.19. Crossover hydrosilylation experiment evaluating the nature of the silyl group transfered to the carbonyl function.

3.3.3.10. Catalytic reaction between acetophenone with an enantioenriched acyclic silane (MeiPrPhSiH)

3.3.3.10.1. Hydrosilylation reaction

A sufficient understanding of the reaction was reached after carrying out the crossover and deuterated experiments defining the source of the hydride and silyl into the final silyl ether product. However, how the silyl transfer to the carbonyl function remained to be solved. Therefore, a reaction to investigate the stereochemical course of the silyl group being transferred was studied.[201,202] The **[SiCSi]FeH(SiMe$_2$Ph)(PMe$_3$)** complex catalyzed the reaction between enantioenriched silane (^{Si}S)-Me*i*PrPhSiH (e.r. >95:5) and acetophenone. As expected, based on the results obtained with Me$_2$PhSiH as the hydrosilane in the catalytic evaluation (see Table 3.3.4, p. 117, entry 11), the reaction was slow. After 6 days a 31% isolated yield was obtained for the silyl ether **1*c*** with poor d.r. ratio 56:44 (Scheme 3.3.20). The remained unreacted silane (^{Si}S)-Me*i*PrPhSiH was separated from the main product by a flash chiral column chromatography. Interestingly, its enantiomeric ratio was found to be unaffected (e.r. >95:5). This result suggests that the Fe–H/Si–H scrambling (see section 3.3.3.5.1) most likely occur in a concerted mechanism involving frontside attack at the asymmetrically substituted silicon likewise the Fe–H/C–H scrambling with the silyl ether product **1*a***.

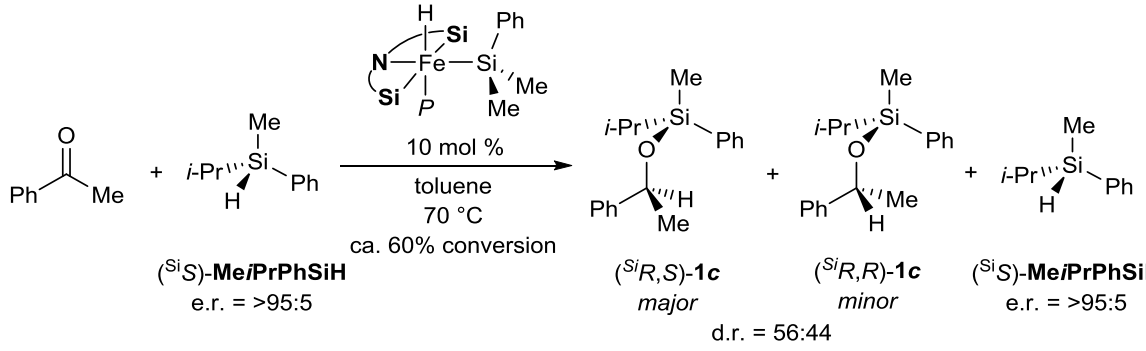

Scheme 3.3.20. Hydrosilylation with enantiomerically enriched (^{Si}S)-**Me*i*PrPhSiH** of acetophenone catalyzed by the **[SiCSi]FeH(SiMe$_2$Ph)(PMe$_3$)** complex.

3.3.3.10.2. Reductive Si–O bond cleavage of silyl ether

Subsequently, the silyl ether **1*c*** was treated with DIBAl−H with the aim to obtain a reductive cleavage of the Si−O bond with chiral retention at the silicon center (Scheme 3.3.21). Remarkably, after this treatment the silane (^{Si}S)-**Me*i*PrPhSiH** presented complete retention of stereochemistry at the silicon atom (e.r. >95:5). This is in strong contrast to other reported metal-catalyzed[199,202,203] or Lewis acid-catalyzed[201] hydrosilylation reactions where an inversion on the silicon center was observed. The observed stereochemical retention would be unlikely in a mechanism involving Lewis acid activation of the silane, which would lead to inversion (see scheme 3.3.12, p. 124). Hence, a concerted mechanism where the iron complex activates the carbonyl function of the ketone must be the key point for this reaction.

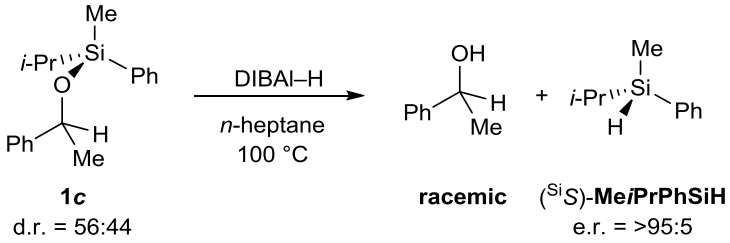

1*c*
d.r. = 56:44

racemic (^{Si}S)-**Me*i*PrPhSiH**
e.r. = >95:5

Scheme 3.3.21. Reductive Si−O bond cleavage with retention at the silicon center.

3.3.3.11. Proposed mechanism

Based on the experimental results a plausible mechanism is proposed. First, the active catalyst is generated from the iron(0) precatalyst **A** by oxidative addition of a silane to the iron(0) center to give the iron-hydrido-silyl complex **B** (Scheme 3.3.22). Due to the sterics around the Fe^{II} center, no dissociation of the trimetylphosphane from the iron center, and the same catalytic performance under the presence of an excess of trimethylphosphane, it is unlikely that the reaction would take place at the metal center. This, in addition of the nature of the hydride and silyl in the final product, the activation must occur in the ketone. Thus, it is proposed that the silicon center, of the silyl ligand, would be sufficiently Lewis acidic to coordinate the ketone substrate.[204] Unfortunately, this adduct must have a low energy barrier because by VT-NMR experiments interaction between acetophenone and the complex **B** was not observed. Therefore, DFT calculations were employed at ωB97X-D/6-

31G(d)[Fe:cc-pVTZ] level of theory to corroborate the existence of this unusual intermediate **C** (Figure 3.3.11). The silicon atom is pentacoordinate in a distorted trigonal bipyramidal structure with Σ<Si3 = 357.46° with the equatorial ligands. The C−O double bond is significantly elongated compared to its equilibrium distance from 1.211 to 1.251 Å, which indicates a weak activation because it is at the range of C−O double bond and not at the C−O single bond of ca. 1.43 Å.[126] The energy of this elusive Lewis pair **C** is +2.8 Kcal/mol more than the substrates, however, it is energetically low enough to serve as an intermediate in the catalytic cycle.

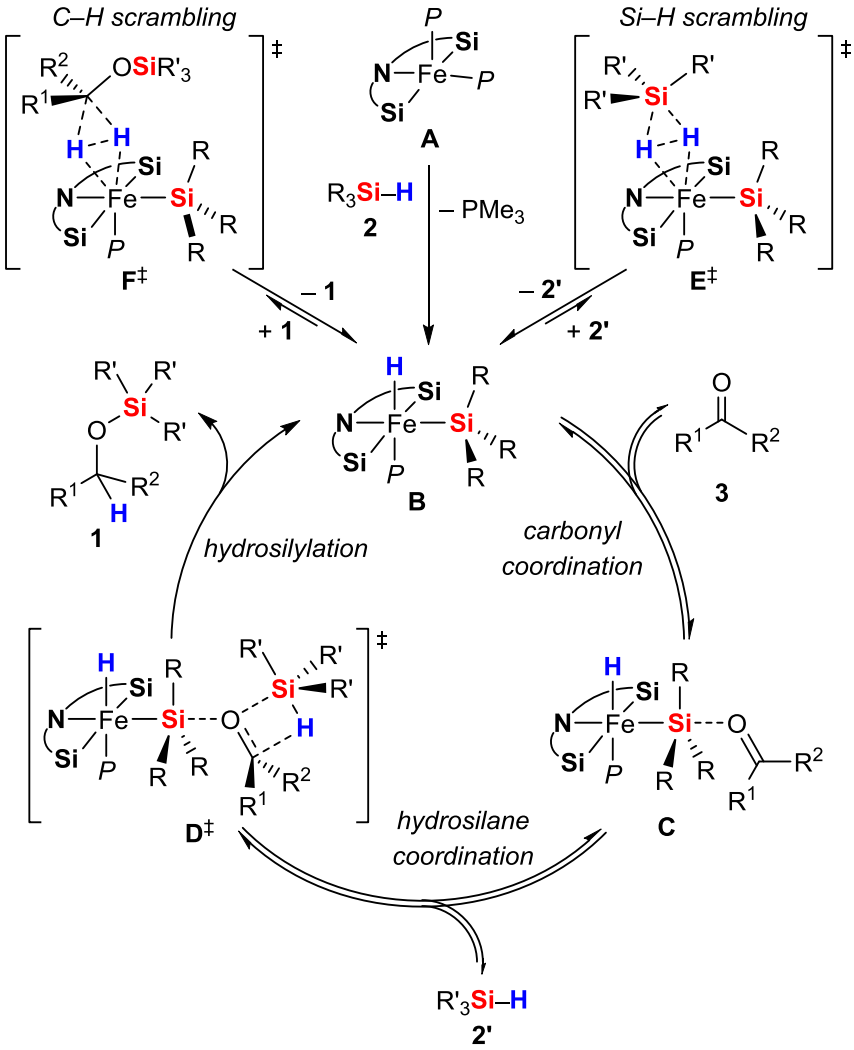

Scheme 3.3.22. Proposed mechanism for the hydrosilylation of ketones catalyzed by hydrido-silyl-iron(II) pincer complexes of type **[SiCSi]FeH(SiR$_3$)(PMe$_3$)**.

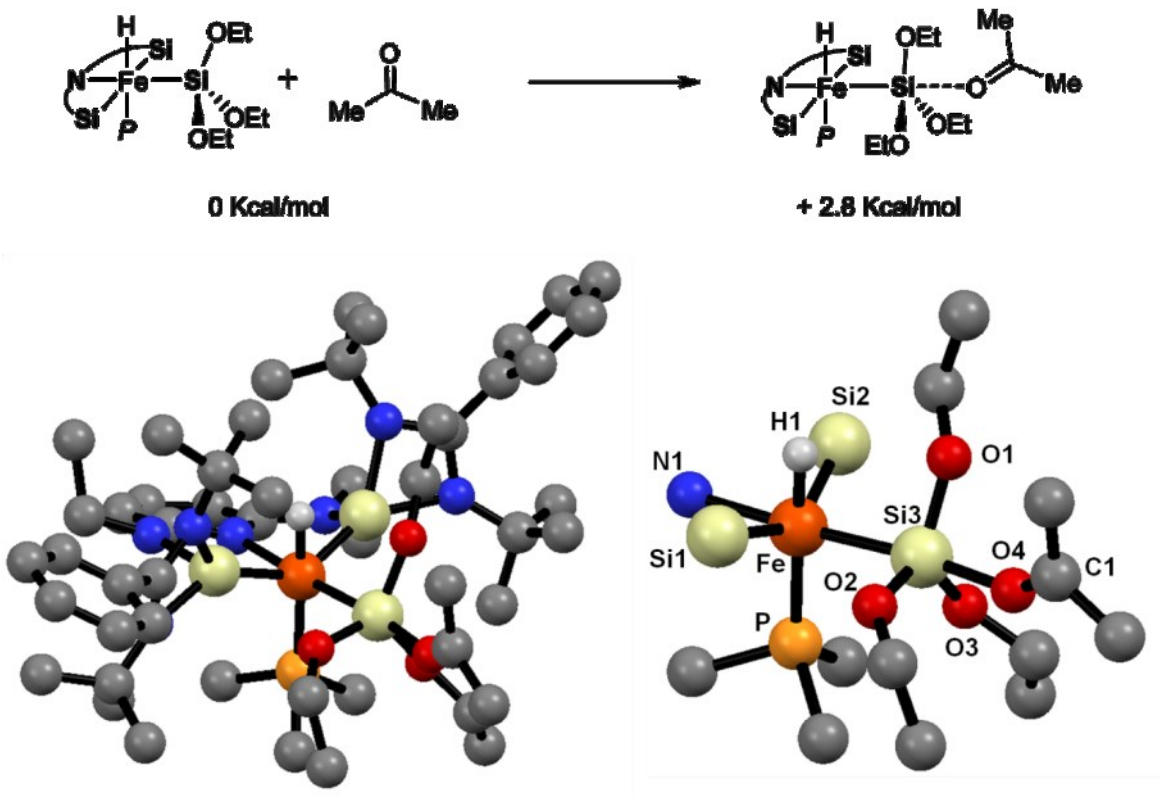

Figure 3.3.11. Calculated structure of the key intermediate C formed from the **[SiCSi]FeH(Si(EtO)$_3$)(PMe$_3$)** complex and acetone at ωB97X-D/6-31G(d)[Fe:cc-pVTZ] level of theory. Selected distances [Å] and angles [°]: Fe−Si1 2.430, Si3−O4 1.931, C1−O4 1.251, Si3−O1 1.746, Si3−O2 1.780, Si3−O3 1.760, Fe−Si3−O4 173.36, Si3−O4−C1 145.96, N1−Fe−Si3 177.25, Σ<(Si3−O123) 357.46.

The catalytic cycle is followed by the hydrosilane coordination to the carbonyl group in **C** producing of the most likely intermediate **D**‡. This intermediate is also supported by the catalytic evaluation using as substrate 4-*tert*-butyl-cyclohexanone (Table 3.3.5, p. 118, entry 20) where exclusively the formation of the *cis*-4-tert-butyl-cyclohexanol was observed. This result can only occur when such a concerted mechanism occur during the hydrosilylation since thehydride attack to the carbonyl in this substrate occur trans to the *t*Bu group. Then, the hydrosilylation process occurs *via* this **D**‡ intermediate with retention at the silicon atom (cf. section 3.3.3.10) forming the product **1** and recovering the resting state **B** of the catalyst. According to the labeling experiments (cf. section 3.3.3.5.2), this is the rate-determining step for the hydrosililation reaction catalyzed by these hydrido-silyl-

Fe^{II} complexes. To further validate this, a competition experiment between electron-rich and electron-deficient ketones was conducted (Scheme 3.3.23). The *para* substitution in the acetophenone shows a pronounced electronic effect, observed by significantly faster consumption of the CF_3-substituted than the MeO-substituted. This reactivity pattern is not unprecedented and it has been observed in silylium-catalyzed hydrosilylation of ketones,[204] which is in agreement with the coordination of the C−O double bond to a electron-poor silicon atom. The electrophilic carbon atom, in the electron-rich ketone **3-MeO,** is more negatively polarized, i.e., less susceptible to hydride attack, than in the electron-deficient ketone **3-CF_3**. This result points out against a carbonyl activation mechanism since the more Lewis-basic ketone **3-MeO** should be more reactive than the less Lewis-basic **3-CF_3**. Outside the catalytic cycle, both the hydrosilane **2** (cf. section 3.3.3.5.1) and the silyl ether **1** (cf. section 3.3.3.6) scramble with the iron(II) hydride **B** by concerted processes *via* the transition states $\mathbf{E}^{\ddagger}$ and $\mathbf{F}^{\ddagger}$, respectively. In conclusion, it has been shown for the first time, to our knowledge, that the metal center is not directly involved in the catalytic process. Activation of substrates occurs at the coordination sphere of the iron center, i.e., on the periphery of the transition metal. This is in contrast to the conventional mechanisms described for ketone hydrosilylation reactions (cf. section 3.3.3.4).

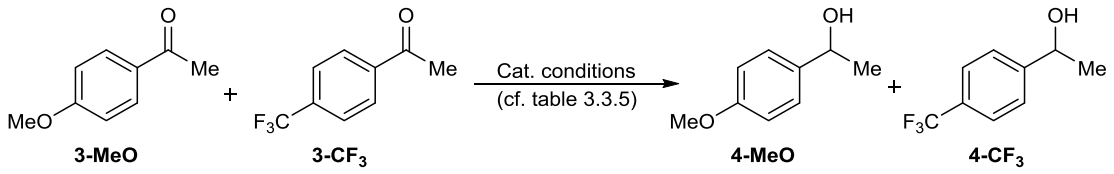

Time (min)	Conv. 4-MeO (%)	Conv. 4-CF_3 (%)
2	4	84
5	21	99
15	32	99

Scheme 3.3.23. Competition experiment with two different ketones highlighting the electronic effects for the catalytic performance. The more electropositive carbon in the ketone reacts faster contrary to a ketone activation process.

4. SUMMARY

The novel pincer ligands based on N-heterocyclic silylenes and germylenes, denominated as **GeCHGe**, **GeCBrGe**, **SiNSi**, and **GeNGe** were synthesized by salt metathesis reactions using the chloro substituted metallylene **5-NHSi** and **1-NHGe**. For the ligands **GeCHGe**, **SiNSi**, and **GeNGe** a direct deprotonation of 4,6-di-*tert*-butylresorcinol or 2,6-diamine-*N,N'*-diethylpyridine by 2 equiv of *n*-BuLi was used. The *in situ* formed dilithiated salt reacted with either **5-NHSi** or **1-NHGe** to afford the ligands in gram scale and high yields (**GeCHGe:** 83%; **SiNSi:** 90%; **GeNGe:** 98%, Figure 4.1).

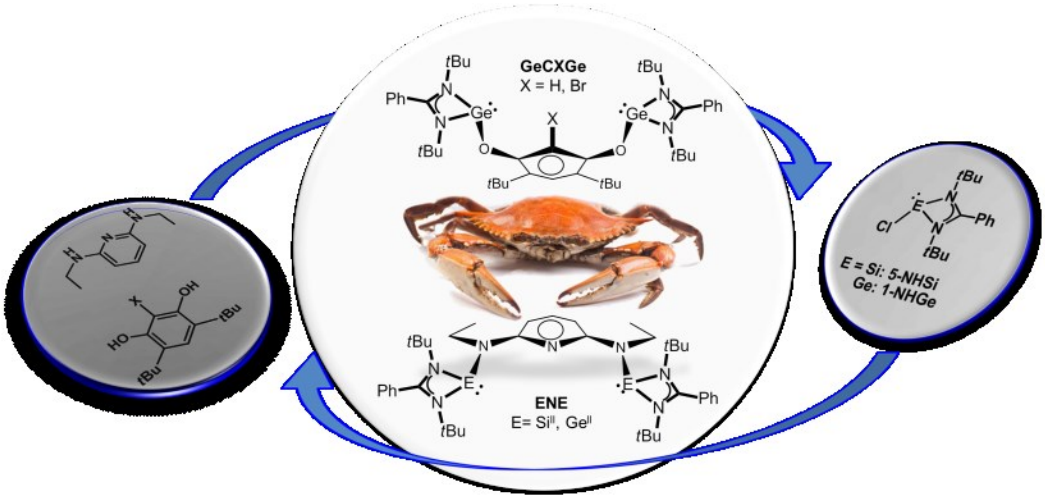

Figure 4.1. Novel bis(metallylene) **GeCXGe** and **ENE** pincer ligands reported in this dissertation (X = H, Br; E = Si^{II}, Ge^{II}).

In contrast, the synthesis of the **ECBrE** ligands resulted more challenging. The **GeCBrGe** ligand was only afforded by a one-pot reation whereas the **SiCBrSi** ligand could not be synthesized due to several side reactions from the **5-NHSi** precursor. Dropwise addition of a LiHMDS solution to a solution mixture of 2-bromo-4,6-di-*tert*-butylresorcinol and **1-NHGe** led to the formation **GeCBrGe** albeit in

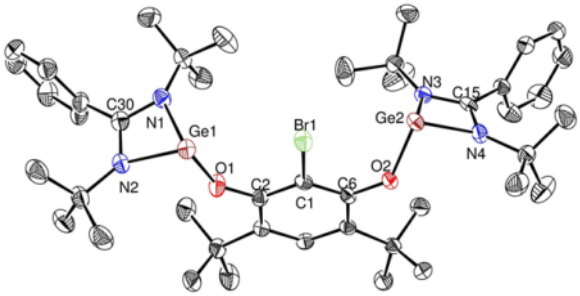

Figure 4.2. Molecular structure of the **GeCBrGe** ligand depicting the pincer-like structure.

moderate yields (68%). The **GeCXGe** and **ENE** were fully characterized by several spectroscopic methods such as ^{1}H, $^{13}C\{^{1}H\}$, $^{29}Si\{^{1}H\}$ NMR, 2D NMR correlation spectroscopy, mass spectrometry, elemental analysis, and XRD structure analysis for **GeCHGe**, **GeCBrBr** (Figure 4.2), and **SiNSi** pincer ligands.

These novel ligands were contrasted to the more common phosphine ***t*Bu-PCHP** and ***i*PrN-PCHP** ligands, synthesized as reference systems (Figure 4.3).

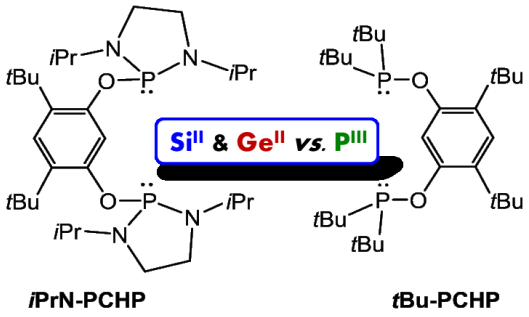

Figure 4.3. References ***i*PrN-PCHP** and ***t*Bu-PCHP** pincer ligands.

The coordination of these novel pincer ligands was studied toward late transition metals of group 8, 9 and 10 metals. First, the iridium(III) complexes of type **[ECE]IrHCl(coe)** were synthesized by reacting the **ECHE** (E = Si^{II}, Ge^{II}) and ***i*PrN-PCHP** with the iridium dimer **$[IrCl(coe)_2]_2$** as Ir^{I} precursor (Scheme 4.1).

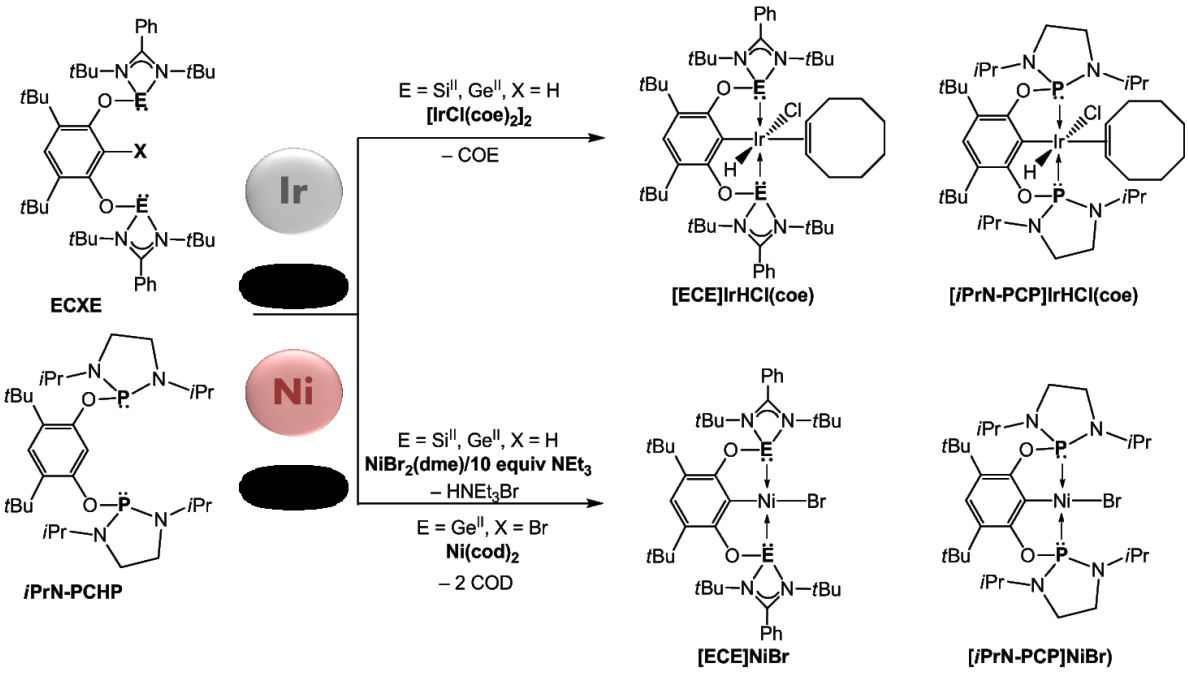

Scheme 4.1. Synthesis of the iridium(III) and nickel(II) metal complexes bearing the monoanionic **[ECE]** pincer ligands.

An oxidative addition of the C_{ipso}–H bond to the Ir^{I} center led to the corresponding novel octahedral **[ECE]IrHCl(coe)** complexes bearing the pincer ligands in a meridional coordination fashion. The products **[SiCSi]IrHCl(coe)** (Figure 4.4), **[GeCGe]IrHCl(coe)**, **[*i*PrN-PCP]IrHCl(coe)** were isolated as white solids in quantitative yields. In contrast, the reaction between ***t*Bu-PCHP** and **[IrCl(coe)$_2$]$_2$** afforded the square-pyramidal **[*t*Bu-PCP]IrHCl** complex without COE coordinated at the metal center. This difference was found to be related with the electronic density at the iridium center. The NMR spectroscopic values and the structural features, at the olefinic group in the ancillary cyclooctene ligand *coe*, permitted the indirect evaluation of the σ-donor strength in this pincer ligand series towards the iridium center. A more deshielded ^{1}H and ^{13}C resonance signals in the NMR spectra for the complex **[SiCSi]IrHCl(coe)**, in addition to a longer C–C double bond length, when compared with the complex **[*i*PrN-PCP]IrHCl(coe)**, indicated that the **[SiCSi]** ligand has the strongest σ-donor ability in this series: **[*t*Bu-PCP]** < **[*i*PrN-PCP]** < **[GeCGe]** < **[SiCSi]** (Figure 4.5).

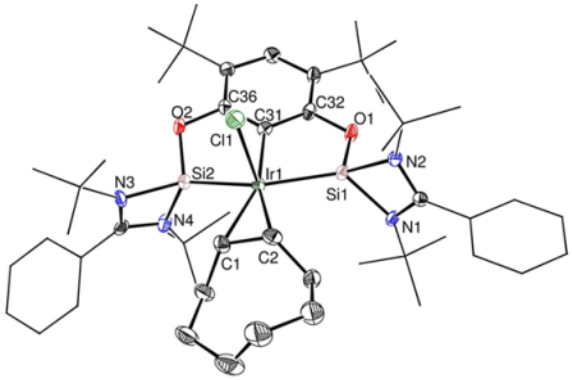

Figure 4.4. Molecular structure of the **[SiCSi]IrHCl(coe)** pincer complex.

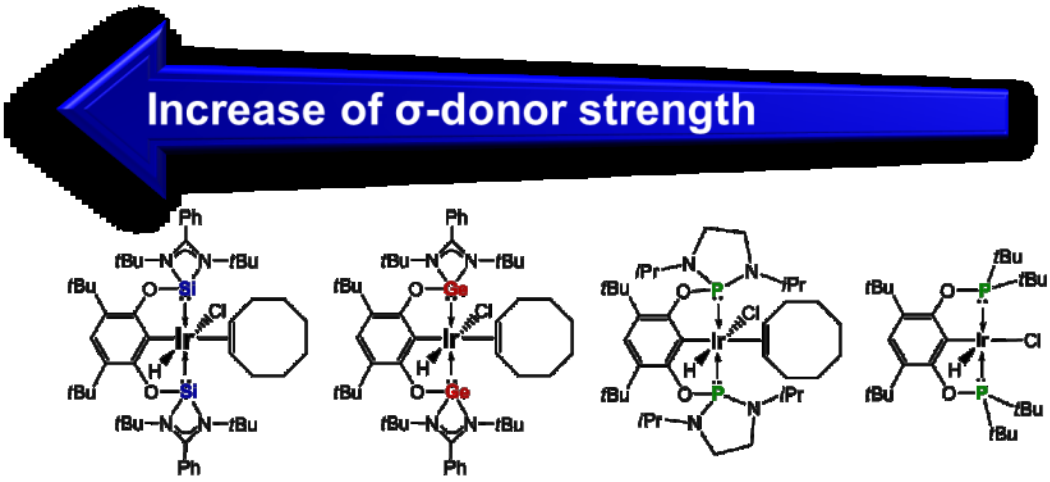

Figure 4.5. Order of σ-donor strength on the ligand series evaluated in the iridium(III) **[ECE]IrHCl(coe)** pincer complexes.

Attracted by the difference in electronic density at the iridium center, the **[ECE]IrHCl(coe)** complexes were explored as precatalyst for the borylation of arenes. Interestingly, the catalytic performance was improved with an additional equivalent of COE as hydrogen acceptor, for the **[SiCSi]**, and **[GeCGe]** ligands: 90 vs. 53 %, and 80 vs. 46 %, respectively; whereas for the **[*t*Bu-PCP]** ligand the presence of COE had no effect (Scheme 4.2). This difference in catalytic behavior is related with the stabilization of the highly electron rich active species by coordination of COE to the iridium center. In strong contrast, for the case of the **[*i*PrN-PCP]** ligand, when an additional equivalent of COE was added, the selectivity varied toward the borylation of COE in 35% yield, with only 21% yield for the borylated benzene. The **[SiCSi]** and **[GeCGe]** pincer ligands proved to be more active than the tested bis(phosphinite) **[*t*Bu-PCP]** and **[*i*PrN-PCP]** ligands, although, they have a moderate activity when compared with the benchmark systems based on bipyridine chelate ligands.

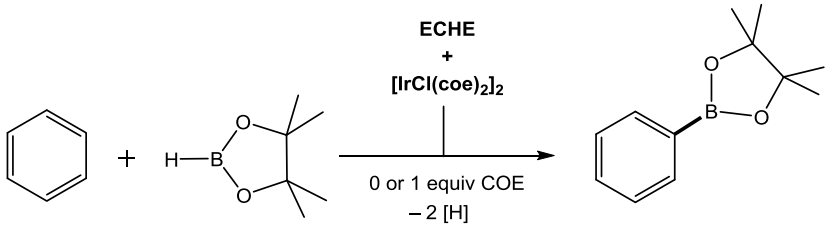

	Yields (%)	
	COE (equiv)	
ECHE	0	1
SiCHSi	53	90
GeCHGe	46	80
*t*Bu-PCHP	60	64
*i*PrN-PCHP	55	21

Scheme 4.2. Borylation of benzene using the *in situ* generated iridium(III) **[ECE]IrHCl(coe)** and **[*t*Bu-PCP]IrHCl** pincer complexes.

The borylation of arenes showed to be controlled by steric effects on the substrate. A high selectivity toward *meta* and *para* borylated substitution was observed when toluene was used as substrate, albeit the yields decreased considerably for the **[GeCGe],** and **[*t*Bu-PCP]** ligands**:** 80 vs. 39 %, and 64 vs. 40%, respectively; whereas the **[SiCSi]** ligand presented the same activity for this substrate: 90 vs. 91%.

As a representative of group 10, the first nickel(II) complexes of type **[ECE]NiBr** were synthesized using the **ECHE** (E = Si^{II}, Ge^{II}), **GeCBrGe**, ***i*PrN-PCHC** pincer ligands. Metallation was carried out by reacting the **ECHE** ligands with $NiBr_2$(dme) (dme = 1,2-dimethoxyethane) *via* a C–H activation, in the presence of NEt_3 as a base, affording the **[ECE]NiBr** complexes in good yields (E= Si:70; Ge: 57; P: 95 %, Scheme 4.1, p.139). Additionally, the **[GeCGe]NiBr** complex was obtained in 88% yield by an oxidative

reaction of the C–Br bond of the **GeCBrGe** ligand when it reacted with $Ni(cod)_2$. The **[ECE]NiBr** complexes (Figure 4.6) were evaluated as precatalysts for the Sonogashira cross-coupling reaction showing moderate yields in the desired coupling product between phenylacetylene and (*E*)-1-octenyl iodide (Scheme 4.3).

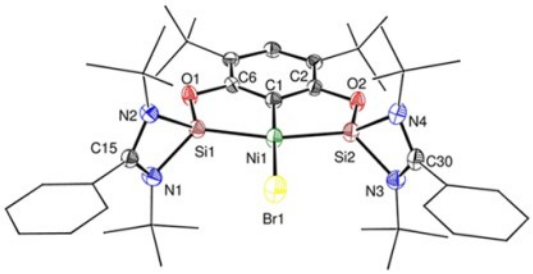

Figure 4.6. Molecular structure of the **[SiCSi]NiBr** pincer complex.

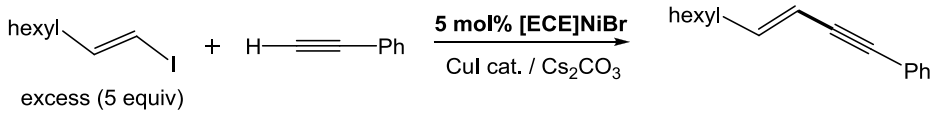

Yields (%)			
[SiCSi]NiBr	**[GeCGe]NiBr**	**[*i*PrN-PCP]NiBr**	**without Ni**
39	53	40	5

Scheme 4.3. Sonogashira cross-coupling reaction catalyzed by the nickel(II) **[ECE]NiBr** complexes.

However, despite of their moderate activity, these novel complexes permitted the isolation of reaction intermediates of the catalytic cycle by conducting stoichiometric reactions in a sequence transmetallation-oxidative addition-reductive elimination. For the first time, the intermediates of the transmetallation reaction between **[ECE]NiBr** with copper acetylides could be isolated and analyzed by single crystal XRD structure analysis. Remarkably, this reaction intermediate **{[ECE]Ni–C≡C–R→CuBr}** (E = Si^{II}, Ge^{II}; R = Ph, *ter*Ph, respectively, Figure 4.7) is composed by the two metal centers, Ni and Cu. DFT calculations performed on these intermediates established the bonding nature between the atoms involved in the four-membered Ni-Si-Cu-C1 cycle. A three-center two-electrons between Ni–E–Cu was defined, whereas the acetylide is end-on coordinated to both

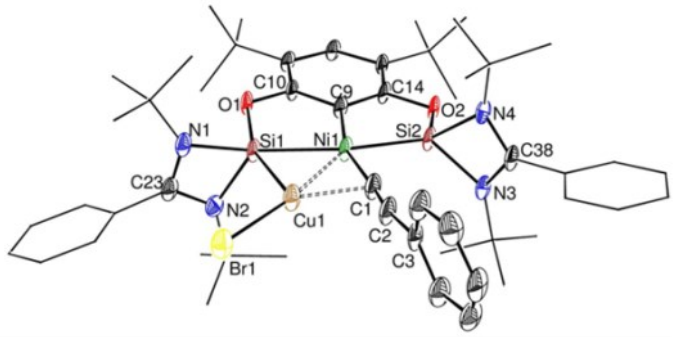

Figure 4.7. Molecular structure of the **{[SiCSi]Ni–C≡C–Ph→CuBr}** transmetallation intermediate.

metal centers Ni and Cu, respectively. Further stoichiometric reaction of these intermediates with the (*E*)-1-octenyl iodide afforded the C(*sp*)–C(sp^2) coupling product and the expected **[ECE]NiI** complex. A catalytic reaction, using a radical clock as substrate, with cyclopropyl as a probe, showed ring opening *via* a radical mechanism. Thus, the second elementary step most likely goes through a single electron transfer (SET) process where a Ni^{III} could be a key intermediate of the reaction. A complete scenario for the Ni-catalyzed Sonogashira cross-coupling reaction is proposed based on the experimental results (Scheme 4.4).

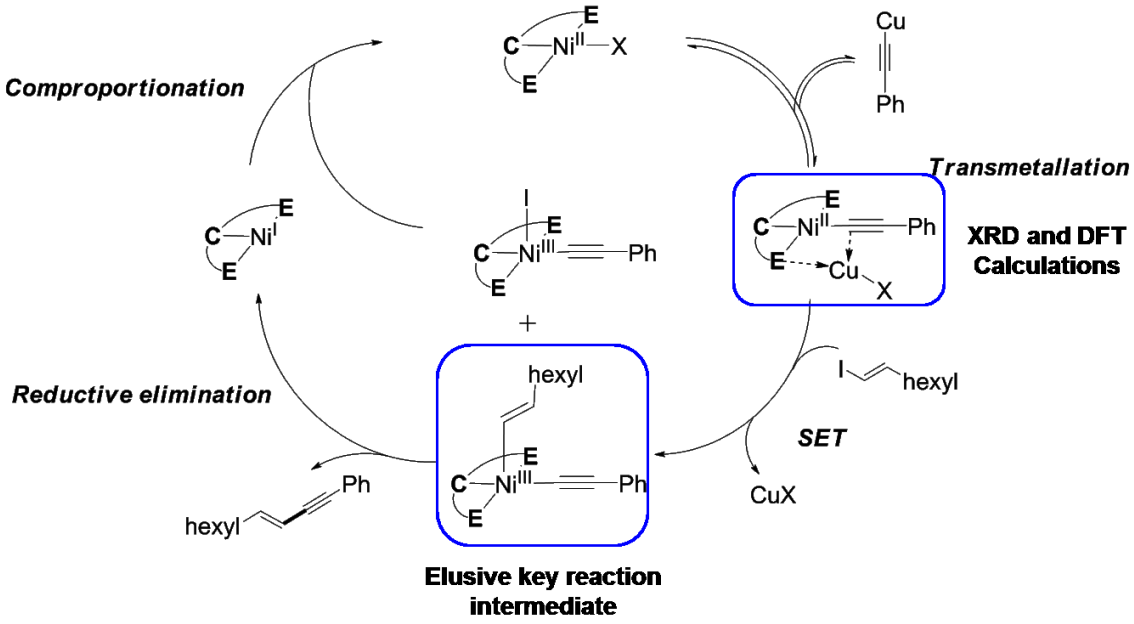

Scheme 4.4. Proposed mechanism for the Ni-catalyzed Sonogashira cross-coupling reaction by the **[ECE]NiBr** pincer complexes.

The neutral **ENE** pincer ligands (E = Si^{II}, Ge^{II}) presented an unusual coordination toward iron in different oxidation states (+2 and 0). Unexpectedly, the reactions between **ENE** and $FeCl_2{\cdot}(THF)_{1.5}$ produced quantitatively the κ^2 coordinated iron complexes ***κ^2E,E'*-[ENE]FeCl$_2$** with the nitrogen at the pyridine reluctant for coordination (Scheme 4.5). Spectroscopic evaluation by ^{57}Fe Mössbauer and magnetic measurements in solutions (Evan's method) supported the presence of tetrahedral high spin iron(II) centers. Reduction of the ***κ^2Si,Si'*-[SiNSi]FeCl$_2$** complex with KC_8 in the presence of PMe_3 afforded the novel iron(0) **[SiNSi]Fe(PMe$_3$)$_2$** complex. In contrast, the **[GeNGe]Fe(PMe$_3$)$_2$** complex was

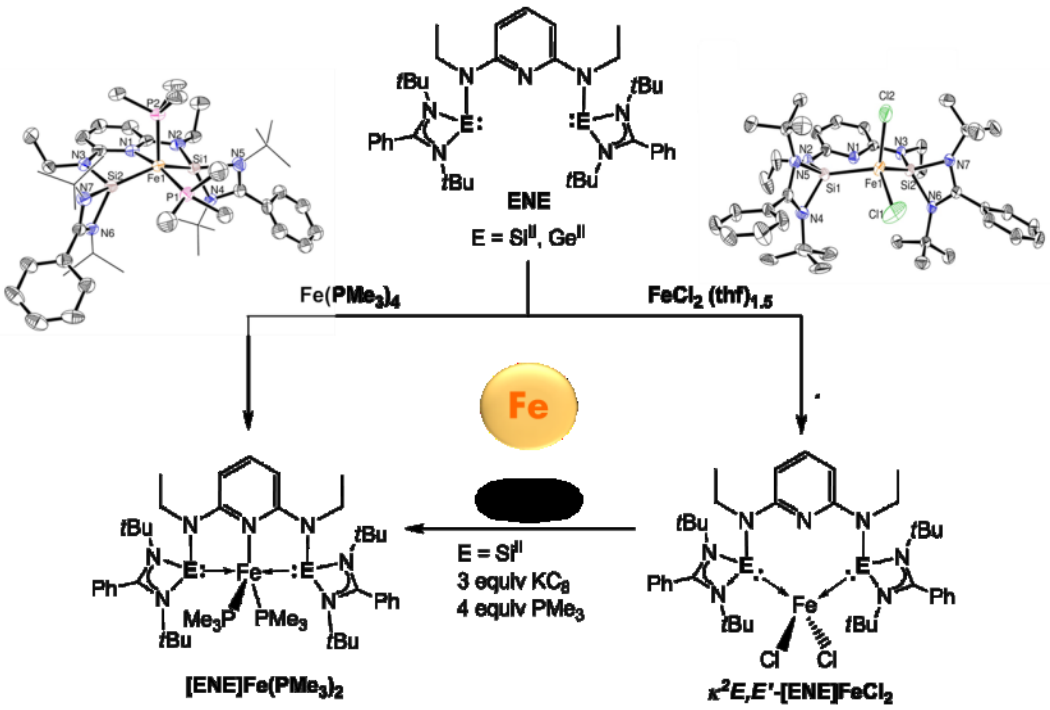

Scheme 4.5. Synthesis of iron complexes bearing the **ENE** pincer ligands and the molecular structures for the iron(0) (top left) and iron(II) (top right) complexes.

synthesized *via* ligand substitution reaction of the PMe_3 in $Fe(PMe_3)_4$ by the **GeNGe** ligand. Interestingly, a variable temperature NMR spectroscopic evaluation of the **[ENE]Fe(PMe$_3$)$_2$** complexes (E = Si^{II}, Ge^{II}) showed a remarkable stability of these complexes in a pseudo-square pyramidal structures along a wide range of temperatures without any observable Berry pseudorotation. This pseudo-square pyramidal structure was unambiguously determined in the **[SiNSi]Fe(PMe$_3$)$_2$** complex by single crystal XDR structure analysis. Evaluation of the electronic structure of the **[ENE]Fe(PMe$_3$)$_2$** complexes by ^{57}Fe Mössbauer spectroscopy, DFT calculations and derivatization to their carbonyl **[ENE]Fe(CO)$_2$** complexes confirmed the redox innocent behavior of these ligand systems. In addition, a single crystal XRD structure analysis of the **[ENE]Fe(CO)$_2$** complexes showed a trigonal bipyramidal coordination geometry around the iron center. The electronic structure of the **[SiNSi]Fe(CO)$_2$** complex, determined by DFT calculations, is similar to the electronic structure of the **[SiNSi]Fe(PMe$_3$)$_2$** complex. Interestingly, this result showed that the stabilization of the pseudo-square pyramidal structure around the iron(0) center in **[SiNSi]Fe(PMe$_3$)$_2$** is intrinsically based on steric effects, of the ancillary PMe_3 ligands, and not on the electronic structure of the iron center.

The iron(0) **[SiNSi]Fe(PMe$_3$)$_2$** complex was tested as precatalyst for hydrosilylation of ketones showing good activity when (EtO)$_3$SiH was used as the reducing agent (Scheme 4.6).

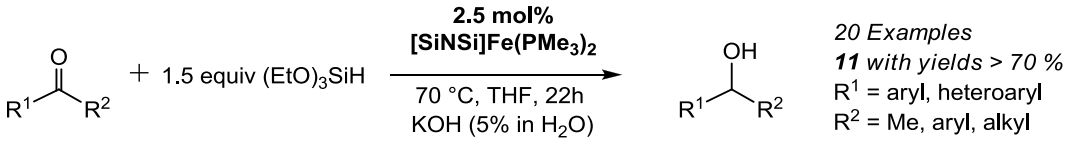

Scheme 4.6. Hydrosilylation of ketones using the iron(0) complex **[SiNSi]Fe(PMe$_3$)$_2$** as precatalyst.

Post-catalytic evaluation of the reaction media by ^{1}H and ^{31}P{^{1}H} NMR showed the formation of a hydrido-silyl-iron(II) complex as the catalyst's resting state. Stoichiometric reaction between **[SiNSi]Fe(PMe$_3$)$_2$** and (EtO)$_3$SiH produced the same NMR resonance signals of the catalyst's resting state *via* an oxidative addition reaction of the Si–H bond to the iron(0) center. Other monohydrosilanes (Me_2PhSiH and $MePh_2SiH$) also reacted with the **[SiNSi]Fe(PMe$_3$)$_2$** in a similar fashion but with lower kinetics. The novel hydrido-silyl-iron(II) **[SiNSi]FeH(SiR$_3$)(PMe$_3$)** complexes presented a distorted octahedral structure around the iron center with the silyl group *trans* to nitrogen of the pyridine and the **[SiNSi]** ligand in a meridional coordination fashion (Figure 4.8). Surprisingly, further reaction with ketone did not afford the carbonyl insertion into the Fe–H bond even at high temperatures (Scheme 4.7, left), in contrast to the reported Ojima mechanism. Moreover, with an additional equivalent of silane the reaction proceeded in quantitative yields (Scheme 4.7, down). Crossover experiments with different silanes and deuterated silanes suggested that neither the hydride nor the silyl groups in the **[SiNSi]FeH(SiR$_3$)(PMe$_3$)** complex are transferred to the ketone. More importantly, a crossover experiment with a chiral silane resulted with retention of stereochemistry at the silicon center after hydrosilylation (Scheme 4.7, right). This result is highly in contrast to activation of silane by a Lewis acid forming a silyloxonium cation. Therefore, the most plausible reaction mechanism must

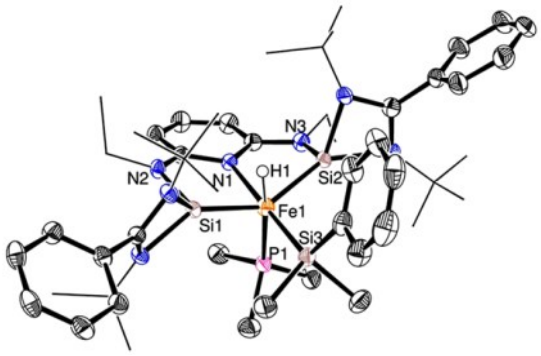

Figure 4.8. Molecular structure of the **[SiCSi]FeH(Me$_2$PhSi)(PMe$_3$)** pincer complex.

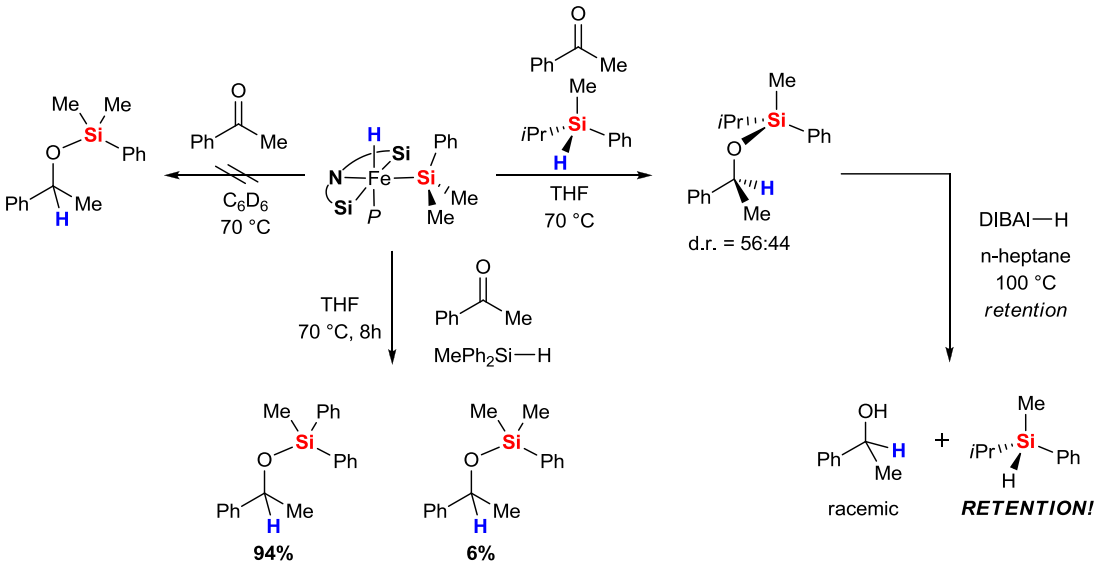

Scheme 4.7. Selected stoichiometric reactions of the **[SiNSi]FeH(SiMe$_2$Ph)(PMe$_3$)** complex with acetophenone and hydrosilanes for mechanistic studies.

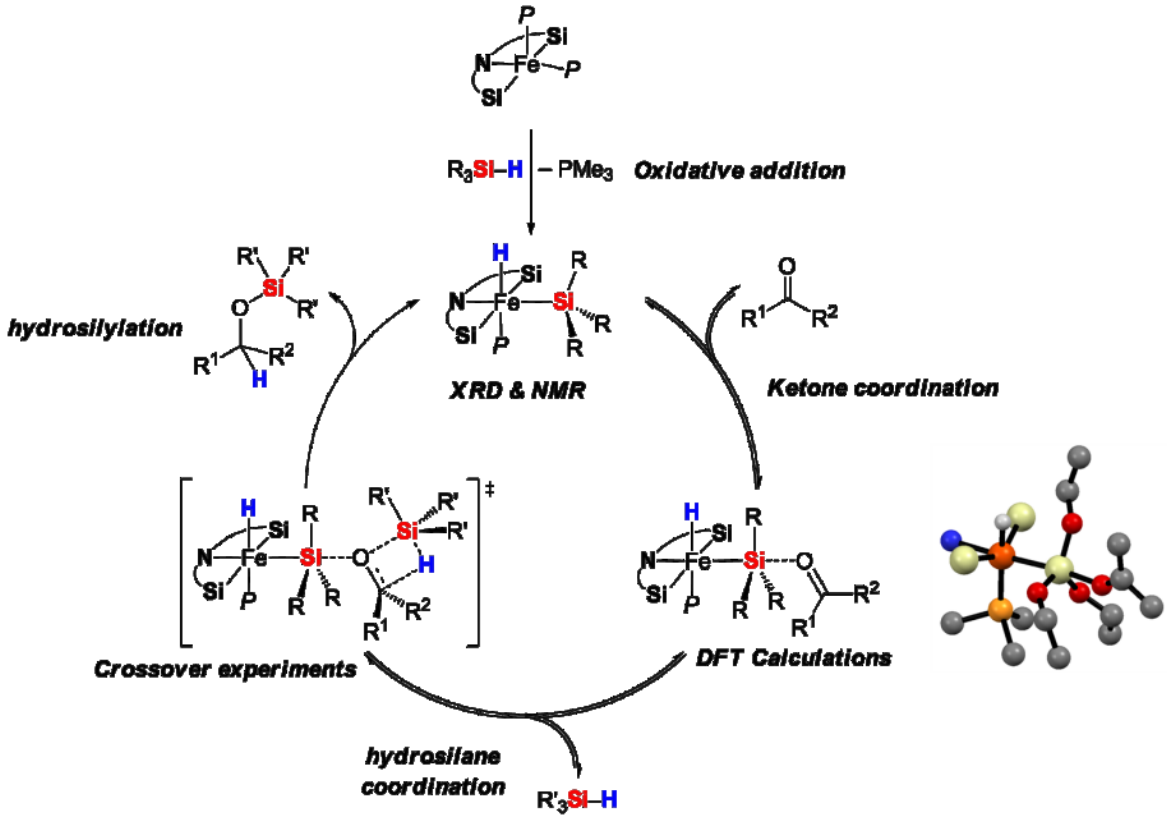

Scheme 4.8. Proposed mechanism for the hydrosilylation of ketones catalyzed by the iron(II) **[SiNSi]FeH(SiR$_3$)(PMe$_3$)** complex according to the experimental results of the mechanistic studies.

involve activation of the ketone by the **[SiNSi]FeH(SiR_3)(PMe_3)** complex. Combination of these results with DFT calculations showed that the most likely intermediate for ketone activation involves the silyl group bound to the iron center acting as a Lewis acid (Scheme 4.8). Remarkably, a complete new mechanism for ketone hydrosilylation was established according to the experimental results. Exceptionally, the iron center remains as a spectator along the reaction where the ketone hydrosilylation process proceeds at its peripheral ligands (Scheme 4.8).

In conclusion, the results presented in this dissertation contribute to broaden the scope of N-heterocyclic silylenes and germylenes as ligands toward late transition metals. The novel bis(silylene) and bis(germylene) **ECXE** and **ENE** pincer ligands (E = Si^{II}, Ge^{II}; X = H, Br) showed applicability as novel steering ligands in metal-based catalysis, a milestone in contemporary inorganic chemistry.

5. EXPERIMENTAL SECTION

5.1. General remarks

All experiments and manipulations were conducted under dry oxygen-free nitrogen using standard Schlenk techniques or in a MBraun drybox with an atmosphere of purified nitrogen. All solvents were purified using conventional procedures and freshly distilled under N_2 atmosphere prior to use. The solvents were stored in Schlenk-vessels containing activated molecular sieves. Benzene, benzene-d_6, toluene, *n*-pentane, *n*-hexane, diethyl ether and THF were purified by distillation from Na/benzophenone. Chloroform and chloroform-*d* were dried by stirring over CaH_2 at ambient temperature. The glassware used in all manipulations was dried at 150 °C prior to use, cooled to ambient temperature under high vacuum, and flushed with N_2. The handling of solid samples and the preparation of samples for spectroscopic measurements were carried out inside a glove-box, where the O_2 and H_2O levels were normally kept below 1 ppm.

The solvents or solutions were tranfered *via* stainless steel cannulas, which were stored in the oven at 120 °C. The transfer was enabled by the vessel of origin being left under a positive pressure of protective gas, and the receptacle vessel of closed with a pressure release value. Filtrations were carried out using stainless steel cannula containing a filter-head at one end. *Whatman* (GF/B 25) filters were affixed to the filter end of the cannula with Teflon tape. After use, cannulas were cleaned immediately by thorough rinsing with acetone, followed by dilute HCl, water, and acetone.

In the case of low temperature reactions, Dewar vessels were filled with acetone/dry-ice mixture until reach the desired temperature. Ethanol/liquid nitrogen was also employed for reactions in needs of −90 °C.

5.2. Analytical methods

NMR Measurements: NMR samples of air and/or moisture sensitive compounds were all prepared under inert atmosphere. The deuterated solvents were dried by stirring over Na (C_6D_6, THF-d_8) or CaH_2 ($CDCl_3$), distilled under N_2 atmosphere and stored in Schlenk-vessels containing activated 4 Å molecular sieves. ^{1}H, ^{13}C, ^{31}P, and ^{29}Si NMR spectra were recorded on Bruker AV500 (^{1}H, 500 MHz; ^{13}C, 126 MHz; ^{29}Si, 99 MHz; ^{31}P, 202 MHz), AV 400 (^{1}H, 400.13 MHz; ^{13}C, 100.61 MHz; ^{29}Si, 79.49 MHz; ^{31}P, 161.80 MHz) or AFM 200 (^{1}H, 200.13 MHz; ^{13}C, 50.32 MHz; ^{31}P, 81.01 MHz) spectrometers. The NMR signals are reported relative to the residual solvent peaks (^{1}H, C_6D_6, 7.15 ppm; C_7D_8, 2.09 ppm; $CDCl_3$, 7.26 ppm; ^{13}C, C_6D_6, 128.0 ppm; C_7D_8, 20.4 ppm; $CDCl_3$, 77.2 ppm) or an external standard (^{31}P, 85% H_3PO_4, 0.0 ppm; ^{29}Si, TMS, 0.0 ppm). All signals were unambiguously assigned by a combination of 2D NMR H-H COSY, HSQC, HMBC correlation spectroscopy. Data are reported as follows: chemical shift, multiplicity (br s = broad singlet, s = singlet, d = doublet, t = triplet, q = quartet, m = multiplet), coupling constants (Hz) and integration.

Infrared spectroscopy: IR spectra (4000 – 400 cm^{-1}) were recorded on a Perkin-Elmer Spectra 100 FT-IR spectrometer and bands are reported in wavenumbers (cm^{-1}). Samples of solids were prepared as KBr pellets. Air or moisture sensitive samples were prepared in the glove-box, and measured immediately.

Mass Spectrometry: Performed at the Institute für Chemie in Technische Universität Berlin. Mass spectra were recorded using APCI or ESI as ionization source and a LTQ Orbitrap XL as analyzer. Solid samples were prepared in glove box and the solution of samples was prepared 15 min before the measurement under N_2 atmosphere.

Elemental analysis: The C, H, N, and S analyses of all compounds were carried out on a Thermo Finnigan Flash EA 1112 Series instrument. Air or moisture sensitive samples were prepared in silver capsules in the glove box.

Single crystal XRD structure analysis: Crystals were mounted on a glass capillary in perfluorinated oil and measured in a cold N_2 flow. The data were collected either on an Agilent Technologies Xcalibur S Sapphire at 150 K (Mo K_α radiation, λ= 0.71073 Å) or an

Agilent Technologies SuperNova (single source) at 150 K (Cu K_α radiation, λ= 1.5418 Å). The structures were solved by direct methods and refined on *F2* with the SHELX-97 software package.[205] The positions of the H atoms were calculated and considered isotropically according to a riding model. The crystallographic data tables for the individual structure solutions from this dissertation are in the Appendix 7.1.

Gas chromatography – Mass spectrometry: GC−MS measurements were conducted on a Shimadzu GC-2010 gas chromatograph (30 m Rxi-5ms column) linked to a Shimadzu GCMA-QP 2010 Plus mass spectrometer.

High Pressure Liquid Chromatography (HPLC): Enantiomeric excesses were determined by analytical HPLC analysis on an *Agilent Technologies* 1290 Infinity or an Agilent Technologies 1200 Infinity instrument with a chiral stationary phase using a *Daicel Chiralcel* OJ-RH column (MeCN/H_2O mixtures as solvent), a *Daicel Chiralcel* OJ-H column (*n*-heptane/*i*PrOH mixtures as solvent) or a *Daicel Chiralpak* IB column (*n*-heptane/*i*PrOH mixtures as solvent).

Quantum Chemical Calculations. Computational details.

Nickel complexes: The structures were calculated by the Kaupp group at the Technische Universität Berlin.

The structures of the copper adducts **{[ECE]Ni-CC-Ph/*ter*Ph→CuBr}** were optimized at the B3LYP/def2-TZVP level of theory using the Turbomole 6.31 program package.[206] That is, the global hybrid functional B3LYP[168–170] with 20% of the exact Hartree-Fock exchange admixture, in conjunction with standard Turbomole all-electron def2-TZVP basis sets[171] for all atoms. For the full optimization Grimme's dispersion correction 3 with the Becke-Johnson potential was used.[172,173] The crystal structures of **{[ECE]Ni-CC-Ph/*ter*Ph→CuBr}** complexes were used as initial structures for full optimization (denoted as "fullopt-D3"). For comparison, partial optimization of only the hydrogen-atom positions for the X-ray-based structure of **{[ECE]Ni-CC-Ph/*ter*Ph→CuBr}** was also done at the B3LYP/def2-TZVP level (denoted as "crystal/opt-H"). For full optimization of the **{[ECE]Ni-CC-Ph/*ter*Ph}** complexes the optimized structures of **{[ECE]Ni-CC-Ph/*ter*Ph→CuBr}** were taken and the CuBr removed.

Atomic charges were evaluated at the B3LYP/def2-TZVP level of theory by means of natural population analyses (NPA), using the built-in NBO subroutines of the Gaussian 09 program.[207] Mayer bond orders[208] were evaluated using the program BORDER. The wavefunctions were also analyzed in the DGrid program[209] by means of the electron localization function (ELF)[174–176] and the electron localizability indicator based on the parallel-spin electron pair density (ELI-D).[177,178] For this purpose, the Kohn-Sham orbitals of the (Gaussian 09) single point calculations were transferred to the DGrid and the examined property was calculated on a grid with 100 points per Bohr. The results of ELF analyses was visualized using the Paraview program.[210]

Iron complexes: The structures were calculated by Prof. Dr. Shigeoshi Inoue at the Technische Universität Berlin.

DFT calculations of the compounds **[SiNSi]Fe(PMe$_3$)$_2$** and **[ENE]Fe(CO)$_2$** (E = Si^{II}, Ge^{II}) were performed at the B3LYP level using 6-31G(d) basis set for H, C, N, P and Si atoms and the LANL2DZ basis set for the Fe atom with the Gaussian 03 program.[207] Optimized structure of model compounds were obtained without symmetry constraints. The structures obtained by X-ray analysis were used as the input for these calculations. The NBO approach was used to calculate the orbital populations, Wiberg Bond Indices (WBI), and Natural Population Analysis (NPA).

***Iron hydride*:**The structure of the key reaction intermediate was calculated by Dr. Tibor Szilvási at the Department of Inorganic and Analytical Chemistry, Budapest University of Technology and Economics, Szent Gellért tér 4, 1111 Budapest, Hungary.

The structure for the key intermediate was calculated using **[SiNSi]FeH(Si(EtO)$_3$)(PMe$_3$)** and acetone as substrates. DFT calculations were carried out at ωB97X-D/6-31G(d)[Fe:cc-pVTZ] level of theory[211] using GAUSSIAN 09 program.[207]

5.3. Starting materials

Commercially available starting materials were used as received. All liquids obtained from commercial sources were degased, destilled, and stored under nitrogen.

The following important precursors were prepared according to literature procedures. The references are shown in Table 5.3.1.

Table 5.3.1. Starting materials and references

Compound	References	Compound	References
$GeCl_2$·dioxane	46	**SiCHSi**	92
5-NHSi	50	$Fe(PMe_3)_4$	212
1-NHGe	51	(^{Si}S)-Me*i*PrPhSiH (e.r. >95:5)[††]	213
2-bromo-4,6-di-*tert*-butylresorcinol	215	silyl ether **1*a***[‡]	214
$NiBr_2$(dme)	217	$B(C_6F_5)_3$[‡]	216
NiI_2(dme)	217		

[†††‡] These compounds were synthesized by Toni T. Metsänen in the Oestreich group in a collaboration project.

5.4. Synthesis and characterization of the new compounds

5.4.1. Bis(germylene) GeCHGe pincer ligand

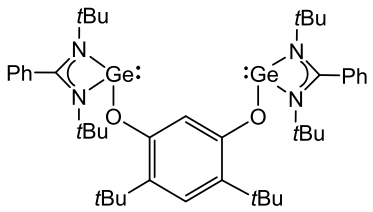

The synthesis of bis-germylene pincer ligand GeCHGe **L1** was conducted following the reported procedure for the bis-silylene analogue **SiCSi**.[92] 3.7 mL of *n*-BuLi (5.9 mmol, 1.6 M in hexane) were added to a pre-cooled solution of 0.645 g of 4,6-di*tert*-butylresorcinol (2.9 mmol) in dry diethyl ether (20 mL) at –30 °C. A white solid in suspension was formed immediately. The cooling bath was removed, and the reaction mixture was stirred at room temperature for 3 hours. The reaction mixture was cooled to –78 °C with a dry ice/isopropanol-bath, and a solution of 2.071 g of *N,N'*-di-*tert*-butylchloro(phenylamidinate)germanium(II) (6.1 mmol) in toluene (20 mL) was added dropwise. After warming up to room temperature under overnight stirring, the solvent was removed *in vacuo*, and the product was extracted with 50 mL of hot hexane via cannula filtration. The solution was concentrated to 10 mL and cooled to –3 °C, which led to the crystallization of the product overnight. Filtration and drying the product *in vacuo* for 2h afforded the product as yellowish crystalline solid in 83% yield.

^{1}H NMR: (400.13 MHz, C_6D_6, 298K): δ(ppm) = 1.10 (s, 36H, NC(CH_3)$_3$), 1.86 (s, 18H, ArC(CH_3)$_3$), 6.91 – 7.05 (m, 8H, $C_{arom.}H$ Ph), 7.38 (m, 2H, $C_{aroma.}H$ Ph), 7.62 (s, 1H, 5-$C_{aroma.}H$), 7.68 (s, 1 H, GeC*H*Ge).

^{13}C{^{1}H} NMR: (100.61 MHz, C_6D_6, 298K): δ(ppm) = 31.2 (ArC(CH_3)$_3$), 32.0 (NC(CH_3)$_3$), 35.0 (Ar*C*(CH_3)$_3$), 52.8 (N*C*(CH_3)$_3$), 109.0 (2-$C_{aroma.}$H Ge*C*Ge), 124.6 (5-$C_{aroma.}$H), 128.4 (4,6-$C_{aroma.}$–*t*Bu), 127.5 ($C_{aroma.}$H Ph), 129.3 ($C_{aroma.}$H Ph), 129.8 ($C_{aroma.}$H Ph), 135.9 ($C_{aroma.}$ quaternary Ph), 159.2 (1,3-$C_{aroma.}$–O), 173.3 (N*C*N).

Elemental analysis: (%) Calcd for $C_{44}H_{66}Ge_2N_4O_2$: C, 63.80; H, 8.03; N, 6.76. Found C, 63.01; H, 7.83; N, 6.53.

5.4.2. Bis(phosphine) *t*Bu-PCHP pincer ligand

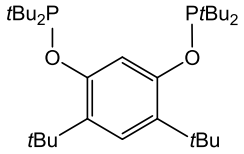

0.245 g of 4,6-di-*tert*-butylresorcinol (1.1 mmol) and 0.092 g of KH (2.3 mmol) were carefully suspended in 50 mL of THF, which led to instantaneous formation of gas. The mixture was heated to reflux for 1 h, until the H_2 evolution ceased. A solution of 0.416 g of di-*tert*-butylchlorophosphine (2.3 mmol) in 5 mL of THF was slowly added via syringe, and the reaction mixture was refluxed for 2 h. All volatile materials were evaporated *in vacuo*, and the product was then extracted with 60 mL of hexane via cannula filtration into a second Schlenk flask. Concentration to 10 mL and cooling to –30°C afforded a colorless and crystalline product in 88% yield. Crystals suitable for single-crystal X-ray analysis were obtained from a saturated hexane solution at –3 °C after 3 days.

^{1}H NMR: (200.13 MHz, C_6D_6, 298K): δ(ppm) = 1.21 (d, $^{3}J_{P–H}$ = 11.8 Hz, 36H, PC(CH_3)$_3$), 1.59 (s, 18H, ArC(CH_3)$_3$), 7.51 (s, 1H, 5-$C_{aroma.}H$), 8.98 (t, $^{4}J_{P–H}$ = 9.6 Hz, 1H, PC*H*P).

^{13}C{^{1}H} NMR: (50.32 MHz, C_6D_6, 298K): δ(ppm) = 28.2 (d, $^{2}J_{C–P}$ = 16.3 Hz, PC(CH_3)$_3$), 31.1 (ArC(CH_3)$_3$), 34.9 (Ar*C*(CH_3)$_3$), 36.0 (d, $^{1}J_{C–P}$ = 29.0 Hz, P*C*(CH_3)$_3$), 108.0 (t, $^{3}J_{C–P}$ = 33.9 Hz, $C_{arom.}$ P*C*P), 126.2 (5-$C_{aroma.}$H), 129.5 (4,6-$C_{aroma.}$–*t*Bu), 156.9 (dd, $^{2}J_{C–P}$ = 9.3 Hz, $^{4}J_{C–P}$ = 2.9 Hz, 1,3-$C_{aroma.}$–O).

^{31}P{^{1}H}: (80 MHz, C_6D_6, 298K): δ(ppm) = 146.45.

Elemental analysis: (%) Calcd for $C_{30}H_{56}O_2P_2$: C, 70.55; H, 11.05. Found: C, 70.38; H, 11.02.

5.4.3. Bis(phosphine) *i*PrN-PCHP pincer ligand

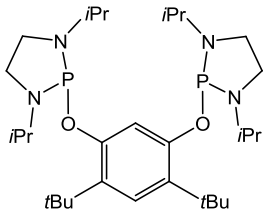

This ligand and its preparation by a different route has been published previsously by Bedford and co-workers.[105]

2.0 mL (5.6 g, 20.8 mmol) of PBr_3 and 8.7 mL (6.3 g, 62.4 mmol) NEt_3 in ca. 50 mL Et_2O were cooled to –78 °C with a dry ice/isopropanol-bath. 3.8 mL of *N,N'*-di-*iso*-propyl-ethylendiamine (3.0 g, 20.8 mmol) were added via syringe, and the solution was warmed to room temperature overnight. All volatile materials were evaporated *in vacuo*, and the product was extracted from the residue with 15 mL of hexane (3×5 mL) via cannula filtration into a second Schlenk flask. Evaporation of the solvent *in vacuo* afforded 2.3 g of the product as yellow oil for a total 54% yield.

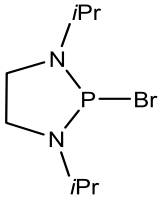

^{1}H NMR: (200 MHz, $CDCl_3$): δ(ppm) = 1.35 (dd, $^3J_{H–H}$ = 6.4 Hz, $^4J_{H–P}$ = 1.5 Hz, 12H, CHCH_3), 3.35 (d, $^3J_{H–H}$ = 6.4 Hz, 2H, CHCH$_3$), 3.40 – 3.56 (m, 4H, CH_2).

^{13}C{^{1}H} NMR: ($CDCl_3$, 50 MHz): δ(ppm) = 21.7 (d, $^3J_{C–P}$ = 10.8 Hz, CHCH$_3$), 48.9 (d, $^2J_{C–P}$ = 10.2 Hz, CH$_2$), 49.0 (d, $^2J_{C–P}$ = 14.5 Hz, CHCH$_3$).

^{31}P{^{1}H}: (80 MHz, $CDCl_3$): δ(ppm) = 191.4 (s).

0.5 g (2.3 mmol) of 4,6- di-*tert*- butylresorcinol and 0.2 g (4.7 mmol) of KH were weighted in a dry 100 mL Schlenk flask. Dry THF (20 mL) were added carefully, and the suspension was stirred at room temperature until the evolution of gas ceased (ca. 30 min). The mixture was heated to 60 °C and stirred for additional 2 hours. A solution of 1.1 g of *N,N'*-di-*iso*-propyl(ethylendiamide)bromophosphine (4.6 mmol) in THF (10 mL) was added dropwise

via syringe, and the mixture was stirred overnight at 60°C. After cooling, all volatile materials were evaporated *in vacuo*, and the sticky yellowish residue was suspended in hexane (3×5 mL), and the suspension was filtered over a small column with neutral Al_2O_3. Removal of the solvent *in vacuo* afforded the product as a colourless oil (0.9 g; 72%).

^{1}H NMR: (200 MHz, $CDCl_3$, 298K): δ(ppm) = 1.16 (dd, $^3J_{H–H}$ = 6.5 Hz, $^4J_{H–H}$ = 8.9 Hz, 12H, CHCH_3), 1.19 (d, $^3J_{H–H}$ = 6.5 Hz, 12H, CHCH_3), 1.29 (s, 18H, ArC(CH_3)$_3$), 3.22 – 3.29 (m, 4H, CHCH$_3$), 3.29 – 3.46 (m, 8H, CH_2), 7.07 (s, 1H, 5-C$_{aroma.}H$), 7.52 (t, $^4J_{C–P}$ = 4.2 Hz, PCHP).

Reported: (300 MHz, $CDCl_3$, 298K): δ(ppm) = 1.02 (d, J = 6.0 Hz, 24H, CH(CH_3)$_2$), 1.26 (s, 18H, C(CH_3)$_3$), 2.76 (hept., J = 6.0 Hz, 4H, CH(CH$_3$)$_2$), 3.07 – 3.27 (m, 8H, CH_2), 7.03 (s, 1H, ArH), 7.48 (t, J = 4.5 Hz, 1H, ArH)

^{31}P{^{1}H}: (80 MHz, $CDCl_3$): δ(ppm) = 118.4 (s).

Reported: (121.5 MHz, $CDCl_3$, 298 K): δ(ppm) = 112.2 (s).

5.4.4. Bis(germylene) GeCBrGe pincer ligand

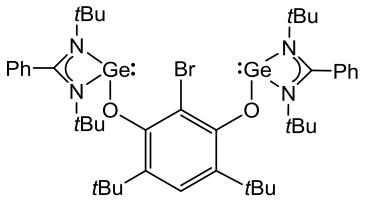

A solution of 0.69 g of 2-bromo-4,6-di-*tert*-butylresorcinol (2.3 mmol) in 20 mL of toluene was slowly added to a solution of 1.54 g of *N,N'*-di-*tert*-butylchloro(phenylamidinate)germanium(II) (4.5 mmol) in 20 mL of toluene at room temperature forming a strong yellow reaction mixture. After stirring for 30 min, a solution of LiHMDS (0.77 g, 4.6 mmol) in 10 mL of toluene was added dropwise in a period of 30 min with concomitant formation of turbidity and color change to terracotta. All volatiles were removed *in vacuo* after stirring overnight at room temperature. Extraction with hot hexane (1×60 mL, 2×20 mL) and filtration *via* cannula produced a colorless solution. The solution was concentrated to 10 mL and crystallized overnight at –3°C as white crystals. Further filtration and dry *in vacuo* afforded 1.40 g of the desired product (68% yield).

^{1}H NMR: (400.13 MHz, C_6D_6, 298K): δ(ppm) = 1.07 (s, 36 H, NC(C*H*$_3$)$_3$), 1.83 (s, 18 H, ArC(C*H*$_3$)$_3$), 6.90 – 7.04 (m, 8 H, C$_{aroma.}$*H* Ph), 7.29 – 7.32 (m, 2 H, C$_{aroma.}$*H* Ph), 7.61 (s, 1 H, 4- C$_{aroma.}$*H*).

^{13}C{^{1}H} NMR: (100.61 MHz, C_6D_6, 298K): δ(ppm) = 31.5 (ArC(*C*H$_3$)$_3$), 32.2 (NC(*C*H$_3$)$_3$), 35.8 (Ar*C*(CH$_3$)$_3$), 53.1 (N*C*(CH$_3$)$_3$), 111.6 (*C*$_{aroma.}$–Br), 123.4 (4-*C*$_{aroma.}$H), 129.6 (3,5-*C*$_{aroma.}$–*t*Bu), 127.4 (*C*$_{aroma.}$H Ph), 129.2(*C*$_{aroma.}$H Ph), 129.9(*C*$_{aroma.}$H Ph), 136.0 (*C*$_{aroma.}$H Ph), 156.9 (2,6-*C*$_{aroma.}$–O), 170.3 (N*C*N).

APCI-MS (m/z) Calcd for [$C_{44}H_{65}BrGe2N_4O_2^{\bullet+}$]: 908.26975. Found: 908.26978 (correct isotope pattern).

Elemental analysis: (%) Calcd for $C_{44}H_{65}BrGe_2N_4O_2$: C, 58.25; H, 7.22; N, 6.18. Found: C, 58.45; H, 7.35; N, 6.18.

5.4.5. 2,6-diamine-*N,N'*-diethylpyridine

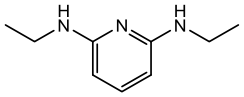

The synthesis was carried out following a reported procedure for reduction of diamides with LAH in THF under reflux.[164–166] 5.29 g (0.027 mol) of the *N,N'*-diacetyl-2,6-diamidepyridine were dissolved in 60 mL of THF and dropwise added into a suspension of 6.56 g (0.173 mol) of LAH in 40 mL of THF at 0°C. After stirring for 1 h at room temperature the reaction was refluxed overnight until completion of the reaction controlled by GC-MS. The excess of LAH was quenched at 0°C with a basic KOH 5% solution obtaining two phases. The phases are separated and the aqueous phase is treated with diethyl ether 3×30 mL. All organic fractions were collected and dried with Na_2SO_4. Filtration and removal of all volatiles *in vacuo* afforded the product in high purity as yellow oil (3.5 g, 77% yield).

^{1}H NMR: (200.13 MHz, $CDCl_3$, 298K): δ(ppm) = 1.22 (t, $^{3}J_{H–H}$ = 7.2 Hz, 6H, C*H*$_3$), 3.21 (q, $^{3}J_{H-H}$ = 7.2 Hz, 2H, C*H*$_2$), 3.24 (q, $^{3}J_{H–H}$ = 7.2 Hz, 2H, C*H*$_2$), 5.70 (d, $^{3}J_{H–H}$ = 7.9 Hz, 2H, 3,5-C$_{aroma.}$*H* py), 7.24 (t, $^{3}J_{H–H}$ = 7.9 Hz, 1H, 4-C$_{aroma.}$*H* py).

$^{13}C\{^{1}H\}$ NMR: (50.32 MHz, $CDCl_3$, 298K): δ(ppm) = 15.0 (CH_3), 36.9 (CH_2), 94.4 (3,5-$C_{aroma.}H$ py), 139.0 (4-$C_{aroma.}H$ py), 158.3 (2,6-$C_{aroma.}H$ py).

ESI-MS (m/z) Calcd for $[C_9H_{15}N_3 + H^+]$: 166.13387. Found: 166.13379 (correct isotope pattern).

5.4.6. Bis(silylene) SiNSi pincer ligand

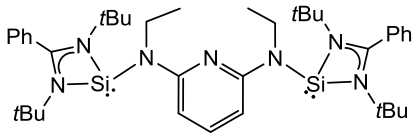

6.40 mL of *n*-BuLi 1.6 M in hexanes (10.2 mmol) were added rapidly to a 30 mL diethyl ether solution of 2,6-*N,N'*-diethylaminopyridine (0.847 g, 5.13 mmol) at –30°C, forming a yellowish solution. After warming up to room temperature, it was refluxed for 3h. The resulting orange solution was cooled down to –78°C and a solution of *N,N'*-di-*tert*-butyl(phenylamidinate)chlorosilylene (3.019 g, 10.2 mmol) in 30 mL of toluene was dropwise added *via* cannula. The color changed with the addition to dark red. All volatiles were removed in *vacuo* after stirring overnight, with slow warming up to room temperature. The product was extracted with 60 mL of hexanes at 60 °C *via* cannula filtration. The solution was concentrated to 10 mL and crystallized at –30°C over three days affording large yellow crystals. Further filtration and drying afforded 2.90 g of the desired product (90 % yield). Suitable crystals for single crystal XRD structure analysis were grown in a concentrated hexane solution at 0°C after 2 days.

Symmetric conformer:

^{1}H NMR: (400.13 MHz, C_6D_6, 298K): δ(ppm) = 1.16 (s, 36H, $NC(CH_3)_3$), 1.63 (t, $^{3}J_{H–H}$ = 6.9 Hz, 6H, NCH_2CH_3), 3.77 (q, $^{3}J_{H–H}$ = 6.9 Hz, 4H, NCH_2CH_3), 6.87 – 7.09 (m, 10H, $C_{aroma.}H$ Ph), 7.34 – 7.50 (m, 3H, $C_{aroma.}H$ py).

$^{13}C\{^{1}H\}$ NMR: (100.61 MHz, C_6D_6, 298K): δ(ppm) = 16.9 (NCH_2CH_3), 31.6 ($NC(CH_3)_3$), 31.9 (NCH_2CH_3), 52.9 ($NC(CH_3)_3$), 101.8 (3,5-$C_{aroma.}H$ py), 127.6 ($C_{aroma.}H$ Ph), 128.5 ($C_{aroma.}H$ Ph), 129.3

($C_{aroma.}$H Ph), 129.3 ($C_{aroma.}$H Ph), 129.4 ($C_{aroma.}$H Ph), 130.0 ($C_{aroma.}$H Ph), 130.5 ($C_{aroma.}$H Ph), 130.5 ($C_{aroma.}$H Ph), 134.7 ($C_{aroma.}$ quaternary Ph), 136.9 (4-$C_{aroma.}$H py), 161.2 (2,6-$C_{aroma.}$ py), 161.4 (N*C*N).

^{29}Si{^{1}H} NMR: (79.49 MHz, C_6D_6, 298K): δ(ppm) = –14.9.

Asymmetric conformer:

^{1}H NMR: (400.13 MHz, C_6D_6, 298K): δ(ppm) = 1.14 (s, 36H, NC(CH_3)$_3$), 1.55 and 1.68 (t, $^{3}J_{H–H}$ = 6.9 Hz, 6H, NCH$_2$CH_3), 3.71 and 4.62 (q, $^{3}J_{H–H}$ = 6.90 Hz, 4H, NCH_2CH$_3$).

^{13}C{^{1}H} NMR: (100.61 MHz, C_6D_6, 298K): δ(ppm) = 18.0 and 16.0 (NCH$_2$*C*H$_3$), 31.4 and 31.5 (NC(*C*H$_3$)$_3$), 36.8 and 43.9 (N*C*H$_2$CH$_3$), 53.3 (N*C*(CH$_3$)$_3$), 103.0 and 103.9 (3,5-$C_{aroma.}$H py), 134.0 and 134.5 ($C_{aroma.}$ quaternary Ph), 136.4 (4-$C_{aroma.}$H py).

^{29}Si{^{1}H} NMR: δ(ppm) = –13.8 and –17.1.

APCI-MS: (m/z) Calcd for [($C_{39}H_{59}N_7Si_2$+OH)$^{\bullet+}$]: 698.43924. Found: 698.43983 (correct isotope pattern).

5.4.7. Bis(germylene) GeNGe pincer ligand

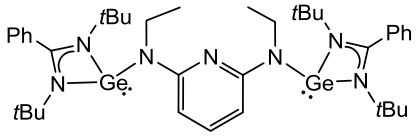

The synthesis of bis(germylene) pyridine pincer ligand proceeded in a similar fashion as for the synthesis of the pincer ligand **SiNSi**. After addition of the *N,N'*-di-*tert*-butyl(phenylamidinate)chlorogermylene (1.788 g, 5.27 mmol) in 30 mL of toluene the color of the reaction mixture changed to an intense yellowish solution. All volatiles were removed *in vacuo* after stirring overnight warming up to room temperature with the cold bath. The product was extracted with 60 mL of hexanes at 60 °C for 1 h *via* cannula filtration. Removal of the solvent produced 1.98 g of a yellowish foamy solid with high purity according to the NMR spectra (98% yield).

^{1}H NMR: (400.13 MHz, C_6D_6, 298K): δ(ppm) = 1.11 (s, 36H, NC(CH_3)$_3$), 1.53 (t, $^3J_{H–H}$ = 7.0 Hz, 6H, NCH_2CH_3), 3.76 (q, $^3J_{H–H}$ = 7.0 Hz, 4H, NCH_2CH_3), 6.34 (d, $^3J_{H–H}$ = 7.9 Hz, 2H, 3,5-$C_{aroma.}H$ py), 6.88 – 7.11 (m, 10H, $C_{aroma.}H$ Ph), 7.46 (t, $^3J_{H–H}$ = 7.9 Hz, 1H, 4-$C_{aroma.}H$ py).

^{13}C{^{1}H} NMR: (100.61 MHz, C_6D_6, 298K): δ(ppm) = 16.8 (NCH_2CH_3), 32.2 (NC(CH_3)$_3$), 38.8 (NCH_2-CH_3), 52.8 (NC(CH_3)$_3$), 95.2 (3,5-$C_{aroma.}$H py), 127.5 ($C_{aroma.}$H Ph), 128.9 ($C_{aroma.}$H Ph), 130.3 ($C_{aroma.}$H Ph), 136.9 (C_{arom} quaternary Ph), 138.7 (4-$C_{aroma.}$H py), 162.6 (2,6-$C_{aroma.}$H py), 167.3 (NCN).

APCI-MS: (m/z) Calcd for [$C_{39}H_{59}Ge_2N_7^{\bullet+}$]: 773.32500. Found: 773.32666 (correct isotope pattern).

Elemental analysis: (%) Calcd for $C_{39}H_{59}Ge_2N_7$: C, 60.74; H, 7.71; N, 12.71. Found: C, 60.47; H, 7.72; N, 12.40.

5.4.8. General procedure for the preparation of complexes of type [ECE]IrHCl(coe) (E = Si^{II}, Ge^{II}, P^{III})

The ligand **ECHE** (2.1 equiv.) and 1 equiv. of [IrCl(coe)$_2$]$_2$ were dissolved in 2 mL of toluene (or benzene) and stirred for 15 min at room temperature. Evaporation of the solvent *in vacuo* yielded a yellow, sticky residue, which was re-dissolved in toluene. The solvent was again evaporated *in vacuo* to remove traces of high-boiling cyclooctene. The yellowish powder was washed with hexanes (2×5 mL), and the residue was dried *in vacuo* for 2 hours.

5.4.9. Iridium(III) complex [SiCSi]IrHCl(coe)

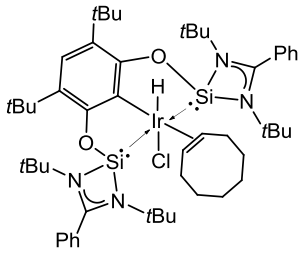

At 0.10 mmol scale: 92% yield; off-white solid. Crystals suitable for XRD structure analysis were obtained by layering a benzene solution with hexane.

^{1}H NMR: (400.13 MHz, $CDCl_3$, 298K): δ(ppm) = –25.65 (s, 1H, Ir–*H*), 0.99 (s, 18H, NC(C*H*$_3$)$_3$), 1.31 (s, 18H, NC(C*H*$_3$)$_3$), 1.43 (s, 18H, C*H*$_2$+C*H*$_3$), 1.67 – 1.70 (m, 2H, CH*H* allyl), 1.81 – 1.93 (m, 4H, C*H*$_2$), 2.97 (br. d, $^{3}J_{H–H}$ = 6.0 Hz, 2H, C*H*H allyl), 3.37 (br. d, $^{3}J_{H–H}$ = 5.4 Hz, 2H, *H*C=C*H*), 6.77 (s, 1H, 4-C$_{arom.}$*H*), 7.43 – 7.45 (m, 2H, C$_{arom.}$*H*), 7.49 – 7.57 (m, 6H, C$_{arom.}$*H*), 7.60 – 7.62 (m, 2H, C$_{arom.}$*H*).

^{13}C{^{1}H} NMR: (100.61 MHz, $CDCl_3$, 298K): δ(ppm) = 26.2 (*C*H$_2$), 30.5 (NC(*C*H$_3$)$_3$), 30.4 (NC(*C*H$_3$)$_3$), 31.6 (*C*H$_2$), 31.6 (ArC(*C*H$_3$)$_3$), 33.7 (*C*H$_2$), 34.7 (Ar*C*(CH$_3$)$_3$), 53.8 (N*C*(CH$_3$)$_3$), 54.2 (N*C*(CH$_3$)$_3$), 55.8 (H*C*=*C*H), 120.1 (4-*C*$_{arom.}$H), 121.7 (*C*–Ir), 124.7 (*C*$_{aroma.}$quaternary Ph), 127.6 (*C*$_{aroma.}$H Ph), 128.4 (*C*$_{aroma.}$H Ph), 130.5 (*C*$_{aroma.}$H Ph), 131.2 (*C*$_{aroma.}$quaternary), 158.4 (2,6-*C*$_{aroma.}$–OSi), 175.2 (N*C*N).

^{29}Si{^{1}H} NMR: ($CDCl_3$, 79.49 MHz, 298K): δ(ppm) = 54.9 (s).

FT-IR (KBr pellet): υ (cm^{-1}) = 2210.18 (w).

Elemental analysis: (%) Calcd for $C_{52}H_{80}ClSi_2IrN_4O_2$: C, 57.99; H, 7.49; N, 5.20. Found: C, 56.90; H, 7.83; N, 5.47.

5.4.10. Iridium(III) complex [GeCGe]IrHCl(coe)

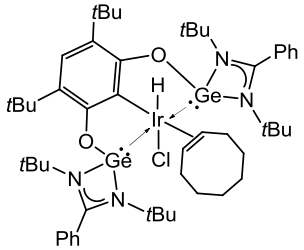

At 0.10 mmol scale: 91% yield; off-white solid

^{1}H NMR: (400.13 MHz, $CDCl_3$, 298K): δ(ppm) = –26.84 (s, 1H, Ir–*H*), 0.99 (s, 18H, NC(C*H*$_3$)$_3$), 1.23 (s, 18H, NC(C*H*$_3$)$_3$), 1.48 (s, 20H, C*H*$_2$ + Ar–C(C*H*$_3$)$_3$), 1.69 – 1.78 (m, 2H, CH*H* allyl), 1.85–1.96 (m, 4H, C*H*$_2$), 3.16 (d, $^{3}J_{H–H}$ = 12.1 Hz, 2H, C*H*H allyl), 4.06 (d, $^{3}J_{H–H}$ = 9.0 Hz, 2H, *H*C=C*H*), 6.86 (s, 1H, 4-C$_{arom.}$*H*), 7.37 (d, $^{3}J_{H–H}$ = 7.2 Hz,

2H, $C_{arom.}H$), 7.47 – 7.55 (m, 6H, $C_{arom.}H$), 7.58 – 7.62 (m, 2H, $C_{arom.}H$).

$^{13}C\{^1H\}$ NMR: ($CDCl_3$, 100.61 MHz): δ(ppm) = 26.1 (CH_2), 30.7 ($NC(CH_3)_3$), 31.2 ($NC(CH_3)_3$), 32.0 ($Ar–C(CH_3)_3$), 32.7 (CH_2), 33.8 (CH_2), 35.3 ($Ar–C(CH_3)_3$), 53.8 ($NC(CH_3)_3$), 55.0 ($NC(CH_3)_3$), 65.1 (HC=CH), 121.0 (4-$C_{arom.}$H), 121.7 (C–Ir), 123.5 ($C_{arom.}$quaternary), 127.9 ($C_{arom.}$), 128.2 (2×$C_{arom.}$), 128.9 ($C_{arom.}$), 130.3 ($C_{arom.}$), 132.4 ($C_{arom.}$quaternary), 157.9 (2,6-$C_{arom.}$–OGe), 174.7 (NCN).

FT-IR (KBr pellet): υ (cm^{-1}) = 2176.89 (w).

ESI-MS (m/z) Calcd for (M–Cl) [$C_{52}H_{80}Ge_2IrN4O_2^{\bullet+}$]: 1133.4. Found: 1133.4 (correct isotope patern).

Elemental analysis: (%) Calcd for $C_{52}H_{80}ClGe_2IrN_4O_2$: C, 53.56; H, 6.91. Found: C, 53.67; H, 6.40.

5.4.11. Iridium(III) complex [SiCSi]Ir(H)$_2$CO

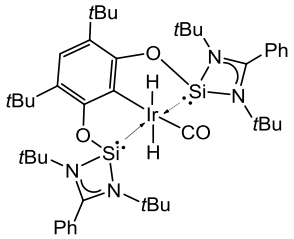

$IrH(CO)(PPh_3)_3$ (30.0 mg, 29.8 mmol) and **[SiCHSi]** (23.1 mg, 31.2 mmol) were weighted into a small Schlenk flask and suspended in 3 mL of toluene. A yellow solution formed upon heating to 100 °C, and the mixture was stirred at that temperature for 1 h. After cooling, the solvent volume was reduced to *ca.* 0.5 mL *in vacuo*, and 5 mL of hexane were added. The product precipitated as white powder and was collected by filtration (25.2 mg; 88%).

^{1}H NMR: (400.13 MHz, $CDCl_3$, 298K): δ(ppm) = –10.21 (s, 2H, Ir–*H*), 1.34 (s, 36H, $NC(CH_3)_3$), 1.82 (s, 18H, $ArC(CH_3)_3$), 6.72 – 6.81 (m, 6H, $C_{arom.}$–*H* Ph), 6.86 – 6.89 (m, 2H, $C_{arom.}$–*H* Ph), 7.13 (d, *J* = 7.9 Hz, 2H, $C_{arom.}$–*H* Ph), 7.35 (s, 1H, 4-$C_{arom.}$–*H*).

$^{13}C\{^1H\}$ NMR: (50 MHz, $CDCl_3$, 298K): δ(ppm) = 31.0 ($ArC(CH_3)_3$), 31.5

(NC(CH_3)$_3$), 35.2 (ArC(CH$_3$)$_3$), 54.9 (NC(CH$_3$)$_3$), 119.5 ($C_{arom.}$), 119.6 ($C_{arom.}$), 125.5 ($C_{arom.}$), 127.2 ($C_{arom.}$), 129.4 ($C_{arom.}$), 129.9 ($C_{arom.}$), 132.1 ($C_{arom.}$), 160.5 (2,6-$C_{arom.}$–OSi), 172.9 (NCN), 182.8 (CO).

^{29}Si{^{1}H} NMR: (79.49 MHz, $CDCl_3$, 298K): δ(ppm) = 35.9 ppm (s).

FT-IR (KBr pellet, cm^{-1}): 2251 (vw), 1957.9 (vs).

CI-MS (m/z) Calcd for (M – H) [($C_{45}H_{67}IrN_4O_3Si_2$ – H)$^+$]: 959.44. Found 959.43 (correct isotope pattern).

Elemental analysis: (%) Calcd for $C_{45}H_{67}IrN_4O_3Si$: C, 56.28; H, 7.03; N, 5.83. Found: C, 56.83; H, 6.77; N, 5.50.

5.4.12. Rhodium(III) complex [SiCSi]RhHClPPh$_3$

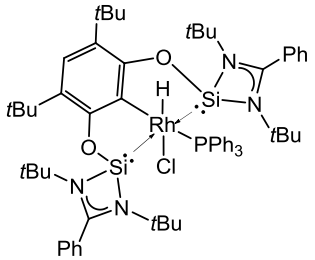

[RhCl(coe)$_2$]$_2$ (30 mg, 41.8 mmol) and PPh$_3$ (44 mg, 168.0 mmol) were weighed into a small Schlenk flask equipped with a stir bar. Toluene (6 mL) was added, and the mixture was stirred for 30 min. During that time, a bright red precipitate formed. **SiCHSi** (65 mg, 87.9 mmol) in 1 mL of toluene was added via cannula, and the suspension was heated to 100 °C. The red precipitate dissolved completely after 30 min, and the color of the solution turned yellow. The solvent volume was reduced to ca. 1 mL in vacuo, and 8 mL of hexane were added to precipitate the product as white powder. The solvent was decanted, and the residue was dried *in vacuo* for 2 hours. 40.1 mg (84% yield).

^{1}H NMR: (400.13 MHz, $CDCl_3$, 298K): δ(ppm) = –17.17 (dd, $^2J_{H–P}$ = 11.0 Hz, $^1J_{H–Rh}$ = 22.2 Hz, 1H, Rh–H), 0.90 (s, 18H, NC(CH_3)$_3$), 1.34 (s, 18H, NC(CH_3)$_3$), 1.88 (s, 18H, ArC(CH_3)$_3$), 6.80 – 6.84 (m, 2H, $C_{arom.}H$), 6.92 – 6.93 (m, 4H, CH3), 7.08 – 7.14 (m, 5H, $C_{arom.}H$), 7.21 (br.q, J = 6.4 Hz, 8H, CH), 7.53 (s, 1H, $C_{arom.}H$), 8.15 (t, J =

8.9 Hz, 6H, $C_{arom.}H$).

$^{13}C\{^1H\}$ NMR: (400.13 MHz, $CDCl_3$, 298K): δ(ppm) = 31.4 (ArC(CH_3)$_3$), 32.0 (ArC(CH_3)$_3$), 35.3 (ArC(CH_3)$_3$), 53.7 (NC(CH_3)$_3$), 55.0 (NC(CH_3)$_3$), 121.3 ($C_{arom.}$), 125.4 (d, 2JC–P = 1.1 Hz, C–Rh), 127.6 ($C_{arom.}$), 127.7 ($C_{arom.}$ PPh_3), 127.8 (d, JCP = 8.6 Hz, CH), 128.3 ($C_{arom.}$), 128.5 ($C_{arom.}$), 129.6 ($C_{arom.}$), 129.9 ($C_{arom.}$), 135.1 (d, JCP = 11.3 Hz, $C_{arom.}$ PPh_3), 141.1 (s, JCP = 31.8 Hz, CP), 159.4 (s, COSi), 175.4 (NCN).

$^{29}Si\{^1H\}$ NMR: (79.49 MHz, $CDCl_3$, 298K): 66.4 (dd, $^2J_{Si–P}$ = 20.6 Hz, $^1J_{Si–Rh}$ = 59.4 Hz).

FT-IR (KBr pellet, cm^{-1}): 2105.8 (w).

ESI-MS (m/z) Calcd for (M – Cl) [$C_{62}H_{81}N_4O_2PRhSi_2^+$]: 1103.47. Found: 1103.47 (correct isotope pattern).

Elemental analysis: (%) Calcd for $C_{62}H_{81}ClN_4O_2PRhSi_2$: C, 65.33; H, 7.16. Found: C, 65.56; H, 6.59.

5.4.13. Iridium(III) complex [*t*Bu-PCP]IrHCl

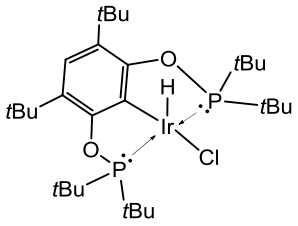

[IrCl(coe)$_2$]$_2$ (25.0 mg, 27.9 mmol) and ***t*Bu-PCHP** (29.2 mg, 57.2 mmol) were weighed into a small Schlenk flask equipped with a stir bar, and 3 mL of toluene were added. The solution was heated to 100 °C and stirrred for 45 min. The color of the solution turned from yellow to dark red during that time. The solvent was evaporated *in vacuo*. The residue was redissolved in toluene, and the solvent was evaporated again *in vacuo* to remove traces of high-boiling cyclooctene. The red residue was dissolved in a minimum amount of hexane, and the solution was placed into the freezer (–30°C). Red crystals (suitable for single crystal X-ray diffraction) formed over the course of three days. The crystals were collected via filtration and dried *in vacuo* (33 mg, 94%).

^{1}H NMR: (200 MHz, $CDCl_3$, 298K): δ(ppm) = –41.61 (t, $^{2}J_{H–P}$ = 13.1 Hz, 1H, Ir–*H*), 1.39 (*virtual*-t, $^{3}J_{H–P}$ = 7.2 Hz, 18H, P(C(CH_3)$_3$)$_2$), 1.42 (*virtual*-t, $^{3}J_{H–P}$ = 7.3 Hz, 18H, P(C(CH_3)$_3$)$_2$), 1.42 (s, 18H, ArC(CH_3)$_3$), (6.83 (s, 1H, 4-C$_{aroma.}$*H*).

^{13}C{^{1}H} NMR: (50 MHz, $CDCl_3$, 298K): δ(ppm) = 27.9 (*virtual*-t, 2*J*CP = 3.1 Hz, P(C(*C*H$_3$)$_3$)$_2$), 28.2 (*virtual*-t, $^{2}J_{C–P}$ = 3.2 Hz, P(C(*C*H$_3$)$_3$)$_2$), 30.5 (s, ArC(*C*H$_3$)$_3$), 34.3 (s, Ar*C*(CH$_3$)$_3$), 39.8 (*virtual*-t, $^{1}J_{C–P}$ = 12.9 Hz, P(*C*(CH$_3$)$_3$)$_2$), 43.3 (t, $^{1}J_{C–P}$ = 11.7 Hz, P(*C*(CH$_3$)$_3$)$_2$), 120.5 (*virtual*-t, $^{2}J_{C–P}$ = 3.3 Hz, *C*–Ir), 121.4 (s, 4-*C*$_{aroma.}$H), 126.2 (*virtual*-t, $^{3}J_{C–P}$ = 4.6 Hz, 3,5-*C*$_{aroma.}$H), 162.9 (*virtual*-t, $^{2}J_{C–P}$ = 5.4 Hz, 2,6-*C*$_{aroma.}$H).

^{31}P{^{1}H} NMR: (80 MHz, $CDCl_3$, 298K): δ(ppm) = 176.6 (s).

FT-IR (KBr pellet, cm^{-1}): 2013.74 (w, Ir–H).

CI-MS (m/z) Calcd for [$C_{30}H_{56}ClIrO_2P_2^{\bullet+}$]: 738.30. Found: 738.31 (M, correct isotope pattern), 703.34 (M – Cl, correct isotope pattern).

Elemental analysis: (%) Calcd for $C_{30}H_{56}ClIrO_2P_2$: C, 48.80; H, 7.64. Found: C, 48.73; H, 7.28.

5.4.14. Iridium(III) complex [*i*Pr-PCP]IrHCl(coe)

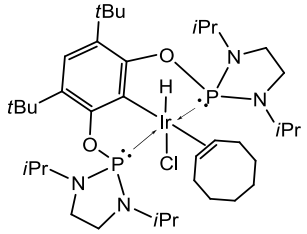

[IrCl(coe)$_2$]$_2$ (30.0 mg, 33.5 mmol) was weighed into a 50 mL Schlenk flask equipped with a stir bar, and 5 mL of CH_2Cl_2 were added to the flask. The suspension was cooled to –78°C with a dry ice/isopropanol bath, and a precooled solution of 38.0 mg (67.0 mmol) ***i*PrN-PCHP** in 3 mL of CH_2Cl_2 was added slowly via cannula while stirring. The reaction mixture was allowed to warm to room temperature overnight yielding a slightly yellow solution. The solvent volume was reduced to ca. 0.5 mL, filtered, and the residue washed with 2 mL of hexane. The combined organic phases were placed in a freezer overnight,

yielding the product in as colorless, microcrystalline material. The solvent was decanted, and the product dried *in vacuo* (54.5 mg, 90%). Crystals suitable for XRD structure analysis were obtained by slow evaporation of hexane solution.

^{1}H NMR: (400 MHz, $CDCl_3$, 298K): δ(ppm) = –24.61 (t, $^{2}J_{H–P}$ = 15.1 Hz, 1H, Ir–*H*), 0.94 (d, $^{3}J_{H–H}$ = 6.6 Hz, 6H, 2×CHC*H*$_3$), 1.04 (d, $^{3}J_{H–H}$ = 6.6 Hz, 6H, 2×CHC*H*$_3$), 1.22 (d, $^{3}J_{H–H}$ = 7.0 Hz, 6H, 2×CHC*H*$_3$), 1.25 (d, $^{3}J_{H–H}$ = 7.0 Hz, 6H, 2×CHC*H*$_3$), 1.34 (s, 18H, ArC(C*H*$_3$)$_3$), 1.42 – 1.49 (m, 6H, C*H*H allyl + C*H*$_2$ coe), 1.65 – 1.74 (m, 4H, CH*H* allyl + C*H*$_2$ coe), 3.18 – 3.28 (m, 2H, NC*H*$_2$), 3.32 – 3.41 (m, 2H, NC*H*$_2$), 3.43 – 3.51 (m, 4H, NC*H*(CH$_3$)$_2$), 3.53 – 3.59 (m, 2H, NC*H*$_2$), 4.31 (br.s, 2H, *H*C=C*H*), 4.90 (m, 2H, NC*H*$_2$), 6.78 (s, 1H, 4-C$_{aroma.}$*H* Ph).

^{13}C{^{1}H} NMR: (50 MHz, $CDCl_3$, 298K): δ(ppm) = 20.5 (s, CH*C*H$_3$), 20.8 (s, CH*C*H$_3$), 22.0 (d, $^{3}J_{C–P}$ = 4.6 Hz, CH*C*H$_3$), 22.1 (d, $^{3}J_{C–P}$ = 4.4 Hz, CH*C*H$_3$), 26.4 (s, *C*H$_2$ coe), 27.9 (s, *C*H$_2$ coe), 30.5 (s, ArC(*C*H$_3$)$_3$), 32.1 (s, *C*H$_2$ coe), 39.8 (s, N*C*H$_2$), 40.8 (s, N*C*H$_2$), 43.8 (virtual-t, $^{2}J_{C–P}$ = 4.4 Hz, *C*HCH$_3$), 44.1 (virtual-t, $^{2}J_{C–P}$ = 4.4 Hz, *C*HCH$_3$), 81.6 (s, H*C*=*C*H coe), 120.7 (s, 4-*C*$_{aroma.}$H Ph), 124.9 (t, $^{2}J_{C–P}$ = 5.7 Hz, *C*–Ir), 128.3 (3,5-*C*$_{aroma.}$H Ph), 153.2 (virtual-t, $^{2}J_{C–P}$ = 8.3 Hz, 2,6-*C*$_{aroma.}$ Ph).

^{31}P{^{1}H} NMR: (80 MHz, $CDCl_3$, 298K): δ(ppm) = 110.05 (s), 110.09 (s).

FT-IR (KBr pellet, cm^{-1}): 2220 (w, Ir–H).

ESI-MS (m/z) Calcd for (M – Cl) [$C_{30}H_{56}IrN_4O_2P_2^+$]: 869.46. Found: 869.46 (correct isotope pattern).

Elemental analysis: (%) Calcd for $C_{38}H_{70}ClIrN_4O_2P_2$: C, 50.45; H, 7.80; N, 6.19. Found: C, 50.19; H, 7.92; N 5.86.

5.4.15. General procedure for the preparation of complexes of type [ECE]NiX (E = Si, Ge, P; X = Br, I)

General procedure with $NiBr_2$(dme). NEt_3 (10.0 equiv.) were added to a suspension of $NiBr_2$(dme) (1.1 equiv.) in THF forming a dark blue solution. After stirring for 20 min, a solution of **ECHE** (1.0 equiv) in toluene was added *via* cannula and the reaction mixture was heated to reflux for 4 h. The mixture was allowed to cool to room temperature, filtered through a short plug of Celite and all volatiles were removed *in vacuo*. The residue was extracted with hexane (1×50 mL, 2×20 mL) at 50°C. The combined organic solutions were concentrated slowly *in vacuo* until small crystals formed at the glass wall. Further cooling in the freezer at –30°C resulted in the crystallization of the pure products in form of needles, which were collected by filtration and dried *in vacuo* for 2 h.

Procedure with GeCBrGe and $Ni(cod)_2$. $Ni(cod)_2$ (0.15 g, 0.53 mmol) was dissolved in 20 mL of toluene at -30°C. A solution of **GeCBrGe** (0.53 g, 0.58 mmol) in 20 mL of toluene was added dropwise through a syringe. The stirred reaction mixture was slowly warmed up to room temperature over the course of 8 h, resulting in a dark red solution, which was filtered. All volatiles from the filtrate were removed *in vacuo*, and the solid was washed with cold hexane (2×10 mL). The residue was dried *in vacuo* for 2 h, obtaining **[GeCGe]NiBr** as a dark red powder (0.45 g, 88 % yield).

5.4.16. Nickel(II) complex [SiCSi]NiBr

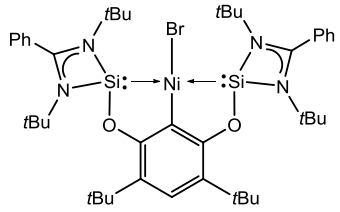

(1.4 mmol scale: 70% yield; yellow needles):

^{1}H NMR: (400.13 MHz, C_6D_6, 298K): δ(ppm) = 1.34 (s, 36 H, NC(CH_3)$_3$), 1.75 (s, 18 H, ArC(CH_3)$_3$), 6.79 – 6.91 (m, 8 H, $C_{aroma.}H$ Ph), 7.48 (s, 1 H, 4-$C_{aroma.}H$), 7.69 – 7.71 (m, 2 H, $C_{aroma.}H$ Ph).

^{13}C{^{1}H} NMR: (100.61 MHz, C_6D_6, 298K): δ(ppm) = 30.8 (s, ArC(CH_3)$_3$), 31.5 (s, NC(CH_3)$_3$), 35.3 (s, ArC(CH_3)$_3$), 54.1 (s, NC(CH_3)$_3$), 123.8 (s,

4-$C_{aroma.}$H), 126.5 (s, 3,5-$C_{aroma.}$ *t*Bu), 128.4 (s, $C_{aroma.}$H Ph), 130.3 (s, 2C, $C_{aroma.}$H Ph), 131.3 (s, *C*–Ni), 131.4 (s, $C_{aroma.}$ quaternary Ph), 162.7 (s, 2,6-$C_{aroma.}$–O), 173.1 (s, N*C*N).

^{29}Si{^{1}H} NMR: (79.49 MHz, C_6D_6, 298K): δ (ppm) = 20.2.

APCI-MS (m/z) Calcd for [$C_{44}H_{65}BrN_4NiO_2Si_2^{\bullet+}$]: 874.31774. Found: 874.31805 (correct isotope pattern).

Elemental analysis: (%) Calcd for $C_{44}H_{65}BrN_4NiO_2Si_2.C_6H_{14}$: C, 62.36; H, 8.27; N, 5.82. Found: C, 62.72; H, 8.43; N, 6.22.

5.4.17. Nickel(II) complex [SiCSi]NiI. NiI_2(dme) as the precursor

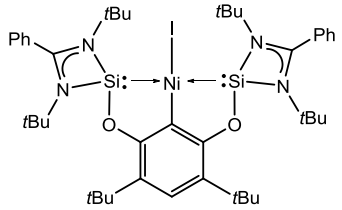

(0.3 mmol scale: 66% yield; orange needles):

^{1}H NMR: (200 MHz, C_6D_6, 298K): δ(ppm) = 1.33 (s, 36 H, NC(CH_3)$_3$), 1.77 (s, 18 H, ArC(CH_3)$_3$), 6.80 – 6.97 (m, 8 H, C $_{aroma.}$*H* Ph), 7.54 (s, 1 H, 4-C $_{aroma.}$*H*), 7.85 – 7.88 (m, 2 H, C $_{aroma.}$*H* Ph).

^{13}C{^{1}H} NMR: (50.32 MHz, C_6D_6, 298K): δ(ppm) = 30.8 (s, ArC(CH_3)$_3$), 31.5 (s, NC(CH_3)$_3$), 35.4 (s, Ar*C*(CH_3)$_3$), 54.1 (s, N*C*(CH_3)$_3$), 123.9 (s, 4-$C_{aroma.}$H), 126.6 (s, 3,5-$C_{aroma.}$*t*Bu), 130.2 (s, $C_{aroma.}$H Ph), 130.3 (s, $C_{aroma.}$H Ph), 131.4 (s, $C_{aroma.}$ quaternary Ph), 135.7 (s, *C*–Ni), 162.5 (s, 2,6-$C_{aroma.}$–O), 173.4 (s, N*C*N).

^{29}Si{^{1}H} NMR: (79.49 MHz, C_6D_6, 298K): δ (ppm) = 30.7.

APCI-MS (m/z) Calcd for [$C_{44}H_{65}IN_4NiO_2Si_2^{\bullet+}$]: 922.30387. Found: 922.30396 (correct isotope pattern).

Elemental analysis: (%) Calcd for $C_{44}H_{65}IN_4NiO_2Si_2$: C, 57.21; H, 7.09; N, 6.06. Found: C, 56.44; H, 6.47; N, 7.17.

5.4.18. Nickel(II) complex [GeCGe]NiBr

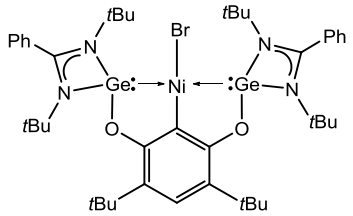

0.5 mmol scale, 57% yield; red needles.

^{1}H NMR: (400.13 MHz, C_6D_6, 298K): δ (ppm) = 1.21 (s, 36 H, NC(CH_3)$_3$), 1.83 (s, 18 H, ArC(CH_3)$_3$), 6.78 – 6.91 (m, 8 H, C$_{aroma.}$*H* Ph), 7.06 – 7.10 (m, 2 H, C$_{aroma.}$*H* Ph), 7.56 (s, 1 H, 4-C$_{aroma.}$*H*).

^{13}C{^{1}H} NMR: (100.61 MHz, C_6D_6, 298K): δ (ppm) = 31.0 (s, ArC(*C*H$_3$)$_3$), 31.5 (s, NC(*C*H$_3$)$_3$), 35.8 (s, Ar*C*(CH$_3$)$_3$), 54.4 (s, N*C*(CH$_3$)$_3$), 125.1 (s, 4-*C*$_{aroma.}$H), 125.4 (s, 3,5-*C*$_{aroma.}$*t*Bu), 126.8 (s, C$_{aroma.}$ quaternary Ph), 128.7 (s, CH$_{arom}$), 128.7 (s, *C*$_{aroma.}$H Ph), 130.0 (s, *C*$_{aroma.}$H Ph), 132.3 (s, *C*–Ni), 162.6 (s, 2,6-*C*$_{aroma.}$–O), 175.0 (s, N*C*N).

APCI-MS (m/z) Calcd for [$C_{44}H_{65}BrGe_2N_4NiO_2^{\bullet+}$]: 966.20510. Found 966.20721 (correct isotope pattern).

Elemental analysis: (%) Calcd for $C_{44}H_{65}BrGe_2N_4O_2$: C, 54.71; H, 6.78; N, 5.80. Found: C, 54.22; H, 7.06; N, 5.51.

5.4.19. Nickel(II) complex [*i*PrN-PCP]NiBr

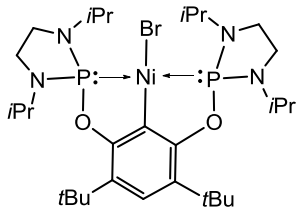

(95% yield, yellow needles)**.**

^{1}H NMR: (200.13 MHz, $CDCl_3$, 298K): δ (ppm) = 1.31 (s, 18H, C(CH_3)$_3$), 1.32 (d, $^{3}J_{H–H}$ = 6.6 Hz, 24 H, CH(CH_3)$_2$), 3.25 – 3.32 (m, 4H, CH_2), 3.33 – 3.39 (m, 4H, CH_2), 3.73 – 3.86 (m, 4H, C*H*(CH$_3$)$_2$),

6.93 (br. s, 1H, 4-$C_{aroma.}H$).

$^{13}C\{^1H\}$ NMR: (50.32 MHz, $CDCl_3$, 298K): δ (ppm) = 21.8 (t, $^3J_{C-P}$ = 2.5 Hz, $NCH(CH_3)_2$), 22.6 (t, $^3J_{C-P}$ = 2.8 Hz, $NCH(CH_3)_2$), 29.9 (s, $ArC(CH_3)_3$), 43.5 (s, CH_2), 47.1 (t, $^2J_{C-P}$ = 7.1 Hz, $NCH(CH_3)_2$), 123.8 (s, 4-$C_{aroma.}H$), 126.2 (t, $^3J_{C-P}$ = 5.7 Hz, 3,5-$C_{aroma.}t$Bu), 134.2 (t, $^2J_{C-P}$ = 24.7 Hz, *C*–Ni), 156.5 (t, $^2J_{CP}$ = 13.2 Hz, 2,6-$C_{aroma.}$–O).

$^{31}P\{^1H\}$ NMR: (81.01 MHz, $CDCl_3$, 298K): δ (ppm) = 134.6 (s).

EI-MS (m/z) Calcd for $[C_{30}H_{55}BrN_4NiO_2P_2^{\bullet+}]$: 704.23166. Found 704.17770 (correct isotope pattern).

5.4.20. General procedure for the preparation of complexes of type *κ²E,E'*-[ENE]$FeCl_2$ (E = Si^{II}, Ge^{II})

A suspension of $FeCl_2$ (1.1 equiv) was heated in 30 mL of THF at 60 °C for 2 h. After cooling to room temperature, a solution of **SiNSi** (1.0 equiv) in 20 mL of THF was dropwise added *via* cannula dissolving all suspended solid. After stirring at room temperature for 3 h, all volatiles were removed under vacuum forming a yellowish solid. The product was extracted with toluene (1 × 60 mL, 1 × 30 mL) and filtered off *via* cannula. Concentration *in vacuo* to 10 mL and crystallization at –30°C afforded the desired product as yellow crystals.

5.4.21. Iron(II) complex *κ²Si,Si'*-[SiNSi]$FeCl_2$

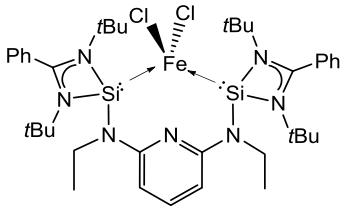

At 1.0 mmol scale: 73% yield; yellow blocks. Suitable crystals for XRD structure analysis were grown from a concentrated toluene solution at 0°C after 3 days.

^1H NMR: paramagnetic (200.13 MHz, C_6D_6, 298K): δ(ppm) = – 2.25 (36 H), 1.24 (6 H), 2.80 (2 H), 5.61 (2 H), 6.53 (2 H), 10.29 (1 H), 10.66 (2 H), 13.32 (2 H), 21.83 (4 H), 24.41 (2 H).

Evans: (C_6D_6, tetramethylsilylsilane capillary, concentration 0.031 g mL^{-1}, 200 MHz for ^1H): μ_{eff} = 4.65 μ_B.

^{57}Fe Mössbauer: at 77K (Zero field): δ = 0.73(1) mm s^{-1}, ΔE_Q = 3.06(1) mm s^{-1}, Γ_{FWHM} = 0.34(1) mm s^{-1}.

APCI-MS : (m/z) Calcd for $[C_{39}H_{59}Cl_2FeN_7Si_2^{\bullet+}]$: 807.30915. Found 807.30914 (correct isotope pattern).

Elemental analysis: (%) Calcd for $C_{39}H_{59}Cl_2FeN_7Si_2.C_7H_8$: C, 61.32; H, 7.50; N 10.88. Found: C, 59.61; H, 7.58; N, 10.99.

5.4.22. Iron(II) complex *κ²Ge,Ge'*-[GeNGe]FeCl$_2$

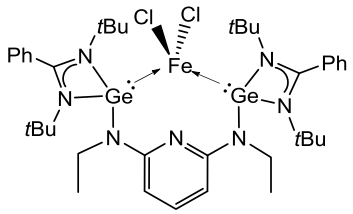

At 1.0 mmol scale: 83% yield; yellow blocks. Suitable crystals for XRD structure analysis were grown from a concentrated toluene solution at -78°C after 3 days.

^{1}H NMR: paramagnetic (200.13 MHz, C_6D_6, 298K): δ(ppm) = – 0.11 and 0.36 (two signals, overlapping, 36 H), 1.00 – 1.42 (5 H), 3.29 (2 H), 4.90 (2 H), 5.17 (1 H), 5.95 (2 H), 8.06 (2 H), 8.86 (2H), 11.93 (1 H), 26.70 (4 H).

Evans: (C_6D_6, tetramethylsilylsilane capillary, concentration 0.029 g mL^{-1}, 200 MHz for ^1H): μ_{eff} = 4.71 μ_B.

^{57}Fe Mössbauer: at 77K (Zero field): δ = 0.82(1) mm s^{-1}, ΔE_Q = 2.57(1) mm s^{-1}, Γ_{FWHM} = 0.46(1) mm s^{-1}.

APCI-MS : (m/z) Calcd for $[C_{39}H_{59}Cl_2FeGe_2N_7^{\bullet+}]$: 899.19765. Found 899.19928 (low intensity). Calcd for $[(C_{39}H_{59}Cl_2FeGe_2N_7 - Cl)^+]$: 864.22935. Found: 864.38190 (correct isotope pattern).

Elemental analysis: (%) Calcd for $C_{39}H_{59}Cl_2FeGe_2N_7.C_7H_8$: C, 55.80; H, 6.82; N, 9.90. Found: C, 55.06; H, 7.01; N, 10.20.

5.4.23. Iron(0) complex [SiNSi]Fe(PMe$_3$)$_2$

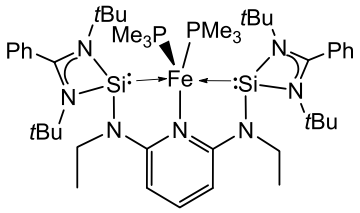

Method A. A strong yellow solution of [SiNSi]FeCl$_2$ (414 mg, 0.511 mmol) in 30 mL of THF was dropwise added *via* cannula to a Schlenk flask containing KC_8 (220 mg, 1.63 mmol) at –10 °C. After 15 min stirring, a solution of PMe_3 (1.0 M in hexanes) (2.0 mL, 2.0 mmol) was added dropwise *via* syringe with a change in color to red. After warming to room temperature and for 24 h stirring the reaction mixture was a dark purple color. The solution was filtered *via* cannula and all volatiles removed *in vacuo* producing a sticky purple solid. The product was extracted with pentane (1 × 50 mL, 1 × 20 mL) and concentrated *in vacuo* affording 350 mg (77% yield) of a purple solid after 3 freeze-thaw cycles in high purity according to the NMR spectra. Suitable crystals for XRD structure analysis were grown in a concentrated pentane solution at 0°C after *ca.* 1 week. **Method B.** A solution of **SiNSi** (160 mg, 0.235 mmol) in 10 mL of hexane was dropwise added to a solution of Fe(PMe$_3$)$_4$ (85 mg, 0.24 mmol) in 10 mL of hexane at room temperature. The mixture was warmed up to 50 °C for 8 h under continuous stirring. The solvent was pumped off and the product extracted with 40 mL of pentane. Concentration, crystallization, filtration and drying *in vacuo* afforded 100 mg of the desired product (48% yield).

^{1}H NMR: (200.13 MHz, C_6D_6, 298K): δ(ppm) = 1.09 (s, 18H, 2×NC(C*H*$_3$)$_3$), 1.29 (d, 9H, $^2J_{H–P}$ = 4.0 Hz, P^A(C*H*$_3$)$_3$), 1.52 (s, 18H, NC(C*H*$_3$)$_3$), 1.58 (t, 6H, $^3J_{H–H}$ = 7.0 Hz, NCH'HC*H*$_3$), 1.89 (d, 9H, $^2J_{H-P}$ = 4.0 Hz, P^B(C*H*$_3$)$_3$), 3.49 (dq with roof effect, 2H, $^2J_{H–H}$ = 14.0 Hz, $^3J_{H–H}$ = 7.0 Hz, NCH'*H*CH$_3$), 3.70 (dq with roof effect, 2H, $^2J_{H–H}$ = 14.0 Hz, $^3J_{H–H}$ = 7.0 Hz, NC*H'*HCH$_3$), 6.04 (d, 2H, $^3J_{H-H}$ = 7.7 Hz, 3,5-C$_{aroma}$.*H* py), 6.96 – 7.06 (m, 6H, C$_{aroma}$.*H* Ph), 7.19 – 7.27 (m, 3H, C$_{aroma}$.*H* Ph and 4-C$_{aroma}$.*H* py), 7.42 – 7.51 (m, 2H, C$_{aroma}$.*H* Ph).
(400.13 MHz, C_7D_8, 298K): δ(ppm) = 1.07 (s, 18H, 2×NC(C*H*$_3$)$_3$),

1.21 (d, 9H, $^{2}J_{H–P}$ = 4.4 Hz, $P^{A}(CH_3)_3$), 1.51 (s, 18H, 2×NC(CH_3)$_3$), 1.56 (t, 6H, $^{3}J_{H–H}$ = 7.0 Hz, NCH'HCH_3), 1.83 (d, 9H, $^{2}J_{H–P}$ = 6.1 Hz, $P^{B}(CH_3)_3$), 3.46 (dq with roof effect, 2H, $^{2}J_{H–H}$ = 14.0 Hz, $^{3}J_{H–H}$ = 7.0 Hz, NCH'*H*CH_3), 3.69 (dq with roof effect, 2H, $^{2}J_{H–H}$ = 14.0 Hz, $^{3}J_{H–H}$ = 7.0 Hz, NC*H'*HCH_3), 5.95 (d, 2H, $^{3}J_{H–H}$ = 8.0 Hz, 3,5-$C_{aroma.}H$ py), 7.18 (td, 1H, $^{3}J_{H–H}$ = 8.0 Hz, $^{6}J_{H–P}$ = 1.8 Hz, 4-$C_{aroma.}H$ p), 6.99 – 7.08 (m, 6H, $C_{aroma.}H$ Ph), 7.24 – 7.28 (m, 2H, $C_{aroma.}H$ Ph), 7.44 – 7.48 (m, 2H, $C_{aroma.}H$ Ph).

$^{13}C\{^{1}H\}$ NMR: (100.61 MHz, C_7D_8, 298K): δ(ppm) = 15.6 (NCH_2CH_3), 25.9 (d, $^{1}J_{C–P}$ = 10.8 Hz, $P^{A}(CH_3)_3$), 33.9 (dd, $^{1}J_{C–P}$ = 13.1 Hz, $^{3}J_{C–P}$ = 5.6 Hz, $P^{B}(CH_3)_3$), 31.6 (NC(CH_3)$_3$), 33.3 (NC(CH_3)$_3$), 38.9 (NCH_2CH_3), 53.3 (NC(CH_3)$_3$), 53.5 (NC(CH_3)$_3$), 93.3 (d, $^{4}J_{C–P}$ = 2.2 Hz, 3,5-$C_{aroma.}$H py), 126.6 (d, $^{5}J_{C–P}$ = 3.3 Hz, 4-$C_{aroma.}$H py), 127.3 ($C_{aroma.}$H Ph), 127.4 ($C_{aroma.}$H Ph), 130.5 ($C_{aroma.}$H Ph),, 135.3 ($C_{aroma.}$ quaternary Ph), 165.3 (d, $^{3}J_{C–P}$ = 3.3 Hz, 2,6-C_{arom} py), 168.5 (N*C*N).

$^{29}Si\{^{1}H\}$ NMR: (79.49 MHz, C_7D_8, 298K): 68.3 (dd, $^{2}J_{Si–P}$ = 22.4 Hz, 91.9 Hz).

$^{31}P\{^{1}H\}$ NMR: (161.97 MHz, C_7D_8, 298K): 7.2 (bs, $P^{A}(CH_3)_3$), 20.8 (bs with satellites $^{2}J_{P–Si}$ = 91.9 Hz, $P^{B}(CH_3)_3$)

^{57}Fe Mössbauer: at 77K (Zero field): δ = 0.24(1) mm s^{-1}, ΔE_Q = 1.66(1) mms^{-1}, Γ_{FWHM} = 0.30(1) mm s^{-1}.

APCI-MS : (m/z) Calcd for [$C_{45}H_{77}FeN_7P_2Si_2^{\bullet+}$]: 889.45982. Found: 889.45978 (correct isotope pattern).

5.4.24. Iron(0) complex [GeNGe]Fe(PMe_3)$_2$

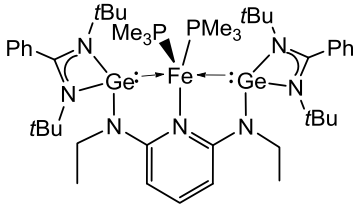

The synthesis of this complex was ONLY affordable by **method B** described above for **[SiNSi]Fe(PMe$_3$)$_2$** complex. Extraction with pentane and removal of the solvent in *vacuo* afforded a foamy like dark red solid in high purity. At 0.5 mmol scale: 90% yield.

^{1}H NMR: (400.13 MHz, C_6D_6, 298K): δ(ppm) = 1.08 (s, 18H, NC(CH_3)$_3$), 1.29 (d, $^2J_{H–P}$ = 5.3 Hz, 9H, P^A(CH_3)$_3$), 1.47 (s, 18H, NC(CH_3)$_3$), 1.57 (t, $^3J_{H–H}$ = 7.0 Hz, 6H, NCH'HCH_3), 1.76 (d, $^2J_{H-P}$ = 6.6 Hz, 9H, P^B(CH_3)$_3$), 3.76 (dq with roof effect, $^2J_{H–H}$ = 14.0 Hz, $^3J_{H–H}$ = 7.0 Hz, 2H, NCH'*H*-CH_3), 3.95 (dq with roof effect, $^2J_{H–H}$ = 14.0 Hz, $^3J_{H–H}$ = 7.0 Hz, 2H, NC*H*'HCH_3), 6.00 (d, $^3J_{H–H}$ = 7.9 Hz, 2H, 3,5-C$_{aroma.}$*H* py), 6.97 – 7.05 (m, 6H, C$_{aroma.}$*H* Ph), 7.22 – 7.29 (m, 3H, C$_{aroma.}$*H* Ph and 4-C$_{aroma.}$*H* py), 7.33 – 7.39 (m, 2H, C$_{aroma.}$*H* Ph).

(400.13 MHz, C_7D_8, 298K): δ(ppm) = 1.06 (s, 18H, NC(CH_3)$_3$), 1.23 (d, $^2J_{H–P}$ = 5.33 Hz, 9H, P^A(CH_3)$_3$), 1.46 (s, 18H, NC(CH_3)$_3$), 1.56 (t, $^3J_{H–H}$ = 7.0 Hz, 6H, NCH'H-CH_3), 1.73 (d, $^2J_{H–P}$ = 7.0 Hz, 9H, P^B(CH_3)$_3$), 3.73 (dq with roof effect, $^2J_{H–H}$ = 14.0 Hz, $^3J_{H–H}$ = 7.0 Hz, 2H, NCH'*H*-CH$_3$), 3.93 (dq with roof effect, $^2J_{H–H}$ = 14.0 Hz, $^3J_{H–H}$ = 7.0 Hz, 2H, NC*H*'HCH$_3$), 5.93 (d, $^3J_{H–H}$ = 7.9 Hz, 2H, 3,5-C$_{aroma.}$*H* py), 7.16 (t, $^3J_{H–H}$ = 7.9 Hz, 1H, 4-C$_{aroma.}$*H* py), 7.03 – 7.08 (m, 6H, C$_{aroma.}$*H* Ph), 7.27 – 7.32 (m, 2H, C$_{aroma.}$*H* Ph), 7.35 – 7.40 (m, 2H, C$_{aroma.}$*H* Ph).

^{13}C{^{1}H} NMR: (100.61 MHz, C_7D_8, 298K): δ(ppm) = 16.0 (NCH$_2$*C*H$_3$), 25.4 (d, $^1J_{C–P}$ = 14.4 Hz, P^A(*C*H$_3$)$_3$), 32.9 (NC(*C*H$_3$)$_3$), 33.3 (dd, $^1J_{C–P}$ = 15.9 Hz, $^3J_{C–P}$ = 3.7 Hz, P^B(*C*H$_3$)$_3$), 33.4 (NC(*C*H$_3$)$_3$), 40.5 (N*C*H$_2$CH$_3$), 53.7 (N*C*(CH$_3$)$_3$), 91.7 (d, $^4J_{C–P}$ = 1.4 Hz, 3,5-*C*$_{aroma.}$H py), 127.3 (*C*$_{aroma.}$H Ph), 127.5 (*C*$_{aroma.}$H Ph), 128.4 (d, $^5J_{C–P}$ = 3.3 Hz, 4-

$C_{aroma.}$H py), 130.6 ($C_{aroma.}$H Ph),, 137.0 ($C_{aroma.}$ quaternary Ph), 164.1 (d, $^3J_{C-P}$ = 2.1 Hz, 2,6- $C_{aroma.}$H py), 169.0 (N*C*N).

$^{31}P\{^1H\}$ NMR: (161.97 MHz, C_7D_8, 298K): δ(ppm) = 10.2 (d, $^2J_{P-P}$ = 20.8 Hz, $P^A(CH_3)_3$), 27.2 (d, $^2J_{P-P}$ = 20.8 Hz, $P^B(CH_3)_3$).

^{57}Fe Mössbauer: at 77K (Zero field): δ = 0.36(1) mm s^{-1}, ΔE_Q = 1.87(1) mm s^{-1}, Γ_{FWHM} = 0.35(1) mm s^{-1}.

APCI-MS : (m/z) Calcd for [$(C_{45}H_{77}FeGe2N_7P_2 - 2PMe_3)^{\bullet+}$]: 827.26139. Found 827.26380 (correct isotope pattern).

5.4.25. Iron(0) complex [SiNSi]Fe(CO)$_2$

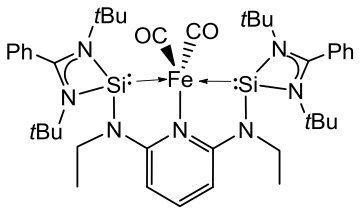

A solution of **[SiNSi]Fe(PMe$_3$)$_2$** (79 mg, 0.089 mmol) in 20 mL of pentane was set up under CO atmosphere after 3 freeze-pump thaw cycles. The reaction mixture was stirred overnight affording an orange solid in suspension with an orange solution. The solid was filtered off by cannula and dried *in vacuo* affording a first crop of the desired product in high purity (40 mg). Concentration, crystallization, filtration and drying in *vacuo* of the remaining solution in pentane afforded the second crop of the product (20 mg) for a total yield of 60 mg of the product (85% yield).

^{1}H NMR: (400.13 MHz, C_6D_6, 298K): δ(ppm) = 1.39 (s, 36H, NC(CH_3)$_3$), 1.39 (t, overlapping with singlet at 1.39 ppm, 6H, NCH_2CH_3), 3.52 (q, $^3J_{H-H}$ = 7.1 Hz, 4H, NCH_2CH_3), 6.18 (d, $^3J_{H-H}$ = 8.0 Hz, 2H, 3,5-$C_{aroma.}$H py), 6.81 – 7.06 (m, 10H, $C_{aroma.}$H Ph), 7.31 (t, $^3J_{H-H}$ = 8.0 Hz, 1H, 4-$C_{aroma.}$H py).

$^{13}C\{^1H\}$ NMR: (100.61 MHz, C_6D_6, 298K): δ(ppm) = 15.2 (NCH_2CH_3), 31.1 (NC(CH_3)$_3$), 38.9 (NCH_2CH_3), 54.6 (NC(CH_3)$_3$), 95.8 (3,5-$C_{aroma.}$H py), 127.3 ($C_{aroma.}$H Ph), 129.7 ($C_{aroma.}$H Ph), 129.7 ($C_{aroma.}$H Ph),

130.9 (4-$C_{aroma.}$H py), 132.4 ($C_{aroma.}$ quaternary Ph), 165.0 (2,6-$C_{aroma.}$ py), 172.3 (N*C*N), 222.0 (*C*O).

^{29}Si{^{1}H} NMR: (79.49 MHz, C_6D_6, 298K): δ(ppm) = 98.3.

IR: (KBr pellet): ν_{CO}(cm^{-1}) = 1830, 1778.

APCI-MS : (m/z) Calcd for [$C_{41}H_{59}FeN_7O_2Si_2^{\bullet+}$]: 793.36127. Found 793.36353 (correct isotope pattern).

5.4.26. Iron(0) complex [GeNGe]Fe(CO)$_2$

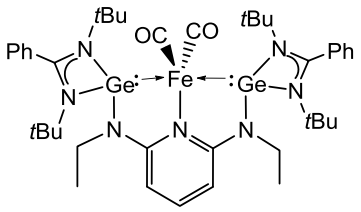

The synthesis of these complexes was carried out in a fashion similar to the synthesis of [SiNSi]Fe(CO)$_2$ described previously. At 0.11 mmol scale. ***[GeNGe]Fe(CO)$_2$*** 39% yield.

^{1}H NMR: (400.13 MHz, C_6D_6, 298K): δ(ppm) = 1.26 (s, 36H, NC(C*H*$_3$)$_3$), 1.39 (t, $^{3}J_{H–H}$ = 6.8 Hz, 6H, NCH$_2$C*H*$_3$), 3.71 (q, $^{3}J_{H–H}$ = 6.8 Hz, 4H, NC*H*$_2$CH$_3$), 6.24 (d, $^{3}J_{H–H}$ = 8.0 Hz, 2H, 3,5-C$_{aroma.}$*H* py), 6.86 – 7.05 (m, 10H, C$_{aroma.}$*H* Ph), 7.34 (t, $^{3}J_{H–H}$ = 8.0 Hz, 1H, 4-C$_{aroma.}$*H* py).

^{13}C{^{1}H} NMR: (100.61 MHz, C_6D_6, 298K): δ(ppm) = 15.5 (NCH$_2$*C*H$_3$), 31.4 (NC(*C*H$_3$)$_3$), 40.5 (N*C*H$_2$CH$_3$), 54.8 (N*C*(CH$_3$)$_3$), 94.9 (3,5-$C_{aroma.}$H py), 127.3 ($C_{aroma.}$H Ph), 129.4 ($C_{aroma.}$H Ph), 129.7 ($C_{aroma.}$H Ph), 132.1 (4-$C_{aroma.}$H py), 133.7 ($C_{aroma.}$ quaternary Ph), 162.8 (2,6-$C_{aroma.}$H py), 172.0 (N*C*N), 220.6 (*C*O).

IR: (KBr pellet) ν_{CO}(cm^{-1}) = 1855, 1805.

ESI-MS: (m/z) Calcd for [$C_{41}H_{59}FeGe_2N_7O_2^{\bullet+}$]: 883.25067. Found 883.25446 (correct isotope pattern).

5.4.27. Iron(II) complexes of type [SiNSi]FeH(SiR$_3$)(PMe$_3$) (SiR$_3$ = Si(OEt)$_3$, SiMe$_2$Ph, SiMePh$_2$)

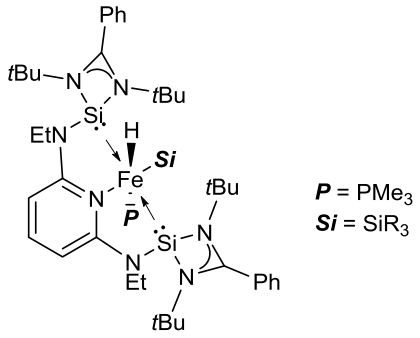

General procedure: Complex **[SiNSi]Fe(PMe$_3$)$_2$** was weighed (44.5 mg, 50.0 µmol, 1 equiv) in a Schlenk flask with a magnetic stirrer. The hydrosilane (0.15 mmol, 3 equiv) was weighed in a vial and dissolved in 2.0 mL of toluene (0.5 mL of C_6D_6 for NMR studies) and added into the Schlenk flask. The reaction mixture was heated in an oil bath at 70 °C changing the color from dark purple to dark red. The time for completion (100% conversion by NMR) varied depending on the silane used: $(EtO)_3SiH$ 12 h, Me_2PhSiH 6 days, and $MePh_2SiH$ reached 90% conversion after 6 days. The reaction mixture was concentrated and the product was obtained as a crude red oil. The crude product was redissolved in C_6H_6 and cold sublimation of the solvent *in vacuo* afforded the desired product as a red powder.

***Si* = (EtO)$_3$Si:** [SiNSi]FeH(Si(EtO)$_3$)PMe$_3$

^{1}H NMR: (500 MHz, C_6D_6, 298 K): δ(ppm) = –14.84 (d, $^2J_{H\text{-}P}$ = 3.4 Hz, $^2J_{H\text{-}Si}$ = 19.3 Hz, 1H, Fe–H), 1.18 (s, 18H, NC(C*H*$_3$)$_3$), 1.40 (t, $^3J_{H\text{-}H}$ = 7.0 Hz, 6H, NCH'H-C*H*$_3$), 1.46 (s, 18H, NC(C*H*$_3$)$_3$), 1.48 (d, $^2J_{H\text{-}P}$ = 6.5 Hz, 9H, P(C*H*$_3$)$_3$), 1.57 (t, $^3J_{H\text{-}H}$ = 7.0 Hz, 9H, SiOCH$_2$C*H*$_3$), 3.37 (dq, $^2J_{H\text{-}H}$ = 14.0 Hz, $^3J_{H\text{-}H}$ = 7.0 Hz, 2H, NCH'*H*–CH$_3$), 3.56 (dq, $^2J_{H\text{-}H}$ = 14.0 Hz, $^3J_{H\text{-}H}$ = 7.0 Hz, 2H, NC*H*'H–CH$_3$), 4.32 (q, $^3J_{H\text{-}H}$ = 7.0 Hz, 6H, SiOC*H*$_2$CH$_3$), 5.90 (d, $^3J_{H\text{-}H}$ = 8.0 Hz, 2H, 3,5-H py), 6.96-7.08 (m, 6H, C$_{arom.}$*H*), 7.24 (t, $^3J_{H\text{-}H}$ = 8.0 Hz, 1H, 4-H py), 7.22 (d, $^3J_{H\text{-}H}$ = 7.4 Hz, 2H, C$_{arom.}$*H*), 7.72 (d, $^3J_{H\text{-}H}$ = 7.4 Hz, 2H, C$_{arom.}$*H*).

^{13}C{^{1}H} NMR: (126 MHz, C_6D_6, 298 K): δ(ppm) = 15.3 (NCH$_2$–*C*H$_3$), 19.8 (SiOCH$_2$*C*H$_3$), 25.9 (d, $^1J_{C\text{-}P}$ = 18.2 Hz, P(*C*H$_3$)$_3$), 31.9

(NC(CH_3)$_3$), 32.6 (NC(CH_3)$_3$), 38.9 (NCH_2-CH_3), 53.7 (NC(CH$_3$)$_3$), 54.1 (NC(CH$_3$)$_3$), 56.9 (SiOCH_2CH$_3$), 94.2 (3,5-C$_{arom.}$ py), 127.1(C$_{arom.}$), 128.5 (C$_{arom.}$), 129.0 (C$_{arom.}$), 129.7 (C$_{arom.}$), 131.0 (4-C$_{arom.}$ py), 132.7 (C$_{arom.}$ quaternary Ph), 133.9 (C$_{arom.}$), 168.1 (2,6-C$_{arom.}$ py), 171.7 (NCN).

^{29}Si{^{1}H} NMR (80 MHz, C_6D_6, 298 K): δ(ppm) = 33.7 (d, $^{2}J_{Si-P}$ = 58.8 Hz, Si(OEt)$_3$), 79.2 (d, $^{2}J_{Si-P}$ = 24.3 Hz, Si:→Fe)

^{31}P{^{1}H} NMR (202 MHz, C_6D_6, 298 K): δ(ppm) = 16.8.

***Si* = Me$_2$PhSi:** [SiNSi]FeH(SiMe$_2$Ph)PMe$_3$

^{1}H NMR: (500 MHz, C_6D_6, 298 K): δ(ppm) = –13.95 (br s, 1H, Fe–H), 1.06 (s, 18H, NC(CH^{A}_3)$_3$), 1.08 (s, 6H, Si(CH_3)$_2$Ph), 1.28 (s, 18H, NC(CH^{B}_3)$_3$), 1.38 (t, $^{3}J_{H-H}$ = 7.0 Hz, 6H, NCH'H-CH_3), 1.44 (d, $^{2}J_{H-P}$ = 6.3 Hz, 9H, P(CH_3)$_3$), 3.33 (dq, $^{2}J_{H-H}$ = 13.2 Hz, $^{3}J_{H-H}$ = 6.6 Hz, 2H, NCH'H-CH$_3$), 3.57 (dq, $^{2}J_{H-H}$ = 13.2 Hz, $^{3}J_{H-H}$ = 6.6 Hz, 2H, NCH'H-CH$_3$), 5.90 (d, $^{3}J_{H-H}$ = 7.6 Hz, 2H, 3,5-H py), 6.93-7.02 (m, 8H, C$_{arom.}H$), 7.24 (t, $^{3}J_{H-H}$ = 7.6 Hz, 1H, 4-H py), 7.33 (t, $^{3}J_{H-H}$ = 7.1 Hz, 1H, 3-C$_{arom.}H$ SiPh), 7.45 (m, 1H, C$_{arom.}H$ SiPh), 7.50 (m, 2H, C$_{arom.}H$ SiPh), 7.76 (m, 2H, C$_{arom.}H$ Ph). 8.57 (d, $^{3}J_{H-H}$ = 7.1 Hz, 1H, 2-C$_{arom.}H$ SiPh).

^{13}C{^{1}H} NMR: (126 MHz, C_6D_6, 298 K): δ(ppm) = 15.1 (NCH$_2$-CH_3), 16.3 (Si(CH_3)$_2$), 25.7 (d, $^{1}J_{C-P}$ = 16.5 Hz, P(CH_3)$_3$), 31.7 (NC(CH^{A}_3)$_3$), 32.5 (NC(CH^{B}_3)$_3$), 38.8 (NCH$_2$-CH$_3$), 53.6 (NC(CH$^{B}_3$)$_3$), 54.0 (NC(CH$^{A}_3$)$_3$), 94.3 (3,5-C$_{arom.}$ py), 125.0 (C$_{arom.}$ SiPh), 126.0 (C$_{arom.}$), 126.1 (C$_{arom.}$ SiPh), 126.9 (C$_{arom}$), 128.4 (C$_{arom}$), 128.6 (C$_{arom.}$), 129.6 (C$_{arom.}$), 130.9 (C$_{arom.}$), 132.8 (4-C$_{arom.}$ py), 133.3 (C$_{arom.}$), 134.3 (C$_{arom.}$), 136.4 (o-C$_{arom.}$ SiPh), 160.5 (C$_{arom.}$ quaternary SiPh) 168.3 (2,6-C$_{arom.}$ py), 171.8 (NCN).

^{29}Si NMR, ^{1}H-^{29}Si (500 MHz / 99 MHz, C_6D_6, 298 K): δ(ppm) = 31.1 (SiMe$_2$Ph), 77.2

HMQC NMR: (Si:→Fe).

$^{31}P\{^{1}H\}$ NMR (202 MHz, C_6D_6, 298 K): δ(ppm) = 14.7.

IR: (KBr pellet) ν_{Fe-H} (cm^{-1}) = 2020.

ESI-MS: (m/z) Calcd for $[C_{50}H_{79}FeN_7PSi_3^+]$ $(M - H)^+$ 948.47863; found 948.54423.

***Si* = MePh$_2$Si:** [SiNSi]FeH(SiMePh$_2$)PMe$_3$

^{1}H NMR: (500 MHz, C_6D_6, 298 K): δ(ppm) = –13.69 (br s, 1H, Fe–H), 1.06 (s, 18H, NC(CH^A_3)$_3$), 1.24 (s, 18H, NC(CH^B_3)$_3$), 1.34 (m, 6H, NCH'H-CH_3), 1.36 (m, 9H, P(CH_3)$_3$), 1.37 (m, 3H, SiCH_3Ph$_2$), 3.33 (dq, $^2J_{H-H}$ = 13.0 Hz, $^3J_{H-H}$ = 6.0 Hz, 2H, NCH'*H*-CH_3), 3.56 (dq, $^2J_{H-H}$ = 13.0 Hz, $^3J_{H-H}$ = 6.5 Hz, 2H, NC*H'*H-CH_3), 5.86 (d, $^3J_{H-H}$ = 7.8 Hz, 2H, 3-5-H py), 6.90-7.05 (m, 10H, $C_{arom.}H$), 7.24 (t, $^3J_{H-H}$ = 7.8 Hz, 1H, 4-H py), 7.34 (t, $^3J_{H-H}$ = 7.2 Hz, 4H, 3-$C_{arom.}H$ SiPh), 7.71 (d, $^3J_{H-H}$ = 6.7 Hz, 2H, $C_{arom}H$ SiPh). 8.22 (d, $^3J_{H-H}$ = 6.7 Hz, 4H, 2-$C_{arom.}H$ SiPh).

$^{13}C\{^{1}H\}$ NMR: (126 MHz, C_6D_6, 298 K): δ(ppm) = 15.0 (NCH$_2$-*C*H$_3$), 25.8 (d, $^1J_{C-P}$ = 16.7 Hz, P(*C*H$_3$)$_3$), 29.2 (Si*C*H$_3$Ph$_2$), 31.7 (NC(*C*H$^A_3$)$_3$), 32.4 (NC(*C*H$^B_3$)$_3$), 38.7 (N*C*H$_2$-CH$_3$), 53.7 (N*C*(CH$^B_3$)$_3$), 54.1 (N*C*(CH$^A_3$)$_3$), 94.3 (3,5-$C_{arom.}$ py), 125.0 ($C_{arom.}$ Si*Ph*), 126.2 ($C_{arom.}$ SiPh), 126.8 ($C_{arom.}$), 128.3 ($C_{arom.}$), 129.1 (2×$C_{arom.}$ Si*Ph*), 129.8 ($C_{arom.}$), 130.7 (4-$C_{arom.}$ py), 133.2 ($C_{arom.}$), 135,6 ($C_{arom.}$), 136.4 (o-C_{arom} Si*Ph*), 137.2 ($C_{arom.}$), 159.8 ($C_{arom.}$ quaternary Si*Ph*), 168.5 (2,6-$C_{arom.}$ py), 172.3 (N*C*N).

^{29}Si NMR, ^{1}H-^{29}Si HMQC NMR: (500 MHz / 99 MHz, C_6D_6, 298 K): δ(ppm) = 34.4 (SiMePh$_2$), 76.3 (Si:→Fe).

$^{31}P\{^{1}H\}$ NMR: 202 MHz, C_6D_6, 298 K): δ(ppm) = 16.8.

5.5. Catalytic evaluations and stoichiometric reactions

5.5.1. Borylation of arenes catalyzed by the iridium complexes

*General procedure with the ligand systems **SiCHSi** and **GeCHGe***: In a nitrogen filled drybox, 5.0 mg (5.6 mmol) of $[IrCl(coe)_2]_2$ and 2.1 eq (11.7 mmol) of the ligand were weighed in a 1.5 mL screw cap vial containing a stir bar, dissolved in 0.3 mL of the arene substrate and stirred for 15 minutes. Pinacolborane (HBPin, 28.6 mg, 223.2 mmol) in 0.2 mL of the arene substrate (from a freshly prepared stock solution) were added to the mixture. When an additional equivalent cyclooctene was used, 29.1 mL of COE (24.6 mg, 223.2 mmol) were added via syringe. The vial was closed, removed from the glovebox, and stirred at 100 °C for 24 h. After cooling, all volatile materials were evaporated *in vacuo*. The yields and product distributions were determined by redissolving the crude product in $CDCl_3$ and analyzed by ^1H NMR. CH_2Br_2 (NMR) or dodecane (GC-MS) were used as internal standards depending the evaluation method. A defined amount of dodecane as internal standard was added to the reaction mixture before heating following the kinetics of the reaction by small aliquots analyzed by GC-MS. Aliquots for monitoring the reactions were removed from the vials in a nitrogen filled drybox after cooling.

*General procedure using ligand system **tBu-PCHP***: Same general method as for ligands **SiCHSi** and **GeCHGe**, but the generation of the complex [***t*Bu-PCP]IrHCl** a heating at 100 °C for 45 min was required prior addition of HBPin (time checked by NMR in the synthesis and isolation of [t**Bu-PCP]IrHCl**).

*General procedure using ligand system **iPrN-PCHP***: The *in-situ* preparation of complex [***i*PrN-PCP]IrHCl(coe)** from $[IrCl(coe)_2]_2$ and 2 equiv of ***i*PrN-PCP** was unfruitful at room temperature. Therefore, isolated and purified [***i*PrN-PCP]IrHCl(coe)** was used as catalyst. The same general method was followed as for ligands **SiCHSi** and **GeCHGe**, but 10.1 mg of isolated [***i*PrN-PCP]IrHCl(coe)** were used as precatalyst.

5.5.2. Sonogashira cross-coupling reaction catalyzed by the nickel complexes

General procedure for catalytic evaluation. In a nitrogen filled drybox, **[ECE]NiBr** (5 mol %; 11.4 μmol), CuI (1.1 mg, 5 mol %; 11.4 μmol), Cs_2CO_3 (74.0 mg, 228.0 μmol), phenylacetylene (11.6 mg, 114 μmol) and (*E*)-1-iodooct-1-ene (1-5 equiv) were weighed in a 4.0 mL screw cap vial containing a stirring bar, and dissolved in 1.5 mL of 1,4-dioxane. The sealed vial was removed from the drybox and heated at 100 °C for 24 h. After cooling, the mixture was filtered through short plug of silica and all volatile were evaporated *in vacuo*. The yields of the products were determined by redissolving the crude product in $CDCl_3$ and adding a defined amount of CH_2Br_2 as internal reference; and/or by addition of a defined amount of dodecane as internal standard to the reaction mixture before heating and taking small aliquots for analysis by GC-MS.

Stoichiometric reactions with copper acetylides. In a nitrogen filled drybox, **[ECE]NiBr** (E = Si^{II}, Ge^{II}; 0.02 – 0.07 mmol), [Cu–C≡C–Ph–R]$_4$ (R = H, 3,5-$(CF_3)_2$, 4-OCH_3, 2,6-Ph_2; 0.03 – 0.09 mmol) were weighed in a Schlenk flask or in a capped vial containing a stirring bar and dissolved in the appropriate solvent (toluene or C_6D_6). The sluggish reaction mixture was stirred for 4 h and filtered through a short plug of Celite. Suitable crystals of **{[SiCSi]Ni–C≡C–Ph→CuBr}** for XRD structure analysis were grown at –78 °C after several micro filtrations in a solvent mixture *n*-pentane/toluene (1:1). For the complex **{[GeCGe]Ni–C≡C–*ter*Ph→CuBr}** suitable the crystals were grown layering *n*-pentane on the toluene solution at room temperature.

Catalytic behavior under stoichiometric scale. The **[Cu–C≡C–3,5-$(CF_3)_2C_6H_3$]$_4$** (31 μmol) was added to a solution of **[SiCSi]NiBr** (23 μmol) in C_6D_6. After microfiltration, a solution of (*E*)-1-iodo-1-octene (60 μmol) was added to the NMR tube and the system was heated at 50 °C for 1 h. The resulting solution was treated again with more **[Cu–C≡C–3,5-$(CF_3)_2C_6H_3$]$_4$** to continue the catalytic cycle proceeding as explain above. The reaction mixture was evaluated by ^{1}H NMR in every single step observing the cyclic behaviour.

5.5.3. Hydrosilylation of ketones catalyzed by the iron complexes

A Schlenk flask equipped with a magnetic stirrer was charged with solution of ketone (0.10 mmol, 1.0 equiv), silane **4**, and iron(0) complex **2** in solvent (2 mL). The mixture was stirred at indicated temperature for 22 h. The reaction was quenched with 2 mL of a KOH solution (5% in H_2O). The reaction mixture was stirred for 2 h at room temperature and was extracted with diethyl ether (3 × 5.0 mL). The combined organic layers were dried over Na_2SO_4 and filtered. Anisole (internal standard) was added and an aliquot was taken for GC-MS analysis.

Substrate scope. According to the procedure described above various ketones (0.10 mmol, 1.0 equiv) were hydrosilylated with triethoxysilane (25 mg, 0.15 mmol, 1.5 equiv) and iron(0) complex **[SiNSi]Fe(PMe$_3$)$_2$** (2.2 mg, 2.5 μmol, 2.5 mol %).

Removal of diethyl ether and dissolution in $CDCl_3$ permitted the control also by NMR. The NMR of the corresponding products were in accordance with the already reported alcohols in the corresponding references (Table 3.3.5).

6. REFERENCES

(1) a) Moulton, C. J.; Shaw, B. L. *J. Chem. Soc., Dalton Trans.* **1976**, 1020–1024; b) Empsall, D.; Hyde, E. M.; Markham, R.; McDonald, W. S.; Norton, M. C.; Shaw, B. L.; Weeks, B. *J. Chem. Soc., Chem. Commun.* **1977**, 589–590; c) Crocker, C.; Errington, R. J.; McDonald, W. S.; Odell, K. J.; Shaw, B. L. *J. Chem. Soc., Chem. Commun.* **1979**, 498–499; d) Crocker, C.; Errington, R. J.; Markham, R.; Moulton, C. J.; Odell, K. J.; Shaw, B. L. *J. Am. Chem. Soc.* **1980**, *102,* 4373–4379; e) Errington, J.; McDonald, W. S.; Shaw, B. L. *J. Chem. Soc., Dalton Trans.* **1982**, 1829–1835; f) Errington, R.; Shaw, B. L. *J. Organomet. Chem.* **1982**, *238*, 319–325; g) Crocker, C.; Empsall, H. D.; Errington, R. J.; Hyde, E. M.; McDonald, W. S.; Markham, R.; Norton, M. C.; Shaw, B. L.; Weeks, B. *J. Chem. Soc., Dalton Trans.* **1982**, 1217–1224.

(2) Meltzer, A.; Präsang, C.; Driess, M. *J. Am. Chem. Soc.* **2009**, *131*, 7232–7233.

(3) Blom, B.; Stoelzel, M.; Driess, M. *Chem. Eur. J.* **2013**, *19*, 40–62.

(4) Benedek, Z.; Szilvási, T. *RSC Adv*. **2015**, *5*, 5077–5086.

(5) van Koten, G. *Pure Appl. Chem.* **1989**, *61,* 1681–1694.

(6) Albrecht, M.; van Koten, G. *Angew. Chem. Int. Ed.* **2001**, *49,* 3750–3781.

(7) Morales-Morales, D.; Jensen, C. M., Eds. *The Chemistry of Pincer Compounds;* Elsevier: Amsterdam, **2007**.

(8) van Koten, G.; Milstein, D.; Eds. *Organometallic Pincer Chemistry.* Series Topics in Organometallic Chemistry, *40*, Springer, **2013**.

(9) Choi, J.; MacArthur, A. H. Roy; Brookhart, M.; Goldman, A. S. *Chem. Rev.* **2011**, *111*, 1761–1779.

(10) a) Dedieu, A.; Strich, A. *Inorg. Chem.* **1979**, *18,* 2940–2943; b) Silvestre, J.; Hoffmann, R. *Helv. Chim. Acta*. **1985**, *68,* 1461–1506.

(11) van der Boom, M. E.; Milstein, D. *Chem. Rev.* **2003**, *103*, 1759–1792.

(12) Zhao, J.; Goldman, A. S.; Hartwig, J. F. *Science* **2005**, *307*, 1080–1082.

(13) Bernskoetter, W. H.; Schauer, C. K.; Goldberg, K. I.; Brookhart, M. *Science* **2009**, *326*, 553–556.

(14) Gupta, M.; Hagen, C.; Flesher, R. J.; Kaska, W. C.; Jensen, C. M. *Chem. Commun.* **1996**, 2083–2084.

(15) Langer, R.; Diskin-Posner, Y.; Leitus, G.; Shimon, L. J. W.; Ben-David, Y.; Milstein, D. *Angew. Chem. Int. Ed.* **2011**, *50*, 9948–9952.

(16) Bart, S. C.; Lobkovsky, E.; Chirik, P. J. *J. Am. Chem. Soc.* **2004**, *126*, 13794–13807.

(17) Bart, S. C.; Chłopek, K.; Bill, E.; Bouwkamp, M. W.; Lobkovsky, E.; Neese, F.; Wieghardt, K.; Chirik, P. J. *J. Am. Chem. Soc.* **2006**, *128*, 13901–13912.

(18) Knijnenburg, Q.; Gambarotta, S.; Budzelaar, P. H. M. *Dalton Trans.* **2006**, 5442–5448.

(19) a) Gibson, V. C.; Redshaw, C.; Solan, G. A. *Chem. Rev.* **2007**, *107*, 1745–1776; b) Bullock, R. M.; Ed. *Catalysis Without Precious Metals;* Wiley-VCH Verlag & Co. KGaA: Weinheim, Germany, **2010**.
(20) a) Wang, Z.-X.; Liu, N. *Eur. J. Inorg. Chem.* **2012**, *2012*, 901–911; b) Hu, X. *Chem. Sci.* **2011**, *2*, 1867–1886.
(21) Anderson, T. J.; Jones, G. D.; Vicic, D. A. *J. Am. Chem. Soc.* **2004**, *126*, 8100–8101.
(22) Zhou, J.; Fu, G. C. *J. Am. Chem. Soc.* **2003**, *125*, 14726–14727.
(23) a) Csok, Z.; Vechorkin, O.; Harkins, S. B.; Scopelliti, R.; Hu, X. *J. Am. Chem. Soc.* **2008**, *130*, 8156–8157; b) Vechorkin, O.; Csok, Z.; Scopelliti, R.; Hu, X. *Chem. Eur. J.* **2009**, *15*, 3889–3899; c) Vechorkin, O.; Hu, X. *Angew. Chem., Int. Ed.* **2009**, *48*, 2937–2940; d) Vechorkin, O.; Proust, V.; Hu, X. *J. Am. Chem. Soc.* **2009**, *131*, 9756–9766; e) Ren, P.; Vechorkin, O.; Allmen, K. v.; Scopelliti, R.; Hu, X. *J. Am. Chem. Soc.* **2011**, *133*, 7084–7095; f) Perez-Garcia, P. M.; Di Franco, T.; Orsino, A.; Ren, P.; Hu, X. *Org. Lett.* **2012**, *14*, 4286–4289.
(24) Vechorkin, O.; Godinat, A.; Scopelliti, R.; Hu, X. *Angew. Chem., Int. Ed.* **2011**, *50*, 11777–11781.
(25) Inamoto, K.; Kuroda, J.-i.; Kwon, E.; Hiroya, K.; Doi, T. *J. Organomet. Chem.* **2009**, *694*, 389–396.
(26) a) Vechorkin, O.; Barmaz, D.; Proust, V.; Hu, X. *J. Am. Chem. Soc.* **2009**, *131*, 12078–12079; b) Vechorkin, O.; Proust, V.; Hu, X. *Angew. Chem., Int. Ed.* **2010**, *49*, 3061–3064;
(27) Herrmann, W. A. *Angew. Chem., Int. Ed.* **2002**, *41,* 1290–1309.
(28) Nair, V.; Bindu, S.; Sreekumar, V. *Angew. Chem., Int. Ed.* **2004**, *43*, 5130–5135.
(29) Lin, J. C. Y.; Huang, R. T. W.; Lee, C. S.; Bhattacharyya, A.; Hwang, W. S.; Lin, I. J. B. *Chem. Rev.* **2009**, *109*, 3561–3598.
(30) Díez-González, S.; Marion, N.; Nolan, S. P. *Chem. Rev.* **2009**, *109*, 3612–3676.
(31) Poyatos, M.; Mata, J. A.; Peris, E. *Chem. Rev.* **2009**, *109*, 3677–3707.
(32) Mizuhata, Y.; Sasamori, T.; Tokitoh, N. *Chem. Rev.* **2009**, *109*, 3479–3511.
(33) Asay, M.; Jones, C.; Driess, M. *Chem. Rev.* **2011**, *111*, 354–396.
(34) Bourissou, D.; Guerret, O.; Gabbaï, F. P.; Bertrand, G. *Chem. Rev.* **2000**, *100*, 39–92.
(35) a) Drahnak, T. J.; Michl, J.; West, R. *J. Am. Chem. Soc.* **1979**, *101,* 5427–5428; b) West, R. *Angew. Chem., Int. Ed. Engl.* **1987**, *26,* 1201–1211; c) Karsch, H. H.; Keller, U.; Gamper, S.; Müller, G. *Angew. Chem., Int. Ed. Engl.* **1990**, *29,* 295–296;
(36) Jutzi, P.; Kanne, D.; Krüger, C. *Angew. Chem., Int. Ed. Engl.* **1986**, *25,* 164.
(37) Fischer, E. O.; Grubert, H. *Z. anorg. allg. Chem.* **1956**, *286,* 237–242.
(38) Arduengo, A. J. III.; Harlow, R. L.; Kline, M. *J. Am. Chem. Soc.* **1991**, *113,* 361–363.

(39) Denk, M.; Lennon, R.; Hayashi, R.; West, R.; Belyakov, A. V.; Verne, H. P.; Haaland, A.; Wagner, M.; Metzler, N. *J. Am. Chem. Soc.* **1994**, *116,* 2691–2692.
(40) Nolan, S. P. *N-Heterocyclic Carbenes in Synthesis;* Wiley-VCH Verlag & Co. KGaA: Weinheim, Germany, **2006**.
(41) Herrmann, W. A.; Denk, M.; Behm, J.; Scherer, W.; Klingan, F.-R.; Bock, H.; Solouki, B.; Wagner, M. *Angew. Chem., Int. Ed. Engl.* **1992**, *31,* 1485–1488.
(42) Gans-Eichler, T.; Gudat, D.; Nieger, M. *Angew. Chem., Int. Ed.* **2002**, *41,* 1888–1891.
(43) Charmant, J. P. H.; Haddow, M. F.; Hahn, F. E.; Heitmann, D.; Fröhlich, R.; Mansell, S. M.; Russell, C. A.; Wass, D. F. *Dalton Trans.* **2008**, 6055–6059.
(44) Kira, M.; Ishida, S.; Iwamoto, T.; Kabuto, C. *J. Am. Chem. Soc.* **1999**, *121*), 9722–9723.
(45) Nagendran, S.; Roesky, H. W. *Organometallics* **2008**, *27*, 457–492.
(46) Lemierre, V.; Chrostowska, A.; Dargelos, A.; Baylere, P.; Leigh, W. J.; Harrington, C. R. *Appl. Organometal. Chem.* **2004**, *18*, 676–683.
(47) Ghadwal, R. S.; Roesky, H. W.; Merkel, S.; Henn, J.; Stalke, D. *Angew. Chem., Int. Ed.* **2009**, *48*, 5683–5686.
(48) Filippou, A. C.; Chernov, O.; Schnakenburg, G. *Angew. Chem., Int. Ed.* **2009**, *48*, 5687–5690.
(49) So, C.-W.; Roesky, H. W.; Magull, J.; Oswald, R. B. *Angew. Chem., Int. Ed.* **2006**, *45*, 3948–3950.
(50) Sen, S. S.; Roesky, H. W.; Stern, D.; Henn, J.; Stalke, D. *J. Am. Chem. Soc.* **2010**, *132*, 1123–1126.
(51) Nagendran, S.; Sen, S. S.; Roesky, H. W.; Koley, D.; Grubmüller, H.; Pal, A.; Herbst-Irmer, R. *Organometallics* **2008**, *27*, 5459–5463.
(52) Haaf, M.; Schmedake, T. A.; West, R. *Acc. Chem. Res.* **2000**, *33*, 704–714.
(53) Yao, S.; Xiong, Y.; Driess, M. *Organometallics* **2011**, *30*, 1748–1767.
(54) Xiong, Y.; Yao, S.; Brym, M.; Driess, M. *Angew. Chem., Int. Ed.* **2007**, *46*, 4511–4513.
(55) Metzler, N.; Denk, M. *Chem. Commun.* **1996**, 2657–2658.
(56) Driess, M.; Yao, S.; Brym, M.; van Wüllen, C. *Angew. Chem., Int. Ed.* **2006**, *45*, 6730–6733.
(57) Ding, Y.; Hao, H.; Roesky, H. W.; Noltemeyer, M.; Schmidt, H.-G. *Organometallics* **2001**, *20*, 4806–4811.
(58) Haaf, M.; Schmiedl, A.; Schmedake, T. A.; Powell, D. R.; Millevolte, A. J.; Denk, M.; West, R. *J. Am. Chem. Soc.* **1998**, *120*, 12714–12719.
(59) Yao, S.; Brym, M.; van Wüllen, C.; Driess, M. *Angew. Chem., Int. Ed.* **2007**, *46*, 4159–4162.
(60) a) Jana, A.; Schulzke, C.; Roesky, H. W. *J. Am. Chem. Soc.* **2009**, *131*, 4600–4601; b) Präsang, C.; Stoelzel, M.; Inoue, S.; Meltzer, A.; Driess, M. *Angew. Chem., Int. Ed.* **2010**, *49*, 10002–10005.

(61) Xiong, Y.; Yao, S.; Driess, M. *Chem. Eur. J.* **2009**, *15*, 5545–5551.
(62) Yao, S.; van Wüllen, C.; Sun, X.-Y.; Driess, M. *Angew. Chem., Int. Ed.* **2008**, *47*, 3250–3253.
(63) Ghadwal, R. S.; Sen, S. S.; Roesky, H. W.; Granitzka, M.; Kratzert, D.; Merkel, S.; Stalke, D. *Angew. Chem. Int. Ed.* **2010**, *49*, 3952–3955.
(64) Petz, W. *Chem. Rev.* **1986**, *86,* 1019–1047.
(65) Baumgartner, J.; Marschner, C. *Rev. Inorg. Chem.* **2013**, *34,* 119–152.
(66) Blom, B.; Enthaler, S.; Inoue, S.; Irran, E.; Driess, M. *J. Am. Chem. Soc.* **2013**, *135*, 6703–6713.
(67) Tan, G.; Blom, B.; Gallego, D.; Driess, M. *Organometallics* **2014**, *33*, 363–369.
(68) Schäfer, S.; Köppe, R.; Gamer, M. T.; Roesky, P. W. *Chem. Commun.* **2014**, *50*, 11401–11405.
(69) Meltzer, A.; Inoue, S.; Präsang, C.; Driess, M. *J. Am. Chem. Soc.* **2010**, *132*, 3038–3046.
(70) Jones, C.; Rose, R. P.; Stasch, A. *Dalton Trans.* **2008**, 2871–2878.
(71) Cabeza, J. A.; García-Álvarez, P.; Polo, D. *Dalton Trans.* **2013**, *42*, 1329–1332.
(72) Sen, S. S.; Khan, S.; Nagendran, S.; Roesky, H. W. *Acc. Chem. Res.* **2012**, *45*, 578–587.
(73) Veith, M.; Lisowsky, R. *Angew. Chem., Int. Ed. Engl.* **1988**, *27,* 1087–1089.
(74) Hitchcock, P. B.; Lappert, M. F.; Thorne, A. J. *J. Chem. Soc., Chem. Commun.* **1990**, 1587–1589.
(75) Ahlemann, J.-T.; Roesky, H. W.; Murugavel, R.; Parisini, E.; Noltemeyer, M.; Schmidt, H.-G.; Müller, O.; Herbst-Irmer, R.; Markovskii, L. N.; Shermolovich, Y. G. *Chem. Ber.* **1997**, *130,* 1113–1121.
(76) Ghadwal, R. S.; Roesky, H. W.; Pröpper, K.; Dittrich, B.; Klein, S.; Frenking, G. *Angew. Chem., Int. Ed.* **2011**, *50*, 5374–5378.
(77) Chorley, R. W.; Hitchock, P. B.; Jolly, B. S.; Lappert, M. F.; Lawless, G. A. *J. Chem. Soc., Chem. Commun.* **1991**, 1302–1303.
(78) Avent, A. G.; Drost, C.; Gehrhus, B.; Hitchcock, P. B.; Lappert, M. F. *Z. anorg. allg. Chem.* **2004**, *630*, 2090–2096.
(79) Veith, M.; Rammo, A. *Z. anorg. allg. Chem.* **2001**, *627,* 662–668.
(80) Gehrhus, B.; Hitchcock, P. B.; Lappert, M. F. *Z. anorg. allg. Chem.* **200**5, *631*, 1383–1386.
(81) Cui, C.; Olmstead, M. M.; Fettinger, J. C.; Spikes, G. H.; Power, P. P. *J. Am. Chem. Soc.* **2005**, *127*, 17530–17541.
(82) Wang, X.; Ni, C.; Zhu, Z.; Fettinger, J. C.; Power, P. P. *Inorg. Chem.* **2009**, *48*, 2464–2470.
(83) Sen, S. S.; Kratzert, D.; Stern, D.; Roesky, H. W.; Stalke, D. *Inorg. Chem.* **2010**, *49*, 5786–5788.
(84) Yeong, H.-X.; Xi, H.-W.; Lim, K. H.; So, C.-W. *Chem. Eur. J.* **2010**, *16*, 12956–12961.

(85) a) Hahn, F. E.; Zabula, A. V.; Pape, T.; Hepp, A. *Eur. J. Inorg. Chem.* **2007**, *2007*, 2405–2408; b) Zabula, A. V.; Pape, T.; Hepp, A.; Hahn, F. E. *Organometallics* **2008**, *27*, 2756–2760.
(86) Zabula, A. V.; Hahn, F. E.; Pape, T.; Hepp, A. *Organometallics* **2007**, *26*, 1972–1980.
(87) Wang, W.; Inoue, S.; Yao, S.; Driess, M. *J. Am. Chem. Soc.* **2010**, *132*, 15890–15892.
(88) Zhang, S.-H.; So, C.-W. *Organometallics* **2011**, *30*, 2059–2062.
(89) Summerscales, O. T.; Olmstead, M. M.; Power, P. P. *Organometallics* **2011**, *30*, 3468–3471.
(90) Azhakar, R.; Ghadwal, R. S.; Roesky, H. W.; Wolf, H.; Stalke, D. *Organometallics* **2012**, *31*, 4588–4592.
(91) Wang, W.; Inoue, S.; Enthaler, S.; Driess, M. *Angew. Chem., Int. Ed.* **2012**, *51*, 6167–6171.
(92) Wang, W.; Inoue, S.; Irran, E.; Driess, M. *Angew. Chem., Int. Ed.* **2012**, *51*, 3691–3694.
(93) Hahn, F. E.; Zabula, A. V.; Pape, T.; Hepp, A. *Z. anorg. allg. Chem.* **2008**, *634*, 2397–2401.
(94) Fürstner, A.; Krause, H.; Lehmann, C. W. *Chem. Commun.* **2001**, 2372–2373.
(95) Zhang, M.; Liu, X.; Shi, C.; Ren, C.; Ding, Y.; Roesky, H. W. *Z. anorg. allg. Chem.* **2008**, *634*, 1755–1758.
(96) Blom, B.; Gallego, D.; Driess, M. *Inorg. Chem. Front.* **2014**, *1*, 134–148.
(97) Stoelzel, M.; Praesang, C.; Blom, B.; Driess, M. *Austral. J. Chem.* **2013**, *66,* 1163–1170.
(98) Someya, C. I.; Haberberger, M.; Wang, W.; Enthaler, S.; Inoue, S. *Chem. Lett.* **2013**, *42*, 286–288.
(99) Kireenko, M. M.; Zaitsev, K. V.; Oprunenko, Y. F.; Churakov, A. V.; Tafeenko, V. A.; Karlov, S. S.; Zaitseva, G. S. *Dalton Trans.* **2013**, *42*, 7901–7912.
(100) Tan, G.; Enthaler, S.; Inoue, S.; Blom, B.; Driess, M. *Angew. Chem., Int. Ed.* **2015**, *54*, 2214–2218.
(101) Kamer, P. C. J.; van Leeuwen, P. W. N. M., Eds. *Phosphorus(III) Ligands in Homogeneous Catalysis: Design and Synthesis;* John Wiley & Sons, Ltd.: The Atrium, Southern Gate, Chichester, West Sussex, UK, **2012**.
(102) Wang, W. Synthesis and Characterization of New Low-Valent Silicon, Germanium and Tin Compounds; Doctoral Thesis, Technische Universität Berlin, 31.10/2012.
(103) Hebden, T. J.; St. John, Anthony J.; Gusev, D. G.; Kaminsky, W.; Goldberg, K. I.; Heinekey, D. M. *Angew. Chem., Int. Ed.* **2011**, *50*, 1873–1876.
(104) a) Li, W.; Hill, N. J.; Tomasik, A. C.; Bikzhanova, G.; West, R. *Organometallics* **2006**, *25*, 3802–3805; b) Tomasik, A. C.; Mitra, A.; West, R. *Organometallics* **2009**, *28*, 378–381; c) Gehrhus, B.; Lappert, M. F.; Heinicke, J.; Boese, R.;

Blaser, D. *J. Chem. Soc., Chem. Commun.* **1995**, 1931–1932; d) Haaf, M.; Schmedake, T. A.; Paradise, B. J.; West, R. *Can. J. Chem.* **2000**, *78,* 1526–1533.

(105) Bedford, R. B.; Betham, M.; Charmant, Jonathan P. H.; Haddow, M. F.; Orpen, A. G.; Pilarski, L. T.; Coles, S. J.; Hursthouse, M. B. *Organometallics* **2007**, *26*, 6346–6353.

(106) Göttker-Schnetmann, I.; White, P.; Brookhart, M. *J. Am. Chem. Soc.* **2004**, *126*, 1804–1811.

(107) a) Cope, A. C.; Ciganek, E. *Org. Synth.* **1959**, *39,* 19; b) Park, C. H.; Simmons, H. E. *Org. Synth.* **1974**, *54,* 88; c) Wilson, C. V.; Stenberg, J. F. *Org. Synth.* **1956**, *36,* 48.

(108) Gehrhus, B.; Hitchcock, P. B.; Lappert, M. F.; Maciejewski, H. *Organometallics* **1998**, *17*, 5599–5601.

(109) Avent, A. G.; Gehrhus, B.; Hitchcock, P. B.; Lappert, M. F.; Maciejewski, H. *J. Organomet. Chem.* **2003**, *686*, 321–331.

(110) a) Schmid, G.; Welz, E. *Angew. Chem., Int. Ed.* **1977**, *16,* 785–786; b) Mitchell, G. P.; Tilley, T. D. *Angew. Chem., Int. Ed.* **1998**, *37,* 2524–2526.

(111) Dupont, J.; Consorti, C. S.; Spencer, J. *Chem. Rev.* **2005**, *105*, 2527–2572.

(112) Example with an aldehyde condensation: Kimura, T.; Uozumi, Y. *Organometallics* **2006**, *25*, 4883–4887.

(113) a) Takenaka, K.; Uozumi, Y. *Org. Lett.* **2004**, *6*, 1833–1835; b) Takenaka, K.; Minakawa, M.; Uozumi, Y. *J. Am. Chem. Soc.* **2005**, *127*, 12273–12281.

(114) a) Corey, J. Y.; Braddock-Wilking, J. *Chem. Rev.* **1999**, *99*, 175–292; b) Corey, J. Y. *Chem. Rev.* **2011**, *111*, 863–1071.

(115) Peters, J. C.; Feldman, J. D.; Tilley, T. D. *J. Am. Chem. Soc.* **1999**, *121*, 9871–9872.

(116) Feldman, J. D.; Peters, J. C.; Tilley, T. D. *Organometallics* **2002**, *21*, 4065–4075.

(117) Calimano, E.; Tilley, T. D. *J. Am. Chem. Soc.* **2009**, *131*, 11161–11173.

(118) Jungton, A.-K.; Meltzer, A.; Präsang, C.; Braun, T.; Driess, M.; Penner, A. *Dalton Trans.* **2010**, *39*, 5436–5438.

(119) Hays, M. K.; Eisenberg, R. *Inorg. Chem.* **1991**, *30,* 2623–2630.

(120) Zarate, E. A.; Kennedy, V. O.; McCune, J. A.; Simons, R. S.; Tessier, C. A. *Organometallics* **1995**, *14,* 1802–1809.

(121) Rappoli, B. J.; Janik, T. S.; Churehill, M. R.; Thompson, J. S.; Atwood, J. D. *Organometallics* **1988**, *7,* 1939–1944.

(122) a) Raskatov, J. A.; Spiess, S.; Gnamm, C.; Brödner, K.; Rominger, F.; Helmchen, G. *Chem. Eur. J.* **2010**, *16*, 6601–6615; b) Spiess, S.; Raskatov, J. A.; Gnamm, C.; Brödner, K.; Helmchen, G. *Chem. Eur. J.* **2009**, *15*, 11087–11090; c) Findlater, M.; Cartwright-Sykes, A.; White, P. S.; Schauer, C. K.; Brookhart, M. *J. Am. Chem. Soc.* **2011**, *133*, 12274–12284; d) Liu, W.-B.; Zheng, C.; Zhuo, C.-X.; Dai, L.-X.; You, S.-L. *J. Am. Chem. Soc.* **2012**, *134*, 4812–4821; e) Madrahimov, S. T.; Hartwig, J. F. *J. Am. Chem. Soc.* **2012**, *134*, 8136–8147; f)

Madrahimov, S. T.; Markovic, D.; Hartwig, J. F. *J. Am. Chem. Soc.* **2009**, *131*, 7228–7229.

(123) a) Morales-Morales, D.; Redón, R.; Yung, C.; Jensen, C. M. *Inorg. Chim. Acta* **2004**, *357*, 2953–2956; b) Zhu, K.; Achord, P. D.; Zhang, X.; Krogh-Jespersen, K.; Goldman, A. S. *J. Am. Chem. Soc.* **2004**, *126*, 13044–13053.

(124) Liu, F.; Pak, E. B.; Singh, B.; Jensen, C. M.; Goldman, A. S. *J. Am. Chem. Soc.* **1999**, *121*, 4086–4087.

(125) a) Gupta, M.; Hagen, C.; Kaska, W. C.; Cramer, R. E.; Jensen, C. M. *J. Am. Chem. Soc.* **1997**, *119,* 840–841; b) Morales-Morales, D.; Lee, D. W.; Wang, Z.; Jensen, C. M. *Organometallics* **2001**, *20*, 1144–1147;

(126) Lide, D. R., Ed. *CRC Handbook of Chemistry and Physics;* CRC Press: Boca Raton, FL, 2005.

(127) Chatt, J.; Duncanson, L. A. *J. Chem. Soc.* **1953**, 2939–2947.

(128) Hartwig, J. F. *Organotransition Metal Chemistry. From Bonding to Catalysis;* University Science Books: Sausalito, **2010**.

(129) Göttker-Schnetmann, I.; White, P. S.; Brookhart, M. *Organometallics* **2004**, *23*, 1766–1776.

(130) Liou, S.-Y.; Gozin, M.; Milstein, D. *J. Chem. Soc., Chem. Commun.* **1995**, 1965–1966.

(131) Zargarian, D.; Castonguay, A.; Spasyuk, D. M. *Top. Organomet. Chem.* **2013**, *40,* 131–173.

(132) Ullah, F.; Kühl, O.; Bajor, G.; Veszprémi, T.; Jones, P. G.; Heinicke, J. *Eur. J. Inorg. Chem.* **2009**, *2009*, 221–229.

(133) Denk, M.; Hayashi, R. K.; West, R. *J. Chem. Soc., Chem. Commun.* **1994**, 33–34.

(134) Meltzer, A.; Präsang, C.; Milsmann, C.; Driess, M. *Angew. Chem., Int. Ed.* **2009**, *48*, 3170–3173.

(135) Grenz, V. M.; Hahn, E.; Du Mont, W.-W.; Pickardt, J. *Angew., Chem.* **1984**, *94,* 69–70.

(136) Bazinet, P.; Yap, Glenn P. A.; Richeson, D. S. *J. Am. Chem. Soc.* **2001**, *123*, 11162–11167.

(137) Bender IV, J. E.; Shusterman, A. J.; Banaszak Holl, M. M.; Kampf, J. W. *Organometallics* **1999**, *18*, 1547–1552.

(138) a) Peng, D.; Zhang, Y.; Du, X.; Zhang, L.; Leng, X.; Walter, M. D.; Huang, Z. *J. Am. Chem. Soc.* **2013**, *135*, 19154–19166; b) Nakajima, Y.; Nakao, Y.; Sakaki, S.; Tamada, Y.; Ono, T.; Ozawa, F. *J. Am. Chem. Soc.* **2010**, *132*, 9934–9936; c) Zhang, J.; Gandelman, M.; Herrman, D.; Leitus, G.; Shimon, L. J.; Ben-David, Y.; Milstein, D. *Inorg. Chim. Acta* **2006**, *359*, 1955–1960; d) O'Reilly, R. K.; Gibson, V. C.; White, A. J.; Williams, D. J. *Polyhedron* **2004**, *23*, 2921–2928; e) Danopoulos, A. A.; Tsoureas, N.; Wright, J. A.; Light, M. E. *Organometallics* **2004**, *23*, 166–168; f) Small, B. L.; Brookhart, M.; Bennett, Alison M. A. *J. Am. Chem. Soc.* **1998**, *120,* 4049–4050.

(139) Zlatogorsky, S.; Muryn, C. A.; Tuna, F.; Evans, D. J.; Ingleson, M. J. *Organometallics* **2011**, *30*, 4974–4982.
(140) Meyer, S.; Orben, C. M.; Demeshko, S.; Dechert, S.; Meyer, F. *Organometallics* **2011**, *30*, 6692–6702.
(141) Blom, B.; Tan, G.; Enthaler, S.; Inoue, S.; Epping, J. D.; Driess, M. *J. Am. Chem. Soc.* **2013**, *135*, 18108–18120.
(142) Barclay, J. E.; Leigh, G. J. *J. Chem. Soc., Dalton Trans.* **1988**, 2865–2870.
(143) Hawrelak, E. J.; Bernskoetter, W. H.; Lobkovsky, E.; Yee, G. T.; Bill, E.; Chirik, P. J. *Inorg. Chem.* **2005**, *44*, 3103–3111.
(144) Danopoulos, A. A.; Wright, J. A.; Motherwell, W. B. *Chem. Commun.* **2005**, 784–786.
(145) Macomber, R. S. *A Complete Introduction to Modern NMR Spectroscopy;* John Wiley & Sons, Inc.: New York, USA, **1998**.
(146) Pregosin, P. S. *NMR in Organometallic Chemistry;* Wiley-VCH Verlag & Co. KGaA: Weinheim, Germany, **2012**.
(147) Addison, A. W.; Rao, T. N.; Reedijk, J.; van Rijn, J.; Verschoor, G. C. *J. Chem. Soc., Dalton Trans.* **1984**, 1349–1356.
(148) a) Casey, C. P.; Whiteker, G. T.; Campana, C. F.; Powell, D. R. *Inorg. Chem.* **1990**, *29,* 3376–3381; b) Pelczar, E. M.; Emge, T. J.; Krogh-Jespersen, K.; Goldman, A. S. *Organometallics* **2008**, *27*, 5759–5767.
(149) Schmedake, T. A.; Haaf, M.; Paradise, B. J.; Millevolte, A. J.; Powell, D. R.; West, R. *J. Organomet. Chem.* **2001**, *636*, 17–25.
(150) Yang, W.; Fu, H.; Wang, H.; Chen, M.; Ding, Y.; Roesky, H. W.; Jana, A. *Inorg. Chem.* **2009**, *48*, 5058–5060.
(151) Tobita, H.; Matsuda, A.; Hashimoto, H.; Ueno, K.; Ogino, H. *Angew. Chem., Int. Ed.* **2004**, *43*, 221–224.
(152) Zell, T.; Milko, P.; Fillman, K. L.; Diskin-Posner, Y.; Bendikov, T.; Iron, M. A.; Leitus, G.; Ben-David, Y.; Neidig, M. L.; Milstein, D. *Chem. Eur. J.* **2014**, *20*, 4403–4413.
(153) Darmon, J. M.; Yu, R. P.; Semproni, S. P.; Turner, Z. R.; Stieber, S. Chantal E.; DeBeer, S.; Chirik, P. J. *Organometallics* **2014**, *33*, 5423–5433.
(154) Bart, S. C.; Lobkovsky, E.; Bill, E.; Wieghardt, K.; Chirik, P. J. *Inorg. Chem.* **2007**, *46*, 7055–7063.
(155) Blom, B. Reactivity of Ylenes at Late Transition Metal Centers; Doctoral Thesis, Rheinische Friedrich-Wilhelms-University of Bonn, April **2011**.
(156) a) Wiberg, K. B. *Tetrahedron* **1968**, *24,* 1083–1096; b) Irwin, R. P. *Organometallic Chemistry: Research Perspectives;* Nova Science Pub Inc.: Hauppauge, NY, **2008**.
(157) Trovitch, R. J.; Lobkovsky, E.; Chirik, P. J. *Inorg. Chem.* **2006**, *45*, 7252–7260.
(158) Hartwig, J. F. *Acc. Chem. Res.* **2012**, *45*, 864–873.

(159) Mkhalid, I. A. I.; Barnard, J. H.; Marder, T. B.; Murphy, J. M.; Hartwig, J. F. *Chem. Rev.* **2010**, *110*, 890–931.
(160) Mandal, S. K.; Roesky, H. W. *Chem. Commun.* **2010**, *46*, 6016–6041.
(161) a) Fukatsu, K.; Harada, M.; Hinuma, S.; Ito, Y.; Sasaki, S.; Suzuki, N.; Yasuma, T. Patent no. EP 1559422 A1; b) Osakada, K.; Sakata, R.; Yamamoto, T. *Organometallics*. **1997**, *16,* 5354–5364.
(162) Manna, J.; John, K. D.; Hopkins, M. D. *Adv. Organomet. Chem.* **1995**, *38,* 79–154.
(163) a) Janssen, M. D.; Köhler, K.; Herres, M.; Dedieu, A.; Smeets, Wilberth J. J.; Spek, A. L.; Grove, D. M.; Lang, H.; van Koten, G. *J. Am. Chem. Soc.* **1996**, *118,* 4817–4829; b) Dias, H. V. Rasika; Flores, J. A.; Wu, J.; Kroll, P. *J. Am. Chem. Soc.* **2009**, *131*, 11249–11255.
(164) Lang, H.; Köhler, K.; Rheinwald, G.; Zsolnai, L.; Büchner, M.; Driess, A.; Huttner, G.; Strähle, J. *Organometallics* **1999**, *18*, 598–605.
(165) Köhler, K.; Eichhorn, J.; Meyer, F.; Vidovic, D. *Organometallics* **2003**, *22*, 4426–4432.
(166) Thompson, J. S.; Bradley, A. Z.; Park, K.-H.; Dobbs, K. D.; Marshall, W. *Organometallics* **2006**, *25*, 2712–2714.
(167) Zhao, N.; Zhang, J.; Yang, Y.; Chen, G.; Zhu, H.; Roesky, H. W. *Organometallics* **2013**, *32*, 762–769.
(168) Becke, A. D. *J. Chem. Phys.* **1993**, *98*, 5648–5652.
(169) Lee, C.; Yang, W.; Parr, R. G. *Phys. Rev. B*. **1988**, *37,* 785–789.
(170) Stephens, P. J.; Devlin, F. J.; Chabalowski, C. F.; Frisch, M. J. *J. Phys. Chem.* **1994**, *98,* 11623–11627.
(171) Weigend, F.; Ahlrichs, R. *Phys. Chem. Chem. Phys.* **2005**, *7*, 3297–3305.
(172) Grimme, S.; Antony, J.; Ehrlich, S.; Krieg, H. *J. Chem. Phys.* **2010**, *132*, 154104-1–154104-19.
(173) Grimme, S.; Ehrlich, S.; Goerigk, L. *J. Comput. Chem.* **2011**, *32*, 1456–1465.
(174) Becke, A. D.; Edgecombe, K. E. *J. Chem. Phys.* **1990**, *92*, 5397–5403.
(175) Savin, A.; Jepsen, O.; Flad, J.; Andersen, O. K.; Preuss, H.; von Schnering, Hans Georg. *Angew. Chem., Int. Ed. Engl.* **1992**, *31,* 187–188.
(176) Kohout, K.; Savin, A. *Int. J. Quantum Chem.* **1996**, *60,* 875–882.
(177) Kohout, M. *Int. J. Quantum Chem.* **2004**, *97*, 651–658.
(178) Kohout, M.; Pernal, K.; Wagner, F. R.; Grin, Y. *Theor. Chem. Acc*. **2004**, *112*, 453–459.
(179) a) Corain, B.; Puosi, G. *J. Catal.* **1973**, *30,* 403–408; b) Wang, L.; Liu, C.; Bai, R.; Pan, Y.; Lei, A. *Chem. Commun.* **2013**, *49*, 7923–7925; c) Birdwhistell, K. R.; Lanza, J. *J. Chem. Ed.*. **1997**, *74,* 579–581.
(180) Breitenfeld, J.; Ruiz, J.; Wodrich, M. D.; Hu, X. *J. Am. Chem. Soc.* **2013**, *135*, 12004–12012.
(181) Breitenfeld, J.; Wodrich, M. D.; Hu, X. *Organometallics* **2014**, *33*, 5708–5715.

(182) a) Enthaler, S.; Junge, K.; Beller, M. *Angew. Chem., Int. Ed.* **2008**, *47*, 3317–3321; b) Morris, R. H. *Chem. Soc. Rev.* **2009**, *38*, 2282–2291.
(183) Zhang, M.; Zhang, A. *Appl. Organometal. Chem.* **2010**, *24*, 751–757.
(184) a) Yu, R. P.; Darmon, J. M.; Hoyt, J. M.; Margulieux, G. W.; Turner, Z. R.; Chirik, P. J. *ACS Catal.* **2012**, *2*, 1760–1764; b) Tondreau, A. M.; Atienza, C. C. H.; Weller, K. J.; Nye, S. A.; Lewis, K. M.; Delis, J. G. P.; Chirik, P. J. *Science* **2012**, *335*, 567–570; c) Obligacion, J. V.; Chirik, P. J. *Org. Lett.* **2013**, *15*, 2680–2683.
(185) a) Bridier, B.; López, N.; Pérez-Ramírez, J. *Dalton Trans.* **2010**, *39*, 8464–8471; b) Sonnenberg, J. F.; Coombs, N.; Dube, P. A.; Morris, R. H. *J. Am. Chem. Soc.* **2012**, *134*, 5893–5899; c) Kelsen, V.; Wendt, B.; Werkmeister, S.; Junge, K.; Beller, M.; Chaudret, B. *Chem. Commun.* **2013**, *49*, 3416–3418.
(186) Bhattacharya, P.; Krause, J. A.; Guan, H. *Organometallics* **2011**, *30*, 4720–4729.
(187) Tondreau, A. M.; Lobkovsky, E.; Chirik, P. J. *Org. Lett.* **2008**, *10*, 2789–2792.
(188) Shaikh, N. S.; Enthaler, S.; Junge, K.; Beller, M. *Angew. Chem., Int. Ed.* **2008**, *47*, 2497–2501.
(189) Nishiyama, H.; Furuta, A. *Chem. Commun.* **2007**, 760–762.
(190) Zuo, Z.; Sun, H.; Wang, L.; Li, X. *Dalton Trans.* **2014**, *43*, 11716–11722.
(191) Denmark, S. E.; Ueki, Y. *Organometallics* **2013**, *32*, 6631–6634.
(192) Ruddy, A. J.; Kelly, C. M.; Crawford, S. M.; Wheaton, C. A.; Sydora, O. L.; Small, B. L.; Stradiotto, M.; Turculet, L. *Organometallics* **2013**, *32*, 5581–5588.
(193) Hsu, S.-F.; Plietker, B. *Chem. Eur. J.* **2014**, *20*, 4242–4245.
(194) Lopes, R.; Cardoso, João M. S.; Postigo, L.; Royo, B. *Catal Lett*. **2013**, *143*, 1061–1066.
(195) Taniguchi, T.; Curran, D. P. *Org. Lett.* **2012**, *14*, 4540–4543.
(196) Rendler, S.; Oestreich, M. *Modern Reduction Methods, Eds. Andersson, P. G. and Munslow, Ian J.;* WILEY-VCH: Weinheim, Germany, **2008**. pp 183–207.
(197) Roy, A. K.; A Review of Recent Progress in Catalyzed Homogeneous Hydrosilation (Hydrosilylation); Elsevier, **2007**; Vol. 55; pp 1–59.
(198) Shirobokov, O. G.; Kuzmina, L. G.; Nikonov, G. I. *J. Am. Chem. Soc.* **2011**, *133*, 6487–6489.
(199) Wang, W.; Gu, P.; Wang, Y.; Wei, H. *Organometallics* **2014**, *33*, 847–857.
(200) Ojima, I.; Nihonyanagi, M.; Kogure, T.; Kumagai, M.; Horiuchi, S.; Nakatsugawa, K.; Nagai, Y. *J. Organomet. Chem.* **1975**, *94*, 449–461.
(201) Rendler, S.; Oestreich, M. *Angew. Chem., Int. Ed.* **2008**, *47*, 5997–6000.
(202) Metsänen, T. T.; Hrobárik, P.; Klare, H. F. T.; Kaupp, M.; Oestreich, M. *J. Am. Chem. Soc.* **2014**, *136*, 6912–6915.
(203) Park, S.; Brookhart, M. *Organometallics* **2010**, *29*, 6057–6064.
(204) Müther, K.; Oestreich, M. *Chem. Commun.* **2010**, *47*, 334–336.
(205) Sheldrick, G. M. *SHELX-97: Program for Crystal Structure Refinement:* University of Göttingen, Göttingen, Germany, **1997**.

(206) University of Karlsruhe and Forschungszentrum Karlsruhe GmbH. *Turbomole, version 6.3.1,* **1989-2007**.

(207) Frisch, M. J.; Trucks, G. W.; Schlegel, H. B.; Scuseria, G. E.; Robb, M. A.; Cheeseman, J. R.; Scalmani, G.; Barone, V.; Mennucci, B.; Petersson, G. A.; Nakatsuji, H.; Caricato, M.; Li, X.; Hratchian, H. P.; Izmaylov, A. F.; Bloino, J.; Zheng, G.; Sonnenberg, J. L.; Hada, M.; Ehara, M.; Toyota, K.; Fukuda, R.; Hasegawa, J.; Ishida, M.; Nakajima, T.; Honda, Y.; Kitao, O.; Nakai, H.; Vreven, T.; Montgomery, J. A., Jr.; Peralta, J. E.; Ogliaro, F.; Bearpark, M.; Heyd, J. J.; Brothers, E.; Kudin, K. N.; Staroverov, V. N.; Kobayashi, R.; Normand, J.; Raghavachari, K.; Rendell, A.; Burant, J. C.; Iyengar, S. S.; Tomasi, J.; Cossi, M.; Rega, N.; Millam, J. M.; Klene, M.; Knox, J. E.; Cross, J. B.; Bakken, V.; Adamo, C.; Jaramillo, J.; Gomperts, R.; Stratmann, R. E.; Yazyev, O.; Austin, A. J.; Cammi, R.; Pomelli, C.; Ochterski, J. W.; Martin, R. L.; Morokuma, K.; Zakrzewski, V. G.; Voth, G. A.; Salvador, P.; Dannenberg, J. J.; Dapprich, S.; Daniels, A. D.; Farkas, O.; Foresman, J. B.; Ortiz, J. V.; Cioslowski, J.; Fox, D. J. *Gaussian 09, revision A.02;* Gaussian, Inc.: Wallingford CT, **2009**.

(208) Mayer, I. *BORDER, version 1.0;* Chemical Research Center, Hungarian Academy of Sciences: Budapest, Hungary, **2005**.

(209) Kohout, M. *DGrid, version 4.6:* Radebeul, Germany, **2011**.

(210) Kitware Inc. *Paraview, version 3.98.1:* Clifton Park, NY, U.S., **2013**.

(211) a) Frisch, M. J.; Pople, J. A.; Binkley. J. S. *J. Chem. Phys.* **1984**, *80,* 3265–3269; b) Dunning, T. H. *J. Chem. Phys.* **1989**, *90,* 1007–1023; c) Chai, J.-D.; Head-Gordon, M. *Phys. Chem. Chem. Phys.* **2008**, *10,* 6615–6620.

(212) Karsch, H. H.; Klein, H.-F.; Schmidbaur, H. *Angew. Chem., Int. Ed.* **1975**, 637–638.

(213) Klare, Hendrik F. T.; Oestreich, M.; Ito, J.-i.; Nishiyama, H.; Ohki, Y.; Tatsumi, K. *J. Am. Chem. Soc.* **2011**, *133*, 3312–3315.

(214) Mewald, M.; Doctoral Thesis, Westfälische Wilhelms-Universität Münster, **2012**.

(215) Kajigaeshi, S.; Kakinami, T.; Tokiyama, H.; Hirakawa, T.; Okamoto, T. *Chem. Lett.* **1987***,* 627.

(216) Wang, C.; Erker, G.; Kehr, G.; Wedeking, K.; Fröhlich, R. *Organometallics* **2005**, *24,* 4760–4773.

(217) Pfirrmann, S.; Limberg, C.; Hoppe, E. *Z. anorg. allg. Chem.* **2009**, *635*, 312–316.

7. APENDIXES

7.1. Crystallographic Data and Refinement Details

Compound	GeCHGe	GeCBrGe	*t*Bu-PCHP	SiNSi
Empirical formula	$C_{44}H_{66}Ge_2N_4O_2 \cdot C_6H_{14}$	$C_{44}H_{65}BrGe_2N_4O_2$	$C_{30}H_{56}O_2P_2$	$C_{39}H_{59}N_7Si_2$
M_r	914.36	907.09	510.69	682.11
Space group	*P2₁/n*	*P-1*	*P2₁/n*	*P2₁/c*
Crystal system	Monoclinic	Triclinic	Monoclinic	Monoclinic
a [Å]	8.7268(8)	10.5224(5)	15.7711(7)	18.2187(4)
b [Å]	22.153(5)	13.4646(6)	12.8437(5)	17.8712(3)
c [Å]	27.056(2)	17.1624(6)	16.9355(7)	13.0738(3)
α [°]	90	105.524(4)	90	90
β [°]	92.226(7)	99.379(3)	107.907(5)	102.759(2)
γ [°]	90	97.497(4)	90	90
Z	4	2	4	4
ρ_{calcd} [mg m^{-3}]	1.162	1.326	1.039	1.091
Wavelength [Å]	0.71073	0.71073	0.71073	1.54184
μ ($Mo_{K\alpha}$) [mm^{-1}]	1.188	2.240	0.155	1.031
Temperature [K]	150(2)	173(2)	173(2)	150.00(20)
crystal size [mm^3]	0.26 × 0.14 × 0.12	0.45 × 0.30 × 0.13	0.26 × 0.16 × 0.13	0.21 × 0.09 × 0.04
V [Å^3]	5226.6(13)	2272.45(17)	3264.3(2)	4151.59(15)
Θ limits [°]	3.29 to 25.00	3.36 to 25.00	3.42 to 25.00	3.51 to 67.50
completeness to Θ_{max} [%]	99.7	99.7	99.8	99.9
reflns measured[a]	19729	15890	13270	17427
independent reflns	9198 [$R_{(int)}$ = 0.1416]	7973 [$R_{(int)}$ = 0.0329]	5739 [$R_{(int)}$ = 0.0463]	7478 [$R_{(int)}$ = 0.0485]
restraints / parameters	0 / 543	0 / 496	0 / 325	18 / 475
R_1 (R_1 all data)[b]	0.0956 (0.1756)	0.0357 (0.0511)	0.0615 (0.0855)	0.0491 (0.0776)
wR_2 (wR_2 all data)[c]	0.2115 (0.2667)	0.0818 (0.0874)	0.1350 (0.1440)	0.1127 (0.1298)
GOF	1.085	1.030	1.190	1.033
max. (min.) peaks [eÅ^{-3}]	1.050 (-1.228)	0.597 (-0.390)	0.322 (-0.216)	0.222 (-0.300)

[a] Observation criterion: $I>2\sigma(I)$. [b] $R_1 = \Sigma \mid |F_o| - |F_c| \mid / \Sigma |F_o|$. [c] $wR_2 = \{\Sigma[w-(F_o^2-F_c^2)^2]/\Sigma[w(F_o^2)^2]\}^{1/2}$

Compound	**[SiCSi]IrHCl(coe)**	**[*t*Bu-PCP]IrHCl**	**[*i*PrN-PCP]IrHCl(coe)**	**[SiCSi]NiBr**
Empirical formula	$C_{59}H_{88}ClIrN_4O_2Si_2$	$C_{30}H_{56}ClIrO_2P_2 \cdot 1/2(C_6H_{14})$	$C_{38}H_{70}ClIrN_4O_2P_2$	$C_{44}H_{65}BrN_4NiO_2Si_2 \cdot C_6H_{14}$
M_r	1169.16	780.42	904.57	962.97
Space group	$P2_1/c$	$P\text{-}1$	$P2_1/n$	$P2_1/c$
Crystal system	Monoclinic	Triclinic	Monoclinic	Monoclinic
a [Å]	21.9037(3)	8.3255(4)	14.0443(5)	9.0981(1)
b [Å]	9.7095(2)	12.5254(6)	17.7739(6)	25.6671(2)
c [Å]	27.2368(5)	18.9009(6)	17.7514(7)	22.5949(2)
α [°]	90	97.727(3)	90	90
β [°]	91.6030(10)	98.833(3)	106.652(4)	91.417(1)
γ [°]	90	104.728(4)	90	90
Z	4	2	4	4
ρ_{calcd} [mg m^{-3}]	1.341	1.399	1.415	1.213
Wavelength [Å]	0.71073	0.71073	0.71073	1.54184
μ ($Mo_{K\alpha}$) [mm^{-1}]	2.437	3.788	3.319	2.150
Temperature [K]	173(2)	150(2)	150(2)	173(2)
crystal size [mm^3]	0.23 × 0.14 × 0.13	0.55 × 0.13 × 0.04	0.28 × 0.18 × 0.17	0.32 × 0.06 × 0.04
V [Å^3]	5790.29(18)	1852.32(14)	4245.3(3)	5274.79(9)
Θ limits [°]	3.23 to 25.00	3.33 to 24.99	3.24 to 25.00	3.44 to 67.49
completeness to Θ_{max} [%]	99.7	99.7	99.8	99.9
reflns measured[a]	40197	13999	18476	20510
independent reflns	10185 [$R_{(int)}$ = 0.0552]	6503 [$R_{(int)}$ = 0.0515]	7447 [$R_{(int)}$ = 0.0719]	9490 [$R_{(int)}$ = 0.0432]
restraints / parameters	439 / 758	204 / 388	53 / 467	6 / 569
R_1 (R_1 all data)[b]	0.0397 (0.0510)	0.0333 (0.0425)	0.0551 (0.0821)	0.0577 (0.0622)
wR_2 (wR_2 all data)[c]	0.0749 (0.0784)	0.0714 (0.0733)	0.0805 (0.0877)	0.1575 (0.1641)
GOF	1.097	1.094	1.070	1.447
max. (min.) peaks [eÅ^{-3}]	1.004 (-1.160)	1.440 (-0.805)	1.035 (-1.103)	1.147 (-1.200)

[a] Observation criterion: $I>2\sigma(I)$. [b] $R_1 = \Sigma \mid |F_o| - |F_c| \mid / \Sigma |F_o|$. [c] $wR_2 = \{\Sigma[w-(F_o^2-F_c^2)^2]/\Sigma[w(F_o^2)^2]\}^{1/2}$

Compound	**[GeCGe]NiBr**	**[iPrN-PCP]NiBr**	***κ²Si,Si'*-[SiNSi]FeCl₂**	***κ²Ge,Ge'*-[GeNGe]FeCl₂**
Empirical formula	$C_{50}H_{65}BrGe_2N_4NiO_2$ ·C_7H_8	$C_{30}H_{55}BrN_4NiO_2P_2$ ·CH_2Cl_2	$C_{39}H_{59}Cl_2FeN_7Si_2$ ·C_7H_8	$C_{39}H_{59}Cl_2FeGe2N_7$·C_7H_8
M_r	1057.93	789.27	901.00	990.00
Space group	$P2_1/n$	$P-1$	$P2_1/n$	$P2_1/n$
Crystal system	Monoclinic	Triclinic	monoclinic	monoclinic
a [Å]	9.1417(3)	11.8490(12)	17.1837(2)	17.19290(10)
b [Å]	22.4188(5)	12.0246(8)	17.3409(2)	17.35970(10)
c [Å]	26.2145(8)	14.9184(14)	17.1990(2)	17.50790(10)
α [°]	90	96.481(7)	90	90
β [°]	97.257(3)	108.989(9)	105.2090(10)	105.7790(10)
γ [°]	90	104.065(7)	90	90
Z	4	2	4	4
ρ_{calcd} [mg m^{-3}]	1.318	1.375	1.210	1.308
Wavelength [Å]	0.71073	0.71073	1.54184	1.54184
μ ($Mo_{K\alpha}$) [mm^{-1}]	2.260	1.813	4.191	4.952
Temperature [K]	173(2)	150(2)	150.00(20)	150.00(20)
crystal size [mm^3]	0.29 × 0.07 × 0.03	0.43 × 0.29 × 0.27	0.21 × 0.18 × 0.12	0.25 × 0.22 × 0.21
V [Å^3]	5329.5(3)	1906.5(3)	4945.47(10)	5028.56(5)
Θ limits [°]	3.42 to 25.00	3.35 to 25.00	3.69 to 67.50	3.66 to 67.49
completeness to Θ_{max} [%]	99.7	99.8	97.2	99.7
reflns measured[a]	35241	13828	21889	20836
independent reflns	9362 [$R_{(int)}$ = 0.0507]	6697 [$R_{(int)}$ = 0.0650]	8673 [$R_{(int)}$ = 0.0299]	9044 [$R_{(int)}$ = 0.0184]
restraints / parameters	36 / 594	24 / 429	603 / 625	440 / 634
R_1 (R_1 all data)[b]	0.0462 (0.0661)	0.0631 (0.1108)	0.0398 (0.0477)	0.0287 (0.0315)
wR_2 (wR_2 all data)[c]	0.0871 (0.0932)	0.0869 (0.1007)	0.1002 (0.1103)	0.0747 (0.0762)
GOF	1.081	0.982	0.954	1.044
max., min. peaks [eÅ^{-3}]	0.940 (-0.563)	0.502 (-0.502)	0.728 (-0.544)	0.615 (-0.602)

[a] Observation criterion: $I>2\sigma(I)$. [b] $R_1 = \Sigma \mid |F_o| - |F_c| \mid / \Sigma |F_o|$. [c] $wR_2 = \{\Sigma[w-(F_o^2-F_c^2)^2]/\Sigma[w(F_o^2)^2]\}^{1/2}$

Compound	**[SiNSi]Fe(PMe$_3$)$_2$**	**[SiNSi]Fe(CO)$_2$**	**[GeNGe]Fe(CO)$_2$ + [GeNGe]Fe(CO)$_2$(PMe$_3$)**	***κ^{2}Si,Si'*-[SiNSi]Fe(CO)$_3$**
Empirical formula	$C_{45}H_{77}FeN_7P_2Si_2$	$C_{41}H_{59}FeN_7O_2Si_2$	$C_{90}H_{139}Fe_2Ge_4N_{14}O_4P$	$2\times(C_{42}H_{59}FeN_7O_3Si_2)$ $3\times(C_7H_8)$
M_r	890.11	793.98	1914.18	1920.39
Space group	$P2_12_12_1$	$P2_12_12_1$	*P-1*	$P2_1/c$
Crystal system	Orthorhombic	Orthorhombic	Triclinic	Monoclinic
a [Å]	9.8316(2)	17.3198(4)	13.3190(3)	9.6005(2)
b [Å]	21.2680(5)	19.2095(4)	14.5574(4)	23.9602(6)
c [Å]	26.6117(5)	26.1237(6)	26.7888(7)	22.5839(6)
α [°]	90	90	76.365(2)	90
β [°]	90	90	80.165(2)	99.136(2)
γ [°]	90	90	70.906(2)	90
Z	4	8	2	2
ρ_{calcd} [mg m^{-3}]	1.062	1.214	1.340	1.243
Wavelength [Å]	1.54184	1.54184	1.54184	1.54184
μ ($Mo_{K\alpha}$) [mm^{-1}]	3.379	3.634	4.403	3.184
Temperature [K]	150.00(20)	150.00(10)	150.00(10)	150.00(10)
crystal size [mm^3]	0.36 × 0.18 × 0.08	0.44 × 0.28 × 0.09	0.44 × 0.28 × 0.09	0.25 × 0.12 × 0.05
V [Å^3]	5564.5(2)	8691.5(3)	4745.1(2)	5129.1(2)
Θ limits [°]	3.32 to 67.48	2.86 to 67.50	3.27 to 67.49	2.71 to 67.50
completeness to Θ_{max} [%]	100.0	100.0	99.9	99.9
reflns measured[a]	22845	34954	32470	19881
independent reflns	9979 [$R_{(int)}$ = 0.0629]	15331 [$R_{(int)}$ = 0.0799]	17090 [$R_{(int)}$ = 0.0948]	9242 [$R_{(int)}$ = 0.0699]
restraints / parameters	324 / 667	0 / 983	0 / 1069	91 / 637
R_1 (R_1 all data)[b]	0.0547 (0.0715)	0.0533 (0.0918)	0.0701 (0.0845)	0.0625 (0.0973)
wR_2 (wR_2 all data)[c]	0.1263 (0.1367)	0.1231 (0.1538)	0.1749 (0.1997)	0.1513 (0.1757)
GOF	1.019	0.902	1.028	1.026
max. (min.) peaks [eÅ^{-3}]	0.499 (-0.316)	0.401 (-0.331)	1.441 (-1.353)	1.942 (-0.535)

[a] Observation criterion: $I>2\sigma(I)$. [b] $R_1 = \Sigma \, | |F_o| - |F_c| | \, / \, \Sigma \, |F_o|$. [c] $wR_2 = \{\Sigma[w\text{-}(F_o^2 - F_c^2)^2]/\Sigma[w(F_o^2)^2]\}^{1/2}$

Compound	**{[SiNSi]Ni-C≡C-Ph→CuBr}**	**{[GeNGe]Ni-C≡C-*ter*Ph→CuBr}**	**[SiCSi]NiI**	**[SiNSi]FeH(SiMe$_2$Ph)(PMe$_3$)**
Empirical formula	$C_{52}H_{70}BrCuN_4NiO_2Si2 \cdot C_7H_8 \cdot C_5H_{12}$	$C_{64}H_{78}BrCuGe_2N_4NiO_2 \cdot C_7H_8$	$C_{44}H_{65}IN_4NiO_2Si_2$	$2\times(C_{50}H_{80}FeN_7PSi_3) \cdot C_7H_8$
M_r	2339.33	1374.78	923.79	1992.73
Space group	*C2/c*	*P21/n*	*P-1*	*P-1*
Crystal system	Monoclinic	Monoclinic	Triclinic	Triclinic
a [Å]	34.2351(8)	21.6098(2)	12.2414(4)	11.5288(5)
b [Å]	19.3827(3)	19.9642(2)	20.7843(7)	12.5203(5)
c [Å]	18.1672(3)	32.5982(2)	21.9693(7)	21.1550(11)
α [°]	90	90	73.485(3)	73.555(4)
β [°]	92.620(2)	102.600(1)	74.053(3)	75.604(4)
γ [°]	90	90	73.009(3)	74.650(4)
Z	4	8	4	1
ρ_{calcd} [mg m^{-3}]	1.290	1.331	1.224	1.193
Wavelength [Å]	1.54184	1.54184	1.54184	1.54184
μ ($Mo_{K\alpha}$) [mm^{-1}]	2.315	2.690	6.121	3.379
Temperature [K]	150(2)	150(2)	150(2)	150(2)
crystal size [mm^3]	0.36 × 0.29 × 0.06	0.42 × 0.32 × 0.19	0.24 × 0.08 × 0.06	0.45 × 0.12 × 0.04
V [Å^3]	12042.6(4)	13724.9(2)	5011.9(3)	2774.0(2)
Θ limits [°]	2.62 to 67.50	2.61 to 67.50	3.46 to 67.50	3.76 to 67.50
completeness to Θ_{max} [%]	99.9	99.7	99.8	99.9
reflns measured[a]	38807	52670	40093	18617
independent reflns	10862 [$R_{(int)}$ = 0.0912]	24655 [$R_{(int)}$ = 0.0591]	18041 [$R_{(int)}$ = 0.1232]	9988 [$R_{(int)}$ = 0.0490]
restraints / parameters	532 / 772	213 / 1523	198 / 1084	645
R_1 (R_1 all data)[b]	0.0711 (0.0898)	0.0626 (0.0676)	0.1052 (0.1354)	0.0452 (0.0635)
wR_2 (wR_2 all data)[c]	0.1761 (0.1899)	0.1708 (0.1775)	0.2023 (0.2220)	0.1026 (0.1162)
GOF	1.535	1.681	1.516	1.020
max. (min.) peaks [eÅ^{-3}]	1.472 (-2.038)	1.560 (-1.366)	3.966 (-2.464)	0.475 (-0.389)

[a] Observation criterion: $I>2\sigma(I)$. [b] $R_1 = \Sigma \mid |F_o| - |F_c| \mid / \Sigma |F_o|$. [c] $wR_2 = \{\Sigma[w-(F_o^2-F_c^2)^2]/\Sigma[w(F_o^2)^2]\}^{1/2}$

7.2. DFT Calculations

Table 7.2.1. Assignment of the atom numbers in complexes **{[ECE]Ni-CC-R→CuBr}** and **{[ECE]Ni-CC-R}** (E=Si, R=Ph / E=Ge, R=*ter*Ph) and its fragments

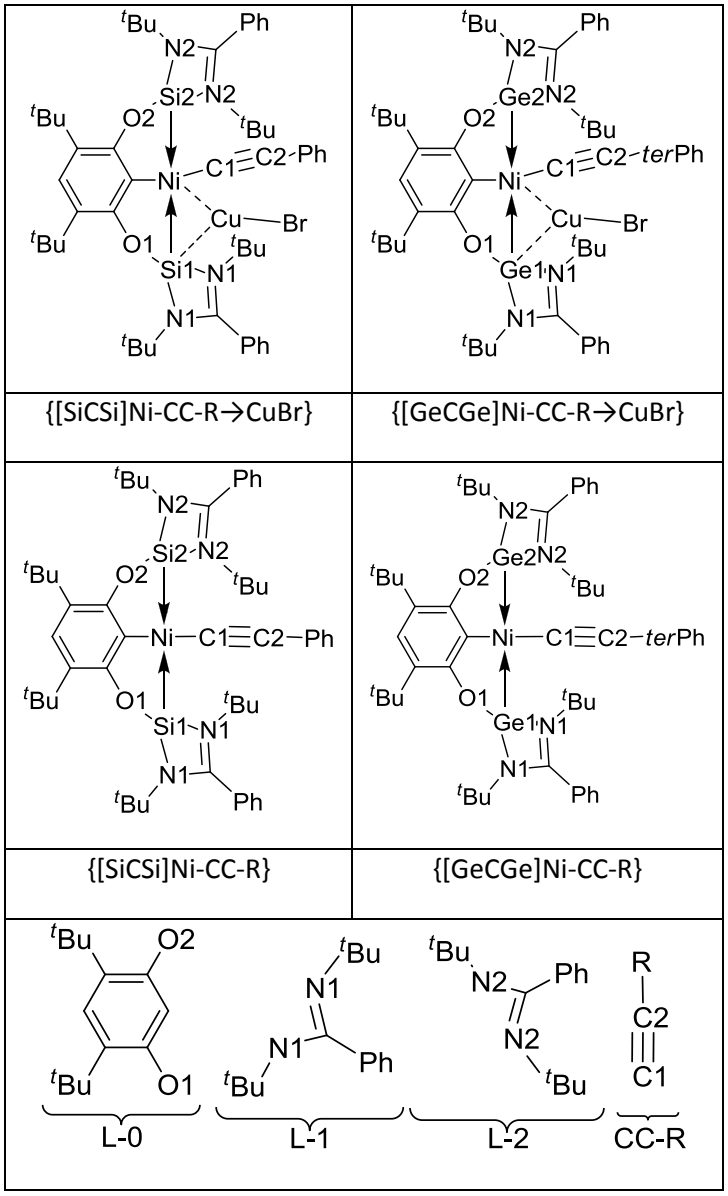

Table 7.2.2. ELF analysis of "Cu-coordination" in **{[ECE]Ni-CC-R→CuBr}** (E=Si, R=Ph / E=Ge, R=*ter*Ph)[a]

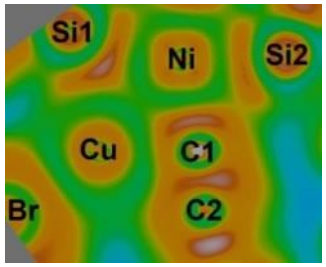

ELI-D Plot: crystal/H-opt{[SiCSi]Ni-CC-Ph→CuBr }

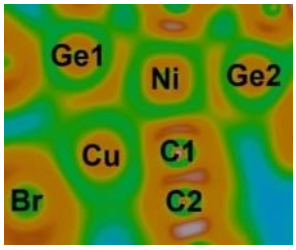

ELI-D Plot: crystal/H-opt{[GeCGe]Ni-CC-*ter*Ph→CuBr }

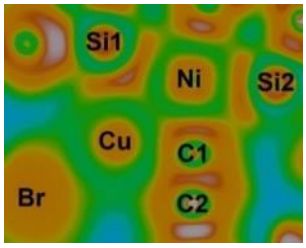

ELI-D Plot: fullopt-D3{[SiCSi]Ni-CC-Ph→CuBr }

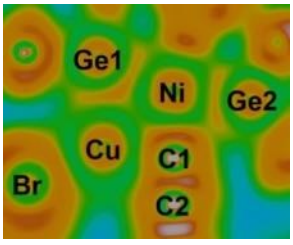

ELI-D Plot: fullopt-D3{[GeCGe]Ni-CC-*ter*Ph→CuBr }

[a] For atom number assignment see Table 7.2.1.

Table 7.2.3. Mayer Bond Order values in complexes **{[ECE]Ni-CC-R→CuBr}** and **{[ECE]Ni-CC-R}** (E=Si, R=Ph / E=Ge, R=*ter*Ph)[a]

MBO - Mayer Bond Order						
	{[ECE]Ni-CC-R→CuBr}				***{[ECE]Ni-CC-R}***	
	crystal/H-opt[b]		**fullopt-D3**[b]		**fullopt-D3**[b]	
	E=Si	*E=Ge*	*E=Si*	*E=Ge*	*E=Si*	*E=Ge*
E1-Ni	0.789	0.757	0.739	0.725	1.128	0.968
E2-Ni	1.011	0.973	1.019	0.919	1.141	0.966
Ni-C1	0.810	1.140	0.980	1.043	1.064	1.082
C1-C2	0.222	1.036	0.728	1.321	1.737	2.076
C2-C ipso,R[c]	0.916	1.086	1.002	1.152	0.977	1.115
C1-E1	-0.259	-0.121	-0.167	-0.026	0.056	0.113
C1-E2	-0.034	0.031	-0.035	0.145	0.051	0.107
C2-E1	0.225	0.107	0.110	0.005	-0.142	-0.088
C2-E2	0.077	0.030	0.062	-0.052	-0.141	-0.087
Cu-C1	1.306	0.999	0.963	0.855	---	---
Cu-C2	-0.448	-0.312	-0.273	-0.247	---	---
Cu-E1	0.152	0.342	0.227	0.462	---	---
Cu-Ni	0.317	0.395	0.362	0.447	---	---

[a] For atom number assignment see Table 7.2.1.
[b] B3LYP/def2-TZVP results (cf. Computational details).
[c] For E=Si → R=Ph, for E=Ge → R=*ter*Ph.

Table 7.2.4. NPA charges in complexes **{[ECE]Ni-CC-R→CuBr}** and **{[ECE]Ni-CC-R}** (E=Si, R=Ph / E=Ge, R=*ter*Ph)[a]

NPA charges						
	{[ECE]Ni-CC-R→CuBr}				***{[ECE]Ni-CC-R}***	
	crystal/H-opt[b]		**fullopt-D3**[b]		**fullopt-D3**[b]	
	E=Si	*E=Ge*	*E=Si*	*E=Ge*	*E=Si*	*E=Ge*
E1	1.752	1.632	1.745	1.642	1.922	1.774
E2	2.016	1.883	2.035	1.893	1.929	1.779
Ni	-0.704	-0.573	-0.690	-0.627	-0.857	-0.755
C ipso,ECE[c]	-0.272	-0.285	-0.267	-0.278	-0.256	-0.269
O1	-0.893	-0.852	-0.887	-0.845	-0.895	-0.864
O2	-0.902	-0.864	-0.901	-0.859	-0.894	-0.865
N1[d]	-0.718	-0.681	-0.720	-0.675	-0.717	-0.678
N2[d]	-0.724	-0.690	-0.730	-0.685	-0.719	-0.681
C1	-0.280	-0.290	-0.285	-0.299	-0.277	-0.281
C2	-0.114	-0.092	-0.106	-0.080	-0.108	-0.094
Cu	0.375	0.383	0.395	0.364	---	---
Br	-0.588	-0.576	-0.598	-0.570	---	---

[a] For atom number assignment see Table 7.2.1.
[b] B3LYP/def2-TZVP results (cf. Computational details). [c] C ipso of the ECE pincer-type ligand.
[d] Average value of both N-atoms is shown.

Table 7.2.5. NPA charges in fragments[a] of complexes **{[ECE]Ni-CC-R→CuBr}** and **{[ECE]Ni-CC-R}** (E=Si, R=Ph / E=Ge, R=*ter*Ph)

NPA charges of fragments				
	{[ECE]Ni-CC-R→CuBr} **fullopt-D3**[b]		***{[ECE]Ni-CC-R}*** **fullopt-D3**[b]	
	E=Si	*E=Ge*	*E=Si*	*E=Ge*
Ni	-0.690	-0.627	-0.857	-0.755
CuBr	-0.203	-0.207	---	---
CC-R[c]	-0.450	-0.438	-0.514	-0.478
L-0	-1.631	-1.584	-1.633	-1.593
E1	1.745	1.642	1.922	1.779
L-1	-0.408	-0.357	-0.423	-0.367
E2	2.035	1.893	1.929	1.774
L-2	-0.397	-0.323	-0.423	-0.360

[a] For assignment of fragments see Table 7.2.1.
[b] B3LYP/def2-TZVP results (cf. Computational details).
[c] For E=Si → R=Ph, for E=Ge → R=*ter*Ph.

7.3. Curriculum vitae

Daniel Gallego Mahecha
CURRICULUM VITAE

PERSONAL DETAILS

Date of birth:	05.02.1986
Place of Birth:	Bogotá D.C., Colombia
Nationality:	Colombian
Actual address:	Bochumer Str. 16, 10555 Berlin, Germany
Telephone:	(+49) 17661347871
E-mail:	dgallegom@mailbox.tu-berlin.de, littlebilbo@hotmail.com

CAREER OBJECTIVE

Continue learning about coordination and organometallic chemistry applied in homogeneous catalysis, chemical sensors, bioinorganic chemistry and metal-based drugs.
Contribute with my knowledge to the society in my country to strength its scientific research.

EDUCATION

2011–present	**PhD studies: *Inorganic Chemistry*** **Supervisor:** Prof. Dr. Matthias Driess Unicat, Technische Universität Berlin, Berlin, Germany. **Title**: Introducing Bis(silylene) and Bis(germylene) Pincer Ligands in Catalysis.
2009–2011	**Master studies: *Advanced Spectroscopy in Chemistry*** **Supervisor:** Prof. Dr. Berthold Kersting Université Lille1 Sciencies et Technologies, Lille, France. Universität Leipzig, Leipzig, Germany. **Title**: Binding of Small Peptides by Macrocyclic Amino-Thiophenolate Complexes.
09.2007–12.2007	**Research internship: *Inorganic and organic synthesis*** **Supervisor:** Prof. Dr. Carlos Lodeiro Espiño Universidade Nova de Lisboa, Lisbon, Portugal. **Title:** Síntesis y Caracterización de Nuevos Ligandos Flexibles Tipo Base de Schiff con Terminales Bitiofeno y Fosfina como Sensores de Iones Metálicos.
2003–2008	**Bachelor studies: *Chemistry*** **Supervisor:** Prof. Dr. Ana Esperanza Burgos C. Universidad Nacional de Colombia, Bogotá D.C., Colombia
1989–2002	**Elementary School and High School** Escuela Pedagógica Experimental (EPE), Bogotá D.C., Colombia

TECHNICAL SKILLS

- **Synthesis**

Organic, inorganic, organometallic, Schlenk techniques

- **Analytical chemistry:**

Spectroscopic methods: NMR, UV-Vis, IR, Raman, XRD, AAS,XAS
Spectrometric methods: Elemental analysis, mass spectrometry

- **Catalysis**

Homogeneous and heterogeneous catalysis

- **Microsoft office**

Work, Excel, PowerPoint

- **Data analysis software**

Matlab, Origin

- **Program language**

C++, Fortran

LANGUAGES

Spanish (1): Native speaker

Level:
1 = excellent
2 = good
3 = fair

English (2): **English courses B2/C1:**
Colombo Institute, Bogotá D.C.
OIINDE Colombia S.A. Institute, Bogotá D.C.
ALEX, Universidad Nacional de Colombia, Bogotá D.C.
Colombian-English Alliance
5 years experience during the master and PhD studies.

French (3): **French course A1/A2**:
Université Lille1 Sciences et Technologies, Lille, France.

German (3): **German course A1/A2**:
Deutsche Akademie, Berlin, Germany.

WORK EXPERIENCE

08.2006 –12.2008 **Laboratory assistant:**
Laboratory of General Chemistry, Universidad Nacional de Colombia

03.2007 – 0.6.2007 **Course assistant:**
Courses of General Chemistry, Universidad Nacional de Colombia

ORGANIZATIONAL SKILLS

01.2007 – 06.2008 **IAESTE**
IAESTE-CIENCIAS. Universidad Nacional de Colombia, Faculty of Sciences

05.2011 – present **ERASMUS MUNDUS**
Erasmus Mundus country representative

08.2011 – present **BIG-NSE Graduated School**
Active student from the *Berlin International Graduated School for Natural Sciences and Engineering* (BIG-NSE)

AWARDS

2008 **Bachelor's Honor Grade**
Best student from the batch of graduate students in Chemistry

08.2009 – 08.2011 **ERASMUS MUNDUS Scholarship**
Master Studies

09.2011 – present **Unicat Scholarship**
PhD Studies

2014 **Si&Me Poster Prize**
ISOS XVII, 3-8 August, Berlin

ARTICLES

13. B. Blom, G. Klatt, **D. Gallego**, G. Tan, M. Driess, *Dalton Trans*. **2015**, 44, 639−644.

12. **D. Gallego**, S. Inoue, B. Blom, M. Driess, *Organometallics* **2014**, *33*, 6885−6897. *ASC Editor's Choice. 3rd Most Read Article of the Year 2014.*
11. B. Blom, M. Pohl, G. Tan, **D. Gallego**, M. Driess, *Organometallics* **2014**, *33*, 5272–5282.
10. G. Tan, B. Blom, **D. Gallego**, E. Irran, M. Driess, *Chem. Eur. J*. **2014**, *20*, 9400–9408.
9. R. Schnitter, **D. Gallego**, B. Kersting, *Dalton Trans*. **2014**, ***43***, 13637–13648.
8. G. Tan, B. Blom, **D Gallego**, M. Driess, *Organometallics* **2014**, *33*, 363–369.
7. B. Blom, **D. Gallego**, M. Driess, *Inorg. Chem. Front*. **2014**, *1*, 134–148.
6. N. C. Breit, T. Szilvási, T. Suzuki, **D. Gallego**, S. Inoue, *J. Am. Chem. Soc*. **2013**, *135*, 17958–17968.
5. **D. Gallego**, A. Brück, E. Irran, F. Meier, M. Kaupp, M. Driess, J.F. Hartwig, *J. Am. Chem. Soc*. **2013**, *135*, 15617–15626.
4. A. Brück, **D. Gallego**, W. Wang, E. Irran, M. Driess, J.F. Hartwig, *Angew. Chem. Int. Ed*. **2012**, *51*, 11478–11482.
3. B. Blom, M. Driess, **D. Gallego**, S. Inoue, *Chem. Eur. J*. **2012**, *18*, 13355–13360.
2. A. Yoboue, A. Susset, A. Tougerti, **D. Gallego**, S. Venkat Ramani, M. Kalyanikar, D.S. Dolzhnikov, S.G. Wubshet, Y. Wang, S. Cristol, V. Briois, C. La Fontaine, R.M. Gauvin, J-F. Paul, E. Berrier, *Chem. Commun*. **2011**, *47*, 4285–4287.
1. Bruno Pedras, **D. Gallego**, P. Figueiredo, J.D. Nunes-Miranda, J.L. Capelo, C. Lodeiro*, Molbank* **2010**, *2010*, M683.

CONGRESS PARTICIPATION

14. XVII International Conference on Organometallic Chemistry, 13-18th July, 2014, Sapporo, Japan. *Assistant with Poster.*
13. SILQCOM-POLYMAT 2013, 13-17th October, **2013**, Huatulco, Mexico. *Oral presentation.*
12. ICIQ-UniCat Summer School, June 30th – July 4th, **2013**, Tarragona, Spain. *Assistant with Poster.*
11. 28th Tag der Chemie, 27th June, **2013**, Potsdam University, Potsdam, Germany. *Assistant with Poster.*
10. 27th Tag der Chemie, 28th June, **2012**, Technical University Berlin, Berlin, Germany. *Assistant with Poster.*
9. UniCat Workshop – Challenges in molecular catalysis, 25th-26th April, **2012**, Technical University Berlin, Berlin, Germany. *Assistant with Poster.*
8. XXIII International Conference on Coordination and Bioinorganic Chemistry – New Trends in Coordination, Bioinorganic, and Applied Inorganic Chemistry, 5th-10th June, **2011**, Smolenice, Slovakia. *Oral presentation*.
7. 7th Koordinationschemie-Treffen, 27th February – 1st March, **2011**, Universität Stuttgart, Stuttgart, Germany. *Assistant.*
6. International Symposium on Molecular Coordination Chemistry, 7th-9th

November, **2010**, Max Planck Institute for Bioinorganic Chemistry, Mülheim an der Ruhr, Germany. *Assistant*.

5. 2nd Gallego meeting of Kinetics and Catalysis, 29th-31st January, **2010**, Portomarín (Lugo), Spain. *Assistant*.
4. XII National Chemistry Students Meeting, 9th-11th October, **2008**, Cartagena de Indias D. T y C., Colombia. *Assistant with Poster.*
3. XIII International Symposium on Luminescence Spectrometry, September 7th-11th, **2008**, Bologna, Italy. *Poster*.
2. 7th Inorganic Chemistry Conference, Chemistry Portuguese Society, 30th November – 1st December, **2007**, Fatima, Portugal. *Assistant with Poster*.
1. 1st Latinamerican Symposium of Organometallic Chemistry (SILQCOM), 29-31th August, **2007**, Bogotá D.C., Colombia. *Assistant.*

ACADEMIC REFERENCES

1. Prof. Dr. Berthold Kersting
   Professor at the Department of Chemistry, Leipzig Universität, Leipzig, Germany.
   E-mail : b.kersting@uni-leipzig.de
2. Prof. Dr. Carlos Lodeiro Espiño
   Assistant Professor at the Department of Chemistry, Faculdade de Ciências e Tecnologia, REQUIMTE - Universidade Nova de Lisboa (FCT-UNL), Moonte de Caparica, Portugal.
   E-mail: cle@fct.unl.pt
3. Prof. Dr. Matthias Driess
   Professor at the Department of Chemistry, Technische Universität Berlin, Berlin, Germany.
   E-mail: matthias.driess@tu-berlin.de

HOBBIES

Learning natural sciences and new cultures. Reading world and adventure literature. Playing sports like soccer, volleyball, basketball, and riding the bike. Listen to all kind of music, especially traditional world music. Watch all kind of human expression by arts. Finally enjoy our wonderful nature every day by the simplicity and/or complexity of each thing.